Multiscale analysis of multi-layered tissues constructs : interfaces in the musculo-skeletal system based on tissue engineered osteotendinous junctions

Alejandro García García

Par **Alejandro GARCÍA GARCÍA**

Multiscale analysis of multi-layered tissues constructs : interfaces in the musculo-skeletal system based on tissue engineered osteotendinous junctions

Thèse présentée
pour l'obtention du grade
de Docteur de l'UTC

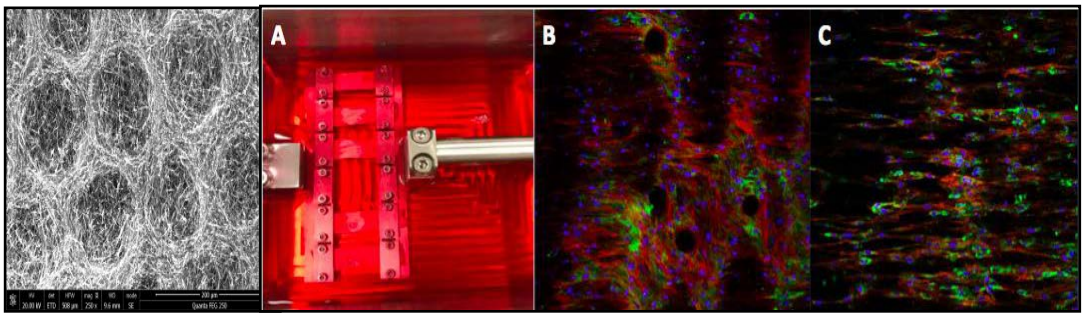

Soutenue le 11 juin 2019
Spécialité : Bio-ingénierie, Biomécanique, Biomatériaux : Unité de Recherche Biomécanique et Bio-ingénierie (UMR-7338)
D2488

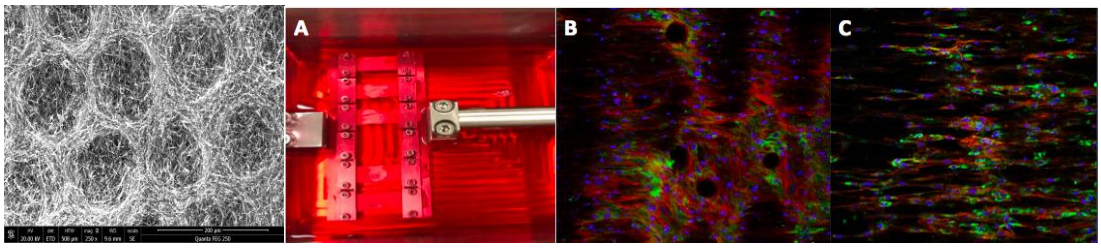

MULTISCALE ANALYSIS OF MULTI-LAYERED TISSUES CONSTRUCTS: INTERFACES IN THE MUSCULO-SKELETAL SYSTEM BASED ON TISSUE ENGINEERED OSTEOTENDINOUS JUNCTIONS

11 Juin 2019

PRESENTED BY : GARCIA GARCIA ALEJANDRO

THESIS SUPERVISORS :

- BEDOUI FAHMI
- LEGALLAIS CECILE

JURY MEMBERS :

- Dr. AMEDEE VILAMITJANA JOELLE, DR INSERM (REFEREE)
- Dr. GANGHOFFER JEAN-FRANCOIS, PROFESSOR (REFEREE)
- Dr. PAUTHE EMMANUEL, PROFESSOR
- Dr. VAYSSADE MURIEL, PROFESSOR
- Dr. BEDOUI FAHMI, MCF HDR
- Dr. LEGALLAIS CECILE, DR CNRS

THESE PRESENTEE POUR L'OBTENTION DU GRADE DE DOCTEUR DE L'UNIVERSITE DE TECHNOLOGIE DE COMPIEGNE SPECIALITE BIO-INGENIERIE, BIOMECANIQUE, BIOMATERIAUX

Résume

L'objectif de cette thèse était le développement d'un substitut bio-hybride pour la reconstruction du continuum tendon-os sur le principe de la ingénierie tissulaire. Après une analyse bibliographique exhaustive des structures natives et de leur environnement, nous avons d'abord proposé la réalisation de chaque système séparément en utilisant des scaffolds en polycaprolactone réalises par electrospinning.

Dans un premier temps, nous avons combiné l'electrospinning et l'electrospraying pour produire un scaffold composé de polycaprolactone et d'hydroapatite avec une structure en forme de nid d'abeille. Notre hypothèse était de doter le substitut d'une structure biomimétique favorisant l'adhésion, la colonisation et la différenciation cellulaire. L'analyse mécanique et biologique in vitro réalisée avec une lignée cellulaire progénitrice et des tests organotypiques a confirmé notre approche originale. Ensuite, le matériel ensemencé avec des cellules souches de moelle osseuse a été implanté avec succès par nos collaborateurs d'Amiens dans le but de traiter un défaut maxillo-facial chez un modèle de rongeur.

Parallèlement, pour la reconstruction du tendon, nous avons réalisé différents scaffolds d'electrospinning, dont la taille et l'organisation (aléatoire/alignée) des fibres varient. Dans une perspective bio-inspirée, nous avons combiné les scaffold avec l'étirement dynamique pour reproduire l'entraînement physique. Sous ces stimulations mécaniques, établies d'abord avec la même lignée cellulaire progénitrice, nous avons démontré dans une deuxième étude que les CSM s'alignaient sur l'axe d'étirement et produisaient une matrice extracellulaire, ce qui a permis de conserver les propriétés mécaniques de la matrice biohybride pendant les deux semaines de la culture.

Nous avons démontré que la différenciation cellulaire vers la lignée tendineuse et osseuse a été réalisée avec succès en l'absence de tout facteur de différenciation, étant spécifiquement lié aux propriétés des matériaux et à la mécanotransduction. Par conséquent, l'étape suivante, qui consiste à assembler les deux échafaudages avec une zone de transition, devrait conduire à la reconstruction de ce continuum osseux-tendon.

Mots clés

Ingénierie tissulaire, os, tendon, interface, electrospinning, biomécanique, cellules souches, polymères

Abstract

The objective of this thesis was the development of a biohybrid substitute for the reconstruction of the bone-tendon continuum based on tissue engineering strategies. After an exhaustive bibliographic analysis of the native structures and their environment, we first proposed the realization of each system separately using electrospun polycaprolactone scaffolds.

At first, we combined electrospinning with electrospraying techniques to produce a PCL-hydroapatite scaffold with honeycomb cavities. Our hypothesis was to provide the substitute with a biomimetic structure favoring cell adhesion, spreading and differentiation. The in vitro mechanical and biological analysis performed with a progenitor cell line and with organotypic assays confirmed our original approach. Then, the material seeded with bone marrow stem cells was successfully implanted by our collaborators in Amiens with the objective of treating a maxillofacial defect in a rodent model.

In parallel, for the tendon reconstruction, we investigated several electrospinning processes, varying fibers' size and organization (random/aligned). In a bioinspired perspective, we combined the choice of the scaffold with dynamic stretching to reproduce physical training. Under those mechanical stimulations, established first with the same progenitor cell line, we demonstrated in a second study that MSCs aligned with the stretching axis and produced extracellular matrix, which in turn allowed to keep the mechanical properties of the biohybrid scaffold all over the 2 weeks of culture.

We demonstrated that cell differentiation towards tendon and bone lineage was successfully achieved in the absence of any differentiation factor, being specifically related to materials properties and mechanotransduction. Therefore, the next step consisting in the assembly of both scaffolds with a transition area should lead to this bone-tendon continuum's reconstruction.

Key words

Tissue engineering, bone, tendon, interface, electrospinning, biomechanics, stem cells, polymer

Laboratories

UMR CNRS 7338: Biomécanique et Bioingénierie (BMBI)

Alliance Sorbonne Université

Université de Technologie de Compiègne

Centre de Recherches

Rue du Docteur Schweitzer

60200 Compiègne

FRE CNRS 2012 : Roberval

Alliance Sorbonne Université

Université de Technologie de Compiègne

Centre de Recherches

Rue du Docteur Schweitzer

60200 Compiègne

List of publications and communications

Publications:

Garcia Garcia A., Beldjilali-Labro M., Farhat F., Bedoui F., Grosset J.F., Dufresne M., Legallais C. **Biomaterials in Tendon and Skeletal Muscle Tissue Engineering: Current Trends and Challenges.** Materials 2018, 11, 1116; doi: 10.3390/ma11071116.

Garcia Garcia A, Hebraud A., Duval J.L., Wittmer C.R., Gaut L., Duprez D., Egles C., Bedoui F., Schlatter G., Legallais C. **Poly(Ɛ-caprolactone)/Hydroxyapatite 3D Honeycomb Scaffolds for a Cellular Microenvironment Adapted to Maxillofacial Bone Reconstruction.** ACS Biomater. Sci. Eng. 2018,4,3317-3326 ; doi : 10.1021/acsbiomaterials.8b00521.

Garcia Garcia A., Perot J.B., Beldjilali-Labro M., Dermigny Q., Naudot M., Le Ricousse S., Legallais C., Bedoui F. **Monitoring mechanical stimulation towards optimal tendon tissue engineering: Mechanical and biological multiscale study.** Draft completed.

International and national congress:

Garcia Garcia A., Schlatter G., Hebraud A., Egles C., Bedoui F., Legallais C. Bone reconstruction with Polycaprolactone/hydroxyapatite scaffolds. **ESB Lyon 2016.** Poster.

Garcia Garcia A., Schlatter G., Hebraud A., Egles C., Bedoui F., Legallais C. Bone tissue engineering with Polycaprolactone/hydroxyapatite biomimetic scaffolds. **43th ESAO Congress 2016, Warsaw, Poland.** Oral presentation.

Garcia Garcia A., Beldjilali-Labro M., Farhat F., Perot J.B., Dermigny Q., Dufresne M., Grosset J.F., Bedoui F., Legallais C. Multi-scale approach to reconstruct a bioartificial system of system: the example of the bone-tendon-muscle continuum. **SOSE 2018 Paris, France.** Poster.

Garcia Garcia A., Perot J.B., Naudot M., Le Ricousse S., Legallais C., Bedoui F. Mechanical stimulation monitoring towards optimal tendon tissue reconstruction. **XLV ESAO Congress 2018, Madrid, Spain.** Oral presentation.

Garcia Garcia A., Perot J.B., Naudot M., Le Ricousse S., Legallais C., Bedoui F. Mechanical stimulation of tendon-engineered construct. **Termis World Congress 2018, Kyoto, Japan.** Poster.

Other scientific communications:

Garcia Garcia A., Naudot M. Comportement de cellules souches mésenchymateuses sur des matériaux électrospinnés pour une application en chirurgie maxillo-faciale. **Quatrième journée scientifique de l'Institut Faire Faces 2017, Amiens, France.**

Fête de la science 2017, Université de Technologie de Compiègne. Participation au stand : De Capitaine Crochet à Iron Man.

Awards

yESAO Exchange Program, European Society for Artificial Organs. Coaxially electrospun and directional solidified scaffolds for bone and vascular tissue engineering. **43th ESAO Congress 2016, Warsaw, Poland.**

List of contents

List of Figures

List of Tables

Abbreviations

3D: Three-dimensional space

ADSC: Adipose derived stem cells

ALP: Alkaline phosphatase

ANF: Aligned nanofiber

ANOVA: Analysis of variance

Aqp1: Aquaporin 1

BCIP/NBT: 5-Bromo-4-chloro-3-indolyl phosphate / 4-Nitro blue tetrazolium chloride

BGLAP: Bone gamma-carboxyglutamate protein

BMP: Bone morphogenetic protein

BMSC: Bone marrow stromal cell

BSP: Bone sialoprotein

BTE: Bone tissue engineering

Cbfa1: Core-binding factor alpha 1

cDNA: Complementary deoxyribonucleic acid

COL1: Collagen type 1

CS: Chitosan

DCM: Dichloromethane

Dlx5: Distal-less Homebox 5

DBM: Demineralized bone matrix

DMF: Dimethylformamide

DNA: Deoxyribonucleic acid

E': Storage modulus

E'': Loss modulus

E*: Complex modulus

ECM: Extracelular matrix

EDS: Energy-dispersive X-ray spectroscopy

ESC: Embryonic stem cell

EthD-1: Ehidium homodimer-1

FBS: Fetal bovine serum

FDA: Food and drug administration

FGF: Fibroblast growth factor

G (needle): Gauge

GPa: Gigapascal

HA: Hydroxyapatite

HCl: Hydrochloric acid

hFOB: human fetal osteoblastic

IBPS: Institut de Biologie Paris-Seine

IBSP: Integrin binding sialiprotein

ICPEES: Institut de chimie et procédés pour l'énergie, l'environnement et la santé

IGF: Insulin growth factor

IMP: Institute für MehrphasenProzessen

iPS: induced pluripotent stem

kV: kilovolt

MPa: Megapascal

MSC: Mesenchymal stem cell

MTT: 3-(4,5-dimethylthiazol-2-yl)-2,5-diphenyltetrazolium bromide

MW: Molecular weight

ND: Non-determined

NF: Nanofiber

OCN: Osteocalcin

OPN: Osteopontin

PAF: Paraformaldehyde

PBS: Phosphate-buffered saline

PCL: Polycaprolactone

PEO: Polyethylene oxide

PHB: Polyhydroxybutyrate

PLA: Poly lactic acid

PLGA: Poly lactic-co-glycolic acid

PLLA: Poly L-lactic acid

RNA: Ribonucleic acid

RNF: Random nanofiber

RP: Rapid prototyping

Rpm: Revolutions per minute

RT-qPCR: Reverse quantitative transcription polymerase chain reaction

SAPC : Service d'analyse physico-chimique

SC: Stem cell

Scx: Scleraxis

SEM: Scanning electron microscopy

SF: Silk fibroin

SOSs: System of systems

SP7: Transcription factor SP7, or Osterix

SPP1: Secreted phosphoprotein 1, or Osteopontin

TCP: Tricalcium phosphate

TDSC: Tendon derived stem cells, or TSPC

TGF: Transforming growth factor

TM: Tensile modulus

TNMD: Tenomodulin, or Tnmd

TS: Tensile strength

TSPC: Tendon stem/progenitor cell, or TDSC

UPJV: Université de Picardie Jules Verne

UTC: Université de Technologie de Compiègne

VEGF: Vascular endothelial growth factor

WJSC: Wharton Jelly stromal cell

Introduction: from bone tissue engineering to the reconstruction of the musculo-skeletal system of system

In a previous study (PhD thesis of T. Baudequin), our laboratory developed a bio-hybrid tissue made of granules of hydroxyapatite on which cells had been seeded and grown within a bioreactor, to produce a hand-able tissue sheet for the further application in maxillofacial reparatory bone surgery. With the synthesis of their own extracellular matrix, cells encompass the particles forming a sheet-like tissue after one month of culture.[1] Very attractive regarding biocompatibility and osteoinduction, the handle-sheet bone like tissue were far from the specifications established by the laboratory regarding its mechanical properties.

To improve these mechanical properties keeping the sheet aspect, electrospun matrices appeared as a clear alternative to granules for maxillofacial regeneration. The combination of elastic properties and fibrous nature similar to the extracellular matrix raised interesting process and solution for tissue engineering. The research group focused then on two polymers, PCL and PLLA, both polyesters with high biocompatibility currently employed in the biomedical field. Interestingly, the investigated polymers not only appears to be promising for bone tissue regeneration, but also seemed to be good candidates for other tissues such as tendon or muscle, other major systems in the musculo-skeletal system of system. These results allowed us to set the framework for the development of a tissue-engineered based model of musculo-skeletal system, with a future emphasis on the reconstruction of the interfaces between the different subsystems, i.e. the osteo-tendinous and the myotendinous junctions. The whole project, involving several researchers at BMBI and Roberval laboratories was selected as a "challenge and funded by the Labex MSST (Maitrise des Systèmes de Systèmes Technologiques)".

Objective of the thesis

In this context, the aim of this PhD thesis was to propose an overall methodology to design and validate a bioartifical system representing the continuum tendon-bone, itself composed of biohybrid systems at different scales. It represents an example of complex bioinspired system of systems (SoSs) in which the different systems are in continuous remodeling and

interactions. The structural complexity (as a reconstructed multi-layered tissue) of the proposed bioengineered system presents a major challenge to understand and predict its mechanical and biological behavior.

To this purpose, the following objectives were defined:

- Characterize the tissues of interest, their components and the key features that should guide their reconstruction. These living tissues are themselves SoSs, formed by the cells, their extracellular matrix and their interaction and are continuously evolving. For this purpose, we perform the review of literature and interact with the experts in physiology and mechanics of musculo-skeletal system at BMBI laboratory

- Establish the requirements and design the appropriate bio-inspired scaffold based on the native structure. In the framework of this PhD thesis, we focus in the development of two sub-systems: reconstructed bone and tendon.

- Analyze the interactions involved within the different subsystems. They are contingent to the biological properties of the developed tissues, but also to the chemical and mechanical properties of the material scaffolds. These interactions will be monitored through the culture process at the relevant scale to first tune the different cell response toward the desired type of tissue and tailor the mechanical properties of the global SoS.

Having in mind this idea of continuum and based on our previous studies, all scaffolds were prepared by electrospinning techniques. Chapter I was dedicated to the literature review regarding first bone and bone tissue engineering, focusing on electrospun scaffolds. Then, a similar survey was achieved for tendon and tendon tissue engineering, under the form of a review paper in which muscle and the myotendinous junction are also described. Finally, the enthesis issues were also briefly analyzed. Chapter II summarized the Materials and Methods employed for this PhD.

For bone bio-hybrid constructs (chapter III), we elaborated 3D scaffolds with a honeycomb-like architecture, based on a technique associating electrospun poly-ε-caprolactone (PCL) nanofibers and electrosprayed hydroxyapatite (HA) nanoparticles. These constructs were designed and built thanks to our collaboration with ICPEES (Dr. G. Schlatter, Dr. A. Hébraud). The biomimetic topography served as a niche for the growth and differentiation of cells. For

in vitro studies, C3H10T1/2 cell line, previously employed in the laboratory thanks to the collaboration with Dr. Delphine Duprez (IBPS), was chosen since these cells are able to differentiate to bone or tendon lineage. Then, in vivo studies were performed by our collaborators at EA 4666 (UPJV) in the framework of a project led by C. Legallais and funded by Région Hauts de France (previously Picardie).

For tendon biohybrid constructs, aligned and random PCL electrospun scaffolds were seeded with cells, in the absence of any differentiation factors. Cyclic stretching was applied to the scaffolds in a bioinspired vision to simulate training. In a first series of investigation (Chapter IV), we also used C3H10T1/2 so as to define culture and stretching conditions in favor of tendon differentiation. Then, we transfer the protocol to rat mesenchymal stem cells (chapter V), to go closer to preclinical in vivo studies. In addition, as these cells present high production of the extracellular matrix, we aimed at studying over time the impact of this neo-synthesis on the mechanical properties of the biohybrid constructs.

Chapter I – State of the art

Chapter I: State of the art

1. Bone Tissue Engineering: Current Trends and Challenges

1.1. Bone Composition and Structure

Bone is a hierarchical and complex hard, dense and highly mineralized connective tissue that support and protect vital organs, allow the body movement, provides the body reservoirs of minerals and growth factors and a site for hematopoiesis.[2] Bone matrix is composed of 70% minerals, 25% of organic compounds and 5% of water.[3] The mineral part is composed mainly of crystals of calcium phosphates (Hydroxyapatite crystals). Type 1 collagen represents around 90% of the organic part of the extracellular matrix. Other collagens such as collagen III, V, XI and XIII, glycoproteins such as Bone Sialo Protein (BSP), vitronectin, osteonectin, thrombospondin, fibronectin and osteonpontin have been also found as constituent for the organic phase of bone matrix.[4]

The skeleton of human adults is composed of around 213 bones that can be classified according to their location, shape, consistency or size.[5] Macroscopically, bones can be categorized into two groups: the cortical and the trabucular bones.[6] Cortical bone, which represents the 80% of bones, is dense and compact with a low porosity (10%), has a slow turnover rate and a high mechanical resistance; and constitutes the outer part of all skeletal structures. Cortical bone provide mechanical strength and protection to the body, but it can also participate in metabolic response, particularly when there is severe or prolonged mineral deficit.[7] It is organized in cylindrical structures called osteons that have a diameter of around 200µm in a human adult. Each osteon consists of concentric layers of compact matrix called lamellae that surrounds a central canal called the harvesian canal, which contains blood vessels and nerves fibers. The remaining 20% is the trabecular bone; less dense, more elastic and porous (30-90%), it has a high turnover rate than cortical bone and constitutes the inner part of long bones, vertebras, pelvis and other large flat bones. Trabecular bones contribute to mechanical support, act as a scaffold for the hematopoietic cells and provide supplies of mineral in acute deficiency states.[7,8] Without osteons, lamellae are organized in a “rod and plate” structure called trabeculae.[9] Relative to its structure and composition there are characteristic mechanical properties for each group of bone. Thus, the cortical bone presented a Young´s modulus of 15-20 GPa and a compressive strength of

100-200MPa and the trabecular bone has a Young´s modulus of 0.1-2GPa and a compressive strength of 2-20MPa.[10]

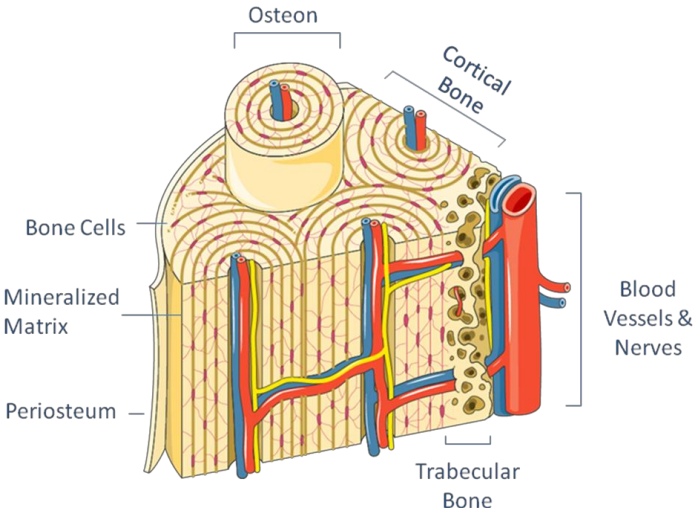

Figure 1. Bone structure, adapted from Sevier Medical Art.

Four different cell types constitute bone tissue: Osteoblasts, bone lining cells, osteocytes and osteoclasts.[11] Osteoblasts, derived from mesenchymal stem cells (MSC), are responsible for new bone synthesis. In their mature form, osteoblasts could undergo two possible pathways: apoptosis or become osteocytes or bone lining cells. Osteocytes, the most abundant cells in bones (90%) are mature osteoblasts located within lacunae surrounded by mineralized bone matrix. Osteocytes are connected creating a network through the lacunae, facilitating the intercellular transport of small signaling molecules, oxygen and nutrients. As osteocytes, bone lining cells derived from osteoblasts. They cover the surface of bones, preventing osteoclasts to enter in contact with bone matrix when matrix resorption should not occur. Osteoclasts are terminally differentiated myeloid cells responsible uniquely to bone resorption.

1.2. Bone Remodeling and Injuries

1.2.1. Remodeling

Bone is a dynamic tissue involved in a continuous cycle of remodeling responsible to the maintain of adult skeleton and mineral homeostasis.[12] This tightly interconnected cycle is constituted of three consecutive phases which involves different phases: (I) Old bone resorption by osteoclasts, (II) a transition phase from resorption to new bone formation, and

(III) formation of new bone by osteoblasts.[13] Apart from other tissues, bone tissues present an inherent ability to regenerate without scaring and this newly formed bone is almost indistinguishable from adjacent uninjured tissue.[14]

1.2.2. Injuries

However in some cases due to trauma, injury, disease or aging damage, bone could present a significant loss of its repair ability.[15] These conditions may lead to non-union, scar formation and long-term persistent bone defects.[16] In these cases in which the self-regeneration of bone tissue is compromised, bone graft appears as the most widespread solution.

1.2.3. Bone Grafts and Subtitutes for Bone Reconstruction

The main function of bone grafts is to ensure growth and healing, whilst providing mechanical support as long as the processes take place.[17] Bone grafts are classified in different categories: autografts, allografts, xenografts and bone grafts substitutes. Each type differs with regard to their properties of osteogenesis, osteoinduction and osteoconduction. [18] Osteogenesis refers to a material which contain living cells that will produce new bone. The osteoconduction is the ability to allow bone growth from vascular and osteogenic host cells. Finally, osteoinduction refers to the ability to induce cell differentiation leading to mature bone cells. [19]

Autographs are considered as the gold standard: they are harvested from the donor and present the three characteristics expected from the bone grafts, they are osteogenic, osteoconductive and osteoinductive. Autograft includes aspirate bone marrow, cortical or cancellous bone and vascularized grafts. [20] In spite of the respect of the specifications for the bone grafts, the limits in terms of quantity and the risk of morbidity make it considerable other ways to overcome bone regeneration and reconstruction.[21]

Bone allografts refer to bone tissue coming from another individual of the same species. Without the preceding limits in terms of quantity and risk of morbidity, allografts are present in various forms including cortical or cancellous bone and derivatives forms as demineralized bone matrix (DMB). [22] While they lack of osteogenicity, allogeneic cortical and cancellous bone presented osteoconductive properties. DMB are processed in such a way that they

provide osteoinduction.[23] As main drawbacks, allografts do not reach a regeneration as complete as autografts, they are immunogenic and they present a risk for the transmission of diseases. [24] Another alternative, xenografts, refers to bony tissue harvested from other species. Moreover, its high immunogenic response turns this possibility into something marginal. Current efforts are made in terms of complete decellularization, deproteination and defatting protocols. [19]

In order to overcome these limitations different alternatives have been deployed as the use of synthetic bone grafts substitutes. Among these biomaterials, we can distinguish calcium phosphate ceramics, bioactive glass and calcium sulfate.[25] Calcium phosphates are the most widespread ceramics available on the market. They are a family of calcium salt compounds consisting of calcium ions and organophosphates. The calcium phosphate family includes monocalcium phosphate, dicalcium phosphate, tricalcium phosphate (TCP), hydroxyapatite (HA) and tetracalcium phosphate.[22] In general, most calcium phosphates are forming mixed compounds in form of blocks, cements or powders.[26,27] Interestingly, HA ($Ca_{10}[PO_4]_6[OH]_2$) is a mineral of natural origin which comprises about 50% of bone weight. Despite their differences in terms of composition, calcium phosphates are osteoconducive, presented a good osteointegration and could promote osteoinduction.[28] Bioactive glasses or bioglass, are synthetic silica-based materials developed in 1970s with osteoconductive and unique bone binding properties.[29] When implanted in the bone a silica-rich layer occurs and on top of this layer, a layer of HA is formed.[22,30] This layer of HA absorbs proteins and attracts osteo-progenitor cells.[31] Calcium sulfate or plaster of Paris (CaSO4) is a osteoconductive and biodegradable ceramic with the faster resorption rate of ceramics, a faster rate than actual bone deposition which compromise bone healing.[22] However their low cost and easy procurement make it an interesting candidate for bone reconstruction if combined with other materials.[31]

1.3. Bone Tissue Engineering

While the aforementioned substitutes for bone allows to a greater or lesser extent for bone reconstruction, none is exempted of further ameliorations to achieve the ideal regeneration: low morbidity, osteoconductive, osteoinductive and osteogenic properties, size restriction, quick accessibility and reasonable cost.[32] In order to achieve all the ideal requirements for

bone regeneration, an emerging field, bone tissue engineering (BTE) has appeared during the last 30 years. BTE requires the combination of the appropriate scaffold, cells and/or signaling factors. The goal is to provide the organism with the right biohybrid scaffold that provides both mechanical support and enough information to allow hosted cells to organize a new bone tissue.

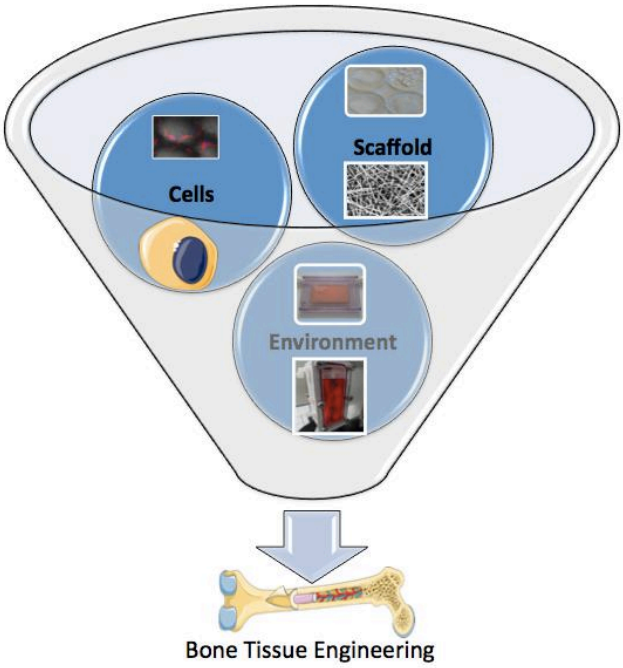

Figure 2. The three pillars of bone tissue engineering: cells are ideally cultivated on a biomimetic scaffold in order to guide their performance as close as in the native bone. The mechanical and biochemical environment are of key relevance in eliciting targeted responses.

1.3.1. Materials and Scaffolds Manufacture

The "right" scaffold should provide a similar three-dimensional structure as bone tissue with osteoconductive, osteoinductive and osteogenic properties. From bioactive inorganic materials as calcium phosphates[33–37] or bioactive glass[38–41] to polymers both naturals as collagen, fibrin, silk, chitosan, alginate or hyaluronic acid, or synthetics as polycaprolactone (PCL)[42,43] polylactic-acid (PLLA)[44,45], poly-lactic-co-glycolic acid (PLGA)[46,47] and polyurethanes (PUs)[48–50] or composites (polymers and inorganic compounds)[51–58] and natural derived tissues (decellularised or demineralized bone), a wide range of materials has been used for BTE applications.

To produce the ideal scaffold, different techniques have been developed during the last years as solvent casting, gas foaming, freeze drying, electrospinning, melt-blown process and rapid prototyping process.[59] Despite the differences among the different processes, it has been highlighted that the optimal scaffold for the bone tissue regeneration must have a sufficient porosity to allow cell colonization, nutrient supply, vascularization and tissue ingrowth, while taking into account the mechanical requirements of the bone tissue. The porosity ranges varies from 100-500 µm and the pore distribution is related to the manufactured technique[60].

1.3.2. Cells

Several cell sources have been investigated for bone tissue engineering. The ideal cell source must meet a series of requirements such as being easily isolated and expanded, as well as presenting an interesting activity in the required field, in this case bone regeneration. Depending on their state of differentiation, we can distinguish between stem cells (SC) or terminally differentiated cells. Only stem cells present a differentiation potential (pluripotent, multipotent or unipotent) and they could be classified into two groups depending of it origin: embryonic or adult.

Embryonic stem cells (ESCs), which are pluripotent, are isolated from the blastocyst. Despite being able to differentiate towards the three germ layers, their use is not exempt of limits such as the risk of immune rejection, as well as ethics' concerns[61]. Recently, induced pluripotent stem (iPS) cells appeared as an alternative to ESCs. iPS are derived from adult somatic cells via the introduction of a series of transcription factors. Recently, some works successfully focused on the differentiation of iPS-derived cells towards bone lineage[62,63]. However, due to the potential for mutagenesis and the low efficiency of transfection, they are not yet authorized for clinical application in humans[64].

Adult mesenchymal stem cells (MSCs) are promising cell sources presenting the ability to differentiate into osteoprogenitors and mature osteoblasts. MSCs could be isolated from several autologous sources as bone marrow, adipose tissue, synovial membrane, dental pulp, skin, cartilage and other sources as umbilical cord. In addition their potential for self-renewal and clonogenicity, make MSCs a relevant source for clinical application. Bone marrow derived stem cells (BMSCs) are the predominant source for adult MSC for bone tissue engineering and are already used in preclinical studies[65]. However they present

several limits including donor site morbidity and lower differentiation potential in aged individuals. Compared to BMSCs, adipose derived stem cells (ADSCs) can be obtained in larger number and in a less invasive procedure. However, further studies should be carried to confirm their bone-forming capacity and safety concerns[66].

Immortalized cells lines are also commonly used for bone tissue engineering. From animal (MC3T3-E1[67–71], C3H10T1/2[72]) or from human (hFOB[73–75]), cells lines offer advantages as they could be grown for prolonged period in vitro and provide homogenous cell population with well-known properties[76]. However, as they have been genetically modified, their phenotype, their native functions, as well as their response capacity to stimuli may be disturbed[77]. These cells are often used in early investigations as proof of concept, or in fundamental studies.

1.3.3. Chemical and Mechanical Environment

Bone healing occurs immediately after a fracture, orchestrated by a cascade of events guided by cytokines, involving different types of cells as inflammatory cells, vascular cells, mesenchymal progenitor cells and osteocytes. According to their activity, we can distinguish among (I) pro-inflammatory, (II) angiogenic and (II) osteogenic factors[78]. The main families regrouping the different growth factors include transforming growth factor superfamily (TGFβs and bone morphogenetic proteins (BMPs)),[79,80] fibroblast growth factor (FGF)[81], vascular endothelial growth factor (VEGF)[82] and insulin-like growth factor (IGF)[83].

TGFβ superfamily comprises over forty members such as the three isoforms of TGFβ (TGFβ1, TGFβ2 and TGFβ3) and BMPs. TGFβ stimulates matrix protein synthesis, enhances the proliferation of mesenchymal cells and osteoblasts in fractures and plays an important role in bone remodeling with it facilitating or suppressing role over the activity on osteoclasts[84,85]. Among TGFBβ superfamily, BMPs are involved in different signaling pathways in bone formation, from promoting recruitment and migration of mesenchymal cells to osteogenic differentiation. While more than 20 different BMPs have been identified, isoforms BMP-2, BMP-4 and BMP-7 are the best characterized ones. BMP-2 and BMP-7 have been incorporated in FDA-approved systems for bone regeneration and are commercially available for surgical use on collagen sponge carrier[86]. FGF displays an important role in bone regeneration and homeostasis. While it does not directly induce osteoblast differentiation, FGF plays a role on osteoblast differentiation. It has been suggested that isoforms FGF-2 and

FGF-9 play an important role on osteoblasts proliferation and angiogenesis[87,88]. Another pro-angiogenic factor is VEGF that stimulates neovascularization by stimulating the proliferation and migration of endothelial cells[82]. IGF regulates different processes as bone development, growth and healing by stimulating proliferation and differentiation of osteoblast precursors. Interestingly, it has also been reported a role on osteoclast survival and remodeling processes[89].

Besides chemical stimulation, it is well known that mechanical stimulation has a preponderant role in bone homeostasis and remodeling. Indeed, during standing and physical activities, mechanical forces are exerted on the bones. This mechanical environment result in a maintenance or gain of bone mass[90]. Lack of physical activity leads to weakening of the bone and consequently, bone fractures could occur[91]. Duncan et al. (1995) summarized the different ranges of physical strains that affect bone homeostasis. Those strains were reported in terms of microstrain (µstrain) where 1000 µstrain corresponds to 0.1% in terms of elongation percentage. Bone resorption occurs below 200 µstrain, the physiological range up to 2500 µstrain, an overuse appears around 5000 µstrain and over this threshold, pathological states appear[92]. Therefore, during the last years, different works have focused on the effect of mechanical stress on bone tissue and the application of a mechanical environment for bone tissue engineering as a key factor towards the proper-engineered construct. This mechanical environment has been generated using different bioreactors that our team summarized in a previous review.[93]

1.4. Biomimetic Electrospun Scaffolds for Bone Tissue Engineering

Electrospun based scaffolds present micron to sub-micron fibres which are similar to the extracellular matrix [94]. In addition to the fibrous nature of the material, the versatility of electrospinning to produce scaffolds with tailored morphology and porosity from a wide range of different polymers could explain its success during the last years in the field of tissue engineering[95]. Different scaffolds have indeed been developed for applications in skin[96], cartilage[97], tendon/ligament[98], nerves[99] and bone[100] reconstruction.

In the electrospinning process, a polymer solution is introduced in a syringe. Under a constant flow rate, the solution is extruded through a thin needle. At the exit of the needle, the solution is held by its surface tension. When subjected to an electric field, generally over

dozen of kilovolts, the polymer solution becomes charged and when the electric charges overcome the surface tension threshold, the high voltage allows the formation of a stable Taylor cone. The polymer is thus carried out towards the collector presenting opposite charges, in the form of a thin and unique continuous fiber. The solvent evaporates as long as the fiber becomes thinner. As a result, a network of fibers is formed on the collector [101]. The fibers and their spatial configuration are influenced by many parameters such as concentration in polymer, type of solvent, humidity, type of collector used, etc.[102]

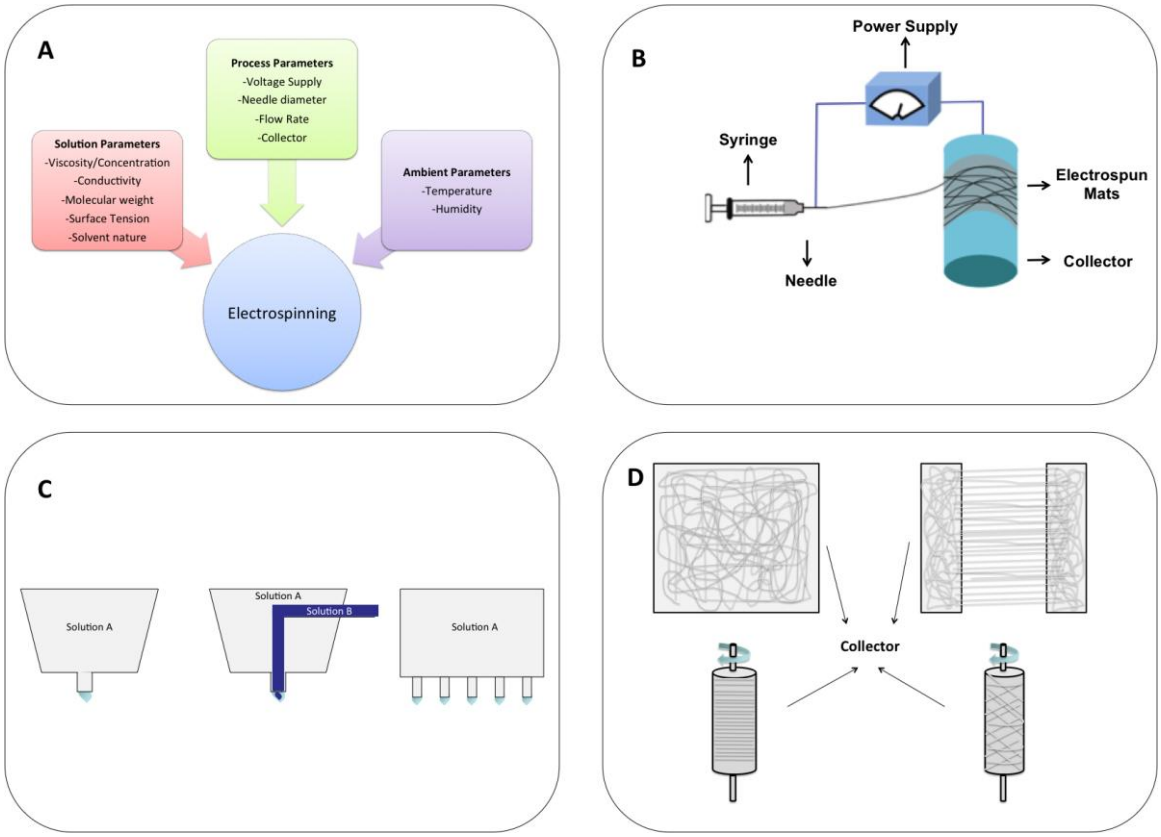

Figure 3. **A.** Scheme of the different parameters involved in the electrospinning process. **B.** General representation of the components of an electrospinning system. **C.** Three types of needles employed in the electrospinning technique. From right to left: single needle, co-axial needle and a multiple needle system. **D.** Different types of collectors for the realization of different organization of electrospun fibers. From right to left and from top to bottom: flat collector, parallel collector, and rotatory drum collector at high speed and rotatory collector at low speed.

While the common electrospinning device consists in a single solution flowing through a capillary and a flat collector, variations of the system are possible. Since the electric field mainly contributes to the attraction towards the collector, the device can be placed vertically or horizontally. The collector can take the form of a rotating cylinder, which will allow greater uniformity of the fiber mat, but especially their alignment at high rotational speed. In addition to these techniques where part of the assembly is in motion, aligned

fibers may be formed using two spaced apart electrical sources operating alternately. Other geometrical modifications of the ground collector could be performed by playing with the surface topography, where fibers are deposited following the design of the surface. Electrospinning also makes it possible to spin polymer mixtures (co-spinning), coaxial fibers or to use multiple jets simultaneously.

We hereafter propose a review of the different materials used for scaffold production, the mechanical properties of the biohybrid constructs, as well as both in vitro and in vivo outcomes. We sorted the references in tables, according to increasing scaffold's complexity.

1.4.1. Materials and Manufacture

A wide range of polymers has been used to produce electrospun fibrous scaffolds for bone tissue engineering (Table 1). Generally, these polymers are classified according in two groups: natural or synthetic. Thanks to their origin, natural polymers (collagen[103–105], gelatin[71,106], silk[107,108,67,73] or chitosan[109]), present correct biocompatibility allowing cell adhesion and proliferation. However, their poor mechanical properties, rapid degradation and costs associated to their isolation and purification limit their use. In contrast, synthetic polymers appeared interesting during the last years because they can easily tailor scaffolds with reproducible porosity, shape and better mechanical properties[59]. Among the examples of synthetics polymers used for bone tissue engineering, we can cite PCL[70,110–112], PLLA[72,74,113], co-polymers as PLGA[114] or PLCL[115]; polystyrenes[69] and polyhydroxyalkanoate as PHB[116]. However, synthetic polymers are less favorable to cell adhesion and proliferation. Therefore, composites of both natural and synthetic polymers have been deployed to meet the entire requirement for bone tissue engineering, i.e. suitable mechanical properties but also bioactivity[70,71,74,104–106,112].

In addition to its fibrous structure, bone specificity depends on its mineralized ECM. Electrospinning setup, by incorporating mineral particles at the polymer solution, is able to produce fibers with nano- to micro-particles, such as TCP[111] or HA[73,75,109,116], already widely used as biomaterials for bone regeneration or repair. Others successfully incorporated demineralized bone matrix (DMB) into a PLLA solution to produce composite scaffolds[113]. Added into the polymer solution[108] or encapsulated by the fibers[109], electrospinning has successfully used as a vehicle for growth factors delivery.

Material	Scaffold Preparation	Shape and Structure of the scaffold	Mechanical Properties of the Scaffold	Ref
PCL/Gelatin	Electrospinning random and aligned fibers	RNFs diameter = 344-347nm ANFs diameter = 355-356nm	RNFs 344nm -> TM=38.6 MPa; TS=7.9 MPa RNFs 334nm -> TM=33.4 MPa; TS=5.5 MPa RNFs 347nm -> TM=26.0 MPa; TS=2.0 MPa ANFs 355nm -> TM=45.3 MPa; TS=20.9 MPa ANFs 335nm -> TM=36.3 MPa; TS=15.6 MPa ANFs 363nm -> TM=30.4 MPa; TS=13.4 MPa	Guo et al. 2015 [70]
PCL/Gelatin	Electrospinning random fibers	RNFs diameter = 10-1000nm	Gelatin NFs -> YM=105 MPa; TS=2.50 MPa PCL NFs -> YM=4.98 MPa; TS=2.70 MPa PCL/Gelatin NFs -> YM=30.8; TS=1.29 MPa	Zhang et al. 2005 [106]
PCL/Collagen	Electrospinning random fibers. 3D scaffolds obtained by wrapping fibers mats	RNFs diameter = 513nm	RNFs -> YM=4.59 MPa Wrapped scaffold in the axial direction => 0.61 MPa Wrapped scaffold in the radial direction =>1.0 MPa	Ekaputra et al. 2009 [104]
PCL/Collagen	Electrospinning random co-axial fibers. Inner PCL and outer fiber Collagen	RNFs coaxial = 442nm	ND	Haslauer et al. 2011 [105]
PLCL/Fibrinogen	Electrospinning random and aligned fibers. 3D honeycomb scaffolds	RNFs diameter = 195-462nm ANFs diameter = 195-491nm HC diameter = 213-445nm	ND	Nedjari et al. 2017 [117]
Collagen	Electrospinning random fibers	RNFs diameter = 50-1000nm	ND	Shih et al. 2006 [103]
PS	Electrospinning random and aligned fibers	RNFs diameter= 1-3.5µm ANFs diameter = 1.5-4.5µm	ND	Terranova et al. 2016 [69]
PCL, PLLA and PCL/PLLA	Electrospinning random, aligned and coaxial fibers	RNFs PCL diameter = 665-1159nm RNFs PLLA diameter = 681nm ANFs PCL diameter = 1032nm CNFs PCL/PLLA diameter = 1928-2461nm	RNFs PCL -> YM = 21-30MPa RNFs PLLA -> YM = 24MPa ANFs PCL -> YM = 15MPa CNFs PCL/PLLA -> YM = 32-60MPa	Baudequin et al. 2017 [72]

Chitosan/HA	Electrospinning random fibers	RNFs chitosan diameter = 138nm RNFs chitosan/HA diameter = 214nm	ND	Zhang et al. 2008 [75]
PLLA PLLA/HA PLLA/Collagen/HA	Electrospinning random fibers	RNFs PLLA diameter = 860nm RNFs PLLA/HA diameter = 845nm RNFs PLLA/Collagen/HA diameter = 310nm	RNFs PLLA -> TS = 4.69MPa RNFs PLLA/HA -> TS = 3.10MPa RNFs PLLA/Collagen/HA -> TS = 2.05MPa	Prabhakaran et al. 2009 [74]
PLLA/PCL PLA/PCL/HA	Electrospinning random fibers	RNFs PLA/PCL diameter = 776nm RNFs PLA/PCL/HA diameter = 332-583nm	ND	Fang et al. 2010 [68]
PLA/Demineralized Bone Powders	Electrospinning random fibers	RNFs diameter = 300-700nm	ND	Ko et al. 2008 [113]
Fibroin/Chitosan/Ha/BMP2	Electrospinning co-axial fibers	Thick fibers diameter = 534nm; outer layer 167nm Thin fibers diameter = 546nm; outer layer 101nm	ND	Shalumon et al. 2015 [109]
Silk/PEO/HA/BMP2	Electrospinning random fibers	RNFs Silk/PEO diameter = 590nm RNFs Silk/PEO diameter = 575nm RNFs Silk/PEO/BMP2 diameter = 570nm RNFs Silk/PEO/HA diameter = 510nm RNFs Silk/PEO/HA/BMP2 diameter = 520nm	ND	Vepari et al. 2006 [108]
Silk	Electrospinning over a modified water bath collector	RNFs diameter = 200-500nm Pores sizes = 0-500µm Porosity = 90-93%	ND	Park et al. 2010 [67]
Silk/HA	Electrospinning over a modified water bath collector	RNFs diameter = 1.49µm Pores sizes = 42.3-301.1µm	Compressive modulus of Silk mats= 3.4-102KPa Compressive modulus of Silk/HA mats = 8.1-29.3KPa	Yang et al. 2015 [73]

PCL/PLLA	Electrospinning aligned fibers to produce yarns. Yarns assembled to create a 3D structure	ANFs diameter = 400-900nm Porosity = 77.61 %	3D structure PCL/PLLA -> EM =57.23-74.91MPa	Cai et al. 2012 [118]
PHB/HA	Electrospinning random fibers. Staked layers to perform a 3D structure	RNFs PHB diameter = 0.7-1.2µm RNFs PHB/HA diameter = 2-2.2µm	RNFs PHB -> TS=1.67 MPa; EM=275.25 MPa RNFs PHB/HA-> TS=3.99 MPa; EM=267.15 MPa Stacked PHB layers -> TS=5.88 MPa; EM=132.78 MPa Stacked PHB/HA layers -> TS=12.43 MPa; EM=798.25 MPa	Chen et al. 2017 [116]
PCL/Starch	Combined rapid prototype (RP) and electrospinning	RNFs PCL diameter = 400nm RP fibers diameter = 300µm RP porosity = 79.4% RNFs and RP porosity = 68.3%	ND	Canha-Gouveia et al. 2015 [112]
PCL/Gelatin	Combined 3D printed and electrospinning	RNFs PCL/Gelatin diameter = 764.55nm 3D printed diameter = 0.39mm Combined scaffold porosity = 79.32%	RNFs PCL/Gelatin -> Compressive modulus=18.55MPa Combined scaffold -> Compressive modulus=30.50MPa	Yu et al. 2016 [71]

Table 1. Material characteristics of electrospinning based strategies for bone tissue engineering. (RNFs = Random Nano Fibers; ANFs = Aligned Nano Fibers.

Cells	Culture Media	Mechanical Properties of Biohybrid Constructs	Major Outcomes	Ref
MC3T3-E1	α-MEM, 10% FBS	ND	Aligned fibers resulted in better cell attachment, proliferation, alignment ad ALP activity when compared to random fibers.	Guo et al. 2015 [70]
BMSC from NZ Rabbit	DMEM; 15% FBS	ND	Better cell attachment and deeper infiltration was found on PCL/gelatin scaffolds, compared to PCL alone.	Zhang et al. 2005 [106]
BMSC from Pig	DMEM; 10% FBS; 10nM dexamethasone; 50µM ascorbic acid; 10mM β-glycerophosphate.	ND	Tubular PCL/Col/BMSCs cell constructs presented positive levels of collagen deposition and osteogenic differentiation with calcium deposition and osteocalcin production.	Ekaputra et al. 2009 [104]
ADSCs from Human	α-MEM; 10% FBS; 0.1µM dexamethasone; 50µM ascorbic acid; 10mM β-glycerophosphate.	ND	Collagen covering PCL fibers enhanced early cell spreading and increased calcium deposition	Haslauer et al. 2011 [105]
ADSCs from Human	DMEM/F12; 10% FBS; 100nM dexamethasone; 10mM β-glycerophosphate; 50µM ascorbic acid.	ND	Cell proliferation didn't differs among random, aligned or honeycomb scaffolds, cells cultured over honeycomb-like scaffolds up-regulated osteogenic differentiation, mineralization and ALP activity.	Nedjari et al. 2017 [117]
BMSCs from Human	IMDM; 10% FBS; 0.1mM dexamethasone; 10mM β-glycerophosphate; 0.2mM ascorbic acid.	ND	Collagen nanofibers supported osteogenic differentiation with positive levels of transcripts as osteocalcin, osteonectin and osteopontin, and ALP activity.	Shih et al. 2006 [103]
MC3T3-E1	α-MEM; 10% FBS; 10nM; dexamethasone; 50µg/ml ascorbic acid	ND	Cell attachment was better on large fibers Cell proliferation was better on aligned fibers and large random fibers compared to smallest random fibers. Large aligned fibers showed better ALP activity compared to small random fibers.	Terranova et al. 2016 [69]

C3H10T1/2	DMEM; 10% FBS	ND	C3H10T1/2 cells cultured on nanofibrous scaffolds presented up-regulated bone transcripts while fibers from micrometric range up-regulated tendon transcripts	Baudequin et al. 2017 [72]
hFOB	DMEM/F12; 10% FBS	ND	Incorporation of HAP on chitosan fibrous scaffolds improves cell proliferation and mineral deposition.	Zhang et al. 2008 [75]
hFOB	DMEM/F12; 10% FBS	ND	Cells cultured on PLLA/Coll/HAP nanofibrous scaffolds showed higher cell proliferation, increased ALP activity and mineralization.	Prabhakaran et al. 2009 [74]
MC3T3-E1	α-MEM; 10% FBS	ND	PCL/PLA/HAP nanofibrous scaffolds provide a better cell spreading and proliferation.	Fang et al. 2010 [68]
MSCs from Human	DMEM; 10% FBS; 10nM dexamethasone; 10mM β-glycerophosphate; 50µg/ml ascorbic acid.	ND	PLA/DPB scaffolds support the growth of MSCs without compromising their osteogenic differentiation. Mineralization was higher compared to PLA scaffolds.	Ko et al. 2008 [113]
MSCs from Human	DMEM; 10% FBS; 0.1µM dexamethasone; 10mM β-glycerophosphate; 50µM ascorbic acid	ND	While either SF/CS/HAP and SF/CS/HAP/BMP-2 resulted in good biocompatibility, cell proliferation, ALP-activity and mineralization; the combination of SF/CS/HAP/BMP-2 resulted in up-regulated bone differentiation.	Shalumon et al. 2015 [109]
BMSCs from Human	DMEM; 10% FBS; 10nM dexamethasone; 50µg/ml ascorbic acid; 7mM β-glycerophosphate.	ND	The combination of HAP and BMP-2 in silk scaffolds induce up-regultated bone transcripts and highest amount of calcium deposition.	Vepari et al. 2006 [108]
MC3T3-E1	α-MEM; 10% FBS	ND	Medium pores size scaffolds (100-200 µm), improves cell proliferation, cell viability and ALP activity.	Park et al. 2010 [67]
hFOB	DMEM/F12; 10% FBS	ND	Silk scaffolds provides a good environment for cell survival and colonization.	Yang et al. 2015 [73]

hMSCs derived from ESCs	DMEM; 10% FBS; 10nM dexamethasone; 50µg/ml ascorbic acid; 10mM β-glycerophosphate	ND	3D scaffolds provide better environment for cell proliferation and ECM mineralization.	Cai et al. 2012 [118]
BMSCs from Rabbit	DMEM; 10% FBS; 100nM dexamethasone, 10mM β-glycerophosphate and 0.2mM ascorbic acid.	ND	Composite scaffolds of NHB/HAP showed better cell proliferation, up-regulated bone transcripts and improved ALP activity than PHB scaffolds.	Chen et al. 2017 [116]
WJSCs from Human	α-MEM; 10% FBS; 10nM dexamethasone, 10mM β-glycerophosphate and 50µg/ml ascorbic acid.	ND	Combining PCL nanofibers meshes with TCP improves cells attachement, proliferation and differentiation towards bone lineage. This effect is accentuated in the presence of an osteogenic medium. In addition, dynamic culture improves cell differentiation and ALP activity even without osteogenic supplementation medium.	Canha-Gouveia et al. 2015 [112]
MC3T3-E1	α-MEM; 10% FBS	ND	The combination of 3D printing and electrospinning improves cells migration and proliferation.	Yu et al. 2016 [71]

Table 2. In vitro performances of biohybrid scaffolds in bone tissue engineering

Animal Model and Tissue Site Implantation	Mechanical Stimulation before Implantation	Mechanical Properties of the Biohybrid Construct Following Implantation	Biological Outcomes	Ref
Murine (Rat) full-thickness bony calvaria defect	None	ND	After 12 weeks, the PLA/DBP nanofibrous scaffolds implanted presented almost complete bone healing with more bone density than PLA scaffolds alone.	Ko et al. 2008 [113]
Ectopic transplation in a mice mode	None	ND	SF/CS/HAP/BMP-2 induces ectopic bone formation even in absence of cells. Pre-cultured scaffolds resulted in higher ECM deposition and OCN expression.	Shalumon et al. 2015 [13]
Murine (Rat) full-thickness bony calvaria defect	None	ND	After 7 weeks, medium pores sizes scaffolds presented more bone formation and good scaffold resorption after.	Park et al. 2010 [67]
Murine (Rat) full-thickness bony calvaria defect	None	ND	New bone formation was more prominent than control after 8 weeks. The addition of BMP-2 augmented the amount of new bone formation.	Yang et al. 2015 [73]
Rabbit bone tibia deffect	None	ND	After 6 weeks, tibia bone defect filled with 3D scaffold presented cortical-bone like tissue and vascularization.	Cai et al. 2012 [118]
Ectopic transplation in a mice mode	None	ND	After 2 months into an ectopic bone formation mice model, PHB/HAP composite scaffolds presented more vascularization and bone-like tissue formation.	Chen et al. 2017 [116]

Table 3. In vivo performances of biohybrid constructs in bone tissue engineering.

Combining natural and synthetic polymers to produce hybrid scaffolds

Table 1 highlights the different potential association of natural and synthetic polymer to produce electrospun fibers. In general, it should be noticed that comparisons are very difficult to make since the diameter of the fibers (from 10 nm to 4500 nm) and their configuration (random / aligned) varied from one study to the other.

Zhang et al. (2004) were the first to produce a combined gelatin and PCL electrospun scaffold with fibers diameters from a range of 10 to 1000nm, to combine the advantages of natural and synthetic polymers. This blend scaffold presented a lower tensile strength of 1.29 MPa than those of PCL and gelatin alone, 2.70 MPa and 2.50 MPa respectively, although its Young Modulus was higher than PCL alone (30.8MPa vs. 4.98MPa)[106]. Results are uneasy to interpret since PCL concentration was different in the blend. Ekaputra et al. (2009) proposed composite scaffolds of PCL and collagen with a fiber diameter of 513 ± 83 nm. When electrospun together, the Young Modulus was lower compared to PCL alone (4.59 ± 1.46MPa vs. 12.35 ± 3.31MPa)[104]. Prabhakaran et al. (2009) combined PCL with collagen and HA nanoparticles. The addition of collagen resulted in smaller fibers' diameter (310 ± 125nm) compared to the scaffold without collagen (845 ± 140nm) and to decreased tensile strength (2.05 ± 0.10MPa vs. 3.10 ± 0.15MPa).[74] While these authors added either collagen or gelatin together with the synthetic polymer, Haslauer et al. (2011) proposed co-axial electrospinning where the inner part was PCL and the outer layer collagen. Co-axial scaffolds resulted in increased fiber diameter (442 ± 45nm vs. 280 ± 51nm)[105]. Unfortunately, the mechanical properties of such scaffolds were not assessed. In our group, Baudequin et al. (2017) prepared coaxial electrospun fibers combining PCL and PLLA polymers. When PCL was the outer layer and PLLA was the inner one, fibers with a diameter of 1928nm and a Young modulus of 38MPa were obtained. When PLLA was the outer layer, fibers presented a larger diameter (2461nm) but Young Modulus became lower, with 30 MPa.[72]

Due to the wide range of mechanical properties and methods of assessment, it seems thus impossible here to conclude on the benefit of a mixture regarding pure polymer, as far as the mechanical properties are concerned.

Combining polymers with nanoparticles to mimic the mineralized environment

Biomimetic approaches have been developed in order to mimic the native mineralized matrix of bones. Li et al. (2006) produced silk scaffolds loaded with hydroxyapatite nanoparticles. The addition of nanoparticles resulted in fibers with reduced diameter (510 ± 60nm) compared to nude silk scaffolds (590 ± 60nm).[108] Zhang et al. (2008) obtained similar results on chitosan scaffolds for which the addition of hydroxyapatite reduced the fiber diameter from 214 ± 25nm to 138 ± 15nm.[75] Fang et al. (2010) produced combined scaffolds of PCL and PLA with added nanoparticles of HA. From a ratio of 0.1 to 1, increased amounts of nanoparticles resulted in smaller electrospun fibers. For the maximal concentration of HA fibres presented a diameter of 332 ± 11.3nm, significant smallest compared to 776 ± 15.6nm for PCL and PLA scaffolds without nanoparticles.[68]

In other work, Ko et al. (2008) analyzed the impact of demineralized bone powders (DPBs) to mimic the composition of the bone matrix. Addition of DPBs in a solution of PLLA resulted in reduced fibers when compared to PLLA scaffold alone.[113]

The mechanical response of scaffolds might be affected by the addition of nanoparticles. Phrabhakaran et al. (2009) showed that when HA nanoparticles were added to PLLA scaffolds, the tensile strength was reduced from 4.69 ± 0.19MPa to 3.10 ± 0.15MPa.[74] However, recently Chen et al. (2017) found opposite effects when PHB scaffolds were loaded with HA nanoparticles. PHB fibres diameter tends to augment with the addition of HA (2-2.2µm vs. 0.7-1.2 µm). When nanoparticles were added tensile strength passes from 1.67 ± 0.65MPa for PHB to 3.99 ± 0.57MPa for PHB/HA while the elastic modulus remained constant.[116]

Again, as far as materials and mechanical properties are concerned, it is very difficult to draw any conclusion since the changes in the electrospinning process, adding nanoparticles, affected other characteristics of the fibers such as their diameter.

Combining polymers with Growth Factors

Growth factors can be included during the electrospinning process in order to endow the fibers with a biological activity. Li et al. (2006) directly added BMP-2 into the polymeric solution of silk. The addition of BMP-2 did not affect the size of the different electrospun fibers.[108] Instead of combining the growth factors with the polymer solution entrapping the

factors within the fibers, Shalumon et al. (2015) encapsulated BMP-2 within the fiber by coaxial electrospinning where the outer layer was made of a combination of silk fibroin, chitosan and hydroxyapatite nanoparticles, and the inner layer containing BMP-2 in a phosphate-buffered saline solution. Two sizes of the outer layer were investigated, a thick one (167 ± 41nm) and a thin one (101 ± 9nm), keeping the whole fiber diameter constant (about 540 nm). In both types of fibers, 80 % of BMP-2 was released during the first 2 weeks but more BMP-2 was released at each time point for the thinner layer, which seems logical since the diffusive length was decreased.[109]

Effect of fibers alignment

Different studies have been carried on the effect of fiber diameter and structure, which have an influence on scaffolds mechanical properties and cell activity. Baudequin et al. (2017) investigated the effect of fiber diameter and alignment on PCL, PLLA and blended scaffolds of both polymers. It appeared that the larger the fibers' diameter, the higher the Young Modulus. When comparing aligned vs random PCL scaffolds with the same concentration in PCL, fibers with similar diameters (1032nm vs 1159nm) presented higher Young Modulus when aligned (63MPa vs 36MPa).[72] Similar results were obtained by Guo et al. (2015) comparing aligned vs random PCL/gelatin scaffolds : aligned fibers presented higher tensile strength (13.45 ± 3.49MPa vs. 2.05 ± 0.31MPa), and higher tensile modulus (30.45 ± 9.15MPa vs. 26.03 ± 5.73MPa) compared to random scaffolds.[70]

From these few studies, it seems that fiber alignment provided improved mechanical properties to the scaffold, probably because the fibers already aligned decreased the overall material elasticity, while random fibers could be submitted to a larger extension during equivalent stretching strain.

Effect of complex 3D structures

Although the micro- to nano-fibers present advantages such as similarity with the extracellular matrix, electrospinning is not devoid of limitations. Its major drawbacks remain in the reduced pores size of the whole layer, which reduces cellular migration and infiltration through the scaffold[119] and in the mechanical properties far under those of the native bone.

To overcome these limitations, different approaches have been deployed in order to create more complex structures attempting to mimic the 3D structure of bone and its mechanical stability. These methods focus on changes on the design of the electrospinning process such as electrospinning changing the collector nature (electrospinning on a solvent bath)[67,73] or combining 3D scaffolds with electrospinning[112] or post-treatment of scaffolds (overlaying electrospun scaffolds[116], folding scaffolds to make yarns[118] or filling electrospinning fibers in a more complex structure[71]).

Park et al. (2010) electrospun silk fibroin into a methanol coagulation bath to get a fibrous silk network with fibers diameter ranging from 200 to 500nm. The final scaffold thickness was 1.5mm, much higher than classical ones (about 200 – 300 µm). The fibrous scaffold reached a total porosity of 70%. In the same experiment, authors combined the coagulation bath with salt leaching using sodium chloride particles of different sizes producing three groups of porous scaffolds. They presented a real porosity about 90-93% with pores sizes distribution: <100, 100-200 and >300µm, respectively[67]. In similar experiments, Yang et al. (2015) produced porous electrospun silk scaffolds with fibers of 1.49 ± 0.30µm diameter. A solution containing silk/HA was then added into each scaffold and freeze-dried. Resulting scaffolds presented pores sizes ranging between 42.30 ± 9.73µm and 301.10 ± 69.34µm depending on silk concentration. Adding HA nanoparticles resulted in an increase of the compressive modulus up to 30.8 ± 0.89 KPa, compared to silk scaffold with the same polymer concentration (14.4 ± 1.09 KPa) [73].

Cai et al. (2012) proposed a three-dimensional macroporous scaffold by folding several times aligned electrospun scaffolds of PCL and PLLA. Once folded, yarns of electrospinning were made by cryostat microtome resulting in aligned yarns with a width of 100-200µm. Yarns were honeycombed at 65ºC (melting temperature of PCL) creating a 3D scaffold were melted PCL combined tightly with PLLA fibers. Final scaffolds presented a porosity of 77.61 ± 6.35% with pore sizes ranging from 60-130µm and an ultimate tensile strength of 71.68 ± 5.61MPa[118]. Chen et al. (2017) proposed laminated electrospun scaffolds of PHB fibers loaded with HA. Each scaffolds was formed by the superimposition of 8 layers. Compared to single layer, multilayered scaffolds presented higher ultimate tensile strength (12.43 ± 1.21MPa vs. 3.99 ± 0.57MPa) and elastic modulus (798.25 ± 120.07MPa vs. 267.15 ± 64.18MPa)[116]. Canha-Gouveia et al. (2015) combined electrospinning PCL with rapid prototyping (RP) of blended starch and polycaprolactone to produce combined microfibers

from RP (average diameter of 300µm) and nanofibers from electrospinning (diameter range from 400nm to 1.4µm) in the same structure. The objective was to associate mechanical stability from RP process and cell interactions with electrospun fibers. Electrospun fibers meshes were made apart and superimposed between 2 layers of RP, resulting in a final scaffold made by 6 layers of RP and 5 layers of electrospun meshes. While the combination of both techniques resulted in a final scaffold with reduced porosity (68.3%) compared to RP scaffolds (79,4%), a fully interconnected porous structure was successfully manufactured.[112]

Instead of overlapping 3D and electrospinning, Yu et al. (2016) produced 3D printed PCL scaffolds and electrospun PCL/collagen meshes separately. Electrospinning meshes were then dispersed into short nanofibers with a high-speed dispersion homogenizer. Once dispersed, previous 3D printed scaffolds were filled with the nanofibers and the composite material were lyophilized and cross-linked with glutaraldehyde. The resulted scaffold was made of combined nano electrospun fibers with an average diameter of 764.55 ± 283.29nm and microfibers from 3D printing with a diameter of 0.39 ± 0.02mm, a porosity of 79.32 ± 8.32% and a compressive modulus of 18.55 ± 0.56MPa.[71]

As last example, Nedjari et al. (2017) proposed honeycomb scaffolds made of PLCL and fibrinogen by electrospinning over a microstructured honeycomb collector. Scaffolds were composed of thick (462 ± 117 nm) and thin fibers (195 ± 50 nm). Interestingly, honeycomb scaffolds presented a structure with cavities with a difference of 10µm between the top and the bottom of the honeycomb structure. However, the impact on the mechanical behavior of the scaffold was not analyzed.[117]

1.4.2. Biological Outcomes

The biological outcomes performed by the different scaffolds listed in the previous part are summarized in Table 2 and analyzed hereafter. From the table, the first view highlights the diversity of the cultured cells, outlining again the lack of standardized procedures to evaluate biocompatibility and cell-materials interactions. In addition, one should pay attention on the presence, or not, of differentiation factors in the culture medium, such as … In the positive case, it is then difficult cell differentiation to the scaffolds' characteristics.

Hypothesis regarding hybrid natural/synthetic scaffold

Zhang et al. (2004) cultured New Zealand White rabbit BMSCs PCL/gelatin scaffolds. After 1 week of culture, cells presented better attachment, proliferation and infiltration through the scaffold, indicating a 3D cell growth compared to pure PCL scaffolds where cells remained at the surface[106]. In a longer study (28 days), Ekaputra et al. (2009) confirmed that PCL/gelatin scaffolds presented a higher ability for cell proliferation and osteoinduction, acknowledged by an over synthesis of protein classically present in bone cells, i.e. COL1, OCN and OPN. Of note, mineralization only occurred on combined PCL/gelatin scaffolds[104]. Prabhakaran et al. (2009) compared the effect of adding collagen to PLLA/HA scaffolds on the activity of hFOB. After 20 days of culture, cells proliferation, ALP activity and mineralization were increased on PLLA/collagen/HA scaffolds compared to PLLA/HA scaffolds[74]. In Haslauer et al. study (2011) hADSCs cultured over coaxial fibers (PCL inside, collagen outside) presented high cell spreading and increased calcium deposition after 14 days of culture. [105] It thus confirms that the addition of natural polymers could increase the scaffold biocompatibility.

Effect of scaffold's functionalization

Li et al. (2006) investigated the effect of loading silk scaffolds with HA nanoparticles and BMP-2 on hBMSCs' response. After 14 days, cells cultivated in the presence of BMP-2 and/or HA showed better differentiation (BSP). When cell culture was prolonged for 31 days, combined scaffolds presented higher mineralization compared to scaffolds without HA.[108] For Zhang et al. (2008), when HA was loaded into chitosan scaffolds, hFOBs presented higher proliferation and mineralization after 10 and 15 days of culture.[75] Fang et al. (2010) investigated the effect of adding HA on PCL/PLLA scaffolds on MC3T3-E1 activity. Nanofibrous scaffolds with HA provide better cell spreading, proliferation and mineralization.[68] Chen et al. (2017) analyzed the impact of HA on laminated electrospun PHB scaffolds. After 7 days of culture, rMSCs presented higher early proliferation. After 14 days cells cultured over PHB/HA presented higher bone activity (ALP activity) and differentiation (OCN, ALP) than its homologous without HA. After 2 months into an ectopic bone formation mice model, PHB/HAP composite scaffolds showed more vascularization and bone-like tissue formation[116]. When adding demineralized bone powder (DBP) into PLA, Ko et al. (2008) demonstrated that after 21 days of culture, both PLA and PLA/DPB scaffolds supported

hMSCs proliferation, differentiation (OCN, ALP, Cbfa1) and mineralization. After 12 weeks of implantation in a rat critical-sized skull defect, PLA/DPB scaffolds presented almost complete bone healing and higher bone density compared to PLA scaffolds[113].

There is thus a consensus to demonstrate the potential of using HA nano or microparticles, or even other components of the mineralized bone, to promote cell proliferation and osteogenic differentiation.

Effect of fiber alignment

Baudequin et al. (2017) cultured C3H10T1/2 on different PCL or PLLA scaffolds randomly organized or aligned. Interestingly, after 96 hours of culture, although morphology of cells was different, both aligned and random scaffolds let to the expression of bone-related markers (BGLAP). However, when C3H10T1/2 were cultured on scaffolds with larger fibers (≥2µm), tendon-related markers were found[72]. In another study, Guo et al. (2015) analyzed the impact of PCL/gelatin fibers alignment on MC3T3-E1. When cultured on aligned scaffolds, cell attachment, proliferation and ALP activity were higher compared to random scaffolds[70]. These results were more or less unexpected, since other studies demonstrated that fiber alignment could favor cell differentiation towards tendon lineage.[70]

Effect of complex 3D structures

Park et al. (2010) analyzed the effect of their 3D silk scaffolds porous structure on cell behavior. When seeded with MC3T3-E1, scaffolds with pores sizes from 100-200µm provided the best environment for cell adhesion, viability, proliferation and ALP activity. After 7 weeks of implantation in a critical bone defect in rat calvaria, porous scaffolds (100-200µm) presented a good resorption and higher bone formation compared to non-porous ones.[67] Cai et al. (2011) compared the 3D scaffold based on PLLA/PCL yarn assembly with its 2D homologous. hMSCs presented higher proliferation and mineralization on 3D structures. After 6 weeks of implantation in a rabbit tibia bone defect, 3D scaffold presented cortical-bone like tissue and vascularization.[118] In another study, Canha-Gouveia (2015) analyzed the impact of combined electrospun PCL with 3D PCL/starch RP structure on hWJSCs. Combined scaffold provided better seeding performance and viability. In addition, ALP activity, cell differentiation towards bone lineage (Runx2, SP7, IBSP, BGLAP and SPP1) and mineralization

were up-regulated compared to 3D scaffolds without electrospun fibers.[112] A similar study was conducted by Yu et al. (2016) where the authors also follow the effect of combined electrospun PCL/gelatin fibers in a 3D-printed PCL scaffold. After 14 days of culture, MC3T3-E1 cells presented higher proliferation and infiltration compared to 3D printed scaffold alone.[71] Finally, Nedjari et al. (2017) analyzed the impact of honeycomb morphologies on cell differentiation. When compared to random or aligned scaffolds, ADMSCs presented higher ALP activity, mineralization and up-regulated osteogenic differentiation (RunX2, ALP).[117]

2. Review: Biomaterials in Tendon and Skeletal Muscle Tissue Engineering: Current Trends and Challenges

materials

MDPI

Review

Biomaterials in Tendon and Skeletal Muscle Tissue Engineering: Current Trends and Challenges

Megane Beldjilali-Labro [1,†], Alejandro Garcia Garcia [1,†], Firas Farhat [1,†], Fahmi Bedoui [2], Jean-François Grosset [1], Murielle Dufresne [1] and Cécile Legallais [1,*]

1 CNRS, UMR 7338, Biomécanique-Bioingénierie, Sorbonne Universités, Université de Technologie de Compiègne, 60200 Compiègne, France; megane.beldjilali-labro@utc.fr (M.B.-L.); alejandro.garcia-garcia@utc.fr (A.G.G.); firas.farhat@utc.fr (F.F.); jean-francois.grosset@utc.fr (J.-F.G.); murielle.dufresne@utc.fr (M.D.)

2 CNRS FRE 2012, Laboratoire Roberval, Sorbonne Universités, Université de Technologie de Compiègne, 60200 Compiègne, France; fahmi.bedoui@utc.fr

* Correspondence: cecile.legallais@utc.fr

† These authors contributed equally to this work.

Received: 31 May 2018; Accepted: 25 June 2018; Published: 29 June 2018

Abstract: Tissue engineering is a promising approach to repair tendon and muscle when natural healing fails. Biohybrid constructs obtained after cells' seeding and culture in dedicated scaffolds have indeed been considered as relevant tools for mimicking native tissue, leading to a better integration in vivo. They can also be employed to perform advanced in vitro studies to model the cell differentiation or regeneration processes. In this review, we report and analyze the different solutions proposed in literature, for the reconstruction of tendon, muscle, and the myotendinous junction. They classically rely on the three pillars of tissue engineering, i.e., cells, biomaterials and environment (both chemical and physical stimuli). We have chosen to present biomimetic or bioinspired strategies based on understanding of the native tissue structure/functions/properties of the tissue of interest. For each tissue, we sorted the relevant publications according to an increasing degree of complexity in the materials' shape or manufacture. We present their biological and mechanical performances, observed in vitro and in vivo when available. Although there is no consensus for a gold standard technique to reconstruct these musculo-skeletal tissues, the reader can find different ways to progress in the field and to understand the recent history in the choice of materials, from collagen to polymer-based matrices.

Keywords: collagen; sponge; electrospinning; stem cells; elastic modulus; stretching

1. Introduction

The most advanced studies on tissue engineering (TE) concerning the musculo-skeletal system focus on bone and cartilage tissue engineering [1–3]. TE aims at better understanding and mimicking the intrinsic properties of each tissue and its interface, such as the complete regeneration of the enthesis [4]. Applications on tendon and muscle tissues are less widespread and still emergent, with various approaches that are still far from clinical applications, but very useful for progress in understanding these specific tissues. The numerous parameters that influence the biological or mechanical outcomes make it uneasy to derive any experimental rationale. This lack of rationale has hampered the emergence of a gold standard experimental protocol for the reconstruction of such biohybrid tissues.

Therefore, to unite the efforts that are made by the various teams, the present review focuses on tissue engineered reconstructions of tendon and skeletal muscle tissues, as well as the

myotendinous junction (MTJ), which is a key element for further implantation. As with other forms of tissue engineering, muscle or tendon tissue engineering relies on three pillars: cells, biomaterials, and environment, ensured by chemical or physical factors (Figure 1). Bioreactors are often required to perform three-dimensional (3D) cultures and mimic the cells' in vivo niche and environment, while ensuring the better control of cell culture conditions and possibly inducing cell responses to mechanical stimuli.

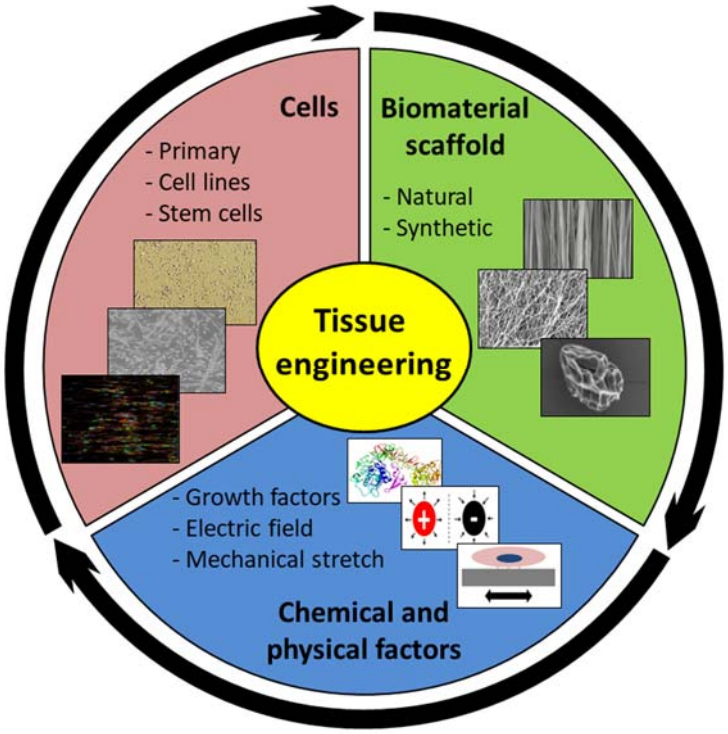

Figure 1. The three pillars of tendon/muscle tissue engineering: cells are cultured on a scaffold where they can attach, proliferate, or differentiate, giving them a phenotype relevant for the renewal of tissue functions. The mechanical and biochemical environments are of prime importance for triggering specific responses.

For this review, we have chosen to present biomimetic or bioinspired strategies that are based on an understanding of the native tissue structure/functions/properties of the tissue of interest. We postulate that in-depth understanding of the native functions of muscle and tendon, as well as their alterations, should guide the research program leading to their reconstruction. These two tissues are involved in the transmission of efforts to bone tissue, ensuring body motion. Interestingly, they have the same embryogenic origin and present similarities in their multi-scale organization, but also have differences at various levels (Figure 2), which will lead to completely different approaches in terms of tissue reconstruction. Therefore, to highlight the efforts that are made to understand native structures, the first part will present the multi-scale organization of the tissue of interest (tendon or muscle), followed by a second part showing the alterations, leading to the need for reconstruction. Then, we will provide information about the various types of materials, cells, and environment (the three pillars) that have been assessed for bioconstruction, and propose a classification. Finally, we will show how the shape of the materials themselves, which is made possible by means of different production techniques, can guide not only the structure and mechanical properties of the scaffold, but also the biological responses, and we will analyze to what extent these integrated approaches can lead to a functional reconstructed tissue.

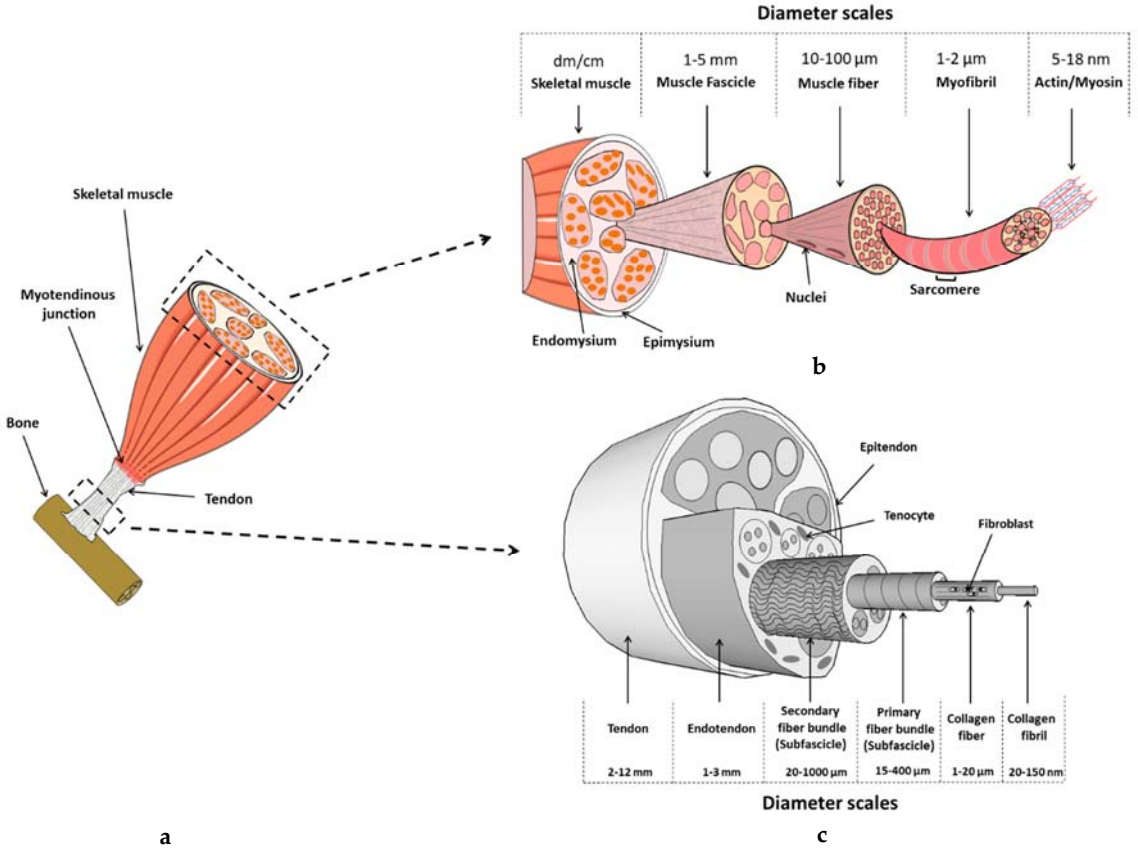

Figure 2. Overview of the bone-tendon-muscle continuum in the human musculo-skeletal system (**a**). Multi-scale description of a skeletal muscle (**b**) and a tendon (**c**).

2. Tendon

2.1. Tendon Composition and Structure

Tendons are specialized fibrous tissues that join skeletal muscle to bone and make body motion possible through the forces that are generated by the skeletal muscles to bone tissues [5]. They act as highly adapted elastic springs that stretch and store energy, which returns to the system through elastic recoil, thus improving locomotor efficiency. This function is closely related to the tendon's composition and structure. Tendon is a dense, connective tissue with limited cell content, vascularization, and innervation [6]. The main component of tendon is water (60% to 80% in weight) [7].

Collagen represents the major component (60% to 85% dry weight) of the extracellular matrix (ECM), type I collagen being the most abundant and responsible for the fibrous structure [8]. Type I collagen molecules aggregate to form collagen fibrils, the basic nanostructural tendon unit. Bundles of fibrils form fibers, fibers group into fiber bundles or fascicles; and, fascicles bundle together within connective tissue sheaths (endotenon) to form larger bundles that are surrounded by another connective tissue sheath (epitenon) [9] (see Figure 2). Collagen fibers display a wave pattern, which is also known as a crimp [10]. Non-fibrous molecules are present on each level, the main ones being proteoglycans (PGs) [11–15], such as decorin [11,16] and aggrecan [17]. ECM also contains glycoproteins, including tenascin-C and fibronectin [18,19].

Tendon cells are key players in tendon growth, maintenance, adaptation to changes in homeostasis, and remodeling in the case of minor or more severe disturbances to tissue. The cells are responsible for the synthesis and turnover of tendon ECM components and its related structure. Mature tendon contains predominantly tenocytes/tenoblasts [20], which account for around 90–95% of the cell population. Tenocytes are terminally differentiated cells typically anchored to the collagen and located

throughout tendon tissue. Tenoblasts are immature tendon cells that give rise to tenocytes. Recently, a new cell type has been characterized in tendon tissue: resident tendon stem/progenitor cells (TSPC). TSPCs represent 1–4% of tendon resident cells, and they exhibit the same characteristics as adult mesenchymal stem cells (MSC) [21].

Regarding the composition and structure of the ECM, tendon appears to be an anisotropic and viscoelastic material that is capable of resisting high tensile forces [22]. At a fixed strain rate, the stress-strain curve of tendons has three distinct regions (Figure 3). The tendons stress strain response is strain rate dependent leading to higher stiffness and lower strain break while keeping the same chronological damage process when stretched at high strain rate [23]. The toe region corresponds to low strains (<2%), where the crimp structure is straightened. Once the collagen fibrils have been straightened, the load-deformation relationship becomes relatively linear, representing the physical stretching of the collagen fibrils (~2–4%). Beyond this region, additional loading causes micro failures to individual fibrils up to a failure of the whole tendon over ~8% of strain [24]. The in vivo evaluation of human tendon mechanical properties depends on the investigation method (ultrasound, magnetic resonance imaging) and stretching protocols used. For human tibialis anterior and gastrocnemius tendons, Maganaris et al. (2002) [25] calculated an elastic modulus (EM) around 1.2 GPa, while an EM value of 600 MPa was reported for the patella tendon [26].

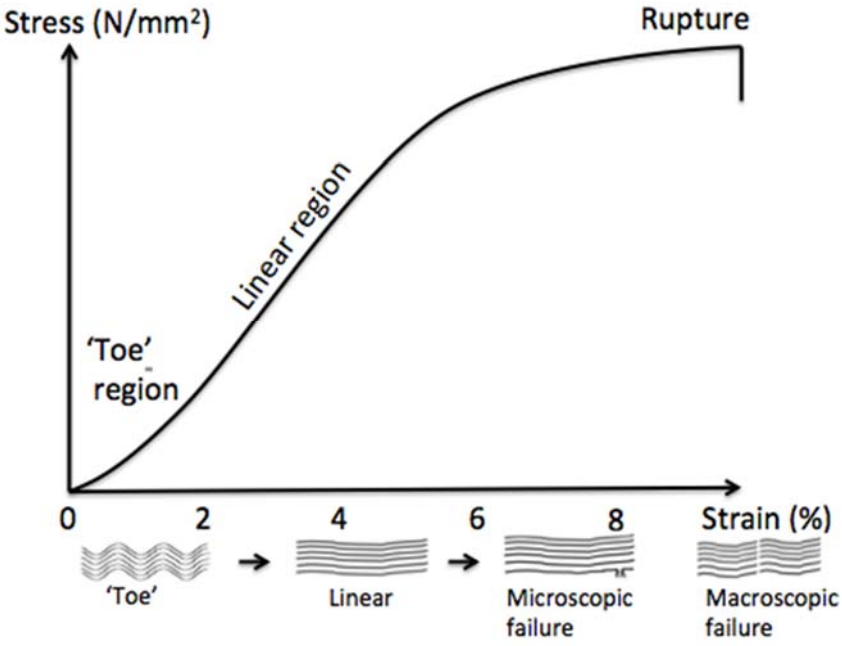

Figure 3. Typical tendon response to stretching at fixed strain rate: stress-strain curve illustrating the various deformations of the collagen fibrils.

2.2. Tendon Injuries and Healing

As a result of physical activity (sport or professional activities), trauma, or aging, tendinopathies, which is a clinical syndrome characterized by the combination of pain, swelling, and impaired performance, are an increasing health problem that affects an estimated number of 100 million people worldwide annually [16]. Owing to its hypovascularity and hypocellularity, tendon has a weak intrinsic healing ability and it often responds poorly to pharmaceutical treatments [20]. Thus, total repair requires prolonged rehabilitation in most cases. Tendon healing follows three well-described steps: inflammatory, proliferative, and remodeling phases, the latter characterized by the alignment of collagen fibers parallel to the muscle force direction, which determines the recovery of the tendon tissue's biomechanical properties [27]. The biomechanical cues for repaired tissue are mostly inferior

to those of native tissue, causing an increasing rate of tendon re-injuries. To overcome the inability of the repaired tissue to regenerate the functions of native tendon, and to improve healing rates, surgical approaches, such as sutures or transplantation of autografts, allografts, or xenografts have been described and clinically performed. Autografts remain the gold standard for surgical procedures for tendon repair. Alternatives, such as: (1) allografts such as GraftJacket™ (Wright Medical Technology, Arlington, TN, USA) or AlloPatch HD® (MTF Sports Medicine, Edison, NJ, USA); (2) xenografts, such as TissueMend® (Stryker Howmedica Osteonics, Kalamazoo, MI, USA) or CuffPatch® (Arthrotek, Warsaw, IN, USA); and, (3) artificial prostheses, such as STR Graft™ (Biorez Inc., New Haven, CT, USA) or SeriCuff™ (Serica Technologies, Medford, MA, USA) have been developed and commercialized [28]. However, these approaches usually result in fibrotic tissue with low mechanical properties when compared to native tendon, and so far none of these techniques has provided complete healing for tendon disorders [29].

2.3. Tendon Tissue Engineering

Tissue engineering is a promising alternative to the natural healing process for tendon repair, especially in the reconstruction of large damaged tissues. The inability of native tendon to neosynthesize ECM is expected to be overcome by the design and production of a scaffold that hosts cells differentiated into a tendon lineage.

After reviewing the literature on the approaches that were adopted in this field in the last fifteen years, we present the papers selected in three tables (Figure 4).

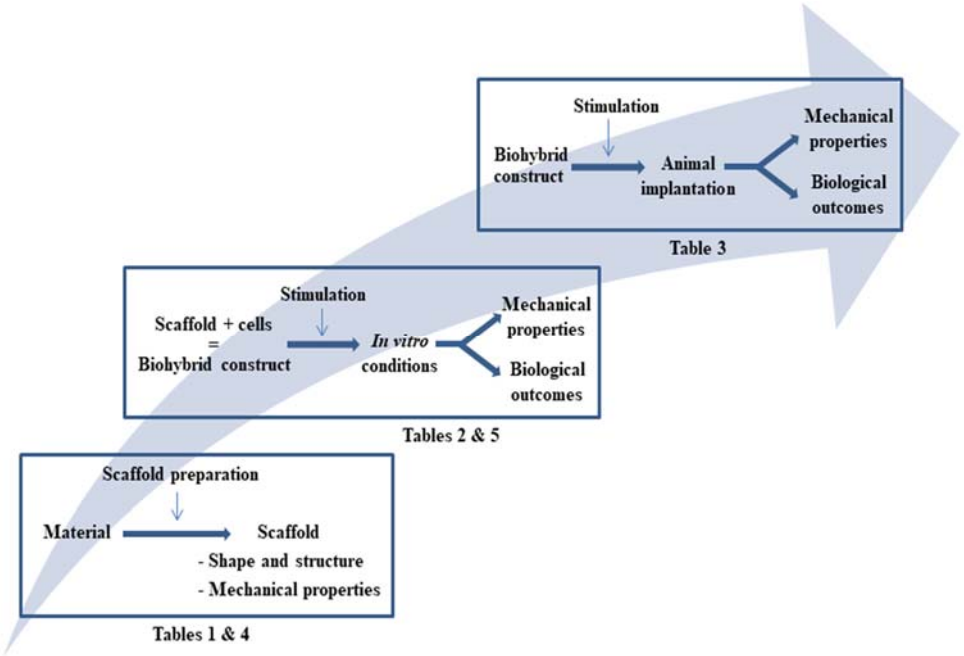

Figure 4. Rationale for the choice of studies and contents reported in the tables, for tendon, and muscle tissue engineering, respectively.

Table 1 is dedicated to a summary of details of the major materials and methods, including, if present, the mechanical characteristics of the scaffold. Table 2 focuses on in vitro studies performed with the same scaffolds, identifying, if present, the effect of physical stimulation. Finally, Table 3 provides the in vivo outcomes, i.e., the behavior of the same TE constructs after their implantation into animal models, when available. After an analysis of the selected articles over the period of interest, we decided to only select those in which an in vitro/in vivo application was presented, and which were detailed enough to bring up trends for current progress in research in the field. The list was

ordered according to the shape of the scaffolds. In the following chapters, we will first briefly focus on the three pillars of tendon TE (in Section 2.3), to outline the major trends and guidelines, and are provided in Section 2.4, the mechanical and biological outcomes arising from the tendon biohybrid reconstructed tissues. Current research mainly focuses on obtaining mechanical properties that are similar to those of native tendon, and on efficient cell differentiation into tenocyte lineage, capable of producing a new ECM.

2.3.1. Cells

Several cell sources can be used for tendon tissue engineering (Table 2). Adult mesenchymal stem cells (MSCs) are a promising cell source as they present the potential for self-renewal, clonogenicity, and multi-lineage differentiation, including tenogenicity. They regulate the inflammation response through the secretion of paracrine factors, and exhibit an immunomodulatory effect, which avoids immunosuppressive treatments after allogenic transplantation. MSCs can be extracted from a variety of tissues, including bone marrow (BMSC), adipose tissue (ASC), or directly from tendon [21]. BMSCs are the most widely-used stem cells in tendon engineering [30–39]. Related to BMSCs, ASCs are present in great quantities in adipose tissues and are harvested by less invasive techniques [40]. Recent work has shown that ASCs have a minor tenogenic differentiation capacity when compared to BMSCs, in vitro and in vivo after implantation in nude mice [41]. To drive the tenogenic differentiation of BMSC and ASC, adding different growth factors and differentiation factors to the culture medium has been used with success [42].

A murine pluripotent cell line, C3H10T1/2 is another relevant stem cell model [43] used in embryology and tendon repair studies [44], also employed by several teams in tendon engineering approaches [45–47].

Tendon Stem/Progenitor Cells (TSPCs) are quite heterogeneous and present common features with adult MSCs. Even if their roles in tendon healing and maintenance remain unclear, these cells are a promising tool in tendon engineering [21,30,48]. Isolated from the mid-substance of patellar tendon, TSPCs may be characterized by various markers [48]. TSPCs have the advantage of having inherent pro-tenogenic abilities and being an autologous source of cells. When compared with BMSCs, TSPCs display the highest levels of tendon-related markers (scleraxis, tenomodulin, cartilage oligomeric matrix protein, and tenascin-C), high clonogenecity, and proliferation. When injected into the injured tendon region in a rat model, TSPCs pretreated in vitro with pro-tenogenic differentiation molecules improve tendon repair [49]. However, they have the same disadvantages as tenocytes, i.e., their scarcity in tendon tissue and a risk of morbidity at the site of tissue extraction [50].

Tenocytes are terminally differentiated tissue-resident cells, which are responsible for the synthesis and homeostasis of the components of the ECM of tendons. Despite the advantages of using autologous cells and the cell type in charge of intrinsic healing tendon [51–55], the use of tenocytes raises a series of obstacles: limited capacity to proliferate, scarcity of donor tendons from which tenocytes can be extracted, low quantity of tenocytes in tendons that make them difficult to collect, cell de-differentiation processes during culture expansion, and a risk of major donor site morbidity [56]. To overcome these limitations, dermal fibroblasts (DFs) have been proposed as an alternative source of cells for tendon reconstruction as it is relatively easy to extract and expand them, and, thanks to their high potential, produce ECM components from them [57]. However, using DFs can result in scar formation, leading to poor mechanical properties when compared to native tissue [58].

2.3.2. Modulation of the Environment

Biochemical Stimulation

Once tendons suffer from an injury, a cascade of events takes place to repair the damaged tissue. Cytokines and growth factors that are released by tendon cells or inflammatory cells recruited into the damaged area play a key role during the early phase of tendon healing via the induction of cell

proliferation, ECM synthesis, and remodeling [59]. Of these factors, vascular endothelial growth factor (VEGF) [60], insulin-like growth factor-1 (IGF-1) [61], platelet-derived growth factor (PDGF) [62], basic fibroblast growth factor (bFGF) [63], members of the transforming growth factor β (TGF-β) superfamily [64], Interleukin-6 (IL-6) [65–67], and connective tissue growth factor (CTGF) [49] have also been characterized in vivo and in vitro. They are up-regulated during the different stages of the healing process, resulting in increased cellularity and tissue volume [33].

TGF-β (isoforms TGF-β1, -2, and -3), and IGF-1 interfere at all stages of tendon healing stimulating inflammatory cell migration, proliferation of fibroblasts and other cells at the injury site, collagen, and ECM production [42]. It is well documented that the TGF-β activation pathway in response to injury is associated with scar formation and fibrous adhesion formation, and the suppression of the TGF-β1 signaling pathway enhances tendon healing in a rat model [68]. The three isoforms of TGF-β present different temporal patterns of expression over the course of tendon healing [69], suggesting that more detailed studies are needed in order to improve the outcomes of TGF-β applications in tendon healing.

Bone morphogenetic proteins (BMPs) are members of the TGF-β superfamily and play important roles in tendon healing. BMP-12 gene transfer in tendon cells increased the tensile strength and stiffness of lacerated tendons [70].

PDGF is also essential for tendon healing. Its administration in rat patella tendons increased the mechanical properties and tissue remodeling when delivered at a late stage after injury [71]. PDGF up-regulated tendon cell growth, collagen production, and ECM remodeling in vitro, but, according to recent work, PDGF may favor a trans-differentiation effect in tenocytes in culture [72].

Platelet-rich plasma containing high growth factor concentrations, among them tendino-inductive factors, gives promising therapeutic effects in vitro and in pre-clinical studies when delivered at the site of injury [73,74].

Biomaterials have been developed extensively to deliver growth factors to the site of injury. Understanding of scaffold design and manufacturing has been accumulated to allow for growth factors to be incorporated into the ECM or immobilized on its surface. In parallel, numerous studies have demonstrated the sensitivity of MSCs towards pro-tenogenic growth factors [29]. New techniques combining stem cells seeded on to scaffolds impregnated with growth factors could stimulate and guide tendon regeneration through the slow diffusion of biomolecules. Hydrogels have been explored to retain bioactive molecules to develop engineered tendon substitutes [75]. The use of a tenogenic differentiation medium (containing BMP-14, also known as growth and differentiation factor-5 (GDF-5)), was recently shown to enhance tendon-like matrix production from ASCs that are seeded on to poly(l/d)lactide (PLA) copolymer filament [76]. These authors reported a similar elastic modulus in bioengineered tissue and in native Achilles tendons.

Mechanical Stimulation

Tendons are subject to loads during movement, and are thus permanently under the effects of mechanical strains of different natures. It has been highlighted that application of physiological loads is necessary for maintaining tendon homeostasis, as well as for preventing excessive degradation of the ECM [77–79]. As a result, tendons are then in a continuous process of remodeling, adapting their metabolism, and structure [80]. These adaptations are made possible by the presence of cells in tendons. Fibroblasts have demonstrated their mechanosensitivity by proliferating [81] and producing collagen [82] when stretched through activation and/or the effects of a number of growth factors (details above). It has also been shown that mechanical force drives the development of tendons during embryogenesis [83]. In addition to growth factors, mechanical stimulation modulates cell differentiation, driving MSCs towards a tenocyte lineage [84]. In vitro studies outlined the importance of mechanical cues for the healing process of a lacerated tendon [85]. Thus, mechanical stimulation appears to be necessary for achieving correct tendon reconstruction by means of TE. Current strategies apply cyclic strain to achieve this goal, with a wide range of strains, frequencies, and rest periods [35,38,39,45,54,86,87].

2.3.3. Materials

Biological Origin

Tendon composition and structure are mostly driven by type I collagen. For this reason, most research has focused on collagen alone or mixed with other molecules, such as proteoglycans as a support for tendon tissue engineering [88]. Different strategies have been explored to produce the ideal collagen-based scaffold, such as sponges [38,39,51,55,87,89], extruded collagen fibers [52,53,90], or electrochemically-aligned collagen [33,34,91], all being suitable for tendon reconstruction. In this review, simple films or collagen coatings are not presented because their inner mechanical properties are not relevant for TE applications.

Due to its rapid degradability, cost issues, and poor mechanical properties, alternatives to collagen for tendon reconstruction have appeared, including silk fibroin, one of two components synthesized by *Bombyx mori* silkworms during cocoon production [92]. With a fibrous nature, silk fibroin is a material with biocompatibility, low immunogenicity, and remarkable tensile strength as its main properties [93]. Silk fibroin has therefore been widely used for biomedical applications [94], such as silk yarns [95], knitted scaffolds [37,96,97], or electrospun materials [98].

More recently, decellularized matrices from tendons or other tissue origins were proposed as the "perfect" scaffold as they preserve biochemical composition, offering cells a full biomimetic environment. The chemical treatments performed to effectively remove donor cells may cause an inflammatory response when implanted into the host [99]. Of these chemical treatments, detergents, such as sodium dodecyl sulfate (SDS), 4-ocylphenol polyethoxylate (Triton X-100), or tri(n-butyl)phosphate (TnBP) are the most appropriate for fully removing cells from the tissue. Tendons from a wide range of species, including humans, rabbits, dogs, pigs, equines, rats, chickens, or bovines have been tested in order to find the best way to remove cells and to provide the suitable environment for tendon tissue engineering [100].

Synthetic Material

Synthetic polymers are very attractive candidates for TE as their material properties are typically more flexible than those of natural materials. Synthetic constructs present tunable and reproducible mechanical and chemical properties, they are relatively inexpensive to produce [73] and easy to mold into a variety of forms—meshes, foams, hydrogels, and electrospun. They can be non-toxic [101], and in many cases, processed under mild conditions that are compatible with cells [74,102,103].

Varied approaches have been deployed to generate scaffolds, such as electrospinning [35,45,46,54,104–107], yarns [35,107,108], knitting [36,37,97,109], and 3D printing [110], using a wide range of synthetic polymers such as poly (-caprolactone)(PCL) [35,111], poly-L-lactic acid (PLLA) [30,112], poly (lactic-co-glycolic) acid (PLGA) [105,106,113], or poly urethanes (PUs) [45,46,114].

Hybrid Material

Biologic-derived scaffolds have the advantage of being biocompatible and bioactive, recognized by cells, and favoring cell adhesion, migration, and proliferation. However, their rapid degradability and their low mechanical properties might limit their use in tissue engineering [115]. On the other hand, synthetic materials usually present low bioactivity, but better mechanical properties and slower degradation.

Hybrid scaffolds are based on the synergistic effect between natural and synthetic materials. Usually, the biological compound tends to act as cells' carrier, stimulating proliferation and migration over the support, while the synthetic one provides the construct with the stiffness needed to reach mechanical properties near the tendinous native tissue [100]. For tendon tissue engineering, such biohybrid scaffolds have been produced from mixture of collagen and polyesters [107].

Table 1. Material characteristics for tendon tissue engineering.

Material	Scaffold Preparation	Shape and Structure of the Scaffold	Mechanical Properties of the Scaffold	Ref.
Collagen	Freeze drying	Sponges L = 11, 23 or 51 mm 94% porosity, pore size = 62 µm	For L = 23 mm spec. EM = 0.02 MPa Linear Stiffness = 0.05 N/mm Maximum Stress = 0.005 MPa	[38,39]
Collagen/Chondroitin Sulfate		Sponge pore size = 53 µm	Linear Stiffness = 0.025 N/mm	[87]
Collagen/Chondroitin Sulfate		Isotropic sponge pore size = 87 µm Anisotropic pore sizes = 55, 152, 243 µm	ND	[51,55]
Collagen	Extrusion	EDC Crosslinked fiber diameter = 215 µm EDC/EDGE Crosslink diameter = 137 µm	Fiber diameter 215 µm → EM = 19.3 MPa Fiber diameter 137 µm → EM = 46.2 MPa	[52,53]
Collagen	ELAC	Collagen thread diameter = 50–100 µm	ND	[33]
Collagen		Woven collagen scaffold with 81% of porosity	Stiffness = 23.8 N/mm	[34]
PLGA	Electrospinning	Random nanofibers = 568 nm Aligned fibers = 320, 680 and 1800 nm	Random nanofibers → EM = 107 MPa Aligned fibers → EM = 341–510 MPa	[105,106]
PLLA		Aligned nanofiber diameter = 430 nm Random nanofiber diameter = 450 nm	Aligned nanofibers → Stiffness = 3.48 N/mm; EM = 22.76 MPa Random nanofibers → Stiffness = 0.07 N/mm; EM = 0.63 MPa	[30]
PLDLLA		Crimped fiber diameter = 880 nm Amplitude = 5.2 µm Wavelength = 46 µm	Crimped fiber Modulus = 3 MPa	[54]
PEEUR		Aligned or random fiber diameters <1 µm, 1–2 µm or >2 µm	EM = 4.2–9.2 MPa	[45,46]
PCL		Yarned made of twisted aligned fibers (200 µm diameter)	UTS = 17 MPa EM = 30 MPa	[35]
P(LLA-CL)/Collagen		Fiber diameter = 643 nm Final yarn thickness = 150 µm Pore size = 28.5 µm	Yarns EM = 2 MPa Ultimate deformation = 250%	[107]
PLGA	Knitting	Scaffold with 3 yarns. 20 filaments/yarn 25 µm diameter of filament + electrospun nanofibers	Initial failure load = 56.3 N Initial Elastic Stiffness = 5.80 N/mm Initial toe region Stiffness = 0.34 N/mm	[36]
Silk		Combined knitted silk fibers and silk sponge pores size from 20 to 100 µm	Maximum Tensile Load = 252 N Tensile Stiffness = 40 N/mm	[37]
Silk/Collagen		Combined knitted silk scaffold and freeze dryed collagen sponge	Failure force = 21.65 N	[97]

All abbreviations regarding materials can be found in the text. ELAC: Electrochemically aligned collagen fibers.

Table 2. In vitro performances of biohybrid scaffold in tendon tissue engineering (↑ = increase, ↓ = decreases).

Cells	Mechanical Stimulation of the Scaffold	Mechanical Properties of Biohybrid Construct	Major Outcomes	Ref.
BMSCs from NZ Rabbit	2 days of static culture and 2.4% strain once every 5 min for 8 h/day for 12 days	Long construct (51 mm): LS = 0.066 N/mm after stimulation. Non-stimulated: LS = 0.047 N/mm	Longest constructs: highest linear stiffness in vitro. Still very weak	[37,38]
BMSCs from NZ Rabbit	2 days of static culture and 2.4% strain 8 h/day for 12 days at 100 or 3000 cycles/day	Stimulated constructs 100 cycles LS = 0.080 N/mm; 3000 cycles LS = 0.032 N/mm	100 cycles/day: ↑ linear stiffness 3000 cycles/day: ↑ mRNA levels of *Col1* and *Col3*. ECM not shown	[87]
Primary horse tenocytes	None	ND	Anisotropic sponges: ↑ cell number, alignment and metabolic activity Pores >150 µm: ↑ cell proliferation and activity Smaller pores with high crosslinking density: ↑ differentiation	[51,55]
Sheep patellar tendon fibroblasts	None	ND	EDC/EDGE crosslinking: better mechanical properties, proliferation but ↓ cell viability EDC cross-linked fibers ↑ ECM production	[52]
Human MSCs	None	ND	ELAC threads: ↑ cell adhesion, ↓proliferation, ↑ tendon differentiation compared to random threads	[32]
Human BMSCs	None	ND	Cells aligned in the 3D structure. Up-regulation of tendon-related markers (TNMD and COL1). New matrix deposition	[33]
Human Rotator Cuff Fibroblasts	None	For 600 nm diameter, after 14 days: Aligned Constr: EM = 341 MPa, Random Constructs: EM = 107 MPa	Aligned/random scaffolds: No differences in cell proliferation or cell matrix deposition Nanofiber: ↑ cell proliferation and matrix synthesis Microfiber: ↑ tendon-like gene markers	[105,106]
Human TSPC from foetal Achilles Tendon	None	ND	Aligned scaffolds: ↑ tendon differentiation (aligned cells and expression of COL1, SCX, Eya2)	[29]
Bovine fibroblasts	Short term: 10% of cyclic uniaxial strain at 1 Hz 3 h/day. Long term: 3 h/day at 1 Hz in alternate days for 2/4 weeks	After 4 weeks on dynamic culture: Crimped structures EM = 33 MPa Uncrimped structures EM = 17 MPa For non-stimulated culture: uncrimped EM = 8.7 MPa	Crimped-like fibers: ↑ collagen accumulation Dynamic culture: ↑ ECM production (collagen and proteoglycans)	[54]
C3H10T1/2	2 days static culture + 3 days static (50 mN)/dynamic load (4% strain 0.25 Hz for 30 min)	ND	Static load, larger fibers, non-alignment: ↑ tenogenic differentiation	[45,46]
Human BMSCs	5 days of static culture. Cyclic uniaxial strain at 5% elongation at 1 Hz 1 h/day for 7 or 21 days	After 21 days on dynamic culture, UTS = 50 MPa; EM = 110 MPa. Under dynamic culture UTS = 20 MPa; EM = 110 MPa	aligned fibers: ↑ cell alignment Uniaxial cyclic strain: ↑ tendon-related markers (COL1, COL3, TNC, FN)/unloaded cells	[34]
Rabbit tendon cells	Static culture for 1 day. Cyclic uniaxial strain at 4% elongation at 0.5 Hz 2 h/day for 14 days	ND	Dynamic culture: ↑ Tendon related markers (COL1, COL3, decorin, TNC, Biglycan and ↓ of bone (Runx2) or cartilage related markers (COL2). Cells aligned in both static or dynamic culture	[107]

Table 2. *Cont.*

Cells	Mechanical Stimulation of the Scaffold	Mechanical Properties of Biohybrid Construct	Major Outcomes	Ref.
Pig BMSCs	None	Failure load = 1. 82 N; Elastic Stiffness = 0.64 N/mm; Toe Region Stiffness = 0.05 N/mm	knitted structure + electrospun nanofibers: ↑ cell proliferation, collagen production and tendon-related markers (COL1, Decorin, Biglycan)	[35]
Human BMSCs	None	Tensile Load = 257 M Tensile Stiffness = 50 N/mm	Combined silk scaffolds with cells shows higher proliferation, ECM production (COL1, COL3 and GAGs) than knitted silk scaffolds.	[36]
Rabbit TSPCs	None	ND	No difference in cells attachment, spreading and proliferation Aligned collagen sponges → aligned ECM deposit	[97]

Table 3. In vivo performances of biohybrid construct in tendon tissue engineering (↑ = increase).

Animal Model, Tissue Site and Duration of Implantation	Mechanical Stimulation before Implantation	Mechanical Properties of the Biohybrid Construct Following Implantation	Biological Outcomes	Ref.
Rabbit patellar tendon 12 weeks	2.4% strain every 5 min for 8 h/day for 12 days prior implantation	Stimulated repair: LS = 241.6 N/mm; EM = 441.2 MPa. Non-stimulated repair: LS = 88.6 N/mm; EM = 343.2 MPa	Stimulated repair constructs: ↑ mechanical properties over time than non-stimulated repair	[38]
Sheep patellar tendon 3 or 6 months	None	After 6 months: EDC cross linked: EM = 73 MPa EDC/EDGE cross linked: EM = 68 MPa	EDC cross-linked fibers: ↑ mechanical properties, integration, resorption and tissue ingrowth after 6 months	[53]
-Mice muscle for 1 or 6 weeks -Mice skin for 1 week	None	None	-Cytotoxicity model: aligned cells with more oriented bundles of collagen compared to random scaffolds -Subcutaneous model: ↑ concentration of collagen with aligned morphology in aligned scaffolds	[30]
-In vivo: Mice back for 2, 4 or 8 weeks -In situ: Rabbit tendon for 4 or 12 weeks	In situ: Static or dynamic culture, 4% elongation at 0.5 Hz 2 h/day, 14 days	In situ: EM = 426.69 MPa for dynamic group EM = 41.5 MPa for static group	-In vivo: Mechanical stimulation: ↑ neo-tendon tissue formation with aligned ECM deposition -In situ: Dynamic culture: ↑ alignment of cells and matrix deposition. Larger collagen fibers on pre-stimulated construct	[107]
Rabbit tendon 12 weeks	None	Failure force = 139.85 N Stress at failure = 4.34 MPa Energy = 0.42 J Stiffness = 26.67 N/mm	Combined knitted and collagen-aligned sponge: ↑ ovoid cells, larger and denser collagen fibers	[97]

2.4. From Biohybrid Tendon Design to Reconstructed Tissue's Response

We now propose a review of the different scaffolds, the mechanical properties achieved by the biohybrid constructs, as well as both in vitro and in vivo outcomes. We sorted the papers referenced (Tables 1–3), according to increasing scaffold's complexity.

2.4.1. Macroporous Sponge

Collagen has been widely-used to produce three-dimensional sponges alone [116–120] or in combination with other molecules present in the tendon, such as glycosaminoglycans [38,39,87], to further mimic the rich nature of tendon ECM. In addition, these molecules support cell cultures due to their inherent biocompatibility.

Freeze-drying using ice-crystals as a porogen makes possible the formation of macroporous sponges, allowing for nutriment transport and cell penetration, the main requirements for building a new tissue [117]. The pore structure of sponge mirrors ice-crystal morphology. Generally, interconnected pores with a random (isotropic) configuration are obtained. Anisotropic sponges have been successfully produced by incorporating a directional solidification step into a conventional freeze-drying process.

The group of Harley produced collagen-chondroitin sulfate anisotropic sponges placing the solution in a cold mold prior to sublimation to direct pore formation [38]. Several parameters affected the final pore size and the density of the macroporous sponges, such as solute concentrations or the freeze temperature (−10, −40 and −60 °C): the lower the temperature, the larger the pores' diameter (243, 152 and 55 μm, respectively). Grier et al. (2017) increased the scaffold's density using a cross-linking treatment [55].

In general, sponges have weak mechanical properties (an elastic modulus in the range of 1 kPa), but have nevertheless been used in tendon tissue engineering.

When cultured over anisotropic sponges with oriented pore distribution [38], horse tenocytes presented enhanced proliferation, metabolic activity, and alignment when compared to isotropic sponges. Larger pores (>150 μm) also enhanced cell proliferation and metabolic activity as compared to smaller ones [51]. In contrast, differentiation assessed by up-regulation of tendon-related markers (COL1, COL3, COMP, and DCN) was promoted on sponges with the smaller pores and high cross-linking densities [87].

Butler's group has focused on the effect of mechanical stimulation on cell activity. For their studies, they worked with isotropic porous freeze-dried type I collagen sponges [38,39,87,120] with a mean porosity of 94% and pores with an average size of around 62 μm. Juncosa-Melvin et al. (2006) used these sponges to better understand the role of mechanical stimulation on the biomechanical properties of the final constructs [38]. Rabbit BMSCs were cultured for 12 days on the sponges with or without mechanical stimulation (8 h/day at 2.4% strain, once per minute). When stimulated, the constructs presented a linear stiffness and modulus 2.5 and 4 times higher than the non-stimulated ones. In the same study, the authors used those constructs to heal the patellar tendon in a rabbit model. Constructs that were stimulated prior to implantation presented better mechanical properties when compared to non-stimulated ones after 12 weeks of implantation. In another study, Nirmalanandhan et al. (2008) compared different sizes of sponge, long and short (51 vs. 11 mm of length), to better elucidate the importance of construct length in tendon repair [39]. After 14 days of culture, rabbit BMSCs that were cultured on the longest constructs presented a linear stiffness four times higher than that of short constructs (0.047 vs. 0.011 N/mm). Interestingly, for collagen-chondroitin sulfate constructs, a high level of COL1 and COL3 was found once stimulated at 2.4% of strain for 12 days with 3000 cycles per day when compared to collagen sponges [87].

2.4.2. Collagen Extruded Fibers

As tendon presents an inherent alignment of collagen, the aim of recent studies has been to develop fibers that better mimic the native structure. Extrusion of type I collagen fibers has been successfully achieved, allowing for the production of fibers with a diameter varying from 10 to 2000 µm [121,122]. This fibrillogenesis is generally achieved by extruding a solution of acidic collagen over a gelation bath to shift acid pH to neutral [123].

To avoid rapid degradation, extruded fibers are generally reticulated with a combination of treatments, such as glutaraldheyde, cyanamide, carbodiimide, and dehydrothermal [124]. As a result, the fibers' physical properties depend on the original collagen preparation, the fiber bath formation, the cross-linking treatment and the diameter of the extruded tube. Zegoulis et al. (2009) were the first to compare the mechanical properties of fibers that are produced through extrusion, depending on the cross-linking treatment. For example, non-reticulated collagen extruded fibers presented a fiber diameter of 300 µm and a maximum stress of 3 MPa, while after treatment with genipin, fibers of the same diameter reached a maximum stress of 7 MPa [124].

In a recent study, Enea et al. (2011) compared two methods (EDC or EDC/ethylene-glycol-diglycidyl-ether (EDGE)) to produce reticulated fibers [52]. EDC treatment resulted in softer and smaller fibers (stress at failure of 4.6 MPa; strain at failure 23.2%; modulus 19.3 MPa). EDC/EDGE resulted in stiffer ones (stress at failure 10.5 MPa; strain at failure 23.1%; modulus 46.2 MPa).

Although the cross-linking process provided better mechanical properties and degradation resistance, the reticulated fibers may present a lack of biocompatibility [52,53,125].

After 14 days of culture over the fibers, sheep tenocytes failed on cell colonization, proliferation, and collagen production on EDC/EDGE stiffer fibers when compared to the softer EDC ones [52]. Similarly, Ahmad et al. (2015) compared the effect on biomechanics and biocompatibility of different concentrations of two cross-linking agents, EDC and NHS [125]. While the agents' concentration did not provide any significant effect on the mechanical properties of the fibers, the highest agent concentration resulted in less cell adherence and proliferation.

Following the in vitro study, Enea et al. (2013) used an open array of multiple fibers of extruded collagen to replace the patellar tendon in an ovine model [53]. After six months, EDC implants presented better integration and tissue ingrowth when compared to EDC/EDGE and higher stress to failure (4 vs. 1 MPa). These results highlight the need for the development of the correct cross-linking methods to better provide a biocompatible environment.

In addition, one can notice that most works have been carried out on single fiber experiments and there is still a lack of biological characterization in the presence of cells (differentiation, collagen synthesis). Further studies need to be performed with more complex structures, such as yarns, threads, or knitting scaffolds with collagen fibers.

2.4.3. Electrochemically-Aligned Collagen (ELAC) Fibers

The Akkus team developed electrochemically-aligned type I collagen fibers (ELAC fibers) [33,34,126–130]. In the presence of an electric current (20VDC) produced by parallel electrodes, collagen molecules aligned at the isoelectric point, allowing for the production of collagen-aligned threads with a variable fiber diameter (50–400 µm) [126]. When reticulated with genipin, those ELAC threads showed mechanical properties in the range of those that are found on native tendons, with an ultimate tensile stress of 108 MPa, an ultimate failure strain of 13%, and a Young's modulus of 890 MPa, showing the potential ELAC fibers have as carriers for tendon tissue engineering [129].

Kishore et al. (2012) compared ELAC threads (50–100 µm in diameter) with random collagen threads to better elucidate the influence of collagen alignment on human MSCs [33]. Interestingly, the cells adhered easily in ELAC threads when compared to random ones, but proliferation was higher in random than in ELAC threads. After 14 days, cells that were cultured over ELAC threads presented a spindle-shaped fibroblastic morphology and presented enhanced tendon early (scleraxis) and late

(TNMD) differentiation markers after 3 or 14 days. On the other hand, cells cultured on random threads presented a random morphology and less tendon-related marker expression. The alignment of collagen threads is enough to produce tenogenic differentiation in the absence of any differentiation factors.

In another study, Younesi et al. (2014) showed the possibility of producing 3D bio-textiles with ELAC threads [34]. ELAC yarns (triple thread) were woven in a robust and porous scaffold (81% of porosity). This 3D configuration provided upgraded mechanical properties and a tendon characteristic-compliant toe-region when stretched. Further in vivo and in vitro studies need to be performed with these structures in order to confirm the trend and to ensure the promising results of ELAC threads as a strategy for full tendon replacement.

2.4.4. Electrospun Scaffolds

Scaffold Structure and Mechanical Properties

Electrospinning leads to the production of fibers that mimic the ECM and therefore create a suitable environment for cell development [131]. There are a remarkable number of parameters that influence the structure of the final scaffold, such as the nature and concentration of the polymer and solvent, but also the form of the collector, conductivity, and displacement (static or rotating) [132]. The major materials that are employed in electrospinning techniques for further tendon engineering applications are polyhydroxyesters, such as PLLA [30], PLGA [105], or PCL [35] alone or combined [47], polyurethanes [45,46], and natural polymeric biomaterials, such as silk fibroin [133,134]. Generally, the fibers produced can thus be randomly deposited or aligned [30,46,47,105], flat, or three-dimensionally structured [35,135].

According to native structure, fiber alignment appears to be a target for mimicking the organization of collagen fibers in tendons. Moffat et al. (2009) produced PLGA random and aligned fibers using a rotating ground collector [105]. When the collector speed was high (20 m/s), the resulting scaffolds were composed of aligned fibers. The elastic modulus of aligned fibers was three times higher than random fibers (341 vs. 107 MPa). In another study, Yin et al. (2010) produced PLLA-aligned fibers using a rotator mandrel turning at 4000 rpm [30]. The mechanical properties of the aligned scaffolds were also enhanced with stiffness and modulus 46 and 36 times higher, respectively, when compared to random materials. As collagen fibers have a crimp-like structure of a variable range of wavelengths (between 45 to 65 μm) and amplitude of 5 to 10 μm [54], further studies have investigated the production of crimped scaffolds [136] and their role in promoting tendon-like tissues. To produce those fibers, Surrao et al. (2012) electrospun PLDLLA into a rotating wire mandrel made by two circular pieces allowing for the production of aligned fibers [54]. Once the final material was placed in a solution with a temperature 10 °C above the glass-transition (T_g), the crimp patterns appeared as a result of the release of the energy stored during collection. This process made it possible to create a final electrospun scaffold made pf fibers with a diameter of 0.88 μm and a crimp amplitude and wavelength of 5.2 and 46 μm, respectively. The final modulus of the crimp scaffold was 3 ± 0.3 MPa.

Electrospinning is also a highly adaptable technique that allows for the production of a fibrous micron to sub-micron matrix. In the literature, one can find fibers from 40 to 2000 nm [137]. Erisken et al. (2013) produced PLGA fibers with diameters of 320 nm, 680 nm, and 1800 nm by modifying the polymer concentration [106]. Improved modulus and reduced ductility were found with the highest diameter fibers. In a similar study, Cardwell et al. (2014) synthesized different electrospun poly (esterurethane urea) (PEUUR) scaffolds with fiber sizes of <1 μm, 1–2 μm, and >2 μm aligned or random [46].

Although a thin layer of an electrospun material is very porous, the high packing density of such scaffolds prevents the correct colonization of cells through the material. In addition, when present as a fibrous sheet, electrospinning cannot be considered as a 3D environment. For these reasons, some researchers have been working on modified electrospun set-up devices in order to produce improved scaffolds with high porosity and a 3D structure. Sacrificial fibers [138],

air-gap [139], water bath collection [107,140,141], or twisted electrospinning to make yarns [35,107,141], have appeared to be a promising solution to confer electrospun scaffolds a superior ultrastructure.

Bosworth et al. (2014) proposed three-dimensional electrospun yarns by continuous strands of twisted aligned PCL fibers resulting in yarns with a final diameter of ~150–200 µm [35]. When compared to a two-dimensional (2D) aligned scaffold, 3D yarns presented a higher ultimate tensile strength and Young Modulus (5 and 14 MPa vs. 1 and 5 MPa). In another study, Xu et al. (2013) produced electrospun yarns through a modified water bath collection system [107]. First, P(LLA-CL) and type I collagen fibers were collected in a water basin with a hole in its bottom. As water was continuously drained, the collection system created a vortex flow, producing twisted yarns, and then collected the yarns in a rotating drum. The final yarns were made of aligned fibers with a diameter of 640 nm. When compared to it homologous 2D aligned electrospun scaffold, nanofibrous yarns presented a lower Young's Modulus (2 vs. 4.5 MPa) and lower tensile strength (4 vs. 6 MPa), but higher break at elongation (150% vs. 250%).

In the following section, the interactions between cells and scaffold structures, such as fiber distribution (aligned vs. random, and fiber size), or 2D vs. 3D structure will be presented.

Biological Response

To analyze the effect of scaffold alignment, Moffat et al. (2009) cultured human rotator cuff fibroblasts on PLGA scaffolds with different structures (random vs. aligned) [105]. After 14 days of culture, no differences in cell proliferation were observed. The aligned fiber scaffolds maintained their mechanical properties longer than the random ones in culture, and fiber alignment appeared to be the main contact guidance to make cell attachment and alignment possible along the fiber axis. In a similar study, Yin et al. (2010) compared the effect of PLLA fiber alignment on hTSPCs [30]. When cultured over aligned scaffolds, hTSPCS showed a spindle-shaped morphology, a classic fibroblastic phenotype. In addition, cells that were cultured on aligned fiber scaffolds presented tendon up-regulated expression and matrix deposition (collagen) and resisted bone induction when compared with random scaffolds. When the same scaffolds were implanted in an ectopic murine model, aligned morphology and collagen synthesis were also found to be enhanced when fibers were aligned.

The effects of fiber diameter on cell activities have been investigated. In a study by Erisken et al. (2013) human rotator cuff fibroblasts were cultured over scaffolds of PLGA with different fiber sizes [106]. In contact with the different mats, cells presented high production of a tendon-like matrix (COL and GAGs) in nano-fibrous scaffolds, but high tendon-related marker expression (COL1, COL3, and TNMD) in larger fiber scaffolds after 28 days of culture. In a similar study, Cardwell et al. (2014) were interested in the effect of fiber diameter on the differentiation of C3H10T1/2 cells into tendon/ligament lineage [46]. After nine days of culture, cells achieved tendon/ligament-differentiation and produced more collagen on larger fibers, regardless of fiber alignment. Taken together, it seems that small, nano-scale random fibers provide a cell environment similar to that found in the inflammatory phase of the tendon healing process, promoting the synthesis of the ECM and cell proliferation, while larger aligned fibers mimic the normal structure of collagen in tendon, maintaining the tendon cell phenotype. This could explain why larger fibers promote high levels of tendon-related gene expression, ensuring the maintenance of the fibroblast phenotype [142].

Bosworth et al. (2013) compared the effect of scaffold structure on cell behavior [143]. When seeded with equine tendon fibroblasts, the cells presented an alignment through the direction of the fibers and an augmented proliferation over time (14 days), however, proliferation was less pronounced on yarns due to the smaller surface area when compared to flat 2D electrospun scaffolds. In a similar study, Xu et al. (2013) compared cell activity over P(LLA-CL)/collagen yarns and its 2D equivalent [107]. After 14 days of culture, primary tendon cells that were cultured on yarns presented enhanced expression of tendon-related ECM genes (*COL1*, *Decorin*, *TNC* and *Biglycan*), proliferation and colonization compared to 2D-aligned scaffolds.

Effect of Mechanical Stimulation

Independently of fiber diameter or alignment, mechanical stimulation was suggested to induce tendon-like cell responses with up-regulation of the expression of tendon-specific markers and ECM production both in vivo and in vitro [28,29]. Cardwell et al. (2015) studied the effect of both fiber diameter and mechanical stimulation (static or dynamic load) on cell activity [45]. These authors plated C3H10T1/2 cells on PEUUR fibers with different sizes (600 vs. 1750 nm) under static (50 mN) or a dynamic load (4% cyclic strain for 30 min at 0.25 Hz daily). After three days of culture, no significant changes in COL1, COL3, DCN, or cell alignment was found. Moreover, cells in contact with larger fibers under static load presented elevated levels of TNC and TNMD, suggesting that the fiber diameter and the mechanical environment may alter cell activity.

For Jha et al. (2011), when bovine fibroblasts were cultured over crimp patterns and submitted to mechanical stimulation above the unfolding region of the crimp structures, cells produced more tendon/ligament-like tissue (collagen and proteoglycans), and interestingly, crimped scaffolds retained their mechanical properties over time [139]. In 3D nanofibrous electrospun yarns, Bosworth et al. (2014) investigated the response of human mesenchymal stem cells (hMSC) when cultured under dynamic loading [35]. During the experiment, electrospun yarns were stimulated for 7 or 21 days, once per day at 5% of elongation and 1 Hz. When submitted to dynamic load, the cells underwent morphological changes and an up-regulation of tendon-related markers (COL1, COL3, TNC, FN). Under dynamic conditions, the cells presented on the outer circumference of the yarns, were more round and the cell layer was thicker when compared to the static conditions. Xu et al. (2014) also investigated the effect of mechanical stimulation over electrospun nanofibrous yarns [141]. After 14 days under dynamic loading (4% elongation at 0.5 Hz, 2 h/day), rabbit TDSCs presented an aligned morphology in both static or dynamic cultures, but major proliferation and tendon ECM production (COL1, COL3, TNC) and enhanced expression of tendon-related markers (COL1, COL3, decorin, TNC, biglycan) under dynamic load. After twelve weeks of implantation in a full-size defect in a rabbit model, biohybrid scaffolds that were prepared under dynamic conditions presented better cell alignment, ECM synthesis, and mechanical properties than those that were prepared under static culture.

On the basis of this literature review, it is possible to say that there is still no consensus on the effect of mechanical stimuli on cell differentiation and production of ECM. This might be due to the absence of consensus regarding the frequency and amplitude of the stimulation to apply.

2.4.5. Knitted Scaffolds

The application of textiles techniques has been widely-used for tissue engineering as it offers the possibility of creating complex hierarchical 3D structures with tailored mechanical properties similar to native tissues [144]. Knitting offers the possibility of creating 3D structures made of interconnected loops of yarns or threads [109] that determine both their mechanical properties and their porosity [37]. To create these structures, a combination of biological and/or synthetic materials, such as silk or PLGA, has been tested [36,37,97,145]. Combined with electrospinning or sponges, this makes it possible to produce multi-hierarchical structures that mimic the nature of the rich tendon ECM.

Sahoo et al. (2006) produced a combined nano-micro fibrous knitted scaffold with the combination of PLGA micro fibers (yarns of 25 μm) and electrospun PLGA nano fibers (300–900 nm) [36]. The final combined construct presented pore size from 2 to 50 μm, an initial failure load of 56.3 N and an initial elastic stiffness of 5.80 N/mm. After 14 days of culture, BMSCs showed increased proliferation, collagen production, and up-regulation of tendon related-markers (COL1, decorin, and biglycan) when compared to the PLGA knitted control without electrospun fibers.

In another study, Liu et al. (2008) developed a knitted silk scaffold resulting from interconnected loops with a pore size of 1 mm and good mechanical properties, with a maximum tensile load of 252 N and a stiffness of 40 N/mm [37]. One of the main problems of knitted scaffolds is finding the right way to load the cells. To improve cell loading and proliferation, these authors placed the knitted construct in a silk solution. Once freeze-dried, this made it possible to produce a combined

scaffold with final pore sizes from 20 to 100 µm. The mechanical properties of this combined scaffold were similar to those of simple knitting, with a maximum tensile load of 255 N and a stiffness of 45 N/m. After 14 days of culture, human BMSCs showed enhanced proliferation and ECM production (COL1, COL3 and GAGs) in combined scaffolds compared to simple silk knitted scaffolds. In a similar study, Zheng et al. (2017) studied the effect of the pore direction of the collagen macroporous sponge on knitted scaffolds [97]. Twelve silk yarns (pore size of 1 × 1 mm) were placed in a type I collagen solution. Unidirectional freezing made it possible to produce aligned pores, while random sponges were made by classic freeze-drying. The final pore size of aligned sponges (110 µm) was smaller than that of the random ones. After seven days of culture, rabbit TSCPs presented the same attachment, spreading and proliferation in both constructs while ECM deposition was aligned into knitting constructs combined with aligned pores, and random constructs with random pores. In a tendon repair model in rabbits, rectangular defects (10 × 5 mm) in the rotator cuff tendon were filled with random or aligned constructs for 4, 8, and 12 weeks. After 12 weeks, the regenerative tissue was more organized and with more ovoid cells, and collagen fibers were larger and denser in aligned constructs when compared to random constructs, similar to the results found in normal tendons.

3. Skeletal Muscle

3.1. Skeletal Muscle's Composition and Structure

Skeletal muscle is a dynamic tissue that is responsible for voluntary movement, postural maintenance, and soft tissue support, through the conversion of chemical energy into mechanical force applied to bone via tendinous tissue. Skeletal muscle is the most abundant tissue in the human body, representing approximately 40% of body mass [146]. The architecture of skeletal muscle is characterized by a highly ordered arrangement of muscle fibers associated with connective tissue [147] (Figure 2). The cellular structural unit of skeletal muscle is the myofiber. A myofiber is a multinucleated single muscle cell, which ranges from approximately 20–100 µm in diameter. Myofibers are arranged in parallel, with length ranging from a couple of mm to several tens of mm depending on the muscle [148]. Myofibers are wrapped in a fibrous ECM, the endomysium, and bundled in fascicles, each of which is supported by the perimysium (Figure 2). There are thus three fibrous layers of connective tissue in skeletal muscle, i.e., the endo-, peri-, and epi-mysium, the latter enveloping the muscle, and supporting the structural and functional continuity of the muscle-tendon junction. They are composed of collagen (types I and III, mainly) and proteoglycans mostly from the family of small leucine-rich proteoglycans (SLRPs). Decorin is the major proteoglycan in the perimysium [149].

The differentiation of skeletal muscle cells is stimulated by a contact-dependent process. Myofibers are thus formed when undifferentiated muscle cells (myoblasts) fuse together to form elongated, multinucleated myotubes, gathering nuclei in a central position. As the myotubes mature to form myofibers, the nuclei adopt positions near the plasma membrane at the cell periphery [150]. At the ultrastructural level, the major components of myofibers are myofibrils, which represent the molecular machinery that is capable of controlling muscle stretching thanks to a sliding movement between the thin, actin filaments, and the thick myosin ones. Actin and myosin proteins represent approximately 70% of the total protein content of a single fiber [151] and are the main component of sarcomeres, the smallest chain of contractile units (approximately 2.3 µm long). Each myofibril is composed of hundreds of sarcomeres in series. It should be noted that skeletal muscle fibers differ in their phenotypes depending on their myosin heavy chain isoform, which results in differences in twitch speed. Type I fibers express slow-twitch myosin heavy chain (MyHC) isoforms and are suited for endurance while type II fibers express fast-twitch MyHCs that are suited for short and high intensity work [152].

Collinsworth et al. (2002) etablished that skeletal muscle cells exhibited viscoelastic behavior that changed during differentiation: the apparent elastic modulus increased from 11.5 ±1.3 kPa for undifferentiated myoblasts to 45.3 ± 4.0 kPa after eight days of differentiation [153].

As well evidenced by Heinemeier et al. (2013), skeletal muscle is a very physiologically active tissue. The high rate of tissue turnover leads to continuous renewal of core muscle. This remarkable capacity for regeneration found in skeletal muscle is made possible through the activation of resident multipotent cells to compensate for muscle tissue turnover or in response to injury [154,155]. The most important cells implicated in the regenerative response of muscles are satellite cells. They are an quiescent population of resident muscle progenitor stem cells, which, in response to injury, are activated and migrate to the defect site, expand, and undergo myogenic differentiation or self-renewing of the satellite cell pool [156].

During muscle regeneration, satellite cell behavior is regulated through a cascade of complex signaling pathways controlled by intrinsic factors within satellite cells, as well as extrinsic factors that compose the muscle stem cell niche/microenvironment [157]. Behind these major muscle resident progenitors, fibro/adipogenic progenitors (FAP) have also been described as promoting muscle regeneration through ECM deposition and promyogenic factor secretion. In the case of chronic muscle injuries, the controlled response of FAP may be unbalanced in favor of excessive ECM deposition, leading to fibrosis and impaired muscle regeneration efficiency [158].

3.2. Muscle Injuries and Healing

Skeletal muscle injuries typically result from traumatic incidents, such as contusions and strains during sports activities, as well as trauma due to accidents or surgical resection of tumors, and are designated as volumetric muscle losses (VMLs). Approximately 35–55% of all sports injuries involve skeletal muscle damage to the myofibers and/or connective tissue [159]. Furthermore, about 5.8 million reconstructive surgical procedures are performed annually as a result of cancer ablation or road traffic accidents [160]. The detailed healing process of skeletal muscle following trauma has already been well described elsewhere [148,161–163]. Briefly, the healing process is composed of three phases: destruction, repair, and remodeling. During the destruction phase, after necrosis of the ruptured myofibers, the propagation of this necrosis is stopped within a couple of hours by a contraction band in the shelter of which the rupture is sealed by a sarcolemma. The broken myofibers contract and the gap between the stumps is filled by a hematoma, meaning that an inflammatory cell reaction occurs. The repair phase starts with phagocytosis of the necrosis surface by blood-derived monocytes. The myogenic process is then activated by activation of the satellite cells. This activation leads to differentiation into myoblasts, followed by a proliferation stage over 24 h, which contributes to the formation of myoblasts. Finally, these myoblasts fuse to form myotubes within a couple of days. After 5–6 days, the necrotic part is replaced by the regenerated myofibers. Revascularization of the injured site occurs three days after the injury with the formation of angiogenic capillary sprouts. The last repair phase, the remodeling phase, is characterized by the maturation of the newly regenerated myofibers, i.e., a maturation of the contractile material and attachment of the ends of the regenerated myofibers to the intervening scar by a newly-formed musculo-tendinous junction.

3.2.1. Grafts

Critical-sized tissue loss of muscle mass (more than 20%) impairs endogenous repair mechanisms [164]. In these cases, the gold standard procedure is most often achieved by autologous tissue transfer (graft) from an uninjured site in the patient [165], such as the muscle flap transfer [166]. Although frequently successful, harvesting soft tissue from the patient creates new defects and the possibility of increased morbidity. Allografts are used to bypass the drawbacks of autografts, but they are beset by limitations in supply, tissue condition at the time of transplant, and concerns over immunogenicity, morbidity, and cost [167].

3.2.2. Cell Therapy

Cells therapies have been investigated when the regenerative capacity of the skeletal muscle is partly depleted, as in severe myopathies, such as Duchenne or Becker muscular dystrophy.

This therapeutic strategy relies on the delivery of myogenic precursors or stem cells to the muscle tissue to improve regeneration and tissue repair thanks to structural and functional integration in the host tissue. It requires a suitable cell population, which is capable of proliferating in vitro to generate sufficient cell quantities for transplantation. Of the cellular candidates, satellite cells, primary myoblasts, fibro-adipogenic progenitors (FAP), and human pluripotent stem cells are considered as promising cell sources thanks to their high regenerative potential in situ or their unlimited proliferative capability.

Despite the potential efficacy of cell-based therapies in muscle regeneration, the poor outcomes of preclinical and clinical trials identified a number of issues [168]. The injected cells face a harsh environment, not only because of the inflammatory response to the muscle injury, but also due to the injection process itself. Intramuscular injections can further damage the tissue, while going through the systemic system, the cells may be unable to attain the injured muscle and instead engraft on to other tissues or organs [139]. Thus, regardless of the approach used, most cells fail to survive a few hours after injection. The cell culture conditions used to expand the cell before the transplantation step need to be improved to maintain the "stemness" or myogenicity characteristics of cells [169]. Interesting studies have shown the influence of substrate physical properties on skeletal cell differentiation. The substrate, on which cells are cultivated, with compliance and elasticity cues mimicking those of the muscle cell micro-environment, may be a regulator for myogenicity [170,171]. Some of the problems that are associated with cell therapies may be fixed by adopting an approach that includes biomaterials as a niche for cells, leading to muscle tissue-engineering strategies.

3.3. Skeletal Muscle Tissue Engineering

In this part, we selected the publications of interest, as described in Section 2.3. However, in contrast with tendon, skeletal muscle's properties (and specifically contractility) are mainly driven by cell behavior. The main approaches that can be found in the literature in muscle TE thus focus more on the end behavior of the cells after culture in a scaffold. The mechanical and biological outcomes investigated are thus quite different to those observed in tendon TE. The major biological issues concern myotube formation from myocytes, and contractility properties. The mechanical properties of a biohybrid construct are poorly documented, with the scaffold appearing mostly as a guide for cell organization and differentiation. In addition, one can point out that muscle tissue engineering is a recent approach, with the first papers appearing in 2005.

The publications of interest are presented in two tables. The first (Table 4) deals with general details of the Materials and Methods part, the second (Table 5) reports in vitro outcomes. Due to a lack of information, there is no table summarizing in vivo results.

3.3.1. Cells

The choice of an appropriate cellular source is fundamental for generating functional muscle in vitro. Fishman et al. (2013) established a non-exhaustive list of criteria that cells should meet to be suitable candidates for muscle engineering [172]. According to the literature data (Table 4), four cell types are predominantly employed in muscle engineering: the mouse C2C12 myoblast cell line [173–198], primary myoblast-derived satellite cells (SCs) [175,199,200], primary myoblast from different species [181,201–204], and mesenchymal stem cells (MSCs) [177,205]. SCs are an appealing solution as they are relatively easy to isolate and are also the direct precursor of myoblasts. Unfortunately, SCs maintained in vitro suffer a severe reduction in their ability to produce myofibers, and a decrease in their proliferative capacity [206]. The C2C12 cell line manages to decrease the variability of primary cell isolation. In addition, using the C2C12 cell line for muscle engineering studies makes possible an objective comparative analysis with works that are published in skeletal muscle bioengineering as it mainly uses this cell type [207].

All of these four cell types are helpful for preliminary design, but there is, to our knowledge, no attempt to cultivate myoblasts or satellite cells of human origin in scaffolds for TE yet.

3.3.2. Modulation of the Environment

Functional muscle formation is an intriguing and highly complex process that requires features, such as cell differentiation and maturation [208]. As shown in Figure 5, several intracellular pathways are responsible for enhancing proliferation and differentiation expression of cell genes during muscle development [209]. The effects of a wide variety of chemical and/or physical factors on muscle cell progenitor cultures have been investigated extensively. Many previous studies have demonstrated the ability of chemical stimulation to induce muscle cells and differentiation by studying the effect of certain growth factors [210–212]. At the same time, many studies suggest the benefits of using physical factors because of their potential ability to accelerate growth and development in skeletal muscle engineering [213–216]. Electric and mechanical factors are the most commonly used in the literature. Electrical stimulation is of particular interest because of the indisputable role of the electrical cues issued by the central nervous system in the development of skeletal muscles in vivo [217]. The understanding of its effect and how to use it are increasingly controlled. The parameters of the electric field applied can be modulated, according to the type of response desired. It has been shown that depending on whether the regimen applied is direct or alternative, and depending on the voltage/intensity range, it accelerates sarcomere assembly, promoting cell proliferation, differentiation, and/or muscle cell alignment [173,183,192,194,199,200,202,218–220]. Some studies pointed out that electrical stimulation makes intracellular calcium and NO release possible [221]. Others showed that it acts via the activation of PI3K, p38 signaling pathways [222,223]. In parallel, mechanical stresses also play a role in muscle cell growth, differentiation, and function because of the contractile and elastic nature of skeletal muscle [224]. When cells grow on a scaffold, a variety of stretch regimes can be applied. Thus, by modulating the cycle, stretching elongation and duration, muscle cell changes and functionality can be modulated [171,174–176,185,203,225,226]. It seems that cell stretching induces the activation of FAK via integrin, leading to an increase in gene expression [227]. Other studies suggest that stretching may also influence the passage of calcium via the ion channels [228,229] and activate PI3K and p38 signaling pathways [230,231].

It has now been clearly shown that several signaling pathways can be modulated in order to control muscle cell development in tissue engineering. The most recent studies are based on cell culture methods while using a combination of chemical and physical stimulations. More importantly, there is growing evidence that a combination of chemical and physical stimulations in addition to surface topography and scaffold composition may be a solution for generating safe and functional muscle constructs in vitro [184,232]. However, the chronology of these different stimuli actions during the development of muscle cells in vivo remains unclear. It may be of particular interest to investigate not only a combination, but also successive different stimulations (chemical, mechanical, electrical).

IGF, insulin-like growth factor; HGF, Hepatocyte growth factor; FGF, fibroblast growth factor; PI3K, phosphatidylinositol-3-kinase; MKKs, McKusick-Kaufman syndrome; ERK, Extracellular signal-regulated kinases; p38, mitogen-activated protein kinases; JNK, c-Jun NH2-terminal kinases; sGC, soluble guanylyl cyclase; calp, calpain; calc, calcineurin; CaMK, Ca^{2+}—calmodulin-dependent protein kinase.

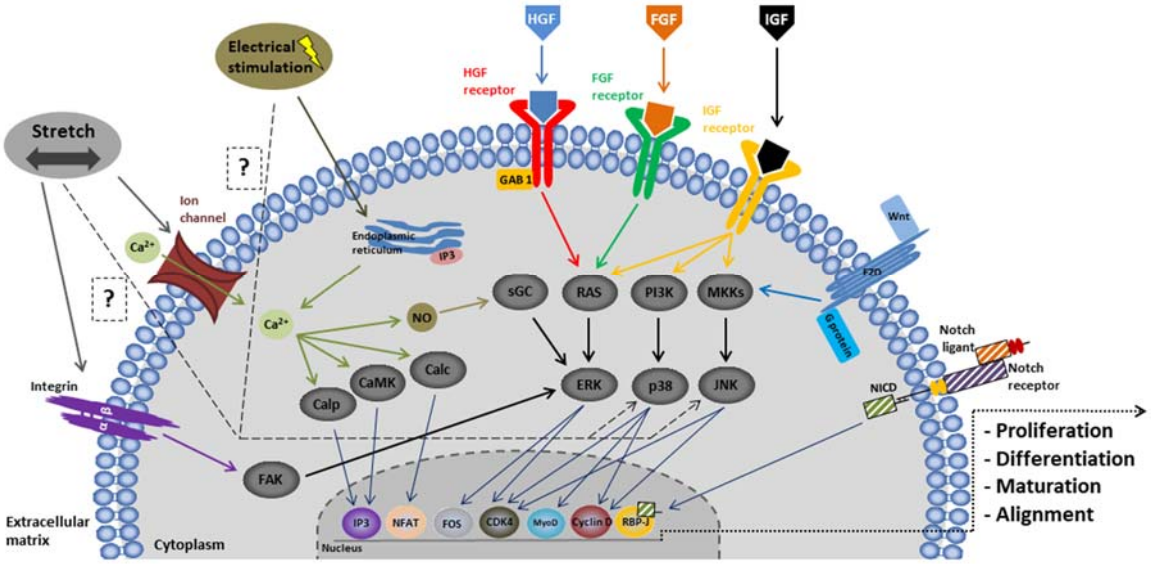

Figure 5. Schematic representation of skeletal muscle cell mechanotransduction: chemical signals are initiated by growth factors such as insulin-like growth factor (IGF), Hepatocyte growth factor (HGF), and fibroblast growth factor (FGF) binding to their respective receptors to trigger RAS, phosphatidylinositol-3-kinase (PI3K), and McKusick-Kaufman syndrome (MKKs) signaling cascades and activate Extracellular signal-regulated kinases (ERK), mitogen-activated protein kinases (p38), and c-Jun NH2-terminal kinases (JNK) pathways, respectively [233–235]. Electrical stimulation induces calcium release from the endoplasmic reticulum [236]. Calcium can act by activating either ERK [237] or calp, camk and calc [238–240]. Mechanical stretching signals involve the transmembrane protein integrin and the calcium ion channel [241]. Activating integrin triggers the FAK signaling pathway. Electrical and mechanical stimulations are also likely to activate the JNK and p38 pathways. Other pathways may be involved, such as wnt/frizzled and notch. All these signaling pathways up-regulate the expression of some of the genes responsible for skeletal muscle progenitor development.

3.3.3. Materials

Biological Origin

The macromolecular composition and structure of protective sheets surrounding muscle fibers (e.g., sarcolemma, endomysium) are mostly driven by various types of collagen [173,174,176,199,200,242,243]. For this reason, collagen and gelatin have been widely used as materials for muscle tissue engineering [182,183,194,244]. Non-mammalian sources of naturally derived materials have also been explored to produce suitable scaffolds for muscle reconstruction, such as alginate [177,245], fibrin [175,202,246,247], or chitosan [205,248]. They have the capacity to be configured into various shapes, including film, hydrogel, and sponge. Some of these materials are responsive to fabrication methods, such as chemical modification to add cross-linkers [249], or specific functional groups to improve cell attachment [250], or mechanical properties [251], in order to obtain structural control similar to that of native muscle.

Recently, as with tendons, scaffolds that were derived from decellularized skeletal muscle may be the optimal biomimetic biomaterials for repairing large skeletal muscle defects. In the literature, implants of decellularized muscles have been reported with contrasting results. Lin et al. (2014) showed that the enzyme detergent method for removing cells from mouse skeletal muscle, made it possible to maintain the biomechanical properties at a level that was comparable to that of native tissue [252]. Several other authors did not observe any myoblast migration towards the scaffold in vivo [253,254]. More recently, Porzionate et al. (2015) performed a comparative analysis between different decellularization protocols on muscles from different species, and especially on

human samples. The study evaluated the integration capacity of the decellularized scaffold in vivo. They observed good integration of the scaffold surrounding the native muscle structure and signs of neo-vascularization [255].

Synthetic Materials

Most of the synthetic polymers used for muscle tissue engineering scaffolds are manufactured from polyesters, which include poly(vinyl alcohol) (PVA) [198,205], (PGA) [256,257], poly(lactic acid) (PLA) [258,259], poly(caprolactone) (PCL) [190,191,260], and their copolymer poly[(lacticacid)-co-(glycolic acid)] (PLGA) [113,186,190,195,261,262]. These polymers are well characterized and have been approved by the Food and Drug Administration (FDA) for certain human uses [263]. They can be tailored into porous sponges, fibers, or microspheres for cell encapsulation [261]. PDMS (polydimethylsiloxane) [178,220], which is a type of silicone, is also used for other bio-microsystem applications. Although there are many applications in TE, their lack of biological cues for promoting desirable cell adhesion and responses may be a problem and requires specific coatings [178,220,264].

Hybrid Materials

Hybrid scaffolds consist of the combination of synthetic polymer and natural derived components, in an attempt to benefit from and exploit each asset. Natural components bring bioactivity, favorable environments for cell adhesion, and proliferation, along with remodeling properties, while synthetic materials can obtain the target mechanical properties. Although this type of approach is quite recent for muscle reconstruction, several configurations and combinations can be found in Table 4: PDMS and fibrin [247], PEG and fibrin [204], PLGA and collagen [195], PCL and collagen [265], and PCL and silk fibroin [196].

3.4. From Biohybrid Muscle Design to Reconstructed Tissue's Response

3.4.1. Films and Hydrogels

Effect of Scaffold Structure and Mechanical Properties on Biological Response

Of the materials used, collagen [173,174,176,188,199,200,203,213,243], fibrin [175,202,204,246,266], gelatin [182,183,194,267], alginate [177,245], and polymers, such as PLLA [180], PDMS [178,220], or PEG [196,268] generally functionalized or coated with adhesion peptides, are the most commonly found. To compensate for the mechanical weakness of hydrogels and their lack of conductive properties, which are useful in muscle tissue engineering [269,270], nanomaterials have often been added to the initial polymer. These include gold nanostructures [265,271], graphene [179,195,272], and carbon nanotubes [192,194,198,273,274]. The rationale for developing conductive polymers is the need for the transmission of the electrical impulse, which in turn may influence cell behavior, specifically for cardiac and skeletal muscle [275].

Natural polymers were first used in the form of simple coatings, to efficiently exploit the inherent capacity of cells to produce their own extracellular matrices and assemble themselves into organized and functional tissues. The gel-like structure and smooth aspect of the coating induce cells to proliferate and differentiate in a random orientation. To overcome this anarchic cell arrangement and favor myotube alignment, which is one of the most critical factors in skeletal muscle regeneration, Vandenburgh et al. (1988) anchored the gel between two fixed points acting as an artificial tendon. Mechanical tension between the anchor points promoted myofiber alignment and stimulated muscle growth [276].

Several studies outlined the role of film stiffness on myotube differentiation into the physiological striated state. The best results were obtained on materials with muscle tissue-like stiffness (elastic modulus around 10 $\pm$ 4 kPa) [170,277]. Baniasadi et al. (2016) worked on cross-linked-oxidized

alginate/gelatin hydrogels and investigated the impact of mechanical properties and degradation rate on the behavior of cultured cells [177]. In order to contract, muscle fibers need to grow parallel [278] to one another with identical anisotropy [279]. This can be achieved using a film with a specific topography to induce this behavior via contact guidance [280].

Topographical nano- [281] or micro-patterning have thus been investigated in grooves [282], waves [178], or more complex configurations [283] to enhance rat satellite cells or C2C12 myoblast fusion thanks to alignment and myotube formation. This approach mainly applied 2D films on to which myoblasts were cultured as monolayers until the formation of mature myotubes. Then, the mature cell layer can be transfer into a 3D contruct hydrogel [247], in order to be transplanted into a rat model. Several studies have shed light on the effect of optimized surface features, such as groove depth [180], width [181], and periodicity [178] on the formation of longer, functional myotubes with striated structures and contractile behavior in vitro [284]. According to these authors, optimal depth varied between 1 to 2.5 µm for a width of 10 µm, with a periodicity of 6 mm. Bajaj et al. (2011) demonstrated that hybrid 30° patterned structures led to the best C2C12 cell differentiation, as assessed by myosin and nuclei staining, as well as the size and orientation of the resulting myotubes [220].

Hydrogels were also developed in 3D to embed/encapsulate the seeded cells. Costantini et al. (2016) prepared a chemically-modified gelatin hydrogel and demonstrated the positive impact of mechanical stiffness and geometrical confinement on myoblast culture. Their results showed a parallel orientation of cells cultured in the smallest hydrogel string structure. Interestingly, the highest amount of myotube formation was obtained in a 3D hydrogel with stiffness in the range of 3 kPa, when compared to hydrogels whose stiffness was closer to that of native tissues. They speculated that C2C12 cells, when cultured in a 3D environment, exhibit specific focal adhesion configurations that influence cell polarization and signaling pathways, which were not observed in 2D constructs [285].

In contrast, Cvetkovic et al. (2014) produced strips of cross-linked collagen and fibrin with very high elastic moduli from 200 to 400 kPa that they placed on a specific holding tool named "biobiot". Despite the considerable stiffness of the material, cells aligned during gel compaction and formed myotubes, more specifically, under the effect of IGF added to the gel [286].

Hydrogels can be shaped as sponges, with an interpenetrating network structure favoring cell colonization within the 3D scaffold. For example, Bandyopadhyay et al. (2013) developed a biocompatible and biodegradable porous sponge that is made with poly(L-lactide-co-ε-caprolactone) copolymers using phase inversion [201]. This type of scaffold, which is characterized by a pore size of around 300 µm, supports adult human myoblast growth and differentiation into multinucleated myotubes in vitro and favors cell colonization in vivo in an ectopic rat model. Similarly, Kin et al. (2007) prepared cross-linked atelocollagen sponge using a freeze-drying technique (−80 °C), with pores in the range of 50–100 µm, and successful cell colonization of the scaffold was achieved in an ectopic rabbit model [243]. Although the hydrogel/sponge manufacturing process is relatively easy to implement, pore size and full interconnectivity remain difficult to control [287,288]. Another way of controlling 3D hydrogel porosity is to mold them into previously prepared PDMS structures that are designed by photolithography. In the study by Bian et al. (2012), primary muscle cells from rats were mixed with matrigel/fibrin gel to form an elongated hexagonal structure of various sizes. They demonstrated that the networks with the most elongated pores resulted in the best cell response in terms of alignment and contractility [204,278].

Effect of Electrical Stimulation on Biological Response

Recently, both Kasper et al. (2018) and Rangarajan et al. (2014) highlighted the attractive strategy of electrical stimulation for activating the signaling pathways that are presented in Figure 5 [289,290]. Hashimoto et al. (2012) demonstrated the effect of electric field on the differentiation and contraction of cultured C2C12 cells. More specifically, they showed that optimized parameters (1s pulse of 8V for three days) had a beneficial influence whereas higher electric stimulation damaged myocytes [173].

Serena et al. (2008) aimed partly to mimic neuronal activation by means of an adequate electrical field (pulse of 70 mV/cm for 3 ms). Applying this to muscle precursor cells (MPCs) cultured in 3D collagen scaffolds, they observed enhanced proliferation when compared to non-stimulated cultures. However, ten days after implantation in mice, cell number and distribution were no different in the two conditions [199]. Cvetkovic et al. (2014) subjected their constructs that were located on "biobots" to electrical stimulation (20 V, 1 to 4 Hz), representative of action potentials observed in vivo. They managed to coordinate the contraction of multiple myotubes in the artificial muscle strip [286]. In contrast, Stern-Straeter et al. (2005) focusing on the influence of electrical stimulation of primary myoblast cultures in a 3D degradable fibrin matrix, described the negative impact that is induced by their stimulation on the myogenic differentiation process, with a down-regulation of the transcription factor in the MRF-family [202]. Coordinating the electrical stimulation within the differentiation process of muscle progenitor cells is delicate and should not be introduced too early [200].

Effect of Mechanical Stimulation on Biological Response

A number of studies applied mechanical loading to cell-laden scaffolds in order to develop functional and structurally-biomimetic muscle constructs. Mechanical stimulation is another important factor during myogenesis [203,208], through the continuous passive tension applied to skeletal muscle by bone growth during both embryogenesis and neonatal development, as described in Figure 3. It also has a significant impact on the diameter of mature skeletal muscle fibers, as well as on cell numbers and myofiber composition [291].

Twenty years ago, Okano et al. (1997) described the impact of cyclic mechanical stretching (frequency: 60 Hz, amplitude: 5%, for four days) on encapsulated C2C12 myoblasts in a collagen type I gel, and reported an assembly of highly dense and oriented myotubes [176]. More recently, Powell et al. (2002) outlined that repetitive stretch/relaxation cycles applied to muscle cells suspended in collagen/Matrigel enhanced the diameter and area of myotubes by 12% and 40%, respectively, and increased the elasticity of the muscle construct, after eight days [203]. Pennisi et al. (2011) mobilized uniaxial or equibiaxial cyclic tensile strain (15% of stretch, 0.5 Hz) to induce assembly and differentiation in C2C12 skeletal myocytes seeded on to flexible-bottom plates precoated with collagen-I. The uniaxial strain resulted in a highly aligned array of cross-striated fibers, with the major axis of most cells aligned in a perpendicular manner in relation to the axis of the strain, and caused faster cell differentiation; on the other hand, equibiaxial strain did not induce any clear orientation and it displayed signs of membrane damage and impaired differentiation [174].

The mechanical stimulation of muscle constructs has not been systematically associated with an improved biological response, depending on the strain parameters used (duration, frequency, direction) [203]. For instance, Boonen et al. (2010) investigated the effects of a two day uniaxial ramp stretch (2%), followed by four days of uniaxial intermittent dynamic stretch (4%) at a frequency of 1Hz on the C2C12 or MPC cells in 2D or 3D constructs. They observed either no effect or a lowered effect on the maturation and differentiation of the cells [175]. There is thus not yet any consensus on the protocols to be applied to such constructs.

The simultaneous combination of mechanical forces and geometric constraints imposed by the substrate represents new models for understanding the mechanisms of cell response.

Ahmed et al. (2010) recently designed a flat support, without any micro-grooves, functionalized by adhesion proteins to control cell orientation. C2C12 cells produce different morphological and cytoskeletal responses to mechanical stimulation depending on their alignment relative to the direction of the cyclic tensile strain: strain applied to 0° micro-pattern lines results in the most irregular actin striation when compared to the highly organized stress fiber orientation observed along the 90° micro-pattern. Myoblast nucleus shape and orientation seem to be determined by geometrical constraints, showing that cyclic tensile strain and geometric constraints may be competing forms of stimuli [225].

3.4.2. Electrospun Scaffolds

Effect of Scaffold Structure and Mechanical Properties on Biological Response

The main materials that were used to produce electrospun scaffolds for skeletal muscle engineering are biocompatible and biodegradable synthetic polymers, such as PLGA [186], PCL [189–191,196–198,260,292], PVDF [187], and polyurethane [184,185,192]. These materials can also be of natural origin such as collagen [188,195,292], gelatin, decorin, silk fibroin, alone or mixed [190,196]. As for the gels, conductive elements can be added to the polymer, such as graphene [195], carbon nanotubes [192,194,198], polyaniline (PANi) [191], or gold nanoparticules [265,275].

Parallel configurations were studied to mimic the natural organization of bundles of aligned muscle fibers, which is necessary to develop high contractile forces [176]. Of the parameters that could be adjusted during the electrospinning process, Li et al. (2007) showed that the rotation speed of the collector had a considerable impact on the anisotropy of the resulting fiber mesh, which in turn, influenced the mechanical properties of the scaffolds [260]. For instance, the tensile moduli for random/aligned fibers of polyurethane (PU) were 2.1 $\pm$ 0.4 MPa and 11.6 $\pm$ 3.1 MPa, respectively.

It is well-documented that aligned fibers in electrospun scaffolds cause myoblast cytoskeletal reorganization, cell orientation along the fibers, and cell fusion into myotubes, unlike randomly oriented fibers [184,186,187,190]. Physicochemical cues for polymers influence myoblast differentiation, hydrophilic properties, and low matrix stiffness had a beneficial effect on cell response.

Drexler and Powell (2011) investigated coaxial electrospinning methods to produce scaffolds with tunable stiffness and strength without changing the architecture or the surface chemistry. These authors demonstrated that strength and stiffness were positively correlated with the inner core diameter, with no impact on fiber diameter [293]. This method might then make it possible to produce scaffolds with mechanical properties that are similar to those of native skeletal muscle tissue (≈10 kPa) [170]. Furthermore, hybrid composite fibers composed of natural and synthetic polymers are of great interest in order to benefit from the synergistic effect of mechanical properties and the biocompatibility of polymers in the same scaffold [205,294]. Aligned PCL/collagen electrospun fibers, when compared to randomly orientated nanofibers, showed higher tensile strength in scaffolds, as well as effective human myoblast alignment and differentiation into myotubes [265].

The influence of electrospun fiber diameter on skeletal muscle cell behavior remains poorly documented. Liao et al. (2008) produced polyurethane electrospun fibers with various diameters: 600 nm, and 2 µm to 10 µm by varying the polymer concentration (7%, 10%, and 15%). They did not find any influence of electrospun fiber diameter on the differentiation of C2C12 myoblasts [184]. Sreerekha et al. (2013) designed a multiscale composite scaffold with fibrin nanofibers (50–500 nm) and PCL microfibers (1 to 2.5 µm) [295]. These dimensions mimic the hierarchical structure of ECM that is found in native tissues (Figure 2). Topography scale also has an effect on cell responses: hydrogel micro-patterns designed on electrospun materials or wavy imprinted materials improved C2C12 myotube formation, orientation, and length through a multi-dimensional scale [189,197]. A more complex structure has been proposed in the form of a core-shell scaffold that combines aligned nanofiber yarns in a hydrogel shell to provide a suitable 3D environment successfully guiding the C2C12 myoblast alignment and differentiation [196].

Table 4. Materials characteristic for muscle tissue engineering.

Material	Scaffold Preparation	Shape and Structure of the Scaffold	Mechanical Properties of the Scaffold	Ref.
Collagen I	Hydrogel (Layer)	Membrane Flexcell	EM = 930 kPa	[174]
Collagen		Sheet -smooth	ND	[173]
Collagen I—Matrigel		Layer	ND	[200]
Fibrin		Layer	ND	[175]
Collagen I		3D cylinder hydrogel with inner diameters: 0.90 and 0.53 mm	ND	[176]
Oxidized alginate/gelatin cross-linking		Layer	EM = 1 and 10 kPa	[177]
PMDS/NCO-sP(EO-*stat*-PO) hydrogel/fibronectin coating		Fibronectin lines micropattern (30 μm wide parallel lines with 40 μm spacing) coating on hydrogel	EM ~1 MPa	[225]
PDMS/laminin coating		Micropatterned waves with 3, 6 and 12 μm in periodicity	ND	[178]
PDMS/fibronectin coating		Fibronectin geometrical cues: linear, 30°, circular micropatterns	EM = 100 and 500 Pa	[220]
poly-l-lactide/trimethylene carbonate		Micropatterns with groove widths (5, 10, 25, 50, 100 μm) and depths (0.5, 1, 2.5, 5 μm)	ND	[180]
Gelatin methacryloyl	Hydrogel (3D matrix)	Hydrogel slabs cross sections: 2000 μm × 2000 μm, 1000 μm × 1000 μm, 500 μm × 500 μm	Compressive modulus = 1 to 17 kPa	[182]
Gelatin methacrylate		Micropatterns with groove-ridges: 100 μm/50 μm; 100 μm/100 μm	ND	[183]
Mix of matrigel and fibrin		3D matrix: 1.5 mm thick—hexagonal holes lengths = 0.6, 1.2, or 1.8 mm	ND	[204]
Mix of collagen and matrigel		3D matrix	ND	[203]
Fibrin		None	ND	[202]
ECM proteins		3D matrix	EM = from 200 to 500 kPa; Passive tension = from 860 to 1150 μN	[286]
Polycarbonate polymer and titanium with gold nanoparticulates	Hydrogel (3D porous sponge)	Micropatterns with ridges, grooves, arrays of holes (5–75 μm)	ND	[181]
L-lactide/e-caprolactone copolymer (70/30)		Porous sponge = 3 cm diameter, 2–3 mm thickness with an average pore size of about 320 μm	ND	[201]
Atelocollagen		Porous sponge = pore diameters with a range of 50 to 100 μm	ND	[243]
Collagen		Porous sponge	ND	[199]

Table 4. *Cont.*

Material	Scaffold Preparation	Shape and Structure of the Scaffold	Mechanical Properties of the Scaffold	Ref.
Polyurethane	Electrospinning	Smooth film or random or aligned fibers Aligned fiber size = 600 nm–10 μm	EM = 0.5–1–22 MPa	[184]
Polyesterurethane (DegraPol®)		Highly oriented fiber (10 μm diameter) Scaffold thickness = 200 μm	ND	[185]
PCL		Highly oriented fibers = 438–520 nm range	Non-aligned scaffolds = EM 2.1 MPa	[260]
PLGA		1500 rpm: 0.6–0.9 μm range oriented with standard deviation: 19.5° 300 rpm: 0.4–0.8 μm range random with standard deviation: 74.7°	ND	[186]
ß-PVDF		Fiber diameter = ~200 nm Films with a thickness = ~110 μm	ND	[187]
Collagen I		Spring-shape	ND	[188]
Chitosan/PVA		Random structure: diameter = 137 nm, pore size = 1.9 μm^2	Break strain = 83.42%, Peak stress = 6.63 MPa	[205]
PCL		Parallel -oriented with wavy micropatterns: period. = 90um—depth = 14um—fiber diam. = 148 nm random orientation: size fibers = 265 nm aligned fibers: size fibers = 354 nm	EM = 36 MPA; UTS = 15 MPa; Elongation to break = 4% EM = 7 MPa; UTS = 4 MPa; Elongation to break = 161% EM =17 mMPa; UTS = 14 MPa; Elongation to break = 64%	[189]
PCL blends with PLGA or decorin		Aligned fiber diameters from 0.4–0.7 μm to 0.7–2.7 μm, for 15% *w/v* and 20% *w/v* of polymer solution	ND	[190]
PCL/PANi: (100/0); (85/15); (70/30)		Random 3D interconnected pores or oriented fibers Fiber diameters: PLCL/PANi (100/0) = 516 nm PLCL/PANi (85/15) = 499 nm PLCL/PANi (70/30) = 466 nm	Tensile strain—Elongation at break—EM—conductivity: PLCL/PANi (100/0): 18.2 MPa—248%—4.74 MPa PLCL/PANi (85/15): 16.7 MPa—176%—6.8 MPa—0.160 ± 0.046 S/cm PLCL/PANi (70/30): 14.1 MPa—160%—6.41 MPa—0.296 S/cm	[191]
Polyurethane/carbon nanotubes		Thickness = 36–64 μm range; Fiber diameter = 441–1533 nm range; Pore area = 2.5–12.3 μm^2	EM = 6.1–41.0 MPa range Tensile strength = 9.95–45.02 MPa range; Elongation at break = 115–300% range	[192]
Gelatin crosslinked by GTA, +/−0.5 or 5 mg/mL MWNTs		Fiber diameter from 18 kV = 250 to 900 nm and from 15 kV = 300 to 600 nm	EM (20% Gelatin) = 509 ± 37 kPa EM (20% gelatin −0.5 mg/mL MWNTs) =1170 kPa EM (20% gelatin −5 mg/mL MWNTs) = 1170 kPa	[194]
PLGA/collagen with graphene oxide nanoparticules		Randomly oriented average diameter = 440 nm	Hydrophilicity angle contact = 85°; Surface energy = 32.35 mN/m; Tensile strenghs = 16.8 MPa; E = 460 MPa	[195]

Table 4. *Cont.*

Material	Scaffold Preparation	Shape and Structure of the Scaffold	Mechanical Properties of the Scaffold	Ref.
PCL/collagen sputter-coated with gold nanoparticules		Fiber diameters = from 296 to 334 nm Fiber orientation: - Random parallel - Random perpendicular - Aligned parallel - Aligned perpendicular	Tensile strength—Elongation at break EM: Random parallel: 4.01 MPa—53%—4.33 MPa Random perpendicular: 3.86 MPa—53%—4.07 MPa Aligned parallel: 4.88 MPa—42.33%—4.43 MPa Aligned perpendicular: 3.06 MPa—91.67%—42.93 MPa	[265]
Fibers:PCL/silk fibroin/polyaniline Hydrogel: PEG		Aligned fiber diameters within hydrogel = 600 to 900 nm Yarn diameters within hydrogel = 50, 100, 165 µm	Tensile stress = 1.49 to 4.02 cN by yarn diameter: 25 to 165 µm Strain of yarns with diameters from 76% to 107%,	[196]
PCL/multiwalled carbon nanotubes (MWCNT) Hydrogel: PAA/PVA		Fiber diameter averages: PCL: 1.032 µm PCL-MWCNT: 1.704 µm PCL-MWCNT-Hydrogel:1.861 µm	Electrical conductivity PCL: 0.026 S/cm PCL-MWCNT:0.043 S/cm PCL-MWCNT-Hydrogel: 0.039.011 S/cm	[296]
PCL Hydrogel: PEG		Random, parallel, perpendicular fibers versus hydrogel pattern; Hydrogel pattern: 100 and 200 µm width	ND	[197]

Table 5. In vitro performances of biohybrid construct in muscle tissue engineering (↑ = increase, ↓= decrease).

Cells	Mechanical and/or Electrical Stimulation	Biological Outcomes	Ref.
C2C12	Mechanical: uniaxial cyclic tensile strain (CTS)—semi-sinusoidal tensile stretching pulses with a duration of 1 s. Peak amplitude 15%	Cell alignment perpendicular to the direction of strain ↑ myotube/myoblast ratio and % of myosin-positive myotubes	[174]
C2C12	Mechanical: 24 h of static culture Electrical: period 1 s, duration 0.1 s for 72 h, amplitude: 0.1 V to 12 V	Pulses lower than 8 V: ↑ cell adherence and proliferation Pulses of 0.1 V: ↑ cell differentiation Cell repetitive contraction at 8 days	[173]
MPCs/C2C12	Electrical: 4 V/cm, 6 ms pulses, frequency 2 Hz for 48 h	↑ sarcomere assembly and expression of late muscle maturation markers Faster maturation of myotubes in 3D model system than in 2D MPCs more mature than C2C12 and more susceptible to the electrical stimulation	[200]
MPCs/C2C12	Mechanical: 2 days uniaxial ramp stretch of 0–2% followed by an uniaxial intermittent stretch regime of 2–6% (3 h on, 3 h off)	↓ maturation into functional muscle fibers	[175]
C2C12	Mechanical: Cyclic stretching of 60 Hz −5% amplitude for 4 days	↑ degree of cell orientation and differentiation. Formation of a necrotic core in larger diameter rode	[176]
MSCs	-	Coverage of the total surface hydrogels OA/GEL (30/70) after 14 day culture	[177]
C2C12	Mechanical: orientation relative to the cyclic strain direction: 0°–45°–90°, amplitude 7% at 0.5 Hz for 4 days	Alignment of the actin stress fibers relative to the strain direction Significant effect on stress fiber orientation under geometric constraints of 30 µm width	[225]

Table 5. *Cont.*

Cells	Mechanical and/or Electrical Stimulation	Biological Outcomes	Ref.
C2C12	-	Wave periodicity (6 μm) of scaffold: ↑ alignment of moyblasts and myotubes	[178]
C2C12	Electrical: 20 V, 50 ms pulse, 1 Hz	30° hybrid structure: ↑ differentiation into myotubes with the highest fusion index	[220]
C2C12	-	↑ cell differentiation and maturation with 25 μm grooves width and 0.5–1 μm depth after 7 days of culture	[180]
C2C12	-	GelMA 3 and 4%: ↑ myogenesis Hydrogel structures (500 μm × 500 μm) and (1000 μm × 1000 μm) ↑ cell parallel orientation	[182]
C2C12	Electrical: 48 h of stimulation at 22 mA,1 Hz, and 2 ms	Surface topography with ridge width 50 μm: ↑ myotube orientation compared to width of 100 μm Electrical stimulation ↑ myoblast alignment and myotube diameter	[183]
Neonatal rat skeletal myoblasts	-	Elongated pores: ↑ cell alignment Tissue networks: ↑ fraction of myogenin-positive nuclei, and cell maturation into myotubes	[204]
Primary human skeletal cells	Mechanical: 3 sets (5% strain for 2 days,10% strain for 2 days and 15% strain for 4 days) of 5 stretch/relaxation cycles, each separated by 30 s of rest, with 28 min of rest after the third set	Repetitive stretch/relaxation cycles: ↑ myofiber diameter, area percentage and aligned multinucleated myofibers	[203]
Primary rat myoblast	Electrical: biphasic stimulation 6.8 mA; 4 ms. Electric bursts lasted for 250 ms, delivered at intervals every 4 s	↓ expression of the MRFs, MyoD and myogenin and AChR-ε	[202]
C2C12	Electrical: bipolar pulses: 20 V, amplitude (21.6-V cm^{-1} field strength) and 50 ms pulse	IGF-1: ↑ rate of fusion, maturation and myotube density Electrical stimulation triggered contraction	[286]
C2C12/primary myoblast	-	Microscale topography: modulates myoblast alignment	[181]
Human myoblast	-	↑ desmin and MyoD expression and myotube formation	[201]
MPCs	Electrical: Pulses 70 mV/cm for 3 ms, frequency 33.3 mHz	↑ expression of MyoD and desmin compare to non-stimulated control and ↑ total amount and release rate of NO_X	[199]
C2C12	Electrical: 20 V, 1 Hz, for 1 h with 5 h of rest Synchronized electromechanical: pre-stretching mechanical protocol: 5% cyclic strain at 1 Hz, followed by electrical stimulation	↑ degree of myotube striation when applied during post differentiation period compared to prior one Synchronized elecromechanical stimulation ↑ degree of myotube striation compared to unstimulated control	[184]
C2C12	Mechanical: 5 days of static culture (24 h of stretching at 0.02 mm/h, up to 960 μm displacement) followed by stretching pattern (frequency 0.5 Hz, amplitude 1 mm, 30 sec rest, followed by 28 min rest)	Cyclic stretching pattern stimulation: ↑ myosin accumulation	[185]
C2C12	-	Parallel electrospun fibers ↑ myoblast alignment, myosin expression and sarcomeric protein organization	[186]
C2C12	-	Negative poled ß-PVDF ↑ cell adhesion and proliferation. Oriented ß-PVDF fibers ↑ cell alignment	[187]

Table 5. *Cont.*

Cells	Mechanical and/or Electrical Stimulation	Biological Outcomes	Ref.
C2C12	-	Stained MHC-positive cells at day 7, multi-nucleated with parallel orientation along the microfiber at day 10 Myoblasts showed typical sarcomeric cross-striations The entire tissue continuously pulsated by autonomous contraction	[188]
Rabbit MSCs	-	Hybrid (chitosan/PVA) composition: ↑ myogenesis	[205]
C2C12	-	Periodic grooves: ↑ myotube formation and orientation	[189]
C2C12	-	Aligned PCL/PLGA 50% fibers: ↑ cell growth and differentiation versus to randomly oriented fibers Decorin addition: ↑ cell fusion, myotube length but ↓ myotube alignment	[190]
C2C12	-	PLCL/PANi (85/15) and (70/30): ↑ myotube length and width and ↑ expression of *myogenin*, *troponin T* and *MHC* genes	[191]
C2C12	Electrical: 10 μA at 10 Hz, 6 h/day, 21 days	Modulation of myotube maturation depend on the conductivity of the scaffolds	[192]
C2C12	Electrical: 5 V, 1 Hz, 1 ms for 2 days	↑ speed and the rate of myotube formation and length ↑ myogenin and FAK gene expression Increasing carbon nanotube concentration ↑ maturation and contractibility of myotubes	[194]
C2C12	-	GO-PLGA-Col hybrid scaffold composition ↑ cell attachment and proliferation, myogenic differentiation, myoblast fusion and myotube maturation	[195]
C2C12	-	Hybrid scaffold/hydrogel: ↑ formation of 3D aligned and elongated myotube ↑ Cell adherence, alignment and elongation with 50 and 100 μm yarns embedded in hydrogels	[196]
C2C12	-	PCL-carbon nanotubes-hydrogel: ↑ multinucleated cellular formation	[296]
C2C12	-	Aligned nonofibers: ↑ cells elongation compared to random and perpendicular nanofibers 100 μm pattern sizes on parallel fibrous scaffolds ↑ MHC expression and myogenesis	[197]

Jun et al. (2009) evaluated the effect of PLCL/PANi random fibers on C2C12 myoblast culture. Mechanically, the fibers showed an increase in tensile strength and a decrease in elongation at break as the concentration of PANi increased. While having a minimal effect on the proliferation, the electrically conductive fibers appeared to have a moderate effect on C2C12 cells by increasing the number and length of the myotubes, and enhancing the expression level of myogenic genes [191]. McKeon-Fischer et al. (2011) electrospun PCL with multiwalled carbon nanotubes (MWCNT) and with PAA/PVA hydrogel. The addition of MWCNT increased the mechanical properties of the "actuator" to more than the values of native skeletal muscle. Primary rat muscle cell cultures within a hydrogel were the first to display interactions among actin filaments in the large multinucleated formations [296]. Later, McKeon-Fischer et al. (2014) implanted the same type of scaffold for four weeks on to the *vastus lateralis* muscle of rats. These authors showed that the scaffold displayed early signs of inflammation and fibrotic tissue formation, which decreased over time, while the number of myogenic cells and neovascularization increased, suggesting that this approach could be innovative for muscle repair [297].

Effect of Electrical Stimulation on Biological Response

Electrical stimulation was recently investigated on electrospun bioconstructs to simulate motoneuron activity. Ostrovidov et al. (2014) demonstrated the positive effect of administering electric pulses (5 V, 1 Hz, 1 ms) for two days on the maturation and contractility of myotubes from C2C12 cells. These cells were cultured on gelatin electrospun fibers loaded with carbon nanotubes to promote electrical conduction [194]. The same type of results was observed by Sirivisoot and Harrison (2011) on electrospun polyurethane/carbon nanotube scaffolds (5% and 10% w/v polyurethane), when compared with nonconductive electrospun polyurethane scaffolds after electrical stimulation (Biphasic pulses delivered at 20 Hz) [192].

Effect of Mechanical Stimulation on Biological Response

Candiani et al. (2010) used a bioreactor and PU electrospun scaffold to investigate the effect of mechanical conditioning on the development of murine skeletal muscle cells. They applied an unidirectional stretching phase (24 h of stretching at 0.02 mm/h, up to 960 µm of displacement) to mimic bone growth-associated muscle lengthening during embryonic development, followed by a phase of cyclic stretch (frequency 0.5 Hz, amplitude 1 mm). Cyclic stretching induced an eight-fold increase in myosin heavy chain synthesis after 10 days, and contributed to myotube maintenance in a 3D environment [185]. Also, with electrospun PU, Liao et al. (2008) demonstrated that mechanical (5% or 10% cyclic strain at 1 Hz for two days post differentiation) or synchronized electromechanical stimuli (20 V at 1 Hz starting at day 0, 4, or 7 days post differentiation) increased the percentage of striated myotubes from C2C12 cells and an up-regulation of α-actinin and myosin heavy chains. They highlighted the need to carefully consider the combination of topographical and mechanical stimuli to optimize myogenesis. More specifically, these authors showed that a 5% pre-stretching procedure applied after cell seeding and prior to the application of cyclic strain resulted in enhanced myogenic differentiation. They also evidenced that the timing of electrical stimulation application is a crucial factor for modulating myoblast differentiation [184].

4. Reconstruction of the Myotendinous Junction

Once a bioengineered tissue has been designed, one of the key challenges for implanting it is its integration into neighboring tissues. Very few studies suggested designing and analyzing biohybrid constructs that mimic the interfaces between two different biological tissues subjected to various mechanical stimuli or strains.

Regarding this aspect, the myotendinous junction (MTJ) is of specific interest. Charvet et al. (2012) reviewed the current understanding of MTJ formation, describing changes during morphogenesis and focusing on the crosstalk between muscle and tendon cells that leads to the development of a functional MTJ. As pointed out, the various mechanisms/events leading to a functional MTJ during

embryogenesis are not yet fully understood. However, the structural integrity of MTJs is critical for force transmission from contracting muscle through tendon to bone tissue [298].

The ultrastructure of the MTJ was mostly explored using transmission electron microscopy (TEM), and focused ion beam/scanning electron microscopy (FIB/SEM). At this scale, the MTJ can be described as sarcoplasmic invaginations (ridge-like protrusion), which increase the contact surface between the muscle and tendon. Multidirectional collagen fibers are observed on the tendon side, improving the anchorage between both tissues.

In the past, Larkin's group [299] attempted to reconstruct the junction while using so-called scaffold-free self-organized tendon constructs (SOT). SOT consisted in collagen-rich deposits and flattened, longitudinally-oriented tenocytes extracted from rat tendons. They were put into contact with pre-established cultures of spontaneously contracting multinucleated myotubes. The interface presented an ultrastructure that resembled the fetal/neonatal MTJ. When subjected to tensile tests, rupture was observed on the muscle side [300]. This approach did not imply a specific scaffold, but it provided new insights into the mechanisms that are responsible for the formation and maturation of the junction, in an attempt to mimic the in vivo conditions.

More recently, Atala's group proposed two different approaches that are based on a unique scaffold that is composed of three different areas. In a first study, such scaffolds were prepared by electrospinning and consisted in: (i) an area of collagen/PCL fibers, (ii) an interphase area where fibers of collagen/PCL and collagen/PLLA were co-extruded; and, (iii) an area of collagen PLLA fibers. All of the areas were randomly deposited and fiber size was about 500 nm, independently of the electrospun material. Young moduli were around 4, 20, and 28 MPa, respectively. When C2C12 cells were seeded on to PCL, they formed myotubes, while NIH/3T3 fibroblasts spread on PLLA. There was no evidence of cell reorganization at the interface to form a specific MTJ [301]. In a second study, bioprinting was used with thermoplastic PU and C2C12 myoblasts on the muscle side, and PCL and NIH/3T3 fibroblasts on the tendon side. The interface was created by co-localizing the printing of PU and PCL leading to a 10% overlap. After the composite PU–PCL/C2C12-NIH/3T3 construct was printed, the fibrin-based hydrogel bio-ink was cross-linked. The extruded fibers exhibited a diameter of about 300 µm. According to classic tensile tests, the final construct was elastic on the PU-C2C12 muscle side (E = 0.4 MPa), stiff on the PCL-NIH/3T3 tendon side (E = 46 MPa), and intermediate in the interface region (E = 1.0 MPa). Again, both cell lines grew correctly on their respective surfaces and some interfacial features could be observed under confocal microscopy. This type of approach seems quite promising, because it is relatively easy to set up [302]. The next step would be to use more relevant cell types, as well as performing stimulation inducing mechanical stretching to stress the three areas showing the different mechanical properties, thus leading to different mechanotransduction signals.

It can be seen that the literature on the subject is still quite poor, probably because the biological phenomena leading to the formation of the MTJ have not yet been clearly established. Attempts to engineer such junctions could thus also be helpful for fundamental studies in embryology, for instance, to evaluate hypotheses regarding mechanisms that are potentially involved in the development of such a complex structure.

5. Conclusions and Perspectives—New Challenges

To conclude, it is obvious that tissue engineering of the musculo-tendinous system is still in its early stages. The investigated protocols summarized in the review are helpful for proposing new perspectives in tendon and muscle healing, which are capable of overcoming the limitations of more classic techniques, such as autologous grafts or more recent purely artificial substitutes or cell therapy. Initially, collagen appeared to be the material of reference, as this fibrillary protein is present both in tendon and muscle. However, the variability of the sources and the various limitations mentioned in this text have led to parallel investigations on synthetic polymers, such as PCL for muscle or PLA, mostly for tendons. Of the shapes used, porous gels and fibers that are produced by electrospinning

are the most widely developed. However, there is not yet any consensus regarding the final choice for the material, cell source or stimulation protocol.

Biomimetism or bio-inspiration will probably guide future investigations and this requires in-depth knowledge of the tissue to be reconstructed. In this review, we attempted to follow this process, starting with the biological and mechanical characterization of native tissues (tendon, muscle, and the myotendinous junction), ending with the biological and mechanical outcomes of the reconstructed tissues, as they have been described. Very interestingly, while muscle and tendon might seem quite similar in structure at different scales, they nevertheless present properties that are completely different, as a result of different cell densities (poor in tendon, high with very specialized cells in muscle) and the composition of the ECM.

To date, tissue engineering has designed the scaffold that will host the cells and provide the construct with mechanical properties. In the future, it may be interesting to consider it as a trigger for the "right" cells to produce their own ECM, in a way that is mimicking embryogenesis. Subjected to specific external stimuli, the properties expected of new "smart" materials would thus be different: guiding cell differentiation thanks to their nano/ultrastructure, releasing specific factors on the basis of defined kinetics to mimic the different steps in development, providing signals for cell colonization/differentiation status, or interacting with the new synthesized ECM to provide genuinely hybrid materials with adaptive mechanical properties.

Funding: This work was carried out and funded in the context of the Labex MS2T. It was supported by the French Government, through the program "Investments for the future" managed by the National Agency for Research (Reference ANR-11-IDEX-0004-02) and by Région Picardie (INTIM project).

Conflicts of Interest: The authors declare no conflicts of interest.

Abbreviations

EDC	(1-ethyl-3-(3-dimethylaminopropyl) carbodiimide hydrochloride
ASC	Adipose stem cell
ATMP	Advanced therapy medicinal products
bFGF	Basic fibroblast growth factor
BMSC	Bone marrow stem cell
BMP	Bone morphogenetic protein
JNK	c-Jun NH2-terminal kinases
camk	calmodulin-dependent protein kinases
calc	Calcineurin
Calp	Calpain
COL	Collagen
CTGF	Connective tissue growth factor
CTS	Cyclic tensile strain
DF	Dermal fibroblast
EM	Elastic modulus
ELAC	Electrochemically-aligned collagen
EDGE	Ethylene-glycol-diglycidyl-ether
ECM	Extracellular matrix
ERK	Extracellular signal-regulated kinases
Eya	Eye absent homolog
FAP	Fibro-adipogenic progenitors
FGF	Fibroblast growth factor
FAK	Focal adhesion Kinase
FIB	Focused ion beam
GelMA	Gelatin methacryloyl
GPa	GigaPascal
T_g	Glass transition

GO	Graphene oxydative
GDF	Growth and differentiation factor
HGH	Hepatocyte growth factor
IGF	Insulin-like growth factor
IL	Interleukin
LS	Linear stiffness
MKKs	McKusick-Kaufman syndrome
MSC	Mesenchymal stem cell
p38	Mitogen-activated protein kinases
MWCNT	Multiwalled carbon nanotubes
MPCs	Muscle progenitor cells
MRF	Myogenic regulatory factor
MHC	Myosin heavy chain
MTJ	Myotendinous junction
NHS	*N*-Hydroxysuccinimide
OA	Oxidized alginate
PI3K	Phosphatidylinositol-3-kinase
PDGF	Platelet derived growth factor
PEEUR	Poly (esterurethane urea)
PCL	Poly (ε-caprolactone)
PEG	Poly ethylene glycol
PLGA	poly lactic-co-glycolic acid
PLLA	Poly-L-lactic acid
PAA	Poly(acrylic acid)
PCL	Poly(caprolactone)
	Poly(L-lactide-co-D,L-lactide)
PLA	Poly(l/d)lactide
PVA	Poly(vinyl alcohol)
PLGA	Poly[(lactic acid)-co-(glycolic acid)]
PANi	Polyaniline
PDMS	Polydimethylsiloxane
PGA	Poly(glycolic acid)
PU	Polyurethane
PVDF	Polyvinylidene fluoride
PG	Proteoglycan
Scs	Satellite cells
SEM	Scanning electron microscopy
SCX	Scleraxis
SDS	Sodium dodecyl sulfate
sGC	Soluble guanylyl cyclase
TNC	Tenascin-C
TDSC	Tendon derived stem cell
TSPC	Tendon stem/progenitor cells
TNMD	Tenomodulin
TE	Tissue engineering
TGF-β	Transforming growth factor-β
TEM	Transmission electron microscopy
TnBP	Tri(n-butyl)phosphate
UTS	Ultimate tensile strength
VEGF	Vascular endothelial growth factor
VMLs	Volumetric muscle losses
YM	Young modulus (E)

References

1. Yang, J.; Zhang, Y.S.; Yue, K.; Khademhosseini, A. Cell-laden hydrogels for osteochondral and cartilage tissue engineering. *Acta Biomater.* **2017**, *57*, 1–25. [CrossRef] [PubMed]
2. Huang, B.J.; Hu, J.C.; Athanasiou, K.A. Cell-based tissue engineering strategies used in the clinical repair of articular cartilage. *Biomaterials* **2016**, *98*, 1–22. [CrossRef] [PubMed]
3. Henkel, J.; Woodruff, M.A.; Epari, D.R.; Steck, R.; Glatt, V.; Dickinson, I.C.; Choong, P.F.M.; Schuetz, M.A.; Hutmacher, D.W. Bone Regeneration Based on Tissue Engineering Conceptions-A 21st Century Perspective. *Bone Res.* **2013**, *1*, 216–248. [CrossRef] [PubMed]
4. Font Tellado, S.; Balmayor, E.R.; Van Griensven, M. Strategies to engineer tendon/ligament-to-bone interface: Biomaterials, cells and growth factors. *Adv. Drug Deliv. Rev.* **2015**, *94*, 126–140. [CrossRef] [PubMed]
5. Kirkendall, D.T.; Garrett, W.E. Function and biomechanics of tendons. *Scand. J. Med. Sci. Sports* **2007**, *7*, 62–66. [CrossRef]
6. Hart, D.A.; Kydd, A.; Reno, C. Gender and pregnancy affect neuropeptide responses of the rabbit Achilles tendon. *Clin. Orthop.* **1999**, *365*, 237–246. [CrossRef]
7. Birch, H.L. Tendon matrix composition and turnover in relation to functional requirements. *Int. J. Exp. Pathol.* **1997**, *88*, 241–248. [CrossRef] [PubMed]
8. Kannus, P. Structure of the tendon connective tissue. *Scand. J. Med. Sci. Sports* **2000**, *10*, 312–320. [CrossRef] [PubMed]
9. Silver, F.H.; Freeman, J.W.; Seehra, G.P. Collagen self-assembly and the development of tendon mechanical properties. *J. Biomech.* **2003**, *36*, 1529–1553. [CrossRef]
10. Rigby, B.J.; Hirai, N.; Spikes, J.D.; Eyring, H. The Mechanical Properties of Rat Tail Tendon. *J. Gen. Physiol.* **1959**, *43*, 265–283. [CrossRef] [PubMed]
11. Danielson, K.G.; Baribault, H.; Holmes, D.F.; Graham, H.; Kadler, K.E.; Iozzo, R.V. Targeted disruption of decorin leads to abnormal collagen fibril morphology and skin fragility. *J. Cell Biol.* **1997**, *136*, 729–743. [CrossRef] [PubMed]
12. Derwin, K.A.; Soslowsky, L.J.; Kimura, J.H.; Plaas, A.H. Proteoglycans and glycosaminoglycan fine structure in the mouse tail tendon fascicle. *J. Orthop. Res. Off. Publ. Orthop. Res. Soc.* **2000**, *19*, 269–277. [CrossRef]
13. Kuc, I.M.; Scott, P.G. Increased Diameters of Collagen Fibrils Precipitated in vitro in the Presence of Decorin from Various Connective Tissues. *Connect. Tissue Res.* **1997**, *36*, 287–296. [CrossRef] [PubMed]
14. Schönherr, E.; Witsch-Prehm, P.; Harrach, B.; .Robenek, H.; Rauterberg, J.; Kresse, H. Interaction of biglycan with type I collagen. *J. Biol. Chem.* **1995**, *270*, 2776–2783. [CrossRef] [PubMed]
15. Ezura, Y.; Chakravarti, S.; Oldberg, A.; Chervoneva, I.; Birk, D.E. Differential expression of lumican and fibromodulin regulate collagen fibrillogenesis in developing mouse tendons. *J. Cell Biol.* **2000**, *151*, 779–788. [CrossRef] [PubMed]
16. Mccormick, R.J. Extracellular modifications to muscle collagen: Implications for meat quality. *Poult. Sci.* **1999**, *78*, 785–791. [CrossRef] [PubMed]
17. Vogel, K.G.; Koob, T.J. Structural specialization in tendons under compression. *Int. Rev. Cytol.* **1989**, *115*, 267–293. [PubMed]
18. Martin, J.A.; Mehr, D.; Pardubsky, P.D.; Buckwalter, J.A. The role of tenascin-C in adaptation of tendons to compressive loading. *Biorheology* **2003**, *40*, 321–329. [PubMed]
19. Sharma, P.; Maffulli, N. Biology of tendon injury: Healing, modeling and remodeling. *J. Musculoskelet. Neuronal Interact.* **2006**, *6*, 181–190. [PubMed]
20. Sharma, P.; Maffulli, N. Tendon injury and tendinopathy: Healing and repair. *J. Bone Jt. Surg. Am.* **1995**, *87*, 187–202. [CrossRef]
21. Bi, Y.; Ehirchiou, D.; Kilts, T.M.; Inkson, C.A.; Embree, M.C.; Sonoyama, W.; Li, L.; Leet, A.I.; Seo, B.-M.; Zhang, L.; et al. Identification of tendon stem/progenitor cells and the role of the extracellular matrix in their niche. *Nat. Med.* **2007**, *13*, 1219–1227. [CrossRef] [PubMed]
22. Martin, R.B.; Burr, D.B.; Sharkey, N.A.; Fyhrie, D.P. Mechanical Properties of Ligament and Tendon. In *Skeletal Tissue Mechanics*; Springer: New York, NY, USA, 2015; pp. 175–225.
23. Silver, F.H.; Christiansen, D.L.; Snowhill, P.B.; Chen, Y. Role of storage on changes in the mechanical properties of tendon and self-assembled collagen fibers. *Connect. Tissue Res.* **2000**, *41*, 155–164. [CrossRef] [PubMed]

24. Robi, K.; Jakob, N.; Matevz, K.; Matjaz, V. The Physiology of Sports Injuries and Repair Processes. *Curr. Issues Sports Exerc. Med.* **2013**. [CrossRef]
25. Maganaris, C.N. Tensile properties of in vivo human tendinous tissue. *J. Biomech.* **2002**, *35*, 1019–1027. [CrossRef]
26. O'Brien, T.D.; Reeves, N.D.; Baltzopoulos, V.; Jones, D.A.; Maganaris, C.N. Mechanical properties of the patellar tendon in adults and children. *J. Biomech.* **2010**, *43*, 1190–1195. [CrossRef] [PubMed]
27. Voleti, P.B.; Buckley, M.R.; Soslowsky, L.J. Tendon Healing: Repair and Regeneration. *Annu. Rev. Biomed. Eng.* **2012**, *14*, 47–71. [CrossRef] [PubMed]
28. Longo, U.G.; Lamberti, A.; Maffulli, N.; Denaro, V. Tendon augmentation grafts: A systematic review. *Br. Med. Bull.* **2010**, *94*, 165–188. [CrossRef] [PubMed]
29. Docheva, D.; Müller, S.A.; Majewski, M.; Evans, C.H. Biologics for tendon repair. *Adv. Drug Deliv. Rev.* **2015**, *84*, 222–239. [CrossRef] [PubMed]
30. Yin, Z.; Chen, X.; Chen, J.L.; Shen, W.L.; Hieu Nguyen, T.M.; Gao, L.; Ouyang, H.W. The regulation of tendon stem cell differentiation by the alignment of nanofibers. *Biomaterials* **2010**, *31*, 2163–2175. [CrossRef] [PubMed]
31. Bottagisio, M.; Lopa, S.; Granata, V.; Talò, G.; Bazzocchi, C.; Moretti, M.; Lovati, A.B. Different combinations of growth factors for the tenogenic differentiation of bone marrow mesenchymal stem cells in monolayer culture and in fibrin-based three-dimensional constructs. *Differ. Res. Biol. Divers.* **2017**, *95*, 44–53. [CrossRef] [PubMed]
32. Qin, T.-W.; Sun, Y.-L.; Thoreson, A.R.; Steinmann, S.P.; Amadio, P.C.; An, K.-N.; Zhao, C. Effect of mechanical stimulation on bone marrow stromal cell-seeded tendon slice constructs: A potential engineered tendon patch for rotator cuff repair. *Biomaterials* **2015**, *51*, 43–50. [CrossRef] [PubMed]
33. Kishore, V.; Bullock, W.; Sun, X.; Van Dyke, W.S.; Akkus, O. Tenogenic differentiation of human MSCs induced by the topography of electrochemically aligned collagen threads. *Biomaterials* **2012**, *33*, 2137–2144. [CrossRef] [PubMed]
34. Younesi, M.; Islam, A.; Kishore, V.; Anderson, J.M.; Akkus, O. Tenogenic Induction of Human MSCs by Anisotropically Aligned Collagen Biotextiles. *Adv. Funct. Mater.* **2014**, *24*, 5762–5770. [CrossRef] [PubMed]
35. Bosworth, L.A.; Rathbone, S.R.; Bradley, R.S.; Cartmell, S.H. Dynamic loading of electrospun yarns guides mesenchymal stem cells towards a tendon lineage. *J. Mech. Behav. Biomed. Mater.* **2014**, *39*, 175–183. [CrossRef] [PubMed]
36. Sahoo, S.; Ouyang, H.; Goh, J.C.-H.; Tay, T.E.; Toh, S.L. Characterization of a novel polymeric scaffold for potential application in tendon/ligament tissue engineering. *Tissue Eng.* **2006**, *12*, 91–99. [CrossRef] [PubMed]
37. Liu, H.; Fan, H.; Wang, Y.; Toh, S.L.; Goh, J.C.H. The interaction between a combined knitted silk scaffold and microporous silk sponge with human mesenchymal stem cells for ligament tissue engineering. *Biomaterials* **2008**, *29*, 662–674. [CrossRef] [PubMed]
38. Juncosa-Melvin, N.; Shearn, J.T.; Boivin, G.P.; Gooch, C.; Galloway, M.T.; West, J.R.; Nirmalanandhan, V.S.; Bradica, G.; Butler, D.L. Effects of mechanical stimulation on the biomechanics and histology of stem cell-collagen sponge constructs for rabbit patellar tendon repair. *Tissue Eng.* **2006**, *12*, 2291–2300. [CrossRef] [PubMed]
39. Nirmalanandhan, V.S.; Rao, M.; Shearn, J.T.; Juncosa-Melvin, N.; Gooch, C.; Butler, D.L. Effect of scaffold material, construct length and mechanical stimulation on the in vitro stiffness of the engineered tendon construct. *J. Biomech.* **2008**, *41*, 822–828. [CrossRef] [PubMed]
40. Gimble, J.M.; Katz, A.J.; Bunnell, B.A. Adipose-derived stem cells for regenerative medicine. *Circ. Res.* **2007**, *100*, 1249–1260. [CrossRef] [PubMed]
41. Dai, L.; Hu, X.; Zhang, X.; Zhu, J.; Zhang, J.; Fu, X.; Duan, X.; Ao, Y.; Zhou, C. Different tenogenic differentiation capacities of different mesenchymal stem cells in the presence of BMP-12. *J. Transl. Med.* **2015**, *13*, 200. [CrossRef] [PubMed]
42. Schneider, M.; Angele, P.; Järvinen, T.A.H.; Docheva, D. Rescue plan for Achilles: Therapeutics steering the fate and functions of stem cells in tendon wound healing. *Adv. Drug. Deliv. Rev.* 2017. [CrossRef] [PubMed]
43. Reznikoff, C.A.; Brankow, D.W.; Heidelberger, C. Establishment and characterization of a cloned line of C3H mouse embryo cells sensitive to postconfluence inhibition of division. *Cancer Res.* **1973**, *33*, 3231–3238. [PubMed]

44. Guerquin, M.-J.; Charvet, B.; Nourissat, G.; Havis, E.; Ronsin, O.; Bonnin, M.-A.; Ruggiu, M.; Olivera-Martinez, I.; Robert, N.; Lu, Y.; et al. Transcription factor EGR1 directs tendon differentiation and promotes tendon repair. *J. Clin. Investig.* **2015**, *123*, 3564–3576. [CrossRef] [PubMed]
45. Cardwell, R.D.; Kluge, J.A.; Thayer, P.S.; Guelcher, S.A.; Dahlgren, L.A.; Kaplan, D.L.; Goldstein, A.S. Static and cyclic mechanical loading of mesenchymal stem cells on elastomeric, electrospun polyurethane meshes. *J. Biomech. Eng.* **2015**, *137*, 071010. [CrossRef] [PubMed]
46. Cardwell, R.D.; Dahlgren, L.A.; Goldstein, A.S. Electrospun fibre diameter, not alignment, affects mesenchymal stem cell differentiation into the tendon/ligament lineage. *J. Tissue Eng. Regen. Med.* **2014**, *8*, 937–945. [CrossRef] [PubMed]
47. Baudequin, T.; Gaut, L.; Mueller, M.; Huepkes, A.; Glasmacher, B.; Duprez, D.; Bedoui, F.; Legallais, C. The Osteogenic and Tenogenic Differentiation Potential of C3H10T1/2 (Mesenchymal Stem Cell Model) Cultured on PCL/PLA Electrospun Scaffolds in the Absence of Specific Differentiation Medium. *Materils* **2017**, *10*, 1387. [CrossRef] [PubMed]
48. Rui, Y.-F.; Lui, P.P.Y.; Li, G.; Fu, S.C.; Lee, Y.W.; Chan, K.M. Isolation and characterization of multipotent rat tendon-derived stem cells. *Tissue Eng. Part A* **2010**, *16*, 1549–1558. [CrossRef] [PubMed]
49. Lui, P.P.Y.; Wong, O.T.; Lee, Y.W. Transplantation of tendon-derived stem cells pre-treated with connective tissue growth factor and ascorbic acid in vitro promoted better tendon repair in a patellar tendon window injury rat model. *Cytotherapy* **2016**, *18*, 99–112. [CrossRef] [PubMed]
50. Thaker, H.; Sharma, A.K. Engaging stem cells for customized tendon regeneration. *Stem Cells Int.* **2012**, *2012*, 309187. [CrossRef] [PubMed]
51. Caliari, S.R.; Harley, B.A.C. The effect of anisotropic collagen-GAG scaffolds and growth factor supplementation on tendon cell recruitment, alignment, and metabolic activity. *Biomaterials* **2011**, *32*, 5330–5340. [CrossRef] [PubMed]
52. Enea, D.; Henson, F.; Kew, S.; Wardale, J.; Getgood, A.; Brooks, R.; Rushton, N. Extruded collagen fibres for tissue engineering applications: Effect of crosslinking method on mechanical and biological properties. *J. Mater. Sci. Mater. Med.* **2011**, *22*, 1569–1578. [CrossRef] [PubMed]
53. Enea, D.; Gwynne, J.; Kew, S.; Arumugam, M.; Shepherd, J.; Brooks, R.; Ghose, S.; Best, S.; Cameron, R.; Rushton, N. Collagen fibre implant for tendon and ligament biological augmentation. In vivo study in an ovine model. Knee Surg. Sports Traumatol. *Arthrosc. Off. J. ESSKA* **2013**, *21*, 1783–1793. [CrossRef]
54. Surrao, D.C.; Fan, J.C.Y.; Waldman, S.D.; Amsden, B.G. A crimp-like microarchitecture improves tissue production in fibrous ligament scaffolds in response to mechanical stimuli. *Acta Biomater.* **2012**, *8*, 3704–3713. [CrossRef] [PubMed]
55. Grier, W.K.; Iyoha, E.M.; Harley, B.A.C. The influence of pore size and stiffness on tenocyte bioactivity and transcriptomic stability in collagen-GAG scaffolds. *J. Mech. Behav. Biomed. Mater.* **2017**, *65*, 295–305. [CrossRef] [PubMed]
56. Yang, G.; Rothrauff, B.B.; Tuan, R.S. Tendon and ligament regeneration and repair: Clinical relevance and developmental paradigm. *Birth Defects Res. Part C Embryo Today Rev.* **2013**, *99*, 203–222. [CrossRef] [PubMed]
57. Young, M. Stem Cell Applications in Tendon Disorders: A Clinical Perspective. *Stem Cells Int.* **2012**, *2012*, 1–10. [CrossRef] [PubMed]
58. Liu, W.; Yin, L.; Yan, X.; Cui, J.; Liu, W.; Rao, Y.; Sun, M.; Wei, Q.; Chen, F. Directing the Differentiation ofParthenogenetic Stem Cells into Tenocytes for Tissue-Engineered Tendon Regeneration. *Stem Cells Transl. Med.* **2017**, *6*, 196–208. [CrossRef] [PubMed]
59. Rodrigues, M.T.; Reis, R.L.; Gomes, M.E. Engineering tendon and ligament tissues: Present developments towards successful clinical products. *J. Tissue Eng. Regen. Med.* **2013**, *7*, 673–686. [CrossRef] [PubMed]
60. Zhang, F.; Liu, H.; Stile, F.; Lei, M.-P.; Pang, Y.; Oswald, T.M.; Beck, J.; Dorsett-Martin, W.; Lineaweaver, W.C. Effect of vascular endothelial growth factor on rat Achilles tendon healing. *Plast. Reconstr. Surg.* **2003**, *112*, 1613–1619. [CrossRef] [PubMed]
61. Abrahamsson, S.O.; Lundborg, G.; Lohmander, L.S. Recombinant human insulin-like growth factor-I stimulates in vitro matrix synthesis and cell proliferation in rabbit flexor tendon. *J. Orthop. Res. Off. Publ. Orthop. Res. Soc.* **1991**, *9*, 495–502. [CrossRef] [PubMed]
62. Evrova, O.; Buschmann, J. In vitro and in vivo effects of PDGF-BB delivery strategies on tendon healing: A review. *Eur. Cells Mater.* **2017**, *34*, 15–39. [CrossRef] [PubMed]

63. Najafbeygi, A.; Fatemi, M.J.; Lebaschi, A.H.; Mousavi, S.J.; Husseini, S.A.; Niazi, M. Effect of Basic Fibroblast Growth Factor on Achilles Tendon Healing in Rabbit. *World J. Plast. Surg.* **2017**, *6*, 26–32. [PubMed]
64. James, R.; Kesturu, G.; Balian, G.; Chhabra, A.B. Tendon: Biology, biomechanics, repair, growth factors, and evolving treatment options. *J. Hand Surg.* **2008**, *33*, 102–112. [CrossRef] [PubMed]
65. Skutek, M.; van Griensven, M.; Zeichen, J.; Brauer, N.; Bosch, U. Cyclic mechanical stretching modulates secretion pattern of growth factors in human tendon fibroblasts. *Eur. J. Appl. Physiol.* **2001**, *86*, 48–52. [CrossRef] [PubMed]
66. Heinemeier, K.; Langberg, H.; Olesen, J.L.; Kjaer, M. Role of TGF-beta1 in relation to exercise-induced type I collagen synthesis in human tendinous tissue. *J. Appl. Physiol.* **2003**, *95*, 2390–2397. [CrossRef] [PubMed]
67. Heinemeier, K.M.; Kjaer, M. In vivo investigation of tendon responses to mechanical loading. *J. Musculoskelet. Neuronal Interact.* **2011**, *11*, 115–123. [PubMed]
68. Loiselle, A.E.; Yukata, K.; Geary, M.B.; Kondabolu, S.; Shi, S.; Jonason, J.H.; Awad, H.A.; O'Keefe, R.J. Development of antisense oligonucleotide (ASO) technology against Tgf-β signaling to prevent scarring during flexor tendon repair. *J. Orthop. Res. Off. Publ. Orthop. Res. Soc.* **2015**, *33*, 859–866. [CrossRef] [PubMed]
69. Juneja, S.C.; Schwarz, E.M.; O'Keefe, R.J.; Awad, H.A. Cellular and molecular factors in flexor tendon repair and adhesions: A histological and gene expression analysis. Connect. *Tissue Res.* **2013**, *54*, 218–226. [CrossRef] [PubMed]
70. Lou, J.; Tu, Y.; Burns, M.; Silva, M.J.; Manske, P. BMP-12 gene transfer augmentation of lacerated tendon repair. *J. Orthop. Res. Off. Publ. Orthop. Res. Soc.* **2001**, *19*, 1199–1202. [CrossRef]
71. Chan, B.P.; Fu, S.C.; Qin, L.; Rolf, C.; Chan, K.M. Supplementation-time Dependence of Growth Factors in Promoting Tendon Healing. *Clin. Orthop.* **2006**, *448*, 240–247. [CrossRef] [PubMed]
72. Musson, D.S.; Tay, M.L.; Chhana, A.; Pool, B.; Coleman, B.; Naot, D.; Cornish, J. Lactoferrin and parathyroid hormone are not harmful to primary tenocytesin vitro, but PDGF may be. *Muscles Ligaments Tendons J.* **2017**, *7*, 215–222. [CrossRef] [PubMed]
73. Klatte-Schulz, F.; Schmidt, T.; Uckert, M.; Scheffler, S.; Kalus, U.; Rojewski, M.; Schrezenmeier, H.; Pruss, A.; Wildemann, B. Comparative Analysis of Different Platelet Lysates and Platelet Rich Preparations to Stimulate Tendon Cell Biology: An In Vitro Study. *Int. J. Mol. Sci.* **2018**, *19*, 212. [CrossRef] [PubMed]
74. Andia, I.; Martin, J.I.; Maffulli, N. Advances with platelet rich plasma therapies for tendon regeneration. *Expert Opin. Biol. Ther.* **2018**, 1–10. [CrossRef] [PubMed]
75. Govoni, M.; Berardi, A.C.; Muscari, C.; Campardelli, R.; Bonafè, F.; Guarnieri, C.; Reverchon, E.; Giordano, E.; Maffulli, N.; Della Porta, G. An Engineered Multiphase Three-Dimensional Microenvironment to Ensure the Controlled Delivery of Cyclic Strain and Human Growth Differentiation Factor 5 for the Tenogenic Commitment of Human Bone Marrow Mesenchymal Stem Cells. *Tissue Eng. Part A* **2017**, *23*, 811–822. [CrossRef] [PubMed]
76. Vuornos, K.; Björninen, M.; Talvitie, E.; Paakinaho, K.; Kellomäki, M.; Huhtala, H.; Miettinen, S.; Seppänen-Kaijansinkko, R.; Haimi, S. Human Adipose Stem Cells Differentiated on Braided Polylactide Scaffolds Is a Potential Approach for Tendon Tissue Engineering. *Tissue Eng. Part A* **2016**, *22*, 513–523. [CrossRef] [PubMed]
77. Bhole, A.P.; Flynn, B.P.; Liles, M.; Saeidi, N.; Dimarzio, C.A.; Ruberti, J.W. Mechanical strain enhances survivability of collagen micronetworks in the presence of collagenase: Implications for load-bearing matrix growth and stability. *Philos. Trans. A Math. Phys. Eng. Sci.* **2009**, *367*, 3339–3362. [CrossRef] [PubMed]
78. Nabeshima, Y.; Grood, E.S.; Sakurai, A.; Herman, J.H. Uniaxial tension inhibits tendon collagen degradation by collagenase in vitro. *J. Orthop. Res. Off. Publ. Orthop. Res. Soc.* **1996**, *14*, 123–130. [CrossRef] [PubMed]
79. Flynn, B.P.; Bhole, A.P.; Saeidi, N.; Liles, M.; Dimarzio, C.A.; Ruberti, J.W. Mechanical strain stabilizes reconstituted collagen fibrils against enzymatic degradation by mammalian collagenase matrix metalloproteinase 8 (MMP-8). *PLoS ONE* **2010**, *5*, e12337. [CrossRef] [PubMed]
80. Magnusson, S.P.; Langberg, H.; Kjaer, M. The pathogenesis of tendinopathy: Balancing the response to loading. *Nat. Rev. Rheumatol.* **2010**, *6*, 262–268. [CrossRef] [PubMed]
81. Zeichen, J.; van Griensven, M.; Bosch, U. The proliferative response of isolated human tendon fibroblasts to cyclic biaxial mechanical strain. *Am. J. Sports Med.* **2000**, *28*, 888–892. [CrossRef] [PubMed]

82. Yang, G.; Crawford, R.C.; Wang, J.H.-C. Proliferation and collagen production of human patellar tendon fibroblasts in response to cyclic uniaxial stretching in serum-free conditions. *J. Biomech.* **2004**, *37*, 1543–1550. [CrossRef] [PubMed]
83. Gaut, L.; Duprez, D. Tendon development and diseases. Wiley Interdiscip. *Rev. Dev. Biol.* **2016**, *5*, 5–23. [CrossRef]
84. Doroski, D.M.; Levenston, M.E.; Temenoff, J.S. Cyclic tensile culture promotes fibroblastic differentiation of marrow stromal cells encapsulated in poly(ethylene glycol)-based hydrogels. *Tissue Eng. Part A* **2010**, *16*, 3457–3466. [CrossRef] [PubMed]
85. Tanaka, H.; Manske, P.R.; Pruitt, D.L.; Larson, B.J. Effect of cyclic tension on lacerated flexor tendons in vitro. *J. Hand Surg.* **1995**, *20*, 467–473. [CrossRef]
86. Govoni, M.; Muscari, C.; Lovecchio, J.; Guarnieri, C.; Giordano, E. Mechanical Actuation Systems for the Phenotype Commitment of Stem Cell-Based Tendon and Ligament Tissue Substitutes. *Stem Cell Rev.* **2016**, *12*, 189–201. [CrossRef] [PubMed]
87. Kinneberg, K.R.C.; Nirmalanandhan, V.S.; Juncosa-Melvin, N.; Powell, H.M.; Boyce, S.T.; Shearn, J.T.; Butler, D.L. Chondroitin-6-sulfate incorporation and mechanical stimulation increase MSC-collagen sponge construct stiffness. *J. Orthop. Res. Off. Publ. Orthop. Res. Soc.* **2010**, *28*, 1092–1099. [CrossRef] [PubMed]
88. Longo, U.G.; Lamberti, A.; Petrillo, S.; Maffulli, N.; Denaro, V. Scaffolds in Tendon Tissue Engineering. *Stem Cells Int.* **2012**, *2012*. [CrossRef] [PubMed]
89. Müller, S.A.; Dürselen, L.; Heisterbach, P.; Evans, C.; Majewski, M. Effect of a Simple Collagen Type I Sponge for Achilles Tendon Repair in a Rat Model. *Am. J. Sports Med.* **2016**, *44*, 1998–2004. [CrossRef] [PubMed]
90. Gentleman, E.; Lay, A.N.; Dickerson, D.A.; Nauman, E.A.; Livesay, G.A.; Dee, K.C. Mechanical characterization of collagen fibers and scaffolds for tissue engineering. *Biomaterials* **2003**, *24*, 3805–3813. [CrossRef]
91. Cheng, X.; Gurkan, U.A.; Dehen, C.J.; Tate, M.P.; Hillhouse, H.W.; Simpson, G.J.; Akkus, O. An electrochemical fabrication process for the assembly of anisotropically oriented collagen bundles. *Biomaterials* **2008**, *29*, 3278–3288. [CrossRef] [PubMed]
92. Minoura, N.; Aiba, S.; Gotoh, Y.; Tsukada, M.; Imai, Y. Attachment and growth of cultured fibroblast cells on silk protein matrices. *J. Biomed. Mater. Res.* **1995**, *29*, 1215–1221. [CrossRef] [PubMed]
93. Kuo, C.K.; Marturano, J.E.; Tuan, R.S. Novel strategies in tendon and ligament tissue engineering: Advanced biomaterials and regeneration motifs. *Sports Med. Arthrosc. Rehabil. Ther. Technol.* **2010**, *2*, 20. [CrossRef] [PubMed]
94. Li, G.; Li, Y.; Chen, G.; He, J.; Han, Y.; Wang, X.; Kaplan, D.L. Silk-based biomaterials in biomedical textiles and fiber-based implants. *Adv. Healthc. Mater.* **2015**, *4*, 1134–1151. [CrossRef] [PubMed]
95. Ghiasi, M.; Naghashzargar, E.; Semnani, D. Silk Fibroin Nano-Coated Textured Silk Yarn by Electrospinning Method for Tendon and Ligament Scaffold Application. *Nano Hybrids* **2014**, *7*, 35–51. [CrossRef]
96. Chen, J.L.; Yin, Z.; Shen, W.L.; Chen, X.; Heng, B.C.; Zou, X.H.; Ouyang, H.W. Efficacy of hESC-MSCs in knitted silk-collagen scaffold for tendon tissue engineering and their roles. *Biomaterials* **2010**, *31*, 9438–9451. [CrossRef] [PubMed]
97. Zheng, Z.; Ran, J.; Chen, W.; Hu, Y.; Zhu, T.; Chen, X.; Yin, Z.; Heng, B.C.; Feng, G.; Le, H.; Tang, C.; Huang, J.; Chen, Y.; Zhou, Y.; Dominique, P.; Shen, W.; Ouyang, H.-W. Alignment of collagen fiber in knitted silk scaffold for functional massive rotator cuff repair. *Acta Biomater.* **2017**, *51*, 317–329. [CrossRef] [PubMed]
98. Zhi, Y.; Liu, W.; Zhang, P.; Jiang, J.; Chen, S. Electrospun silk fibroin mat enhances tendon-bone healing in a rabbit extra-articular model. *Biotechnol. Lett.* **2016**, *38*, 1827–1835. [CrossRef] [PubMed]
99. Malcarney, H.L.; Bonar, F.; Murrell, G.A.C. Early Inflammatory Reaction after Rotator Cuff Repair with a Porcine Small Intestine Submucosal Implant: A Report of 4 Cases. *Am. J. Sports Med.* **2005**, *33*, 907–911. [CrossRef] [PubMed]
100. Mallick, K.K.; Cox, S.C. Biomaterial scaffolds for tissue engineering. *Front. Biosci. Elite Ed.* **2013**, *5*, 341–360. [CrossRef] [PubMed]
101. Kim, B.S.; Mooney, D.J. Development of biocompatible synthetic extracellular matrices for tissue engineering. *Trends Biotechnol.* **1998**, *16*, 224–230. [CrossRef]
102. Place, E.S.; George, J.H.; Williams, C.K.; Stevens, M.M. Synthetic polymer scaffolds for tissue engineering. *Chem. Soc. Rev.* **2009**, *38*, 1139–1151. [CrossRef] [PubMed]

103. Peter, S.J.; Miller, M.J.; Yasko, A.W.; Yaszemski, M.J.; Mikos, A.G. Polymer concepts in tissue engineering. *J. Biomed. Mater. Res.* **1998**, *43*, 422–427. [CrossRef]
104. Wang, X.; Ding, B.; Li, B. Biomimetic electrospun nanofibrous structures for tissue engineering. *Mater. Today Kidlington Engl.* **2013**, *16*, 229–241. [CrossRef] [PubMed]
105. Moffat, K.L.; Kwei, A.S.-P.; Spalazzi, J.P.; Doty, S.B.; Levine, W.N.; Lu, H.H. Novel nanofiber-based scaffold for rotator cuff repair and augmentation. *Tissue Eng. Part A* **2009**, *15*, 115–126. [CrossRef] [PubMed]
106. Erisken, C.; Zhang, X.; Moffat, K.L.; Levine, W.N.; Lu, H.H. Scaffold fiber diameter regulates human tendon fibroblast growth and differentiation. *Tissue Eng. Part A* **2013**, *19*, 519–528. [CrossRef] [PubMed]
107. Xu, Y.; Wu, J.; Wang, H.; Li, H.; Di, N.; Song, L.; Li, S.; Li, D.; Xiang, Y.; Liu, W.; Mo, X.; Zhou, Q. Fabrication of electrospun poly(L-lactide-co-ε-caprolactone)/collagen nanoyarn network as a novel, three-dimensional, macroporous, aligned scaffold for tendon tissue engineering. *Tissue Eng. Part C Methods* **2013**, *19*, 925–936. [CrossRef] [PubMed]
108. Horan, R.L.; Collette, A.L.; Lee, C.; Antle, K.; Chen, J.; Altman, G.H. Yarn design for functional tissue engineering. *J. Biomech.* **2006**, *39*, 2232–2240. [CrossRef] [PubMed]
109. Wang, X.; Han, C.; Hu, X.; Sun, H.; You, C.; Gao, C.; Haiyang, Y. Applications of knitted mesh fabrication techniques to scaffolds for tissue engineering and regenerative medicine. *J. Mech. Behav. Biomed. Mater.* **2011**, *4*, 922–932. [CrossRef] [PubMed]
110. Park, S.H.; Choi, Y.-J.; Moon, S.W.; Lee, B.H.; Shim, J.-H.; Cho, D.-W.; Wang, J.H. Three-Dimensional Bio-Printed Scaffold Sleeves With Mesenchymal Stem Cells for Enhancement of Tendon-to-Bone Healing in Anterior Cruciate Ligament Reconstruction Using Soft-Tissue Tendon Graft. *Arthroscopy* **2018**, *34*, 166–179. [CrossRef] [PubMed]
111. Mkhabela, V.J.; Ray, S.S. Poly(epsilon-caprolactone) nanocomposite scaffolds for tissue engineering: A brief overview. *J. Nanosci. Nanotechnol.* **2014**, *14*, 535–545. [CrossRef] [PubMed]
112. Saini, P.; Arora, M.; Kumar, M.N.V.R. Poly(lactic acid) blends in biomedical applications. *Adv. Drug Deliv. Rev.* **2016**, *107*, 47–59. [CrossRef] [PubMed]
113. Zhao, W.; Li, J.; Jin, K.; Liu, W.; Qiu, X.; Li, C. Fabrication of functional PLGA-based electrospun scaffolds and their applications in biomedical engineering. *Mater. Sci. Eng. C Mater. Biol. Appl.* **2016**, *59*, 1181–1194. [CrossRef] [PubMed]
114. Sarkar, D.; Yang, J.-C.; Gupta, A.S.; Lopina, S.T. Synthesis and characterization of L-tyrosine based polyurethanes for biomaterial applications. *J. Biomed. Mater. Res. A* **2009**, *90*, 263–271. [CrossRef] [PubMed]
115. Badylak, S.F.; Gilbert, T.W. Immune response to biologic scaffold materials. *Semin. Immunol.* **2008**, *20*, 109–116. [CrossRef] [PubMed]
116. Glowacki, J.; Mizuno, S. Collagen scaffolds for tissue engineering. *Biopolymers* **2008**, *89*, 338–344. [CrossRef] [PubMed]
117. Schoof, H.; Apel, J.; Heschel, I.; Rau, G. Control of pore structure and size in freeze-dried collagen sponges. *J. Biomed. Mater. Res.* **2001**, *58*, 352–357. [CrossRef] [PubMed]
118. Haugh, M.G.; Murphy, C.M.; O'Brien, F.J. Novel freeze-drying methods to produce a range of collagen-glycosaminoglycan scaffolds with tailored mean pore sizes. *Tissue Eng. Part C Methods* **2010**, *16*, 887–894. [CrossRef] [PubMed]
119. De France, K.J.; Xu, F.; Hoare, T. Structured Macroporous Hydrogels: Progress, Challenges, and Opportunities. *Adv. Healthc. Mater.* **2018**, *7*. [CrossRef] [PubMed]
120. Butler, D.L.; Juncosa-Melvin, N.; Boivin, G.P.; Galloway, M.T.; Shearn, J.T.; Gooch, C.; Awad, H. Functionaltissue engineering for tendon repair: A multidisciplinary strategy using mesenchymal stem cells, bioscaffolds, and mechanical stimulation. *J. Orthop. Res. Off. Publ. Orthop. Res. Soc.* **2008**, *26*, 1–9. [CrossRef] [PubMed]
121. Kato, Y.P.; Christiansen, D.L.; Hahn, R.A.; Shieh, S.J.; Goldstein, J.D.; Silver, F.H. Mechanical properties of collagen fibres: A comparison of reconstituted and rat tail tendon fibres. *Biomaterials* **1989**, *10*, 38–42. [CrossRef]
122. Kew, S.J.; Gwynne, J.H.; Enea, D.; Abu-Rub, M.; Pandit, A.; Zeugolis, D.; Brooks, R.A.; Rushton, N.; Best, S.M.; Cameron, R.E. Regeneration and repair of tendon and ligament tissue using collagen fibre biomaterials. *Acta Biomater.* **2011**, *7*, 3237–3247. [CrossRef] [PubMed]
123. Silver, F.H.; Trelstad, R.L. Type I collagen in solution. Structure and properties of fibril fragments. *J. Biol. Chem.* **1980**, *255*, 9427–9433. [PubMed]

124. Zeugolis, D.I.; Paul, G.R.; Attenburrow, G. Cross-linking of extruded collagen fibers—A biomimetic three-dimensional scaffold for tissue engineering applications. *J. Biomed. Mater. Res. A* **2009**, *89*, 895–908. [CrossRef] [PubMed]
125. Ahmad, Z.; Shepherd, J.H.; Shepherd, D.V.; Ghose, S.; Kew, S.J.; Cameron, R.E.; Best, S.M.; Brooks, R.A.; Wardale, J.; Rushton, N. Effect of 1-ethyl-3-(3-dimethylaminopropyl) carbodiimide and N-hydroxysuccinimide concentrations on the mechanical and biological characteristics of cross-linked collagen fibres for tendon repair. *Regen. Biomater.* **2015**, *2*, 77–85. [CrossRef] [PubMed]
126. Gurkan, U.A.; Cheng, X.; Kishore, V.; Uquillas, J.A.; Akkus, O. Comparison of morphology, orientation, and migration of tendon derived fibroblasts and bone marrow stromal cells on electrochemically aligned collagen constructs. *J. Biomed. Mater. Res. A* **2010**, *94*, 1070–1079. [CrossRef] [PubMed]
127. Kishore, V.; Paderi, J.E.; Akkus, A.; Smith, K.M.; Balachandran, D.; Beaudoin, S.; Panitch, A.; Akkus, O. Incorporation of a decorin biomimetic enhances the mechanical properties of electrochemically aligned collagen threads. *Acta Biomater.* **2011**, *7*, 2428–2436. [CrossRef] [PubMed]
128. Uquillas, J.A.; Kishore, V.; Akkus, O. Effects of phosphate-buffered saline concentration and incubation time on the mechanical and structural properties of electrochemically aligned collagen threads. *Biomed. Mater.* **2011**, *6*, 035008. [CrossRef] [PubMed]
129. Uquillas, J.A.; Akkus, O. Modeling the electromobility of type-I collagen molecules in the electrochemical fabrication of dense and aligned tissue constructs. *Ann. Biomed. Eng.* **2012**, *40*, 1641–1653. [CrossRef] [PubMed]
130. Alfredo Uquillas, J.; Kishore, V.; Akkus, O. Genipin crosslinking elevates the strength of electrochemically aligned collagen to the level of tendons. *J. Mech. Behav. Biomed. Mater.* **2012**, *15*, 176–189. [CrossRef] [PubMed]
131. Kishan, A.P.; Cosgriff-Hernandez, E.M. Recent advancements in electrospinning design for tissue engineering applications: A review. *J. Biomed. Mater. Res. A* **2017**, *105*, 2892–2905. [CrossRef] [PubMed]
132. Li, Z.; Wang, C. *One-Dimensional Nanostructures: Electrospinning Technique and Unique Nanofibers*; SpringerBriefs in Materials; Springer: Berlin/Heidelberg, Germany, 2013; ISBN 978-3-642-36426-6.
133. Teh, T.K.H.; Toh, S.-L.; Goh, J.C.H. Aligned fibrous scaffolds for enhanced mechanoresponse and tenogenesis of mesenchymal stem cells. *Tissue Eng. Part A* **2013**, *19*, 1360–1372. [CrossRef] [PubMed]
134. Chen, C.-H.; Chen, S.-H.; Kuo, C.-Y.; Li, M.-L.; Chen, J.-P. Response of Dermal Fibroblasts to Biochemical and Physical Cues in Aligned Polycaprolactone/Silk Fibroin Nanofiber Scaffolds for Application in Tendon Tissue Engineering. *Nanomaterials* **2017**, *7*, 219. [CrossRef] [PubMed]
135. Barber, J.G.; Handorf, A.M.; Allee, T.J.; Li, W.-J. Braided nanofibrous scaffold for tendon and ligament tissue engineering. *Tissue Eng. Part A* **2013**, *19*, 1265–1274. [CrossRef] [PubMed]
136. Liu, W.; Lipner, J.; Moran, C.H.; Feng, L.; Li, X.; Thomopoulos, S.; Xia, Y. Generation of electrospun nanofibers with controllable degrees of crimping through a simple, plasticizer-based treatment. *Adv. Mater.* **2015**, *27*, 2583–2588. [CrossRef] [PubMed]
137. Reneker, D.H.; Chun, I. Nanometre diameter fibres of polymer, produced by electrospinning. *Nanotechnology* **1996**, *7*, 216. [CrossRef]
138. Voorneveld, J.; Oosthuysen, A.; Franz, T.; Zilla, P.; Bezuidenhout, D. Dual electrospinning with sacrificial fibers for engineered porosity and enhancement of tissue ingrowth. *J. Biomed. Mater. Res. B Appl. Biomater.* **2017**, *105*, 1559–1572. [CrossRef] [PubMed]
139. Jha, B.S.; Colello, R.J.; Bowman, J.R.; Sell, S.A.; Lee, K.D.; Bigbee, J.W.; Bowlin, G.L.; Chow, W.N.; Mathern, B.E.; Simpson, D.G. Two pole air gap electrospinning: Fabrication of highly aligned, three-dimensional scaffolds for nerve reconstruction. *Acta Biomater.* **2011**, *7*, 203–215. [CrossRef] [PubMed]
140. Pant, H.R.; Neupane, M.P.; Pant, B.; Panthi, G.; Oh, H.-J.; Lee, M.H.; Kim, H.Y. Fabrication of highly porous poly (ε-caprolactone) fibers for novel tissue scaffold via water-bath electrospinning. *Colloids Surf. B Biointerfaces* **2011**, *88*, 587–592. [CrossRef] [PubMed]
141. Xu, Y.; Dong, S.; Zhou, Q.; Mo, X.; Song, L.; Hou, T.; Wu, J.; Li, S.; Li, Y.; Li, P.; Gan, Y.; Xu, J. The effect of mechanical stimulation on the maturation of TDSCs-poly(L-lactide-co-e-caprolactone)/collagen scaffold constructs for tendon tissue engineering. *Biomaterials* **2014**, *35*, 2760–2772. [CrossRef] [PubMed]
142. Lee, N.M.; Erisken, C.; Iskratsch, T.; Sheetz, M.; Levine, W.N.; Lu, H.H. Polymer fiber-based models of connective tissue repair and healing. *Biomaterials* **2017**, *112*, 303–312. [CrossRef] [PubMed]

143. Bosworth, L.A.; Turner, L.-A.; Cartmell, S.H. State of the art composites comprising electrospun fibres coupled with hydrogels: A review. *Nanomed. Nanotechnol. Biol. Med.* **2013**, *9*, 322–335. [CrossRef] [PubMed]
144. Aibibu, D.; Hild, M.; Wöltje, M.; Cherif, C. Textile cell-free scaffolds for in situ tissue engineering applications. *J. Mater. Sci. Mater. Med.* **2016**, *27*, 63. [CrossRef] [PubMed]
145. Chen, X.; Qi, Y.-Y.; Wang, L.-L.; Yin, Z.; Yin, G.-L.; Zou, X.-H.; Ouyang, H.-W. Ligament regeneration using a knitted silk scaffold combined with collagen matrix. *Biomaterials* **2008**, *29*, 3683–3692. [CrossRef] [PubMed]
146. Janssen, I.; Heymsfield, S.B.; Wang, Z.M.; Ross, R. Skeletal muscle mass and distribution in 468 men and women aged 18-88 yr. *J. Appl. Physiol.* **2000**, *89*, 81–88. [CrossRef] [PubMed]
147. Frontera, W.R.; Ochala, J. Skeletal muscle: A brief review of structure and function. *Calcif. Tissue Int.* **2015**, *96*, 183–195. [CrossRef] [PubMed]
148. Huard, J.; Li, Y.; Fu, F.H. Muscle injuries and repair: Current trends in research. *J. Bone Jt. Surg. Am.* **2002**, *84*, 822–832. [CrossRef]
149. Gillies, A.R.; Lieber, R.L. Structure and function of the skeletal muscle extracellular matrix. *Muscle Nerve* **2011**, *44*, 318–331. [CrossRef] [PubMed]
150. Roman, W.; Gomes, E.R. Nuclear positioning in skeletal muscle. *Semin. Cell Dev. Biol.* 2017. [CrossRef] [PubMed]
151. Greising, S.M.; Gransee, H.M.; Mantilla, C.B.; Sieck, G.C. Systems biology of skeletal muscle: Fiber type as an organizing principle. Wiley Interdiscip. *Rev. Syst. Biol. Med.* **2012**, *4*, 457–473. [CrossRef] [PubMed]
152. Bottinelli, R.; Reggiani, C. Human skeletal muscle fibres: Molecular and functional diversity. *Prog. Biophys. Mol. Biol.* **2000**, *73*, 195–262. [CrossRef]
153. Collinsworth, A.M.; Zhang, S.; Kraus, W.E.; Truskey, G.A. Apparent elastic modulus and hysteresis of skeletal muscle cells throughout differentiation. *Am. J. Physiol. Cell Physiol.* **2002**, *283*, C1219–C1227. [CrossRef] [PubMed]
154. Heinemeier, K.M.; Schjerling, P.; Heinemeier, J.; Magnusson, S.P.; Kjaer, M. Lack of tissue renewal in human adult Achilles tendon is revealed by nuclear bomb (14)C. *FASEB J. Off. Publ. Fed. Am. Soc. Exp. Biol.* **2013**, *27*, 2074–2079. [CrossRef]
155. Relaix, F.; Zammit, P.S. Satellite cells are essential for skeletal muscle regeneration: The cell on the edge returns centre stage. *Development* **2012**, *139*, 2845–2856. [CrossRef] [PubMed]
156. Kuang, S.; Gillespie, M.A.; Rudnicki, M.A. Niche regulation of muscle satellite cell self-renewal and differentiation. *Cell Stem Cell* **2008**, *2*, 22–31. [CrossRef] [PubMed]
157. Yin, H.; Price, F.; Rudnicki, M.A. Satellite cells and the muscle stem cell niche. *Physiol. Rev.* **2013**, *93*, 23–67. [CrossRef] [PubMed]
158. Judson, R.N.; Low, M.; Eisner, C.; Rossi, F.M. Isolation, Culture, and Differentiation of Fibro/Adipogenic Progenitors (FAPs) from Skeletal Muscle. *Methods Mol. Biol.* **2017**, *1668*, 93–103. [CrossRef] [PubMed]
159. Counsel, P.; Breidahl, W. Muscle injuries of the lower leg. Semin. *Musculoskelet. Radiol.* **2010**, *14*, 162–175. [CrossRef] [PubMed]
160. 2016 Plastic Surgery Statistics. Available online: https://www.plasticsurgery.org/news/plastic-surgery-statistics?sub=2016+Plastic+Surgery+Statistics (accessed on 22 May 2018).
161. Järvinen, T.A.H.; Järvinen, T.L.N.; Kääriäinen, M.; Kalimo, H.; Järvinen, M. Muscle injuries: Biology and treatment. *Am. J. Sports Med.* **2005**, *33*, 745–764. [CrossRef] [PubMed]
162. Äärimaa, V.; Kääriäinen, M.; Vaittinen, S.; Tanner, J.; Järvinen, T.; Best, T.; Kalimo, H. Restoration of myofiber continuity after transection injury in the rat soleus. *Neuromuscular Disord.* **2004**, *14*, 421–428. [CrossRef] [PubMed]
163. Kääriäinen, M.; Järvinen, T.; Järvinen, M.; Rantanen, J.; Kalimo, H. Relation between myofibers and connective tissue during muscle injury repair. *Scand. J. Med. Sci. Sports* **2000**, *10*, 332–337. [CrossRef] [PubMed]
164. Kasukonis, B.; Kim, J.; Brown, L.; Jones, J.; Ahmadi, S.; Washington, T.; Wolchok, J. Codelivery of Infusion Decellularized Skeletal Muscle with Minced Muscle Autografts Improved Recovery from Volumetric Muscle Loss Injury in a Rat Model. *Tissue Eng. Part A* **2016**, *22*, 1151–1163. [CrossRef] [PubMed]
165. Mariscalco, M.W.; Magnussen, R.A.; Mehta, D.; Hewett, T.E.; Flanigan, D.C.; Kaeding, C.C. Autograft versus nonirradiated allograft tissue for anterior cruciate ligament reconstruction: A systematic review. *Am. J. Sports Med.* **2014**, *42*, 492–499. [CrossRef] [PubMed]

166. Reece, E.M.; Oishi, S.N.; Ezaki, M. Brachioradialis flap for coverage after elbow flexion contracture release. *Tech. Hand Up. Extrem. Surg.* **2010**, *14*, 125–128. [CrossRef] [PubMed]
167. Vang, P. Advantages and Disadvantages between Allograft Versus Autograft in Anterior Cruciate Ligament Replacement. Available online: http://hdl.handle.net/10057/957 (accessed on 21 May 2006).
168. Casaroli-Marano, R.P.; Tabera, J.; Vilarrodona, A.; Trias, E. Regulatory issues in cell-based therapy for clinical purposes. *Dev. Ophthalmol.* **2014**, *53*, 189–200. [CrossRef] [PubMed]
169. Shadrin, I.Y.; Khodabukus, A.; Bursac, N. Striated Muscle Function, Regeneration, and Repair. *Cell. Mol. Life Sci.* **2016**, *73*, 4175–4202. [CrossRef] [PubMed]
170. Engler, A.J.; Griffin, M.A.; Sen, S.; Bönnemann, C.G.; Sweeney, H.L.; Discher, D.E. Myotubes differentiate optimally on substrates with tissue-like stiffness: Pathological implications for soft or stiff microenvironments. *J. Cell Biol.* **2004**, *166*, 877–887. [CrossRef] [PubMed]
171. Valentin, J.E.; Turner, N.J.; Gilbert, T.W.; Badylak, S.F. Functional Skeletal Muscle Formation with a Biologic Scaffold. *Biomaterials* **2010**, *31*, 7475–7484. [CrossRef] [PubMed]
172. Fishman, J.M.; Tyraskis, A.; Maghsoudlou, P.; Urbani, L.; Totonelli, G.; Birchall, M.A.; De Coppi, P. Skeletal muscle tissue engineering: Which cell to use? *Tissue Eng. Part B Rev.* **2013**, *19*, 503–515. [CrossRef] [PubMed]
173. Hashimoto, S.; Sato, F.; Uemura, R.; Nakajima, A. Effect of Pulsatile Electric Field on Cultured Muscle Cells In Vitro. *J. Syst. Cybern. Inform.* **2012**, *10*, 1–6.
174. Pennisi, C.P.; Olesen, C.G.; de Zee, M.; Rasmussen, J.; Zachar, V. Uniaxial Cyclic Strain Drives Assembly and Differentiation of Skeletal Myocytes. *Tissue Eng. Part A* **2011**, *17*, 2543–2550. [CrossRef] [PubMed]
175. Boonen, K.J.M.; Langelaan, M.L.P.; Polak, R.B.; van der Schaft, D.W.J.; Baaijens, F.P.T.; Post, M.J. Effects of a combined mechanical stimulation protocol: Value for skeletal muscle tissue engineering. *J. Biomech.* **2010**, *43*, 1514–1521. [CrossRef] [PubMed]
176. Okano, T.; Satoh, S.; Oka, T.; Matsuda, T. Tissue engineering of skeletal muscle. Highly dense, highly oriented hybrid muscular tissues biomimicking native tissues. *ASAIO J.* **1997**, *43*, M749–M753. [CrossRef] [PubMed]
177. Baniasadi, H.; Mashayekhan, S.; Fadaoddini, S.; Haghirsharifzamini, Y. Design, fabrication and characterization of oxidized alginate-gelatin hydrogels for muscle tissue engineering applications. *J. Biomater. Appl.* **2016**, *31*, 152–161. [CrossRef] [PubMed]
178. Lam, M.T.; Sim, S.; Zhu, X.; Takayama, S. The effect of continuous wavy micropatterns on silicone substrates on the alignment of skeletal muscle myoblasts and myotubes. *Biomaterials* **2006**, *27*, 4340–4347. [CrossRef] [PubMed]
179. Bajaj, P.; Rivera, J.A.; Marchwiany, D.; Solovyeva, V.; Bashir, R. Graphene-based patterning and differentiation of C2C12 myoblasts. *Adv. Healthc. Mater.* **2014**, *3*, 995–1000. [CrossRef] [PubMed]
180. Altomare, L.; Gadegaard, N.; Visai, L.; Tanzi, M.C.; Farè, S. Biodegradable microgrooved polymeric surfaces obtained by photolithography for skeletal muscle cell orientation and myotube development. *Acta Biomater.* **2010**, *6*, 1948–1957. [CrossRef] [PubMed]
181. Charest, J.L.; García, A.J.; King, W.P. Myoblast alignment and differentiation on cell culture substrates with microscale topography and model chemistries. *Biomaterials* **2007**, *28*, 2202–2210. [CrossRef] [PubMed]
182. Costantini, M.; Testa, S.; Fornetti, E.; Barbetta, A.; Trombetta, M.; Cannata, S.M.; Gargioli, C.; Rainer, A. Engineering Muscle Networks in 3D Gelatin Methacryloyl Hydrogels: Influence of Mechanical Stiffness and Geometrical Confinement. *Front. Bioeng. Biotechnol.* **2017**, *5*, 22. [CrossRef] [PubMed]
183. Hosseini, V.; Ahadian, S.; Ostrovidov, S.; Camci-Unal, G.; Chen, S.; Kaji, H.; Ramalingam, M.; Khademhosseini, A. Engineered Contractile Skeletal Muscle Tissue on a Microgrooved Methacrylated Gelatin Substrate. *Tissue Eng. Part A* **2012**, *18*, 2453–2465. [CrossRef] [PubMed]
184. Liao, I.-C.; Liu, J.B.; Bursac, N.; Leong, K.W. Effect of Electromechanical Stimulation on the Maturation of Myotubes on Aligned Electrospun Fibers. *Cell. Mol. Bioeng.* **2008**, *1*, 133–145. [CrossRef] [PubMed]
185. Candiani, G.; Riboldi, S.A.; Sadr, N.; Lorenzoni, S.; Neuenschwander, P.; Montevecchi, F.M.; Mantero, S. Cyclic mechanical stimulation favors myosin heavy chain accumulation in engineered skeletal muscle constructs. *J. Appl. Biomater. Biomech.* **2010**, *8*, 68–75. [PubMed]
186. Aviss, K.J.; Gough, J.E.; Downes, S. Aligned electrospun polymer fibres for skeletal muscle regeneration. *Eur. Cells Mater.* **2010**, *19*, 193–204. [CrossRef]
187. Martins, P.M.; Ribeiro, S.; Ribeiro, C.; Sencadas, V.; Gomes, A.C.; Gama, F.M.; Lanceros-Méndez, S. Effect of poling state and morphology of piezoelectric poly(vinylidene fluoride) membranes for skeletal muscle tissue engineering. *RSC Adv.* **2013**, *3*, 17938. [CrossRef]

188. Takeda, N.; Tamura, K.; Mineguchi, R.; Ishikawa, Y.; Haraguchi, Y.; Shimizu, T.; Hara, Y. In situ cross-linked electrospun fiber scaffold of collagen for fabricating cell-dense muscle tissue. *J. Artif. Organs* **2016**, *19*, 141–148. [CrossRef] [PubMed]
189. Guex, A.G.; Birrer, D.L.; Fortunato, G.; Tevaearai, H.T.; Giraud, M.-N. Anisotropically oriented electrospun matrices with an imprinted periodic micropattern: A new scaffold for engineered muscle constructs. *Biomed. Mater.* **2013**, *8*, 021001. [CrossRef] [PubMed]
190. Abarzúa-Illanes, P.N.; Padilla, C.; Ramos, A.; Isaacs, M.; Ramos-Grez, J.; Olguín, H.C.; Valenzuela, L.M. Improving myoblast differentiation on electrospun poly(ε-caprolactone) scaffolds. *J. Biomed. Mater. Res. A* **2017**, *105*, 2241–2251. [CrossRef] [PubMed]
191. Jun, I.; Jeong, S.; Shin, H. The stimulation of myoblast differentiation by electrically conductive sub-micron fibers. *Biomaterials* **2009**, *30*, 2038–2047. [CrossRef] [PubMed]
192. Sirivisoot, S.; Harrison, B.S. Skeletal myotube formation enhanced by electrospun polyurethane carbon nanotube scaffolds. *Int. J. Nanomedicine* **2011**, *6*, 2483–2497. [CrossRef] [PubMed]
193. Maciel, M.M.; Ribeiro, S.; Ribeiro, C.; Francesko, A.; Maceiras, A.; Vilas, J.L.; Lanceros-Méndez, S. Relation between fiber orientation and mechanical properties of nano-engineered poly(vinylidene fluoride) electrospun composite fiber mats. *Compos. Part B Eng.* **2018**, *139*, 146–154. [CrossRef]
194. Ostrovidov, S.; Shi, X.; Zhang, L.; Liang, X.; Kim, S.B.; Fujie, T.; Ramalingam, M.; Chen, M.; Nakajima, K.; Al-Hazmi, F.; et al. Myotube formation on gelatin nanofibers—Multi-walled carbon nanotubes hybrid scaffolds. *Biomaterials* **2014**, *35*, 6268–6277. [CrossRef] [PubMed]
195. Shin, Y.C.; Lee, J.H.; Jin, L.; Kim, M.J.; Kim, Y.-J.; Hyun, J.K.; Jung, T.-G.; Hong, S.W.; Han, D.-W. Stimulated myoblast differentiation on graphene oxide-impregnated PLGA-collagen hybrid fibre matrices. *J. Nanobiotechnol.* **2015**, *13*. [CrossRef] [PubMed]
196. Wang, L.; Wu, Y.; Guo, B.; Ma, P.X. Nanofiber Yarn/Hydrogel Core-Shell Scaffolds Mimicking Native Skeletal Muscle Tissue for Guiding 3D Myoblast Alignment, Elongation, and Differentiation. *ACS Nano* **2015**, *9*, 9167–9179. [CrossRef] [PubMed]
197. Cha, S.H.; Lee, H.J.; Koh, W.-G. Study of myoblast differentiation using multi-dimensional scaffolds consisting of nano and micropatterns. *Biomater. Res.* **2017**, *21*, 1. [CrossRef] [PubMed]
198. McKeon-Fischer, K.D.; Flagg, D.H.; Freeman, J.W. Poly(acrylic acid)/poly(vinyl alcohol) compositions coaxially electrospun with poly(ε-caprolactone) and multi-walled carbon nanotubes to create nanoactuating scaffolds. *Polymer* **2011**, *52*, 4736–4743. [CrossRef]
199. Serena, E.; Flaibani, M.; Carnio, S.; Boldrin, L.; Vitiello, L.; De Coppi, P.; Elvassore, N. Electrophysiologic stimulation improves myogenic potential of muscle precursor cells grown in a 3D collagen scaffold. *Neurol. Res.* **2008**, *30*, 207–214. [CrossRef] [PubMed]
200. Langelaan, M.L.P.; Boonen, K.J.M.; Rosaria-Chak, K.Y.; van der Schaft, D.W.J.; Post, M.J.; Baaijens, F.P.T. Advanced maturation by electrical stimulation: Differences in response between C2C12 and primary muscle progenitor cells. *J. Tissue Eng. Regen. Med.* **2011**, *5*, 529–539. [CrossRef] [PubMed]
201. Bandyopadhyay, B.; Shah, V.; Soram, M.; Viswanathan, C.; Ghosh, D. In vitro and in vivo evaluation of L-lactide/ε-caprolactone copolymer scaffold to support myoblast growth and differentiation. *Biotechnol. Prog.* **2013**, *29*, 197–205. [CrossRef] [PubMed]
202. Stern-Straeter, J.; Bach, A.D.; Stangenberg, L.; Foerster, V.T.; Horch, R.E.; Stark, G.B.; Beier, J.P. Impact of electrical stimulation on three-dimensional myoblast cultures—A real-time RT-PCR study. *J. Cell. Mol. Med.* **2005**, *9*, 883–892. [CrossRef] [PubMed]
203. Powell, C.A.; Smiley, B.L.; Mills, J.; Vandenburgh, H.H. Mechanical stimulation improves tissue-engineered human skeletal muscle. *Am. J. Physiol. Cell Physiol.* **2002**, *283*, C1557–C1565. [CrossRef] [PubMed]
204. Bian, W.; Juhas, M.; Pfeiler, T.W.; Bursac, N. Local tissue geometry determines contractile force generation of engineered muscle networks. *Tissue Eng. Part A* **2012**, *18*, 957–967. [CrossRef] [PubMed]
205. Kheradmandi, M.; Vasheghani-Farahani, E.; Ghiaseddin, A.; Ganji, F. Skeletal muscle regeneration via engineered tissue culture over electrospun nanofibrous chitosan/PVA scaffold. *J. Biomed. Mater. Res. A* **2016**, *104*, 1720–1727. [CrossRef] [PubMed]
206. Shadrach, J.L.; Wagers, A.J. Stem cells for skeletal muscle repair. *Philos. Trans. R. Soc. B Biol. Sci.* **2011**, *366*, 2297–2306. [CrossRef] [PubMed]
207. Liao, H.; Zhou, G.-Q. Development and progress of engineering of skeletal muscle tissue. *Tissue Eng. Part B Rev.* **2009**, *15*, 319–331. [CrossRef] [PubMed]

208. Gilbert, S.F. Myogenesis: The Development of Muscle. In *Developmental Biology*, 6th ed.; 2000. Available online: https://www.ncbi.nlm.nih.gov/books/NBK10006/ (accessed on 22 May 2018).
209. Egerman, M.A.; Glass, D.J. Signaling pathways controlling skeletal muscle mass. *Crit. Rev. Biochem. Mol. Biol.* **2014**, *49*, 59–68. [CrossRef] [PubMed]
210. Mauro, A.; Ciccarelli, C.; De Cesaris, P.; Scoglio, A.; Bouché, M.; Molinaro, M.; Aquino, A.; Zani, B.M. PKCalpha-mediated ERK, JNK and p38 activation regulates the myogenic program in human rhabdomyosarcoma cells. *J. Cell Sci.* **2002**, *115*, 3587–3599. [CrossRef] [PubMed]
211. Michailovici, I.; Harrington, H.A.; Azogui, H.H.; Yahalom-Ronen, Y.; Plotnikov, A.; Ching, S.; Stumpf, M.P.H.; Klein, O.D.; Seger, R.; Tzahor, E. Nuclear to cytoplasmic shuttling of ERK promotes differentiation of muscle stem/progenitor cells. *Development* **2014**, *141*, 2611–2620. [CrossRef] [PubMed]
212. Wang, H.; Xu, Q.; Xiao, F.; Jiang, Y.; Wu, Z. Involvement of the p38 Mitogen-activated Protein Kinase α, β, and γ Isoforms in Myogenic Differentiation. *Mol. Biol. Cell* **2008**, *19*, 1519–1528. [CrossRef] [PubMed]
213. Fujita, H.; Shimizu, K.; Yamamoto, Y.; Ito, A.; Kamihira, M.; Nagamori, E. Fabrication of scaffold-free contractile skeletal muscle tissue using magnetite-incorporated myogenic C2C12 cells. *J. Tissue Eng. Regen. Med.* **2010**, *4*, 437–443. [CrossRef] [PubMed]
214. Ikeda, K.; Takayama, T.; Suzuki, N.; Shimada, K.; Otsuka, K.; Ito, K. Effects of low-intensity pulsed ultrasound on the differentiation of C2C12 cells. *Life Sci.* **2006**, *79*, 1936–1943. [CrossRef] [PubMed]
215. Ricotti, L.; Fujie, T.; Vazão, H.; Ciofani, G.; Marotta, R.; Brescia, R.; Filippeschi, C.; Corradini, I.; Matteoli, M.; Mattoli, V.; et al. Boron Nitride Nanotube-Mediated Stimulation of Cell Co-Culture on Micro-Engineered Hydrogels. *PLoS ONE* **2013**, *8*, e71707. [CrossRef] [PubMed]
216. Salgarella, A.R.; Cafarelli, A.; Ricotti, L.; Capineri, L.; Dario, P.; Menciassi, A. Optimal Ultrasound Exposure Conditions for Maximizing C2C12 Muscle Cell Proliferation and Differentiation. *Ultrasound Med. Biol.* **2017**, *43*, 1452–1465. [CrossRef] [PubMed]
217. Campion, D.R.; Richardson, R.L.; Kraeling, R.R.; Reagan, J.O. Regulation of skeletal muscle development by the central nervous system in the fetal pig. *Growth* **1978**, *42*, 189–204. [PubMed]
218. Khodabukus, A.; Baar, K. Defined electrical stimulation emphasizing excitability for the development and testing of engineered skeletal muscle. *Tissue Eng. Part C Methods* **2012**, *18*, 349–357. [CrossRef] [PubMed]
219. Tanaka, T.; Hattori-Aramaki, N.; Sunohara, A.; Okabe, K.; Sakamoto, Y.; Ochiai, H.; Hayashi, R.; Kishi, K. Alignment of Skeletal Muscle Cells Cultured in Collagen Gel by Mechanical and Electrical Stimulation. Available online: https://www.hindawi.com/journals/ijte/2014/621529/ (accessed on 15 January 2018).
220. Bajaj, P.; Reddy, B.; Millet, L.; Wei, C.; Zorlutuna, P.; Bao, G.; Bashir, R. Patterning the differentiation of C2C12 skeletal myoblasts. *Integr. Biol. Quant. Biosci. Nano Macro* **2011**, *3*, 897–909. [CrossRef] [PubMed]
221. Buvinic, S.; Almarza, G.; Bustamante, M.; Casas, M.; López, J.; Riquelme, M.; Sáez, J.C.; Huidobro-Toro, J.P.; Jaimovich, E. ATP released by electrical stimuli elicits calcium transients and gene expression in skeletal muscle. *J. Biol. Chem.* **2009**, *284*, 34490–34505. [CrossRef] [PubMed]
222. Eltit, J.M.; García, A.A.; Hidalgo, J.; Liberona, J.L.; Chiong, M.; Lavandero, S.; Maldonado, E.; Jaimovich, E. Membrane Electrical Activity Elicits Inositol 1,4,5-Trisphosphate-dependent Slow Ca^{2+} Signals through a Gβγ/Phosphatidylinositol 3-Kinase γ Pathway in Skeletal Myotubes. *J. Biol. Chem.* **2006**, *281*, 12143–12154. [CrossRef] [PubMed]
223. Rahnert, J.A.; Burkholder, T.J. ERK phosphorylation correlates with intensity of electrical stimulation in mouse tibialis anterior. *FASEB J.* **2011**, *25*, 1051.
224. Zöllner, A.M.; Abilez, O.J.; Böl, M.; Kuhl, E. Stretching skeletal muscle: Chronic muscle lengthening through sarcomerogenesis. *PLoS ONE* **2012**, *7*, e45661. [CrossRef] [PubMed]
225. Ahmed, W.W.; Wolfram, T.; Goldyn, A.M.; Bruellhoff, K.; Rioja, B.A.; Möller, M.; Spatz, J.P.; Saif, T.A.; Groll, J.; Kemkemer, R. Myoblast morphology and organization on biochemically micro-patterned hydrogel coatings under cyclic mechanical strain. *Biomaterials* **2010**, *31*, 250–258. [CrossRef] [PubMed]
226. Moon, D.G.; Christ, G.; Stitzel, J.D.; Atala, A.; Yoo, J.J. Cyclic mechanical preconditioning improves engineered muscle contraction. *Tissue Eng. Part A* **2008**, *14*, 473–482. [CrossRef] [PubMed]
227. Zhang, S.J.; Truskey, G.A.; Kraus, W.E. Effect of cyclic stretch on β1D-integrin expression and activation of FAK and RhoA. Am. *J. Physiol. Cell Physiol.* **2007**, *292*, C2057–C2069. [CrossRef] [PubMed]
228. Hara, M.; Tabata, K.; Suzuki, T.; Do, M.-K.Q.; Mizunoya, W.; Nakamura, M.; Nishimura, S.; Tabata, S.; Ikeuchi, Y.; Sunagawa, K.; et al. Calcium influx through a possible coupling of cation channels impacts

skeletal muscle satellite cell activation in response to mechanical stretch. *Am. J. Physiol. Cell Physiol.* **2012**, *302*, C1741–1750. [CrossRef] [PubMed]
229. Tatsumi, R.; Hattori, A.; Ikeuchi, Y.; Anderson, J.E.; Allen, R.E. Release of Hepatocyte Growth Factor from Mechanically Stretched Skeletal Muscle Satellite Cells and Role of pH and Nitric Oxide. *Mol. Biol. Cell* **2002**, *13*, 2909–2918. [CrossRef] [PubMed]
230. Adam, R.M.; Roth, J.A.; Cheng, H.-L.; Rice, D.C.; Khoury, J.; Bauer, S.B.; Peters, C.A.; Freeman, M.R. Signaling Through PI3K/Akt Mediates Stretch and PDGF-BB-Dependent DNA Synthesis in Bladder Smooth Muscle Cells. *J. Urol.* **2003**, *169*, 2388–2393. [CrossRef] [PubMed]
231. Hanke, N.; Kubis, H.-P.; Scheibe, R.J.; Berthold-Losleben, M.; Hüsing, O.; Meissner, J.D.; Gros, G. Passive mechanical forces upregulate the fast myosin heavy chain IId/x via integrin and p38 MAP kinase activation in a primary muscle cell culture. *Am. J. Physiol. Cell Physiol.* **2010**, *298*, C910–920. [CrossRef] [PubMed]
232. Pavesi, A.; Adriani, G.; Rasponi, M.; Zervantonakis, I.K.; Fiore, G.B.; Kamm, R.D. Controlled electromechanical cell stimulation on-a-chip. *Sci. Rep.* **2015**, *5*, 5. [CrossRef] [PubMed]
233. Sørensen, V.; Zhen, Y.; Zakrzewska, M.; Haugsten, E.M.; Wälchli, S.; Nilsen, T.; Olsnes, S.; Wiedlocha, A. Phosphorylation of Fibroblast Growth Factor (FGF) Receptor 1 at Ser777 by p38 Mitogen-Activated Protein Kinase Regulates Translocation of Exogenous FGF1 to the Cytosol and Nucleus. *Mol. Cell. Biol.* **2008**, *28*, 4129–4141. [CrossRef] [PubMed]
234. Suzuki, J.; Yamazaki, Y.; Guang, L.; Kaziro, Y.; Koide, H. Involvement of Ras and Ral in Chemotactic Migration of Skeletal Myoblasts. *Mol. Cell. Biol.* **2000**, *20*, 4658–4665. [CrossRef] [PubMed]
235. Walker, N.; Kahamba, T.; Woudberg, N.; Goetsch, K.; Niesler, C. Dose-dependent modulation of myogenesis by HGF: Implications for c-Met expression and downstream signalling pathways. *Growth Factors* **2015**, *33*, 229–241. [CrossRef] [PubMed]
236. Bustamante, M.; Fernández-Verdejo, R.; Jaimovich, E.; Buvinic, S. Electrical stimulation induces IL-6 in skeletal muscle through extracellular ATP by activating Ca^{2+} signals and an IL-6 autocrine loop. *Am. J. Physiol. Endocrinol. Metab.* **2014**, *306*, E869–E882. [CrossRef] [PubMed]
237. Perez-Ruiz, A.; Gnocchi, V.F.; Zammit, P.S. Control of Myf5 activation in adult skeletal myonuclei requires ERK signalling. *Cell Signal.* **2007**, *19*, 1671–1680. [CrossRef] [PubMed]
238. Cárdenas, C.; Müller, M.; Jaimovich, E.; Pérez, F.; Buchuk, D.; Quest, A.F.G.; Carrasco, M.A. Depolarization of Skeletal Muscle Cells induces Phosphorylation of cAMP Response Element Binding Protein via Calcium and Protein Kinase Cα. *J. Biol. Chem.* **2004**, *279*, 39122–39131. [CrossRef] [PubMed]
239. Dargelos, E.; Dedieu, S.; Moyen, C.; Poussard, S.; Veschambre, P.; Brustis, J.-J.; Cottin, P. Characterization of the calcium-dependent proteolytic system in a mouse muscle cell line. *Mol. Cell. Biochem.* **2002**, *231*, 147–154. [CrossRef] [PubMed]
240. Friday, B.B.; Horsley, V.; Pavlath, G.K. Calcineurin Activity Is Required for the Initiation of Skeletal Muscle Differentiation. *J. Cell Biol.* **2000**, *149*, 657–666. [CrossRef] [PubMed]
241. Low, S.Y.; Taylor, P.M. Integrin and cytoskeletal involvement in signalling cell volume changes to glutamine transport in rat skeletal muscle. *J. Physiol.* **1998**, *512*, 481–485. [CrossRef] [PubMed]
242. Kjaer, M. Role of extracellular matrix in adaptation of tendon and skeletal muscle to mechanical loading. *Physiol. Rev.* **2004**, *84*, 649–698. [CrossRef] [PubMed]
243. Kin, S.; Hagiwara, A.; Nakase, Y.; Kuriu, Y.; Nakashima, S.; Yoshikawa, T.; Sakakura, C.; Otsuji, E.; Nakamura, T.; Yamagishi, H. Regeneration of skeletal muscle using in situ tissue engineering on an acellular collagen sponge scaffold in a rabbit model. *ASAIO J.* **2007**, *53*, 506–513. [CrossRef] [PubMed]
244. Lehto, M.; Kvist, M.; Vieno, T.; Józsa, L. Macromolecular composition of the sarcolemma and endomysium in the rat. *Acta Anat.* **1988**, *133*, 297–302. [CrossRef] [PubMed]
245. Ansari, S.; Chen, C.; Xu, X.; Annabi, N.; Zadeh, H.H.; Wu, B.M.; Khademhosseini, A.; Shi, S.; Moshaverinia, A. Muscle Tissue Engineering Using Gingival Mesenchymal Stem Cells Encapsulated in Alginate Hydrogels Containing Multiple Growth Factors. *Ann. Biomed. Eng.* **2016**, *44*, 1908–1920. [CrossRef] [PubMed]
246. Li, Y.; Meng, H.; Liu, Y.; Lee, B.P. Fibrin gel as an injectable biodegradable scaffold and cell carrier for tissue engineering. *Sci. World J.* **2015**, *2015*, 685690. [CrossRef] [PubMed]
247. Lam, M.T.; Huang, Y.-C.; Birla, R.K.; Takayama, S. Microfeature guided skeletal muscle tissue engineering for highly organized 3-dimensional free-standing constructs. *Biomaterials* **2009**, *30*, 1150–1155. [CrossRef] [PubMed]

248. Tonda-Turo, C.; Ruini, F.; Ramella, M.; Boccafoschi, F.; Gentile, P.; Gioffredi, E.; Labate, G.F.D.; Ciardelli, G. Non-covalently crosslinked chitosan nanofibrous mats prepared by electrospinning as substrates for soft tissue regeneration. *Carbohydr. Polym.* **2017**, *162*, 82–92. [CrossRef] [PubMed]
249. Hennink, W.E.; van Nostrum, C.F. Novel crosslinking methods to design hydrogels. *Adv. Drug Deliv. Rev.* **2002**, *54*, 13–36. [CrossRef]
250. Rowley, J.A.; Mooney, D.J. Alginate type and RGD density control myoblast phenotype. *J. Biomed. Mater. Res.* **2002**, *60*, 217–223. [CrossRef] [PubMed]
251. Davidenko, N.; Schuster, C.F.; Bax, D.V.; Raynal, N.; Farndale, R.W.; Best, S.M.; Cameron, R.E. Control of crosslinking for tailoring collagen-based scaffolds stability and mechanics. *Acta Biomater.* **2015**, *25*, 131–142. [CrossRef] [PubMed]
252. Lin, C.-H.; Yang, J.-R.; Chiang, N.-J.; Ma, H.; Tsay, R.-Y. Evaluation of decellularized extracellular matrix of skeletal muscle for tissue engineering. *Int. J. Artif. Organs* **2014**, *37*, 546–555. [CrossRef] [PubMed]
253. Gamba, P.G.; Conconi, M.T.; Lo Piccolo, R.; Zara, G.; Spinazzi, R.; Parnigotto, P.P. Experimental abdominal wall defect repaired with acellular matrix. *Pediatr. Surg. Int.* **2002**, *18*, 327–331. [CrossRef] [PubMed]
254. Fishman, J.M.; Lowdell, M.W.; Urbani, L.; Ansari, T.; Burns, A.J.; Turmaine, M.; North, J.; Sibbons, P.; Seifalian, A.M.; Wood, K.J.; et al. Immunomodulatory effect of a decellularized skeletal muscle scaffold in a discordant xenotransplantation model. *Proc. Natl. Acad. Sci. USA* **2013**, *110*, 14360–14365. [CrossRef] [PubMed]
255. Porzionato, A.; Sfriso, M.M.; Pontini, A.; Macchi, V.; Petrelli, L.; Pavan, P.G.; Natali, A.N.; Bassetto, F.; Vindigni, V.; De Caro, R. Decellularized Human Skeletal Muscle as Biologic Scaffold for Reconstructive Surgery. *Int. J. Mol. Sci.* **2015**, *16*, 14808–14831. [CrossRef] [PubMed]
256. Saxena, A.K.; Marler, J.; Benvenuto, M.; Willital, G.H.; Vacanti, J.P. Skeletal muscle tissue engineering using isolated myoblasts on synthetic biodegradable polymers: Preliminary studies. *Tissue Eng.* **1999**, *5*, 525–532. [CrossRef] [PubMed]
257. Saxena, A.K.; Willital, G.H.; Vacanti, J.P. Vascularized three-dimensional skeletal muscle tissue-engineering. Biomed. *Mater. Eng.* **2001**, *11*, 275–281.
258. Rimington, R.P.; Capel, A.J.; Christie, S.D.R.; Lewis, M.P. Biocompatible 3D printed polymers via fused deposition modelling direct C_2C_{12} cellular phenotype in vitro. *Lab Chip* **2017**, *17*, 2982–2993. [CrossRef] [PubMed]
259. Ricotti, L.; Taccola, S.; Pensabene, V.; Mattoli, V.; Fujie, T.; Takeoka, S.; Menciassi, A.; Dario, P. Adhesion and proliferation of skeletal muscle cells on single layer poly(lactic acid) ultra-thin films. *Biomed. Microdevices* **2010**, *12*, 809–819. [CrossRef] [PubMed]
260. Li, W.-J.; Mauck, R.L.; Cooper, J.A.; Yuan, X.; Tuan, R.S. Engineering controllable anisotropy in electrospun biodegradable nanofibrous scaffolds for musculoskeletal tissue engineering. *J. Biomech.* **2007**, *40*, 1686–1693. [CrossRef] [PubMed]
261. Kim, M.; Choi, Y.S.; Yang, S.H.; Hong, H.-N.; Cho, S.-W.; Cha, S.M.; Pak, J.H.; Kim, C.W.; Kwon, S.W.; Park, C.J. Muscle regeneration by adipose tissue-derived adult stem cells attached to injectable PLGA spheres. *Biochem. Biophys. Res. Commun.* **2006**, *348*, 386–392. [CrossRef] [PubMed]
262. Xu, J.; Xie, Y.; Zhang, H.; Ye, Z.; Zhang, W. Fabrication of PLGA/MWNTs composite electrospun fibrous scaffolds for improved myogenic differentiation of C2C12 cells. *Colloids Surf. B Biointerfaces* **2014**, *123*, 907–915. [CrossRef] [PubMed]
263. Middleton, J.C.; Tipton, A.J. Synthetic biodegradable polymers as orthopedic devices. *Biomaterials* **2000**, *21*, 2335–2346. [CrossRef]
264. Yamada, K.M. Adhesive recognition sequences. *J. Biol. Chem.* **1991**, *266*, 12809–12812. [PubMed]
265. Choi, J.S.; Lee, S.J.; Christ, G.J.; Atala, A.; Yoo, J.J. The influence of electrospun aligned poly(ε-caprolactone)/collagen nanofiber meshes on the formation of self-aligned skeletal muscle myotubes. *Biomaterials* **2008**, *29*, 2899–2906. [CrossRef] [PubMed]
266. Heher, P.; Maleiner, B.; Prüller, J.; Teuschl, A.H.; Kollmitzer, J.; Monforte, X.; Wolbank, S.; Redl, H.; Rünzler, D.; Fuchs, C. A novel bioreactor for the generation of highly aligned 3D skeletal muscle-like constructs through orientation of fibrin via application of static strain. *Acta Biomater.* **2015**, *24*, 251–265. [CrossRef] [PubMed]
267. Suh, G.C.; Bettadapur, A.; Santoso, J.W.; McCain, M.L. Fabrication of Micromolded Gelatin Hydrogels for Long-Term Culture of Aligned Skeletal Myotubes. *Methods Mol. Biol.* **2017**, *1668*, 147–163. [CrossRef] [PubMed]

268. Salimath, A.S.; García, A.J. Biofunctional hydrogels for skeletal muscle constructs. *J. Tissue Eng. Regen. Med.* **2016**, *10*, 967–976. [CrossRef] [PubMed]
269. Salahshoor, H.; Rahbar, N. Multi-scale mechanical and transport properties of a hydrogel. *J. Mech. Behav. Biomed. Mater.* **2014**, *37*, 299–306. [CrossRef] [PubMed]
270. Pollot, B.E.; Rathbone, C.R.; Wenke, J.C.; Guda, T. Natural polymeric hydrogel evaluation for skeletal muscle tissue engineering. *J. Biomed. Mater. Res. B Appl. Biomater.* **2018**, *106*, 672–679. [CrossRef] [PubMed]
271. Pardo-Yissar, V.; Gabai, R.; Shipway, A.N.; Bourenko, T.; Willner, I. Gold Nanoparticle/Hydrogel Composites with Solvent-Switchable Electronic Properties. *Adv. Mater.* **2001**, *13*, 1320–1323. [CrossRef]
272. Ku, S.H.; Park, C.B. Myoblast differentiation on graphene oxide. *Biomaterials* **2013**, *34*, 2017–2023. [CrossRef] [PubMed]
273. Ramón-Azcón, J.; Ahadian, S.; Estili, M.; Liang, X.; Ostrovidov, S.; Kaji, H.; Shiku, H.; Ramalingam, M.; Nakajima, K.; Sakka, Y.; Khademhosseini, A.; Matsue, T. Dielectrophoretically Aligned Carbon Nanotubes to Control Electrical and Mechanical Properties of Hydrogels to Fabricate Contractile Muscle Myofibers. *Adv. Mater.* **2013**, *25*, 4028–4034. [CrossRef] [PubMed]
274. MacDonald, R.A.; Voge, C.M.; Kariolis, M.; Stegemann, J.P. Carbon nanotubes increase the electrical conductivity of fibroblast-seeded collagen hydrogels. *Acta Biomater.* **2008**, *4*, 1583–1592. [CrossRef] [PubMed]
275. McKeon-Fischer, K.D.; Freeman, J.W. Characterization of electrospun poly(L-lactide) and gold nanoparticle composite scaffolds for skeletal muscle tissue engineering. *J. Tissue Eng. Regen. Med.* **2011**, *5*, 560–568. [CrossRef] [PubMed]
276. Vandenburgh, H.H.; Karlisch, P.; Farr, L. Maintenance of highly contractile tissue-cultured avian skeletal myotubes in collagen gel. *In Vitro Cell. Dev. Biol.* **1988**, *24*, 166–174. [CrossRef] [PubMed]
277. Griffin, M.A.; Sen, S.; Sweeney, H.L.; Discher, D.E. Adhesion-contractile balance in myocyte differentiation. *J. Cell Sci.* **2004**, *117*, 5855–5863. [CrossRef] [PubMed]
278. Bian, W.; Bursac, N. Engineered skeletal muscle tissue networks with controllable architecture. *Biomaterials* **2009**, *30*, 1401–1412. [CrossRef] [PubMed]
279. Courtney, T.; Sacks, M.S.; Stankus, J.; Guan, J.; Wagner, W.R. Design and analysis of tissue engineering scaffolds that mimic soft tissue mechanical anisotropy. *Biomaterials* **2006**, *27*, 3631–3638. [CrossRef] [PubMed]
280. Dalby, M.J.; Childs, S.; Riehle, M.O.; Johnstone, H.J.H.; Affrossman, S.; Curtis, A.S.G. Fibroblast reaction to island topography: Changes in cytoskeleton and morphology with time. *Biomaterials* **2003**, *24*, 927–935. [CrossRef]
281. Yang, H.S.; Ieronimakis, N.; Tsui, J.H.; Kim, H.N.; Suh, K.-Y.; Reyes, M.; Kim, D.-H. Nanopatterned muscle cell patches for enhanced myogenesis and dystrophin expression in a mouse model of muscular dystrophy. *Biomaterials* **2014**, *35*, 1478–1486. [CrossRef] [PubMed]
282. Sanzari, I.; Callisti, M.; Grazia, A.D.; Evans, D.J.; Polcar, T.; Prodromakis, T. Parylene C topographic micropattern as a template for patterning PDMS and Polyacrylamide hydrogel. *Sci. Rep.* **2017**, *7*, 5764. [CrossRef] [PubMed]
283. Janakiraman, V.; Kienitz, B.L.; Baskaran, H. Lithography Technique for Topographical Micropatterning of Collagen-Glycosaminoglycan Membranes for Tissue Engineering Applications. *J. Med. Devices* **2007**, *1*, 233–237. [CrossRef] [PubMed]
284. Qazi, T.H.; Mooney, D.J.; Pumberger, M.; Geißler, S.; Duda, G.N. Biomaterials based strategies for skeletal muscle tissue engineering: Existing technologies and future trends. *Biomaterials* **2015**, *53*, 502–521. [CrossRef] [PubMed]
285. Costantini, M.; Idaszek, J.; Szöke, K.; Jaroszewicz, J.; Dentini, M.; Barbetta, A.; Brinchmann, J.E.; Święszkowski, W. 3D bioprinting of BM-MSCs-loaded ECM biomimetic hydrogels for in vitro neocartilage formation. *Biofabrication* **2016**, *8*, 035002. [CrossRef] [PubMed]
286. Cvetkovic, C.; Raman, R.; Chan, V.; Williams, B.J.; Tolish, M.; Bajaj, P.; Sakar, M.S.; Asada, H.H.; Saif, M.T.A.; Bashir, R. Three-dimensionally printed biological machines powered by skeletal muscle. *Proc. Natl. Acad. Sci. USA* **2014**, *111*, 10125–10130. [CrossRef] [PubMed]
287. Omidian, H.; Rocca, J.G.; Park, K. Elastic, superporous hydrogel hybrids of polyacrylamide and sodium alginate. *Macromol. Biosci.* **2006**, *6*, 703–710. [CrossRef] [PubMed]
288. Lee, J.H.; Lee, S.J.; Khang, G.; Lee, H.B. Interaction of fibroblasts on polycarbonate membrane surfaces with different micropore sizes and hydrophilicity. *J. Biomater. Sci. Polym. Ed.* **1999**, *10*, 283–294. [CrossRef] [PubMed]

289. Kasper, A.M.; Turner, D.C.; Martin, N.R.W.; Sharples, A.P. Mimicking exercise in three-dimensional bioengineered skeletal muscle to investigate cellular and molecular mechanisms of physiological adaptation. *J. Cell. Physiol.* **2018**, *233*, 1985–1998. [CrossRef] [PubMed]
290. Rangarajan, S.; Madden, L.; Bursac, N. Use of flow, electrical, and mechanical stimulation to promote engineering of striated muscles. *Ann. Biomed. Eng.* **2014**, *42*, 1391–1405. [CrossRef] [PubMed]
291. Alberts, B.; Johnson, A.; Lewis, J.; Raff, M.; Roberts, K.; Walter, P. *Genesis, Modulation, and Regeneration of Skeletal Muscle*, 4th ed.; Garland Science: New York, NY, USA, 2002.
292. Choi, Y.-J.; Kim, T.G.; Jeong, J.; Yi, H.-G.; Park, J.W.; Hwang, W.; Cho, D.-W. 3D Cell Printing of Functional Skeletal Muscle Constructs Using Skeletal Muscle-Derived Bioink. *Adv. Healthc. Mater.* **2016**, *5*, 2636–2645. [CrossRef] [PubMed]
293. Drexler, J.W.; Powell, H.M. Regulation of electrospun scaffold stiffness via coaxial core diameter. *Acta Biomater.* **2011**, *7*, 1133–1139. [CrossRef] [PubMed]
294. Kim, M.S.; Jun, I.; Shin, Y.M.; Jang, W.; Kim, S.I.; Shin, H. The development of genipin-crosslinked poly(caprolactone) (PCL)/gelatin nanofibers for tissue engineering applications. *Macromol. Biosci.* **2010**, *10*, 91–100. [CrossRef] [PubMed]
295. Sreerekha, P.R.; Menon, D.; Nair, S.V.; Chennazhi, K.P. Fabrication of fibrin based electrospun multiscale composite scaffold for tissue engineering applications. *J. Biomed. Nanotechnol.* **2013**, *9*, 790–800. [CrossRef] [PubMed]
296. McKeon-Fischer, K.D.; Flagg, D.H.; Freeman, J.W. Coaxial electrospun poly(ε-caprolactone), multiwalled carbon nanotubes, and polyacrylic acid/polyvinyl alcohol scaffold for skeletal muscle tissue engineering. *J. Biomed. Mater. Res. A* **2011**, *99*, 493–499. [CrossRef] [PubMed]
297. McKeon-Fischer, K.D.; Rossmeisl, J.H.; Whittington, A.R.; Freeman, J.W. In vivo skeletal muscle biocompatibility of composite, coaxial electrospun, and microfibrous scaffolds. *Tissue Eng. Part A* **2014**, *20*, 1961–1970. [CrossRef] [PubMed]
298. Charvet, B.; Ruggiero, F.; Le Guellec, D. The development of the myotendinous junction. A review. *Muscles Ligaments Tendons J.* **2012**, *2*, 53–63. [PubMed]
299. Kostrominova, T.Y.; Calve, S.; Arruda, E.M.; Larkin, L.M. Ultrastructure of myotendinous junctions in tendon-skeletal muscle constructs engineered in vitro. *Histol. Histopathol.* **2009**, *24*, 541–550. [PubMed]
300. Larkin, L.M.; Calve, S.; Kostrominova, T.Y.; Arruda, E.M. Structure and Functional Evaluation of Tendon–Skeletal Muscle Constructs Engineered In Vitro. *Tissue Eng.* **2006**, *12*, 3149–3158. [CrossRef] [PubMed]
301. Ladd, M.R.; Lee, S.J.; Stitzel, J.D.; Atala, A.; Yoo, J.J. Co-electrospun dual scaffolding system with potential for muscle-tendon junction tissue engineering. *Biomaterials* **2011**, *32*, 1549–1559. [CrossRef] [PubMed]
302. Merceron, T.K.; Burt, M.; Seol, Y.-J.; Kang, H.-W.; Lee, S.J.; Yoo, J.J.; Atala, A. A 3D bioprinted complex structure for engineering the muscle-tendon unit. *Biofabrication* **2015**, *7*, 035003. [CrossRef] [PubMed]

3. Bone-Tendon Interface: Bioinspired Approach

3.1. The Enthesis: Composition and Structure

The ostotendinous junction or enthesis corresponds the anchorage point between bones and tendons, mediating the integration of the different tissues which present dissimilar cellular, molecular and structural compounds in a tight region of one hundred microns.[120] This natural interface is specifically adapted to allow smooth transmission of strain between tendon and bone, facilitating joint motion.[120,121]

In general, there are two types of bone-to-tendon insertions classified as either fibrous or fibrocartilaginous enthesis.[122] Fibrous entheses, which are less common, are characterised from a direct attachment between the tendon and the bone through perforating mineralized collagen fibers whose structure is similar to the tendon midsubstance and are found in areas where the joint angle does not change during motion.[123] Fibrocartilaginous entheses are the most encountered bone-to-tendon interfaces, and are constituted by four distinct zones allowing a greater integration between both structures. These zones are (1) tendon, (2) fibrocartilage, (3) mineralized fibrocartilage and (4) bone. A great example of this junction is the Achilles tendon. As seen before, the tendon region is characterized by an extracellular matrix composed mainly of aligned and parallel fibers of collagen type I, with fibroblasts as the most important cellular population. The non-mineralized fibrocartilaginous region is characterized by its composition in collagen type I and II and glycosaminoglycans, with fibrochondrocytes as cellular population. The mineralized fibrocartilage, which interdigitates with the bone, also contains a significant amount of collagen type X and hydroxyapatite, with the hypertrophic fibrochondrocytes responsible for mineralization as the main cells. The last zone, the bone region is mostly composed of type I collagen, hydroxyapatite and bone cells (osteoblasts, osteocytes and osteoclasts).[124] The different regions not only differ in cells or ECM composition but also in terms of structure. Moving forward within each zone, the extracellular matrix undergoes a series of morphological changes in order to ensure a smooth transition between each unit. These changes are represented in **Figure 4**.

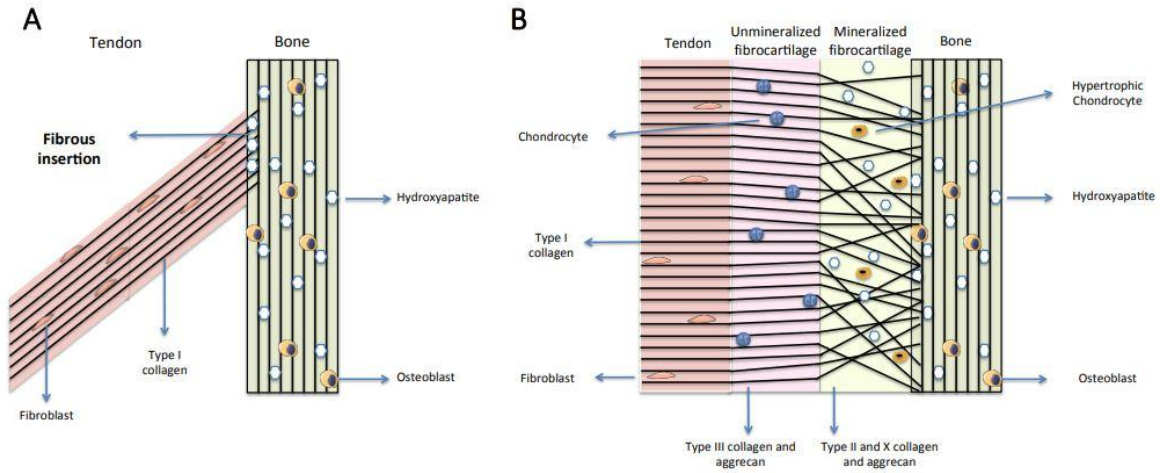

Figure 4. Representation of the two types of enthesis. **A.** Fibrous enthesis. **B.** Fibrocartilaginous enthesis.

Briefly, collagen fibers change in alignment as they approach the bone side and become mineralized. The combination of both phenomena, the increase in mineral content and the reduction in collagen alignment, modifies the mechanical properties of the enthesis throughout its length and translates into a more complaint behaviour at the tendon extremity than at the bone ones.[125]

3.2. First Approaches for the Reconstruction of the Bone-Tendon Interface

As seen before, tendon and bone tissue present different capacity for self-repair. While bone healing can be completed after 11-12 weeks with a resulting tissue with the same structural and mechanical properties as prior to fracture, tendon self-healing is highly limited due to it low vascularity and low cellular composition: it may take up to a year to restore it structure and function.[126] Up to now, tendon grafts mainly focus on the improvement of the mechanical properties of the tendon, without taking into account the complexity and heterogeneity of the insertion junction within bone tissue. Because of this, there is an unsatisfied demand for a tissue-engineering scaffold displaying the sophistication of the bone-to-tendon insertion.[127]

Ideally, the appropriate biohybrid substitute needs to ensure the different biomechanical and biochemical gradients found in the different zones of the enthesis. Therefore, specific attention was paid on a range of materials with mechanical and/or biochemical gradient to ensure a transition similar to the native enthesis.[128–131] They are summarized in extensive

reviews and will not be described in detail here.[125,127,132,133] Kim et al. 2014 proposed a four-layer freeze-dried substitute consisting in a collagen layer for the tendon region, a collagen/chondroïtin layer for the unmineralized region, a low mineralized collagen layer for the mineralized region and a high mineralized collagen layer for the bone region. Each layer presented a change in the mechanical properties along the scaffolds.[128] Erisken et al. 2008 proposed a single electrospun PCL scaffold coated with a β-TCP gradient to mimic the mineral gradient found in enthesis. As in the native enthesis, Young´s modulus increased as the β-TCP concentration was higher.[129] A similar strategy was followed by Liu et al. (2014) where a electrospun PLGA scaffold was immersed in a mineralization solution creating a mineral gradient throughout the scaffold.[130] As far as cells were concerned, there is also no clear choice. Some used fibroblasts, chondrocytes and osteoblasts to mimic the different cell populations found in the enthesis,[128] others focused on multipotent stem cells such as BMSCs or ADSCs following their potential differentiation within the different zones of the engineered substitute.[130] However, the achievement of such complex biohydrid tissue was not demonstrated yet.

Chapter II – Material and Methods

Chapter II: Material and Methods

1. Scaffold Production by Electrospinning

1.1. Electrospinning Device

Three different electrospinning set-ups were used for the production of the different mats analyzed during this thesis. The electrospinning apparatus of Laboratoire Roberval (UTC, FRE 2012, France, Compiègne) consisted in a high-voltage generator (Gamma High Voltage, USA), a syringe pump (Kd Scientific, USA), a 19G needle (Cadence Science, USA) and a 7.5 cm diameter rotating cylindrical collector (Nabond, China) (Figure 5). The collector was equipped with a step motor allowing a rotation up to 1000 rpm. The entire system was placed inside a chemical bench, allowing the solvents to be extracted during the process.

To facilitate the removal of the scaffold, the collector is covered with aluminum foil before the electrospinning process. Both sides of the collector are covered with transparent polypropylene strips, leaving 7 cm of scratches in the center of the collector. This concentrated the polymer jet mainly in this area, leading to a more homogeneous scaffold. Humidity and temperature were not monitored and corresponded to ambient conditions.

Figure 5. Electrospinning device of Laboratoire Roberval.

The device of ICPEES (Université de Strasbourg, France) consisted in a flat rotatory collector on which a honeycomb micropattern was fixed. Those micropatterns were manufactured by means of photolithography. A SU-8 2050 (Microchem) photoresist layer was deposited over

a silicon wafer. The photoresist layer was exposed to UV light through a honeycomb mask using a mask aligner (MJB4, SUSS Microtec). The photoresist layer was then developed and cured to obtain the honeycomb micropatterns. Finally, a Plassys MEB5505 electron beam evaporator was used to deposit a conductive layer on the collectors to allow the electrospinning process. The needle was positioned vertically to the collector. As it was not covered with an aluminum foil, the scaffold was delicately removed at the end of the process from the collector surface to avoid damaging this conductive layer and to be able to use it afterwards. The last device, from the IMP Hannover (Institute für MehrphasenProzessen, Université de Leipzig) consisted of a vertical electrospinning system with a drum rotated collector which could rotate up to 2000 rpm to obtain aligned fibers. The collector was covered with aluminum foil before the electrospinning process to better remove the electrospinning mats after the process.

1.2. Materials used for electrospinning

1.2.1. Polymers

The ε-polycaprolactone (PCL, MW=80kg.mol^{-1}) used for the production of electrospun mats at the Laboratoire Roberval was acquired in the form of beads from Sigma-Aldrich (United States).

1.2.2. Hydroxyapatite Nanoparticles

The hydroxyapatite (HA) nanoparticles (nanopowder with a particle size of ≤200 nm (BET) ≥97% synthetic) used for electrospraying were purchased from Sigma-Aldrich (USA).

1.2.3. Solvents

The different solvents used to dissolve the PCL were dichloromethane (DCM, Sigma-Aldrich) and *N,N*-dimethylformamide (DMF, Sigma-Aldrich).

1.3. Electrospinning Method

The different parameters used for the realization of the electrospun materials as well as their origins are summarized in the **Table 4**.

Structure	Concentration	Solvent	Flow Rate (ml/h)	Voltage (kV)	Speed (rpm)	Distance (cm)	Time (h)
Random	10%	DCM/DMF	1.14	15	1000	15	3.5
Random	12.50%	DCM/DMF	1.2	15	1000	15	3.5
Random	15%	DCM/DMF	1.2	15	1000	15	3.5
Aligned	10%	DCM/DMF	1.2	25	2000	15	2
Honeycomb	15%	DCM/DMF	2	25	100	15	0.13

Table 4. Parameters for the realization of the different PCL scaffolds.

While 10, 12.5 and 15% electrospun scaffold resulted from a continuous process without additives, honeycomb scaffolds arose from successive layers of PCL electrospinning and HA electrospraying. The process to obtain these materials is summarized in **Table 5**.

Layer	Technique	Solution	Time	Voltage	Distance	Needle diameter	Flow rate
1st	Electrospinning	A	8min	25kV	15cm	18G	2,0ml/h
2nd	Electrospraying	B	10min	25,5kV	15,5cm	18G	0,6ml/h
3d	Electrospinning	A	8min	25kV	15cm	18G	2,0ml/h
4th	Electrospraying	B	10min	25,5kV	15,5cm	18G	0,6ml/h
5th	Electrospinning	A	8min	25kV	15cm	18G	2,0ml/h
6th	Electrospraying	B	10min	25,5kV	15,5cm	18G	0,6ml/h
7th	Electrospinning	A	8min	25kV	15cm	18G	2,0ml/h
8th	Electrospraying	B	10min	25,5kV	15,5cm	18G	0,6ml/h
9th	Electrospinning	A	8min	25kV	15cm	18G	2,0ml/h
10th	Electrospraying	B	10min	25,5kV	15,5cm	18G	0,6ml/h
11th	Electrospinning	A	8min	25kV	15cm	18G	2,0ml/h
12th	Electrospraying	B	10min	25,5kV	15,5cm	18G	0,6ml/h
13th	Electrospinning	A	8min	25kV	15cm	18G	2,0ml/h

Table 5. Electrospinning and electrospraying parameters step by step. Solution A: PCL at 15-wt % W/V in DCM/DMF 60/40%; Solution B: HA at 10% W/V in Ethanol.

1.4. Electrospun Scaffold Characterization

1.4.1. Morphological Characterization of the Different Electrospun Scaffolds

The morphology of the different scaffolds was observed by scanning electron microscopy (Philips XL30 ESEM-FEG, Netherlands). Each sample was covered with gold before observation. The diameter of the fibres was measured on 20 fibres randomly taken by the Service d'Analyse Physico-Chimique (SAPC) of UTC.

1.4.2. Chemical Characterization of the Different Electrospun Scaffolds

In addition to the morphology of fibers, hydroxyapatite deposition over the honeycomb-like scaffold was investigated by EDS analysis in order to verify it presence on each scaffold by employing an EDS detector present in the microscope. The measurement is based on the energy and intensity distribution of X- ray signals produced by the electron beam striking the surface of the targeted scaffold.

1.4.3. Mechanical Properties of Electrospun Scaffolds

The elastic modulus of each material was quantified using uniaxial tensile tests. Six samples of each scaffold were cut into strips measuring 1.0 x 3.0 cm. The thickness of each sample was evaluated using a precision dial thickness gauge (Mitutoyo Corporation, Japan) or caliper (minimum scale: 0.1 mm). The samples were attached with the metal grips of the traction machine (Bose Electroforce 3200, TA, USA) and stretched at a speed of 0.1 mm^{-1} using a 22N cell load. The modulus was calculated by analyzing the stress-strain curve in the elastic zone. 10, 12.5 and 15-wt % were tested for both dry and wet conditions (immersion for 45 minutes in ethanol then immersed in PBS for 1 day) while honeycomb scaffolds were only tested for dry conditions.

1.4.4. Statistical Analysis

At least 6 independent experiments were carried out for each analyze. The significance of the results was tested by analysis of variance (ANOVA) with Turkey´s post hoc test.

2. Cell Culture

2.1. The Origin of the Cells

2.1.1. Mesenchymal Stem Cells Line

The murine stem cells C3H10T1/2 (ATTCCCL-226) mouse line was a gift from Université Pierre et Marie Curie (UMR 7622, Institut de Biologie du Développement Paris-Seine). The cells (at passage P10) were cultured on a 75cm^2 flask (T75, BD Falcon, Dutscher, Germany) in DMEM Low-Glucose medium (Hyclone, USA) supplemented with 10% fetal calf serum (FBS, Gibco Invitrogen, USA), 1% Penicillin-Streptomycin (Gibco Invitrogen, USA) and 2mM L-Glutamine (Gibco Invitrogen, USA) under standard culture conditions up to 80% confluence. Once at confluence, the cells were rinsed with PBS 7.4 (Phosphate buffered saline, Thermo Fisher Scientific, USA) and detached from the culture flasks by the action of trypsin EDTA 0.25% (Thermo Fisher Scientific, USA). In a second step, trypsin was inactivated with culture medium containing 10% FBS and the cells were centrifuged at 1060rpm. The cells were re-suspended in the medium supplemented with 10% FBS, counted and seeded in 75 cm^2 (T75) culture flasks until confluence to repeat the protocol or be used. The media was completely renewed every 2-3 days.

2.1.2. Primary Bone Marrow Stromal Cells

Bone marrow stromal cells (BMSCs) were isolated from healthy 5-6 weeks Sprague Dawley rats. Once sacrified, both right and left femur were isolated under sterile conditions and immersed in PBS 7.4 (Phosphate buffered saline, Gibco Invitrogen, USA) supplemented with 100 U/mL penicillin (Gibco Invitrogen, USA). After cutting joint capsules at the ends of the diaphysis a disposable needle was used to perform holes in the spongy bone of each extremity. α-MEM culture medium (PAN BIOTECH, Germany) supplemented with 10% foetal bovine serum (FBS, Gibco Invitrogen, USA), 1% of penicillin-streptomycin (Gibco Invitrogen, USA) and 1% amphotericin B (PAN BIOTECH, Germany) was then used to wash the bone marrow cavity to collect cells in a sterile 6-well dishes (BD Falcon™, USA). This procedure was repeated three times for each bone. After 24h non-adherents cells were carefully discarded and adherent cells were cultured with fresh α-MEM for 6-7 days. Cell culture media was replaced every 3 days. When culture dishes became nearly confluent, the cells

were detached and serially sub cultured. Cells at third passage (P3) were used for cell seeding experiments.

2.2. Cell Culture over Electrospun Scaffolds

For C3H10T1/2 cells, honeycomb scaffolds and 10, 12.5 and 15-wt % scaffolds were cut into squares of 17x17 mm. In addition 10, 12.5 and 15-wt % scaffolds were cut into rectangles of 40 x 12.5 mm for dynamic culture experiments. Once cut, each scaffold was disinfected for 45 minutes in a 70% ethanol solution (Sigma-Aldrich, USA). After three washes with PBS 7.4 (PBS, Sigma-Aldrich, USA), $1x10^5$ cells x cm^{-2} were cultured on each sample. After 2 days of culture, the complete DMEM medium was replaced and cell culture was continuous until the end of the experiments.

For BMSCs, 10-wt % scaffolds were cut into stripes of 40 x 12.5 mm or 35 x 9 mm, disinfected and washed as shown before and soaked into fresh complete α-MEM for 48h before seeding cells to facilitate cell adhesion. Once the time has elapsed, $6x10^4$ cells cm^{-2} were seeded into each scaffold. After 2 days of culture, the complete α-MEM was replaced and cell culture was continuous until the end of the experiments.

2.3. Mechanical Stimulation over Cell-Constructs

The mechanical solicitations were conducted over cell-constructs in two different bioreactors: (1) Bose Biodynamic 5100 (TA Electroforce ®, USA) composed of a culture chamber with a volume of about 200 mL, autoclavable, allowing the capture of a sample between metallic clamps to apply mechanical loads during culture. The device and its use are reported in detail in Chapter 4 and 5. (2) MechanoCulture T6 Mechanical Stimulation System (CellScale Biomaterials Testing, Waterloo, ON, Canada) consisted in a cell culture chamber with a volume of about 400 ml which contained an actuator and screw-driven clamps grips mounted inside and capable of applying uniaxial stretching on 6 parallel samples. The bioreactor and its use are reported in detail in **Chapter 5**.

2.4. Monitoring Cell Activity

2.4.1. Live and Dead

After 5 days of culture on scaffolds, cell-constructs were washed with PBS 7.4 and viability was estimated with a Live/Dead kit (Invitrogen, Waltham, MA, USA). Cells were stained with a solution containing calcein-AM (1 mM) and ethidium homodimer-1 (EthD-1, 1 mM) to stain viable and dead cells, respectively. Then the stained samples were observed using fluorescence microscopy (Leica Microsystem, Wetzlar, Germany).

Fluorochrome	Excitation wavelength	Emission wavelength	Color
Calcein AM	488 nm	491-573 nm	Green
Ethidium homodimer-1	561 nm	581-735 nm	Red

Table 6. Fluorescent stains used for cell viability analysis.

2.4.2. Cell Morphology

Once the cell culture phase was achirved, cell-constructs were washed three times in PBS and fixed for 10 min in a solution of 4% (v/v) paraformaldehyde solution (PAF, Agar Scientific, United Kingdom) in PBS 7.4 or 1h in a Rembaum solution. Once rinsed three times with PBS, each sample was observed by scanning electron microscopy (Philips XL30 ESEM-FEG, Netherlands) or confocal microscopy (Inverted ZEISS 710 confocal microscope, Zeiss, Germany). For SEM analysis, each sample was gold-coated prior observation. For confocal analysis, each sample was permeabilized 10 min in a solution of PBS-Triton X-100 0.5% (v/v) (VWR, United Kingdom), rinsed three times with PBS 7.4 and incubated with a solution containing 5 U/mL of rhodamine-phalloidin (Invitrogen, USA) to selectively stain the F-actin was added for 45 min at room temperature after permeabilization. After washing three times with PBS 7.4, samples are counterstained for cell nuclei with a solution containing 0.5 µg/ml Hoechst 33342 (Sigma-Aldrich, USA) in PBS 7.4.

Fluorochrome	Excitation wavelength	Emission wavelength	Color
Hoechst 33342	346 nm	460 nm	Bleu
Rhodamine-phalloidin	540 nm	565 nm	Red

Table 7. Fluorescent stains used for cell morphology analysis.

2.4.3. Cell Proliferation

2.4.3.1. MTT

MTT assay (3-(4, 5-dimethylthiazol-2yl)-2, 5-diphenyl-2H-tetrazolium bromide, Sigma-Aldrich, USA) was used for the evaluation of cell proliferation on cell-constructs. After each time point, cell-constructs were washed with PBS and each construct was plated with 2.5 mg/mL of MTT in complete culture media. After 3 h of incubation, dimethyl sulfoxide (DMSO, Sigma-Aldrich, USA) was used to dissolve the newly formed formazan crystals. 100 µL of the supernatant are transferred into a 96 well plate (Corning Microplates, USA). The absorbance of the solution was measured using a Spark multimode microplate reader (TECAN, Swiss) at a wavelength of 590 nm.

2.4.3.2. DNA Quantification

After each time point, cell-constructs were removed from cell culture media and placed into separated RNase-free 1.5ml eppendorfs (Microfuge Tubes 1.5ml, Thermo Fisher Scientific, USA). Then samples were lysed by the action of 1ml of Trizol (TRI Reagent®, Sigma-Aldrich, USA) for 5 min at room temperature. Upon addiction of 0.2 ml of chloroform (Sigma-Aldrich, USA) samples were allowing to stand for 15 min. By centrifuging the resulting mixture at 12,000 g for 15 min at 4ºC, DNA is separated in an interphase. To precipitate the DNA from the interphase 0.3 ml of 100% ethanol (Sigm-Aldrich, USA) was added. The mixture was then mixed by inversion and allowed to stand for 2–3 minutes at room temperature. Upon a centrifugation at 2,000 × g for 5 minutes at 4 °C, DNA precipitates into the bottom of the eppendorf. To ensure the quality of the DNA, the final precipitate was washed twice with 1ml of a solution of trisodium citrate 0.1M (Sodium citrate dihydrate, Sigma-Adrich, USA) in a solution of 10%. Once rinsed, DNA was resuspended with a solution of 75% ethanol and dry at room temperature. Dry DNA was finally dissolved in 0.3ml of NaOH 8mM (Sodium Hydroxide, Sigma-Aldrich, USA) and quantified with NanoDrop ND-1000 (Thermo Scientific, USA).

2.4.4. Protein Production

2.4.4.1. Immunofluorescence Staining

For immunofluorescence staining, each sample was permeabilized 10 min in a solution of PBS-Triton X-100 0.5% (v/v) (VWR, United Kingdom), rinsed three times with PBS 7.4 and incubated in a solution containing mouse primary antibodies anti-rat collagen type I (COL1, 1:100, Abcam, United Kingdom) or anti-rat tenomodulin (TNMD, 1:200, Abcam, United Kingdom) in a solution of BSA 0.1% overnight at 4ºC, then washed three times with PBS 7.4 and incubated for 1h at room temperature with secondary fluorescent antibodies donkey anti-mouse 488 (Invitrogen, USA). After washing three times with PBS 7.4, samples are counterstained with a solution containing 0.5 µg/ml Hoechst 33342 (Sigma-Aldrich, USA) in PBS for cell nuclei staining.

Fluorochrome	Excitation wavelength	Emission wavelength	Color
Donkey anti-mouse 488	495	519	Green
Hoechst 33342	346	460	Bleu

Table 8. Fluorescent antibodies used for cell morphology analysis.

2.4.4.2. Hydroxyproline Quantification

After each time point, cell-constructs were removed from cell culture media and placed into separated RNase-free 1.5ml eppendorfs (Microfuge Tubes 1.5ml, Thermo Fisher Scientific, USA). Then samples were lysed by the action of 1ml of Trizol (TRI Reagent®, Sigma-Aldrich, USA) for 5 min at room temperature. Upon addiction of 0.2 mL of chloroform (Sigma-Aldrich, USA), samples were allowed to stand for 15 min. By centrifuging the resulting mixture at 12,000 g for 15 min at 4ºC, proteins are separated in a lower red organic phase. To precipitate the proteins from the lower-phase, 0.3 mL of 100% ethanol (Sigma-Aldrich, USA) was added. The mixture was then mixed by inversion and allowed to stand for 2–3 minutes at room temperature. Upon a centrifugation at 2,000 × g for 5 minutes at 4 °C, soluble proteins were found in the supernatant. Then proteins were precipitated with 1.5ml of 2-propanol (Isopropanol, Sigma-Aldrich, USA) and centrifuged at 12,000 g for 10 min at 4ºC. After precipitation, proteins were washed three times in a 2ml solution of 0.3M-guanidine hydrochloride (Sigma-Adrich, USA) in 95% ethanol. After washing, proteins were resuspended in a solution of ethanol 100%, dryed at 65ºC for 10 min and hydrolysed with a solution of 6N HCl at 120ºC for 3h. Once lysate, 50 µL of the hydrolyzed proteins were

transferred into a 96 well plate (Corning Microplates, USA) and evaporated at 60ºC for 3h. Once evaporated, the samples were incubated for 5 min with a 100µL mixture solution of Chloramine T/Oxidation buffer (Sigma-Aldrich, USA). After 5 minutes, 100µL mixture solution of DMAB/Percloric acid/Isopropanol was added. The mixture was incubated for 90 min at 60ºC and the absorbance was measured at a wavelength of 560nm using a Spark multimode microplate reader (TECAN, Swiss).

2.4.4.3. Alkaline Phosphatase Production

Alkaline phosphatase (ALP) coloration was performed with a solution BCIP/NBT (Sigma-Aldrich, USA). Once the cell-constructs were fixed in a 4% PAF solution and rinsed three times with PBS 7.4, each sample was then permeabilized 10 min in a solution of PBS-Triton X-100 0.5% (v/v) (VWR, United Kingdom), rinsed three times with PBS 7.4 and incubated with 1ml of the ready-to-use BCIP/NBT solution for 1h. Areas that stained purple were considered as positive.

ALP activity was assessed using a quantitative colorimetric Alkaline Phosphatase Assay Kit (Abcam, UK) following manufacturer's instruction. The samples were placed in 500 µL of supplied assay buffer, vortexed and then centrifuged for 3 minutes at 13,000 g. The supernatants were recovered and 80µL of each sample was placed in a 96-well plate. The enzymatic reaction was initiated by adding 5mM of the ALP substrate. The plate was then shake and placed 60 min at 25°C in the dark. Adding 20µL of the stop solution provided by the kit stopped the reaction. The plate was briefly agitated, and then the absorbance was measured using a Spark multimode microplate reader (TECAN, Swiss) at 405nm.

2.4.5. Gene Expression

The gene expression was studied using RT-qPCR (reverse quantitative transcription polymerase chain reaction) on the different samples at the Laboratoire de Biologie du Développment (UPMC, Paris) by Dr. Ludovic Gaut. At each time point, the samples were lysed with 350 µl of RLT buffer (Qiagen, Germany). The lysate was then transferred to an RNase-free 1.5ml eppendorfs (Microfuge Tubes 1.5ml, Thermo Fisher Scientific, USA) and centrifuged to extract ribonucleic acid (RNA) according to the manufacturer's protocol. RNA

was retroactively transcribed into deoxyribonucleic acid (DNA) using a high-capacity cDNA reverse transcription kit (Applied Biosystems, USA) according to the manufacturer's protocol. The RT-qPCR was performed using the Master Mix SYBR Green PCR (Applied Biosystems). Relative mRNA levels were calculated using the 2-ΔΔCt method. The ΔCts were obtained from standardized Ct with the levels of the Rplp0 gene in each sample. The primers are listed in **Table 9** and the reactions were verified before the experiments (efficacy > 80%, R2 > 0.99).

Genes	Primer sequences
Rplp0	Forward 5' ACCTCCTTCTTCCAGGCTTT
	Reverse 5' CTCCCACCTTGTCTCCAGTC
Aqp1	Forward 5' CAATTCACTTGGCCGCAATGACCT
	Reverse 5' TACCAGCTGCAGAGTGCCAATGAT
Col1α1	Forward 5' TGGAGAGAGCATGACCGATG
	Reverse 5' GAGCCCTCGCTTCCGTACT
Dlx5	Forward 5' CGTCTCAGGAATCGCCAACT
	Reverse 5' AGTCAGAATCGGTGGCCG
Bglap	Forward 5' CAGCGGCCCTGAGTCTGA
	Reverse 5' TTATTGCCCTCCTGCTTGGA
RunX2	Forward 5' GGTCCCCGGGAACCAA
	Reverse 5' GGCGATCAGAGAACAAACTAGCTTT
Scx	Forward 5' CCTTCTGCCTCAGCAACCAG
	Reverse 5' GGTCCAAAGTGGGGCTCTCCGTGACT
Tnmd	Forward 5' AACACTTCTGGCCCGAGGTAT
	Reverse 5' AAGTGTGCTCCATGTCATAGGTTTT

Table 9. List of primers used for RT-qPCR.

2.4.6. Biomechanical Evaluation

An analysis of different mechanical properties was carried on electrospun scaffolds in the presence or absence (controls) of cells by recording the strain (ε) and the stress (σ) over the time course of the experiment (Figure 6). In the experiment, we imposed the displacement (strain) and recorded the corresponding force (stress).

$$\varepsilon = \varepsilon_0 \sin \omega t \ (1)$$

$$\sigma = \sigma_0 \sin(\omega t - \delta) \ (2)$$

Where δ is the phase lag.

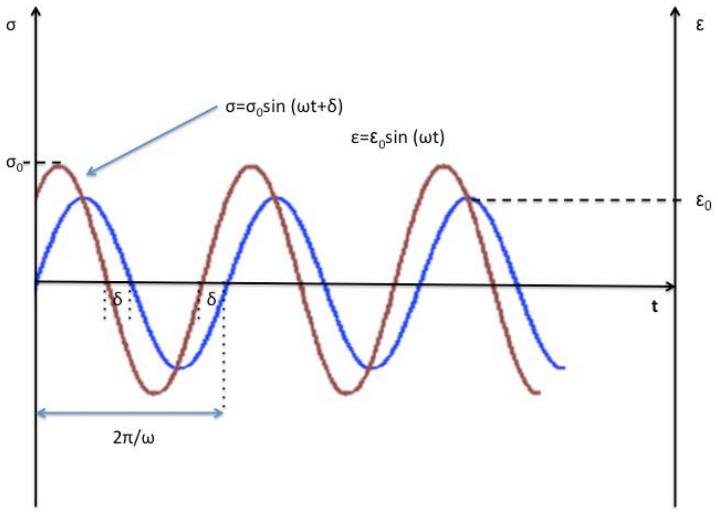

Figure 6: Schematic representation of stress vs strain.

Strain-stress curves could then be drawn (see chapters 4 and 5). Several mechanical parameters such as the dissipated energy (hysteresis), the storage modulus (E'), the loss modulus (E''), the complex modulus (E*), the tan δ, were calculated with Matlab through the work of two internship students, Mortiz von Wrangel and Jean Baptiste Perot, according to the following equations:

$$E' = \frac{\sigma_0}{\varepsilon_0}\cos\delta \quad (3)$$

$$E'' = \frac{\sigma_0}{\varepsilon_0}\sin\delta \quad (4)$$

If we represent E' and E'' we can obtain a relationship between E', E'' and the complex modulus (E*), where E* could be obtained as a geometric function:

$$E^* = \sqrt{E'^2 + E''^2} \quad (5)$$

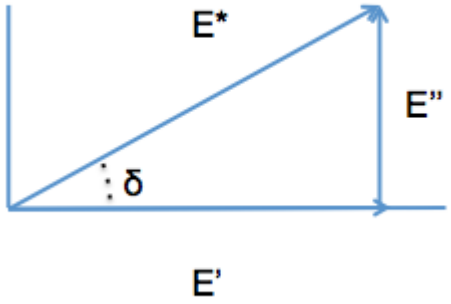

Figure 7: Geometric representation of E' and E'' and their relationship with E*.

In the same manner, by obtaining E* we could calculate E’ and E’’:

$$E' = E^* \cos \delta \quad (6)$$

$$E'' = E^* \sin \delta \quad (7)$$

2.4.7. Statistical analysis

At least 6 independent experiments, except for the biomechanical analysis carried out on chapter 5, were realized for each analyze. The significance of the results was tested by analysis of variance (ANOVA) with Turkey´s post hoc test in the case of multiple comparisons and by Student´s test in the case of two-to-two comparisons.

Chapter III: (Article) Poly (ε-caprolactone)/Hydroxyapatite 3D Honeycomb Scaffolds for a Cellular Microenvironment Adapted to Maxillofacial Bone Reconstruction

ACS Biomaterials SCIENCE & ENGINEERING
Cite This: ACS Biomater. Sci. Eng. 2018, 4, 3317−3326
Article
pubs.acs.org/journal/abseba

Poly(ε-caprolactone)/Hydroxyapatite 3D Honeycomb Scaffolds for a Cellular Microenvironment Adapted to Maxillofacial Bone Reconstruction

Alejandro Garcia Garcia,[†] Anne Hébraud,[‡] Jean-Luc Duval,[†] Corinne R. Wittmer,[‡] Ludovic Gaut,[§,∥] Delphine Duprez,[§,∥] Christophe Egles,[†] Fahmi Bedoui,[⊥] Guy Schlatter,[‡] and Cecile Legallais*[,†]

[†]CNRS, UMR 7338 Laboratory of Biomechanics and Bioengineering, Sorbonne Universités, Université de Technologie de Compiègne, Rue du Dr. Schweitzer, 60200 Compiegne, France

[‡]ICPEES UMR 7515, Institut de Chimie et Procédés pour l'Energie, l'Environnement et la Santé, CNRS, Université de Strasbourg, 25 Rue Becquerel, 67087 Strasbourg, France

[§]CNRS, UMR 7622, IBPS-Developmental Biology Laboratory, Sorbonne Université, 7-9 Quai Saint Bernard, 75005 Paris, France

[∥]Inserm U1156, 7-9 Quai Saint Bernard, 75005 Paris, France

[⊥]Roberval Laboratory for Mechanics, Sorbonne Universités, Université de Technologie de Compiègne, Rue du Dr. Schweitzer, 60200 Compiègne, France

Supporting Information

ABSTRACT: The elaboration of biomimetic materials inspired from the specific structure of native bone is one the main goal of tissue engineering approaches. To offer the most appropriate environment for bone reconstruction, we combined electrospinning and electrospraying to elaborate an innovative scaffold composed of alternating layers of polycaprolactone (PCL) and hydroxyapatite (HA). In our approach, the electrospun PCL was shaped into a honeycomb-like structure with an inner diameter of 160 μm, capable of providing bone cells with a 3D environment while ensuring the material biomechanical strength. After 5 days of culture without any differentiation factor, the murine embryonic cell line demonstrated excellent cell viability on contact with the PCL-HA structures as well as active colonization of the scaffold. The cell differentiation, as tested by RT-qPCR, revealed a 6-fold increase in the expression of the RNA of the Bglap involved in bone mineralization as compared to a classical 2D culture. This differentiation of the cells into osteoblasts was confirmed by alkaline phosphatase staining of the scaffold cultivated with the cell lineage. Later on, organotypic cultures of embryonic bone tissues showed the high capacity of the PCL-HA honeycomb structure to guide the migration of differentiated bone cells throughout the cavities and the ridge of the biomaterial, with a colonization surface twice as big as that of the control. Taken together, our results indicate that PCL-HA honeycomb structures are biomimetic supports that promotes in vitro osteocompatibility, osteoconduction, and osteoinduction and could be suitable for being used for bone reconstruction in complex situations such as the repair of maxillofacial defects.

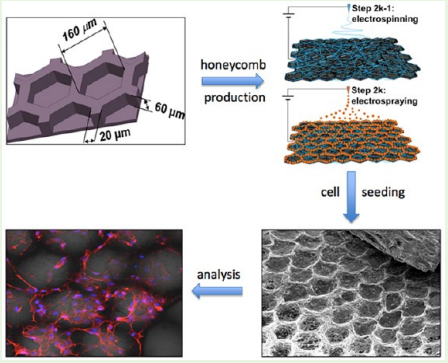

KEYWORDS: *bone, electrospinning, honeycomb, cell differentiation, biomimetic*

INTRODUCTION

Bone is a hierarchical and complex mineralized connective tissue involved in a continuous remodelling process.[1] The remodelling cycle is composed of three consecutive phases: (I) resorption of old bone by osteoclasts, (II) transition from resorption to bone formation, and (III) formation of new bone matrix by osteoblasts.[2] This extracellular matrix is composed of organic components, mainly type I collagen and other inorganic compounds such as calcium phosphates.[3,4] It is organized in cylindrical units called osteons, which have a diameter of around 200 μm in a human adult. There are multiple situations in which bone regeneration is compromised, such as diseases, aging, or major defects, where the bone need reconstruction.[5] For example, maxillofacial defects are still a surgical challenge[6] as a result of trauma and disfigurement.[7] Autologous bone grafts remain the "gold standard"[8,9] but are not free of drawbacks such as a high level of postsurgical morbidity or the limited availability and quality of bone.[10]

The use of biomaterials and recent developments in tissue engineering[11] are promising for complete regeneration of bone defects by combining materials, cells, and growth factors, making possible the creation of a scaffold that resembles native tissue.[12] Different materials have been proposed over the years

Received: May 3, 2018
Accepted: August 20, 2018
Published: August 20, 2018

DOI: 10.1021/acsbiomaterials.8b00521
ACS Biomater. Sci. Eng. 2018, 4, 3317−3326

to mimic the organic and porous part in bone tissue based on either bio-organic molecules[13−17] or on synthetic polymers such as poly(ε-caprolactone) (PCL),[18,19] or others.[20,21] One of the main limitations of organic compounds is their rapid degradation and the lack of mechanical strength, while synthetic polymers suffer from a lack of osteoconduction and osteoinduction, two major requirements for bone healing.[22] There has thus been interest in recent years in combining these polymers with bioceramics such as tricalcium phosphate (TCP) or hydroxyapatite (HA) to benefit from the inorganic composition inherent to the bone.[23−25]

The structure of the extracellular niche and the 3D organization are also of prime importance. Varied approaches have been deployed to generate scaffolds. These include hydrogel formation,[26] freeze-drying,[27] extrusion,[28] or more recently 3D printing.[29] Of these approaches, electrospinning[30] is one of the most promising techniques for creating a fibrous matrix that mimics the extracellular bone matrix, creating a 3D environment suitable for the cells.[31,32] However, although a thin layer of an electrospun material is considered to be very porous, the high packaging density of a scaffold prevents the cells from correct colonization through thick materials. In addition, these structures do not mimic the osteon organization. Very recently, the advantage of using concave areas to stimulate osteoblasts and therefore enhance bone formation was highlighted using a variety of techniques.[33−35] Composite scaffolds with a controlled 3D microstructure could be obtained using cooperative electrostatic interactions during simultaneous electrospinning and electrospraying on a rotating micropatterned collector.[36] As an illustration, honeycomb structures were composed of PCL in which nanoparticles of hydroxyapatite were inserted to control the bilayered structure of the cavities.[37]

Therefore, in this study, we proposed the development of new, multilayered scaffolds made of PCL fibers and HA particles with controlled pore size, mimicking the osteon structure, imagined as a honeycomb network.[38] According to the characterization of its physical and mechanical properties, the colonisation and differentiation in the honeycomb structures were assessed using two approaches: (I) study of the early fate of a mesenchymal stem cell line of mice origin, cultured on the scaffold in the absence of any differentiation factor, and (II) the organotypic culture of bone from chicken embryos, a common biocompatibility test for implantable biomaterials.

MATERIALS AND METHODS

Fabrication of the Honeycomb Collectors. Honeycomb micropattern collectors were manufactured by means of photolithography. An SU-8 2050 (Microchem) photoresist layer with a thickness of 60 μm was deposited over a silicon wafer. The photoresist layer was exposed to UV light through a honeycomb mask using a mask aligner (MJB4, SUSS Microtec). The photoresist layer was then developed and cured to obtain the honeycomb micropatterns. Finally, a Plassys MEB5505 electron beam evaporator was used to deposit a conductive layer (composed of a 120 nm Al layer and a 30 nm Au layer) on the collectors. The micropatterns covered a square area measuring 44 mm × 44 mm. The internal size of the honeycombs was 160 μm, the width and height of the honeycomb walls were 20 and 60 μm, respectively (see Figure 1B).

Scaffold Production by Electrospinning/Electrospraying. A solution of 15 wt % poly(ε-caprolactone) (PCL, MW = 80 kg mol^{-1}, CAPA 6806, Perstorp) was dissolved in dichloromethane (DCM, Sigma-Aldrich)/*N*,*N*-dimethylformamide (DMF, Reagent Plus ≥99%, Sigma-Aldrich) (60/40 v/v) for 24 h before electrospinning. Then 10 wt % hydroxyapatite (HA, Sigma-Aldrich, nanopowder with a particle size of ≤200 nm (BET), ≥97% synthetic) suspension was prepared in ethanol (Sigma-Aldrich) 48 h prior to electrospraying and ultrasonicated for 5 min (Branson Sonifier) just before processing. Alternating deposition (13 layers, Supporting Information, Table S1) of electrospun PCL layers (distance 15 cm; flow rate 2 mL/h; needle diameter 18G; voltage 25 kV) and electrosprayed HA layers (distance 15.5 cm; flow rate 0.6 mL/h; needle diameter 18G; voltage 25.5 kV) was performed over a homemade rotating collector. For control, 15% PCL was electrospun over a flat aluminum foil with the same parameters.

SEM Characterization and Energy Dispersive X-ray Spectroscopy (EDS) Analysis. The morphology and topography of the honeycomb-like scaffolds were observed by scanning electron microscopy (Philips XL30 ESEM-FEG). Electrospun mats were cleaned with ethanol, placed in an ultrasound bath to remove any impurities, and gold coated prior to observation. Hydroxyapatite deposits over the honeycomb-like scaffold were investigated by EDS analysis using the EDS detector present in the microscope. The measurement is based on the energy and intensity distribution of X-ray signals produced by the electron beam striking the surface of the targeted scaffold.

Tensile Testing. The scaffolds modulus was quantified using uniaxial tensile testing. One sample of each scaffold (n = 3) was cut up into a stripe measuring 1.0 cm × 3.0 cm, with a thickness of 31 ± 5 μm. The thickness of the scaffolds was evaluated using a precision dial thickness gauge (Mitutoyo Corporation, Japan). The samples were secured with the metallic grips of the tensile tester (Bose Electroforce 3200, TA, USA) and stretched at a rate of 0.1 mm s^{-1} using a cell load of 22N. Modulus was calculated by analysis of the stress−strain curve in the elastic zone. Ultimate strength (UTS) was measured from the highest peak in the stress−strain curve.

Cell Seeding on Scaffolds. The embryonic murine cell line C3H10T1/2 (ATCCCL-226) was cultured on to a Corning T-75 flask at a confluence of 85% with Dulbecco's Modified Eagle's Medium low-glucose (DMEM; Hyclone, USA) supplemented with 10% fetal bovine serum (FBS, Gibco Invitrogen, USA), 2 mM glutamine (Gibco Invitrogen, USA), and 1% of penicillin−streptomycin (Gibco Invitrogen, USA) under standard culture conditions. To evaluate the response of the cells to materials, the scaffolds were cut into squares measuring 17 mm × 17 mm, disinfected with ethanol 70% (Sigma-Aldrich, USA) for 45 min, and washed with PBS 7.4 (phosphate buffered saline, Gibco Invitrogen, USA) for 10 min before the cell culture experiment. Each scaffold was plated with a density of 1 × 10^5 cells cm^{-2}. After 2 days of culture, the culture media were replaced and the culture was prolonged for three additional days.

Cell Viability and Proliferation. After 5 days of culture cell viability was estimated with a Live/Dead kit (Invitrogen, Waltham, MA, USA). Calcein AM (1 mM) and ethidium homodimer-1 (EthD-1, 1 mM) fluorescent dyes were used to stain viable and dead cells, respectively. The samples were observed using fluorescence microscopy (Leica Microsystem, Wetzlar, Germany), allowing us to qualitatively determine cell viability and distribution. Next, cell proliferation was evaluated at different time points (24, 48, and 96 h) with 3-(4, 5-dimethylthiazol-2yl)-2, 5-diphenyl-2*H*-tetrazolium bromide (MTT) assay. After different time periods, 2.5 mg/mL of MTT in complete culture media was added on each well. After 3 h of incubation, dimethyl sulfoxide (DMSO) was used to dissolve formazan crystals. The absorbance of the solution was measured using a Spark multimode microplate reader (TECAN, Swiss) at a wavelength of 590 nm. SEM (Philips XL30 ESEM-FEG) was used to observe the attachment of the cells to the scaffolds. After 5 days of culture, all the samples were washed twice with PBS, fixed in a solution of Rembaum for 1 h, and then washed twice with permuted water. Each sample was finally gold-coated for SEM observation.

Cell behavior on the scaffold was assessed using rhodamine phalloidin (Invitrogen, USA) to selectively stain the F-actin. The cells were fixed with 4% (w/v) paraformaldehyde solution (PAF, Agar

DOI: 10.1021/acsbiomaterials.8b00521
ACS Biomater. Sci. Eng. 2018, 4, 3317−3326

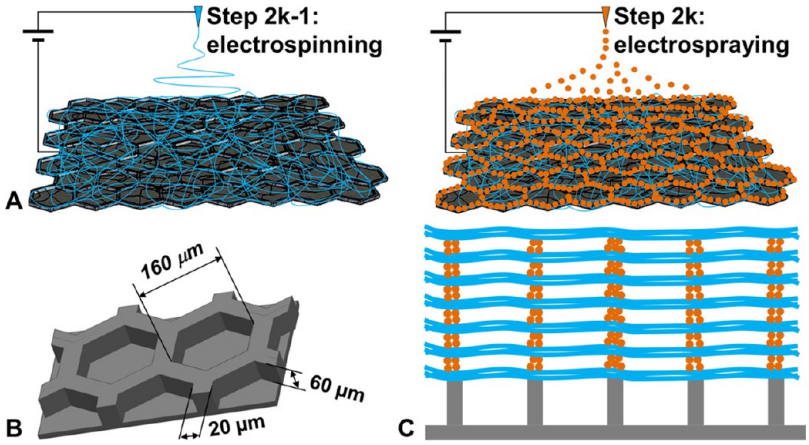

Figure 1. Design of the honeycomb-like scaffolds. (A) Odd steps: electrospinning process. Even steps: electrospraying process. (B) Geometry of the honeycomb collector. (C) Both steps were repeated to achieve the production of a 3D multilayer scaffold with HA microparticles mainly located over the wall of the honeycomb collector thanks to the electrostatic template effect.

Scientific, United Kingdom) in PBS for 10 min then permeabilized with 0.5% Triton X-100 (VWR, United Kingdom) for 10 min. Nonspecific binding sites were blocked by incubating the substrates in 1% (w/v) BSA (Sigma-Aldrich, USA) in PBS for 15 min. The staining solution rhodamine phalloidin was added at 5 U/mL for 45 min. In addition, Hoechst 33342[39] was added to every experiment. Samples were then washed in PBS and observed with an Inverted ZEISS 710 confocal microscope (Zeiss, Germany) and Leica fluorescence microscopy (Leica Microsystems, Germany).

Gene Expression Analyses. Gene expression was studied using RT-qPCR (reverse transcription quantitative polymerase chain reaction) after 5 days of culture on the scaffolds. Briefly, samples were lysed with 350 μL of RLT Buffer (Qiagen, Germany) and centrifuged to extract the RNA (ribonucleic acid) according to the manufacturer's protocol. The RNA was retro-transcribed into DNA (DNA) using a High Capacity cDNA Reverse Transcription Kit (Applied Biosystems, USA) according to the manufacturer's protocol. RT-qPCR was performed using the SYBR Green PCR Master Mix (Applied Biosystems). Relative mRNA levels were calculated using the $2-\Delta\Delta Ct$ method.[40] The ΔCts were obtained from Ct normalized with the Rplp0 gene levels in each sample. The primers are listed in Supporting Information, Table S2, and reactions were checked before the experiments (efficiency >80%, R^2 > 0.99). The results were compared with data from samples cultured without scaffolds, i.e., data were plotted as a ratio to a cell-only control group, highlighting the intrinsic effect of the scaffolds on the gene expression.

Alkaline Phosphatase (ALP) Activity. ALP activity, an early marker of osteoblast differentiation, was assessed using a quantitative colorimetric Alkaline Phosphatase Assay Kit (Abcam, UK) after 5 days of culture following manufacturer's instruction. In addition, BCIP/NBT (Sigma-Aldrich, USA) solution was used according to the manufacturer's protocol to stain alkaline phosphatase. Areas that stained purple were considered as positive.

Organotypic Culture. Slices of bone from chicken embryos explanted tissue were put over the surface of honeycomb scaffolds (n = 20).[41] Every sample was cultured over 2 weeks into Dulbecco's Modified Eagle's Medium low-glucose (DMEM; Hyclone, USA) supplemented with 40% fetal bovine serum (FBS, Gibco Invitrogen, USA), 2 mM glutamine (Gibco Invitrogen, USA), and 0.15% of penicillin–streptomycin (Gibco Invitrogen, USA) under standard culture condition. After 2 weeks of culture, 16 samples were observed with an Optical Microscopy (×25), and four samples were fixed into Rembaum solution for 1 h and then washed twice with permuted water. Each sample was finally coated with gold for SEM observation.

Statistical Analysis. All data are represented as mean ± standard deviation (SD). Mann–Whitney nonparametric statistical test was used to define the significance of the results.

RESULTS

Production and Materials Characterization of Honeycomb-Like Electrospun Scaffold. Honeycomb-like scaffolds were produced by the alternate electrospinning of PCL fiber layers and the electrospraying of HA particle layers over a micropatterned collector as depicted in Figure 1. The mechanisms making microstructuration possible were explained by an electrostatic template effect, which was induced by the fiber portions deposited over the pattern holes during the first step of electrospinning. These portions of fiber, hanging in the air, retained their electric charges, leading to repulsive forces located at precise areas defined by the design of the patterned collector. On the other hand, the portions of fiber in direct contact with the collector patterns were able to dissipate their charges efficiently, thus leading to attractive forces. These repulsive and attractive forces were then able to act after an electrospraying step, resulting in precise deposits of microparticles on the attractive areas thanks to the so-called electrostatic template effect.[37]

We produced the 3D scaffolds with six bilayers (Figure 1): each bilayer consisted of a layer of electrospun PCL fibers with an average fiber diameter of 145 ± 39 nm covered by a layer of electrosprayed HA nanoparticles (Figure 1C). A final layer of PCL fibers was deposited in order to encapsulate the last layer of HA microparticles. The final thickness of the scaffold was measured as 31 ± 5 μm. The main challenge consisted in maintaining the design of the electrostatic template intact during the various electrospinning and electrospraying steps (Figure 2A–C). Enough particles had to be electrosprayed to ensure efficient electric contact with the collector patterns as shown in the inset of Figure 1B. An electrospinning time of 8 min for each layer of fibers and an electrospraying time of 10 min for each layer of particles were necessary to ensure that the honeycomb patterns were preserved throughout the process. These parameters made possible the formation of a 3D composite scaffold with a honeycomb structure, the walls of which were formed by dense deposits of HA microparticles and PCL fibers, whereas the honeycomb cavity of the collector was covered by only few PCL fibers, thus forming 3D cavities with a diameter of 160 μm sparsely filed with PCL fibers (Figure 2D). The HA deposits were verified with EDS analysis, confirming the presence of calcium (Figure 2E,F).

DOI: 10.1021/acsbiomaterials.8b00521
ACS Biomater. Sci. Eng. 2018, 4, 3317–3326

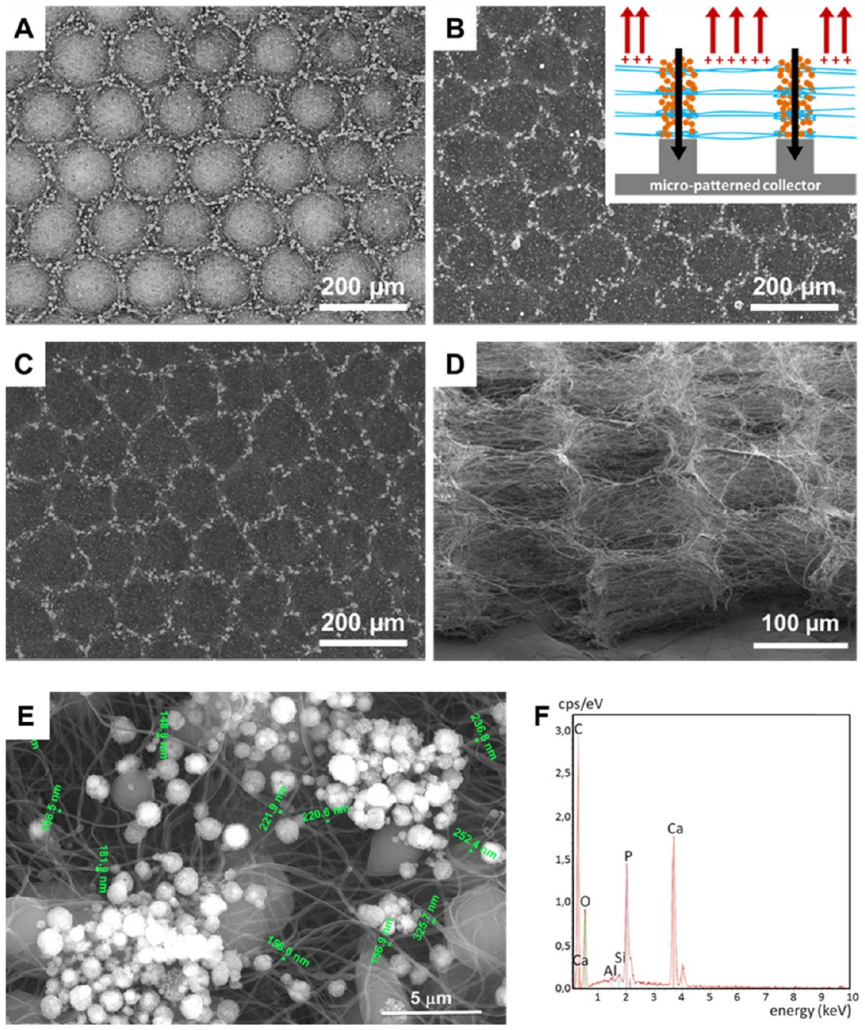

Figure 2. (A–C) SEM images obtained using a backscattered electron detector in order to enhance the contrast between HA and PCL. (A) Top view of a bilayer scaffold obtained from the electrospraying of HA particles over a layer of PCL fibers, which were previously electrospun on to a honeycomb-like micropatterned collector. (B) Top view of a PCL-HA 3D scaffolds obtained from deposits of four bilayers of PCL fibers and HA particles. The inset shows a schematic view of the cross section of this type of scaffold. The black arrows represent the conductive paths formed by the aggregated fibers and particles in contact with the walls of the collector patterns. The red arrows represent the repulsive areas due to the suspended charged fiber segments. (C) Top view of a PCL-HA 3D scaffold obtained from deposits of six bilayers of PCL fibers and HA particles. (D) Cross-section of a PCL-HA 3D scaffold showing the 3D microcavities sparsely filled by PCL fibers. Image obtained with the Everhart–Thornley detector of SEM. (E) SEM micrographs of the honeycomb-like scaffold for EDS and fiber diameter analysis. (F) EDS spectra of the sample focused over nanoparticles presented on the top of honeycomb wall.

To investigate the strength of the material, uniaxial tension tests were performed on three samples (Figure 3). The displacement velocity was set at 0.1 mm s^{-1} to avoid any damage during the loading phase. Application of Hooke's law led to the calculation of a mean modulus of 3.77 ± 0.35 MPa. The ultimate tensile strength was obtained at 971 ± 155 kPa.

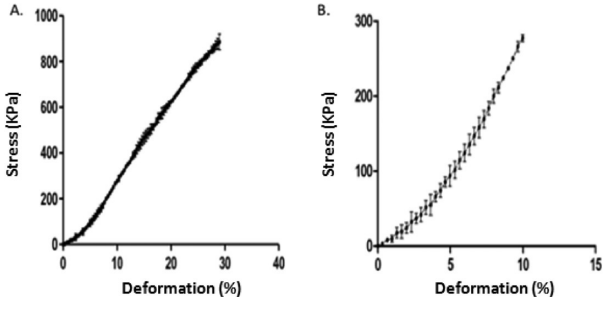

Figure 3. Representative plot of the stress–strain curve of the honeycomb scaffold (with error bars). (A) Ultimate tensile stress (UTS). (B) Linear region where the modulus was calculated from 5 to 10% strain.

Cells' Viability and Scaffold Colonization. The scaffolds were seeded with C3H10T1/2 cells at a density of 10^5 cells/cm^2 without any osteogenic factors in order to assess the effect of the scaffold alone. After 5 days of culture, Live/Dead assays were performed to evaluate the cell viability on the polymeric scaffold (Figure 4). The pictures taken under fluorescence microscopy showed excellent cell viability after 5 days of culture with most of living cells in contact with the fibers of the scaffold. MTT assay (Figure 5) indicated that cells cultured on the honeycomb scaffold proliferated, in contrast with TCP where they were probably already at confluence. This is in agreement with the increased available surface offered by the 3D structure. Indeed, Figure 6 clearly showed that after 2 h, C3H10T1/2 cells still presented a round shape and started to

DOI: 10.1021/acsbiomaterials.8b00521
ACS Biomater. Sci. Eng. 2018, 4, 3317–3326

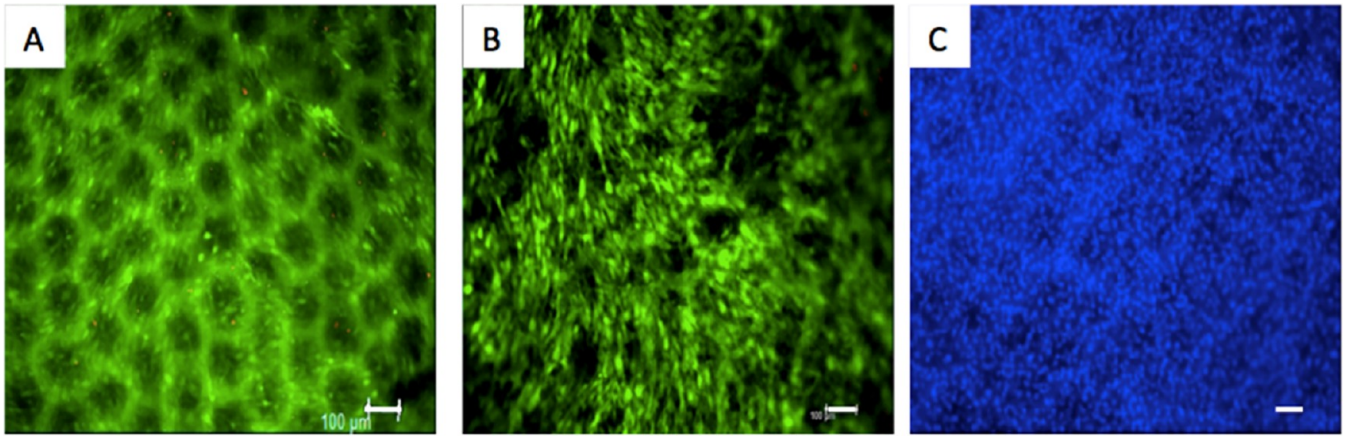

Figure 4. (A–C) C3H10T1/2 viability after 5 days of culture over honeycomb scaffold (n = 3). (A) Live and dead stained cells superposed on the honeycomb scaffold. Calcein AM (green) dye shows living cells membranes. EthD-1 dye (red dots) stained the nuclei of dead cells. (B) Live and dead staining on cells. (C) Hoechst 33342 staining all cell nuclei (blue). Scale bar = 100 μm.

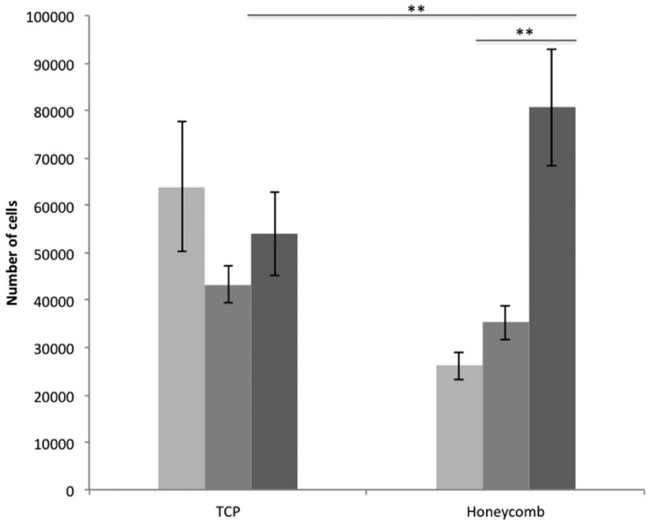

Figure 5. MTT analysis for comparing proliferation of C3H10T1/2 on honeycomb compared to tissue culture plate (TCP) at D1 (light gray), D2 (medium gray), and D5 (dark gray) (n = 3). The data obtained for MTT of the cells cultured on honeycomb-like scaffolds were compared to those of the control cells (tissue culture plate, TCP) with the Mann–Whitney nonparametric statistical test. The p-values are indicated for the tests, showing a significant difference between the two groups (** for p-value = 0.0043).

adhere on the fibers (Figure 6A). It seems that, at first, the cells preferred to attach to the top of the cavity, spreading along the fibers with an elongated shape (Figure 6B). After 48 h of culture, the C3H10T1/2 started to cover the whole depth of the cavity, from the ridge to the bottom (Figure 6C). The cells appeared uniformly distributed without any preference (Figure 6E and Supporting Information, Figure S1). Taken together, these results show that the cells could cover the entire surface of the cavity.

Cell Differentiation. The preferential differentiation outcomes of C3H10T1/2 cells cultured in the honeycomb scaffolds were evaluated though the expression of genes of interest by means of RT-qPCR at the end of 5 days of culture. Tendon- and bone-related markers were simultaneously analyzed on the cells cultured in the honeycomb scaffold and control without any differentiation factors to better demonstrate the role of our material and its specific geometry (Figure 7). *Runx2,* a specific bone transcription factor,[42] and *Bglap* a late marker involved in bone mineralization[43] were used as bone-related genes. To assess to what extent stem cells were committed to the tendon lineage, we used *Scx* (*Scleraxis*), a bHLH transcription factor expressed in tendon progenitors and differentiated cells,[44] and *Tnmd* (*Tenomodulin*) a late tendon-specific marker.[45] The expression of the gene *Col1a1* was also analyzed, although we were aware that *Col1a1* is expressed in both bone and tendon tissues. The relative mRNA levels of bone and tendon genes in the stem cells cultured on the honeycomb-like scaffold and control conditions led to an increase in *Bglap* expression (up to 6-fold increase), associated with decreased expression of the *Scx* tendon-related gene compared to the control plastic cultures, suggesting a shift toward bone differentiation. However, these results must be taken with caution as the late tendon marker *Tnmd* was also significantly upregulated in cells cultured on the honeycomb scaffold compared to their controls cultured on plastic.

C3H10T1/2 are embryonic cells that are not able to produce ALP in conventional cultures when they are not totally differentiated into osteoblast cells. This enzyme was therefore a suitable marker for investigating cell differentiation because of the intrinsic properties of the honeycomb scaffold. As shown in Figure 8, after 5 days of conventional culture (without any growth factors) in the honeycomb scaffold, high ALP-positive staining (in purple) was found (Figure 8C, indicating changes in phenotype toward osteoblast cells. The negative control without cells showed no staining. In addition, ALP synthesis was quantitatively assessed (Figure 8D) under both culture conditions. ALP activity was found 1.7-fold increased on the honeycomb scaffold. Altogether, these results clearly support the positive effect of the honeycomb scaffolds on cells' differentiation toward bone lineage in the absence of any differentiation factor.

Organotypic Culture. The colonisation by cells originating from bone slices of chicken embryos was observed by scanning electron microscopy and optical microscopy after 14 days of culture. The cells from the explanted tissue spread over a surface of 4.7 mm^2 for the control (15% PCL random) (Figure 9A) and 11 mm^2 for the honeycomb scaffolds (Figure 9B). This migration took place over the whole cavity in both the depth and ridge of the honeycomb (Figure 9C,D) with no

DOI: 10.1021/acsbiomaterials.8b00521
ACS Biomater. Sci. Eng. 2018, 4, 3317–3326

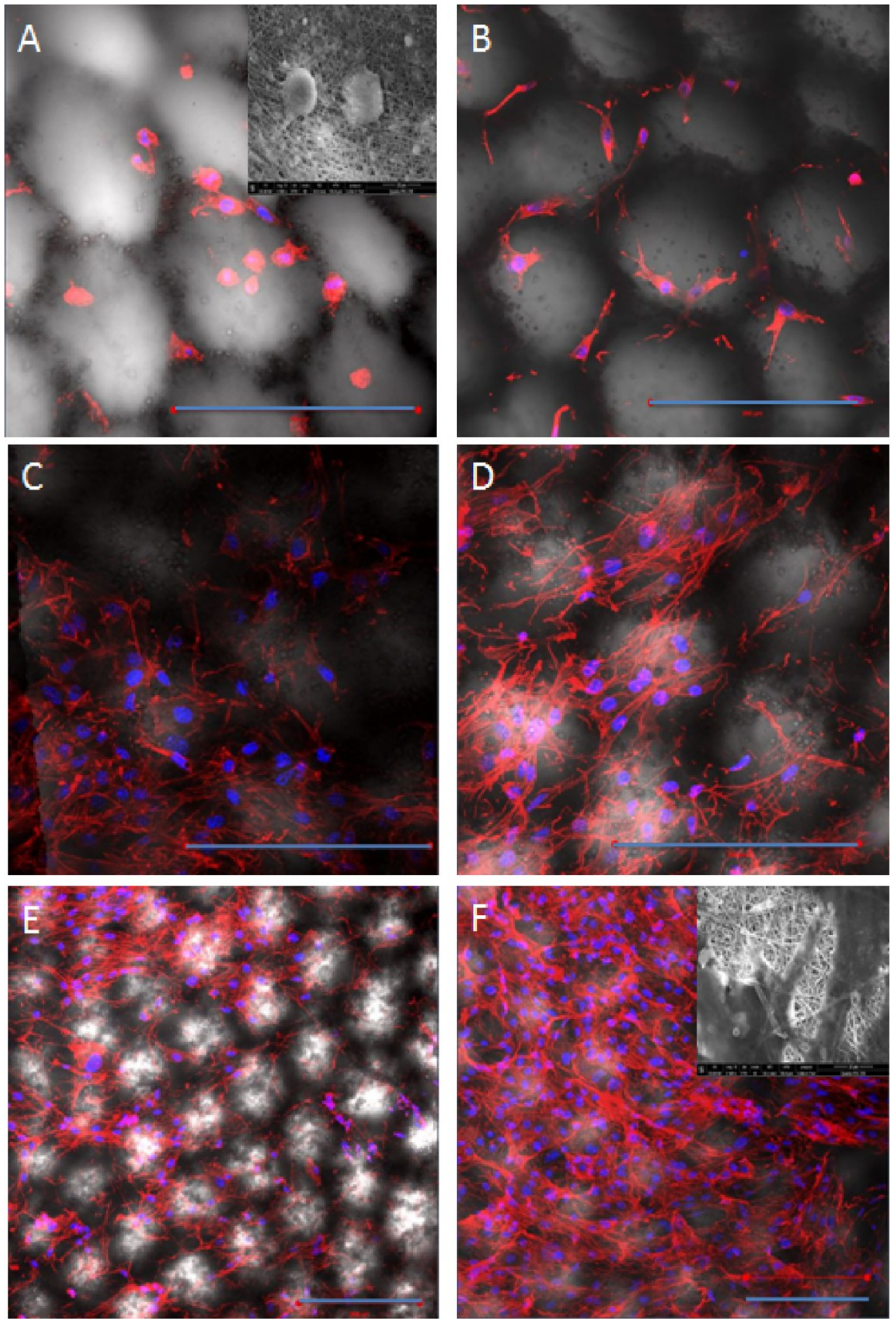

Figure 6. Fluorescence staining of actin cytoskeleton (red) and nuclei (blue) of C3H10T1/2. The cells were cultured for 2 h (A), 24 h (B), 48 h (C), and 96 h (D) free of growth factors over honeycomb-like scaffolds. Magnification ×20. (E,F) Cells cultured for 48 h and 96 h, respectively, over the scaffold. Magnification ×10. Scale bars equal 200 μm. Insert images on (A) and (F) show SEM pictures of adherent cells over the scaffold surface.

preference between regions between the top and bottom of the cavities.

DISCUSSION

In a previous work, we established the advantages for surgeons of using biomaterials produced as sheets with versatile properties for treating defects in the maxillofacial area.[46] These sheets are easy to handle and their final shape can be adjusted to fill the defect. In the present study, we demonstrated that the honeycomb structure composed of PCL electrospun fibers and hydroxyapatite nanoparticles is a relevant candidate for a semi-3D organized support for bone regeneration.

Our first goal was to produce such a specific scaffold, adopting a biomimicry approach in order to improve osteinduction. Our hypothesis was that architecture plays an essential role regarding cell response and the mechanical properties of the substitute obtained with respect to the natural tissue to be regenerated. During bone regeneration, osteoclasts dig cavities in the bone and osteoblasts produce new bone.[47] During this process, osteocytes are formed and remain in the center of a biophysical niche that can be mirrored in our honeycomb architecture. We thus focused on producing a

DOI: 10.1021/acsbiomaterials.8b00521
ACS Biomater. Sci. Eng. 2018, 4, 3317−3326

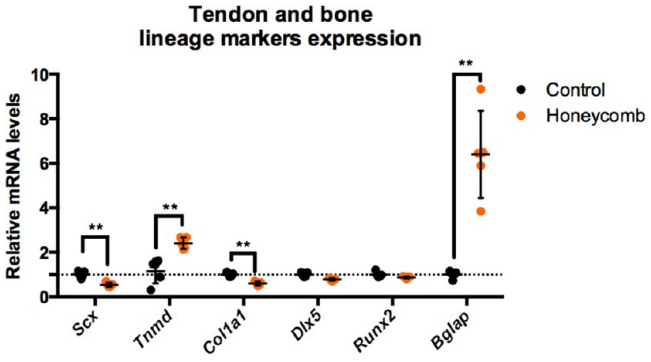

Figure 7. Gene expression of tendon- and bone-related markers in C3H10T1/2 cells cultured on the honeycomb-like scaffolds compared to cells cultured without scaffold. The genes *Scx*, *Tnmd*, and *Col1a1* were uses as tendon markers to assess tenogenic differentiation, although *Col1a1* is also expressed in bones. *Dlx5*, *Runx2*, and *Bglap* were used as bone markers to assess bone differentiation. The results are displayed as scattered dot plots, each plot representing the result of one sample (n = 5 for each condition). The data obtained for gene expression of the cells cultured on honeycomb-like scaffolds (orange dots) were compared to those of the control cells (black dots) with the Mann–Whitney nonparametric statistical test. The p-values are indicated for the tests, showing a significant difference between the two groups (** for p-value = 0.0079).

scaffold mimicking this structure in order to evaluate the relationship between specific morphology properties. It has already been demonstrated that electrospun PCL fibers using template-assisted technique leads to the generation of specific patterns.[48] In previous studies, honeycomb 3D composite micropatterned scaffolds have already been prepared with poly(lactic acid) fibers and PCL particles[36] as well as bilayer micropatterned scaffolds with one layer of hydroxyapatite nanoparticles covering electrospun PCL fibers for lab-on-chip applications.[37] In the present work, we demonstrated the feasibility of electrospraying several layers of hydroxyapatite between PCL layers during the process. We were thus able to develop more complex, three-dimensional structures of greater magnitude and, at the same time, mimicking the morphology and composition of the mineral component present in bone.

The final scaffold presented an overall thickness of around 30 μm in accordance with previously developed sheets.[46] The originality of the scaffold also relied on the presence of honeycomb pores (of around 160 μm diameter) corresponding to domains sparsely filled by the electrospun fibers. This pore size has been described by many authors as being optimal for promoting cell colonization and bone formation.[49−54] The Young modulus was very low (3.77 ± 0.35 MPa) compared to classical scaffolds dedicated to bone regeneration (a range of

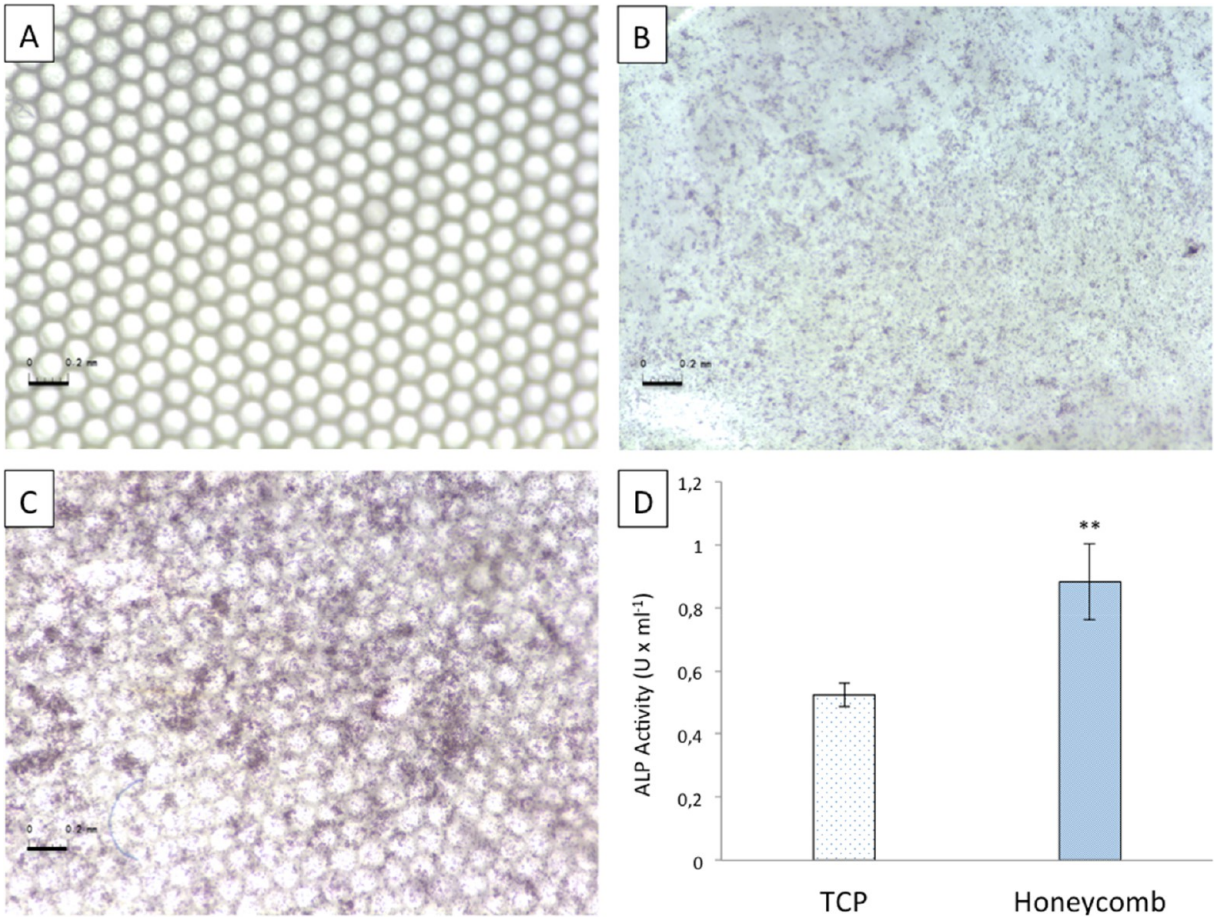

Figure 8. (A–C) Alkaline phosphatase staining on the honeycomb-like scaffold after 5 days of culture. (A) Control honeycomb-like scaffold without cells. (B) C3H10T1/2 cells on culture into TCP control. (C) C3H10T1/2 cells on culture into honeycomb-like scaffold. (D) Alkaline phosphatase activity. The data obtained for alkaline phosphatase activity of the cells cultured on the honeycomb-like scaffolds (blue bar) were compared to those of the control cells cultured on TCP (white bar) with the Mann–Whitney nonparametric statistical test. The p-values are indicated for the test, showing a significant difference between the two groups (** for p-value = 0.0043).

DOI: 10.1021/acsbiomaterials.8b00521
ACS Biomater. Sci. Eng. 2018, 4, 3317–3326

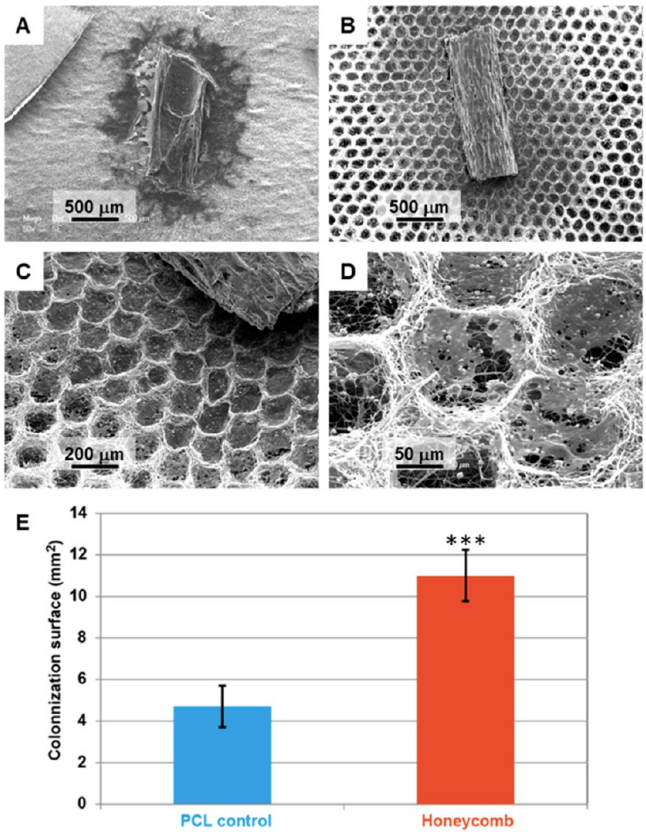

Figure 9. Scanning electron micrographs of honeycomb electrospun scaffold. (A) A 15% polycaprolactone scaffold being colonized by cells from slices of chicken embryos after 14 days. Scale bar = 500 μm. (B–D) represent the scaffold after being colonized by cells from slices of chicken embryos after 14 days. Scale bar = 500, 200, and 50 μm, respectively. (E) Migration surface calculated by correlating cell surface in pixels to mm^2. The data obtained for cell migration of the cells cultured on the honeycomb-like scaffolds (orange bar) were compared to those of the control cells cultured on poly(ε-caprolactone) (blue bar) with the Mann–Whitney nonparametric statistical test. The p-values are indicated for the test, showing a significant difference between the two groups (*** for p-value <0.0001).

hundreds MPa or more). This can be explained by the facts that the scaffolds are poorly dense in fibers. However, such a mechanical property was intended to allow easy manipulation and changes in shape, as already stated in Baudequin.[46]

To assess the impact of such architecture on the fate of cells, the scaffolds were then seeded with mouse pluripotent stem cells: C3H10T1/2. This cell line was chosen for its maintained capacity to differentiate into different tissues such as bone, cartilage, adipose tissue, etc.[55,56] Shea[57] demonstrated that BMP2 treatment of C3H10T1/2 mesenchymal stem cells induces both chondrogenesis and osteogenesis. Takata[58] used them to evaluate the potential of a specific ketone found in raspberries to promote osteogenesis. In the present study, it should be specified that the C3H10T1/2 were seeded on the scaffold in the absence of any differentiation factor to avoid any guided differentiation toward bone lineage that could be only to the result of the presence of BMP2. The cell behavior observed in our experiments was thus expected to be strictly induced by cell–material interactions.

In contact with the 3D honeycomb scaffold, and after 5 days of culture, the cells presented high viability over the entire surface, both in the center of the cavity and in the ridges. We demonstrated that cells arranged themselves according to the shape of the support: they were elongated on the ridges and spread randomly across the width at the bottom of the cavity. Cells were thus able to colonise the whole material, as shown by the proliferation assay, and take advantage of the added surface provided by 3D shapes and the support of the electrospun fibers.

The increase in expression of characteristic bone genes, such as *Bglap*, showed clear differentiation toward the osteoblastic lineage. This finding was corroborated by the clear ALP production and staining observed on the cell-seeded scaffolds. This osteoinduction may be attributed to the combined effect of the presence of hydroxyapatite nanoparticles and of the specific morphology of the scaffold. Gomez-Lizarraga[59] demonstrated that electrospun PCL combined with HA nanoparticles promoted cell viability and proliferation. To deeply analyze the role of the honeycomb structure alone, it would be interesting to compare the outcomes with those of the same scaffold devoid of HA. However, the production of such scaffold with the present method is not possible because HA electrospraying is mandatory to perform layer by layer production of the 3D structure.

Tenomodulin also appeared to increase with respect to the control; this increase might be due to regions located at the top of the cavity, with straight fibers that could promote cell differentiation into tendon lineage. BMSCs were shown to differentiate toward the tendon lineage when the support on which they grew presented an alignment.[60]

Finally, thanks to the organotypic study, we demonstrated that differentiated cells present in the bones of chicken embryos were able to leave and colonize the honeycomb structure. The surface on which cells spread was larger on this support than on a simple support composed of PCL 15%. This shows the potential of this scaffold for osteoconduction, which is a major advantage in case of surgical implantation.

CONCLUSION

In this study, we succeeded in producing a biomimetic scaffold with the relevant properties of osteocompatibility, osteoconduction, and osteoinduction. Successive layers of electrospun PCL and electrosprayed HA nanoparticles on a collector equipped with hexagonal micropatterns led to the production of a scaffold with an overall shape of a sheet but with a 3D honeycomb structure. In this scaffold, mesenchymal stem cells showed a preference for early differentiation toward bone lineage in the absence of any differentiation factors. These results are very promising for exploiting this material in bone reconstruction either in vitro as tissue engineering approaches or directly in vivo as a regenerative supporting biomaterial.

ASSOCIATED CONTENT

Supporting Information

The Supporting Information is available free of charge on the ACS Publications website at DOI: 10.1021/acsbiomaterials.8b00521.

Electrospinning and electrospraying parameters step by step; solution **A**, PCL at 15% W/V in DCM/DMF 60/40%; solution **B**, HA at 10% W/V in ethanol; list of primers used for RT-qPCR; C3H10T1/2 colonization over a honeycomb groove (PDF)

DOI: 10.1021/acsbiomaterials.8b00521
ACS Biomater. Sci. Eng. 2018, 4, 3317–3326

Confocal stack of cells over a honeycomb groove; honeycomb scaffold in gray (white light); cell cytoskeleton in red (Phalloidin-Rhodamine); cell nuclei in blue (Hoechst 3342) (AVI)

AUTHOR INFORMATION

Corresponding Author

*Tel.: +33-344234670. E-mail: cecile.legallais@utc.fr.

ORCID

Anne Hébraud: 0000-0002-6018-1523
Guy Schlatter: 0000-0003-3037-4129
Cecile Legallais: 0000-0002-8061-906X

Notes

The authors declare no competing financial interest.

ACKNOWLEDGMENTS

This work was carried out and funded in the framework of the Labex MS2T. It was supported by the French Government, through the program "Investments for the future" managed by the National Agency for Research (reference ANR-11-IDEX-0004-02) and by Région Hauts de France (INTIM project). A. Hebraud, C. Wittmer, and G. Schlatter also thank the financial support of the project ANR MimHeart (ANR-15-CE08-0010) and Sabine Siegwald for the fabrication of the micropatterned collectors at the clean room STnano (Strasbourg, France).

REFERENCES

(1) Buck, D. W.; Dumanian, G. A. Bone Biology and Physiology: Part I. The Fundamentals. *Plast. Reconstr. Surg.* **2012**, *129* (6), 1314–1320.

(2) Reznikov, N.; Shahar, R.; Weiner, S. Bone Hierarchical Structure in Three Dimensions. *Acta Biomater.* **2014**, *10* (9), 3815–3826.

(3) Alford, A. I.; Kozloff, K. M.; Hankenson, K. D. Extracellular Matrix Networks in Bone Remodeling. *Int. J. Biochem. Cell Biol.* **2015**, *65*, 20–31.

(4) Chai, Y. C.; Carlier, A.; Bolander, J.; Roberts, S. J.; Geris, L.; Schrooten, J.; Van Oosterwyck, H.; Luyten, F. P. Current Views on Calcium Phosphate Osteogenicity and the Translation into Effective Bone Regeneration Strategies. *Acta Biomater.* **2012**, *8* (11), 3876–3887.

(5) Amini, A. R.; Laurencin, C. T.; Nukavarapu, S. P. Bone Tissue Engineering: Recent Advances and Challenges. *Crit. Rev. Biomed. Eng.* **2012**, *40* (5), 363–408.

(6) Rai, R.; Raval, R.; Khandeparker, R. V.; Chidrawar, S. K.; Khan, A. A.; Ganpat, M. S. Tissue Engineering: Step Ahead in Maxillofacial Reconstruction. *J. Int. Oral Health JIOH* **2015**, *7* (9), 138–142.

(7) Glynn, S. M.; Shetty, V.; Elliot-Brown, K.; Leathers, R.; Belin, T. R.; Wang, J. Chronic Posttraumatic Stress Disorder after Facial Injury: A 1-Year Prospective Cohort Study. *J. Trauma* **2007**, *62* (2), 410–418.

(8) Kretlow, J. D.; Young, S.; Klouda, L.; Wong, M.; Mikos, A. G. Injectable Biomaterials for Regenerating Complex Craniofacial Tissues. *Adv. Mater.* **2009**, *21* (32–33), 3368–3393.

(9) Moura, L. B.; Carvalho, P. H. de A.; Xavier, C. B.; Post, L. K.; Torriani, M. A.; Santagata, M.; Chagas Júnior, O. L. Autogenous Non-Vascularized Bone Graft in Segmental Mandibular Reconstruction: A Systematic Review. *Int. J. Oral Maxillofac. Surg.* **2016**, *45* (11), 1388–1394.

(10) LaPrade, R. F.; Botker, J. C. Donor-Site Morbidity after Osteochondral Autograft Transfer Procedures. *Arthrosc. J. Arthrosc. Relat. Surg. Off. Publ. Arthrosc. Assoc. N. Am. Int. Arthrosc. Assoc.* **2004**, *20* (7), e69–73.

(11) Seidi, A.; Ramalingam, M.; Elloumi-Hannachi, I.; Ostrovidov, S.; Khademhosseini, A. Gradient Biomaterials for Soft-to-Hard Interface Tissue Engineering. *Acta Biomater.* **2011**, *7* (4), 1441–1451.

(12) Fernandez-Yague, M. A.; Abbah, S. A.; McNamara, L.; Zeugolis, D. I.; Pandit, A.; Biggs, M. J. Biomimetic Approaches in Bone Tissue Engineering: Integrating Biological and Physicomechanical Strategies. *Adv. Drug Delivery Rev.* **2015**, *84*, 1–29.

(13) Glowacki, J.; Mizuno, S. Collagen Scaffolds for Tissue Engineering. *Biopolymers* **2008**, *89* (5), 338–344.

(14) Dawson, J. I.; Wahl, D. A.; Lanham, S. A.; Kanczler, J. M.; Czernuszka, J. T.; Oreffo, R. O. Development of Specific Collagen Scaffolds to Support the Osteogenic and Chondrogenic Differentiation of Human Bone Marrow Stromal Cells. *Biomaterials* **2008**, *29* (21), 3105–3116.

(15) Oh, B. H. L.; Bismarck, A.; Chan-Park, M. B. Injectable, Interconnected, High-Porosity Macroporous Biocompatible Gelatin Scaffolds Made by Surfactant-Free Emulsion Templating. *Macromol. Rapid Commun.* **2015**, *36* (4), 364–372.

(16) Saravanan, S.; Leena, R. S.; Selvamurugan, N. Chitosan Based Biocomposite Scaffolds for Bone Tissue Engineering. *Int. J. Biol. Macromol.* **2016**, *93*, 1354–1365.

(17) Venkatesan, J.; Bhatnagar, I.; Manivasagan, P.; Kang, K.-H.; Kim, S.-K. Alginate Composites for Bone Tissue Engineering: A Review. *Int. J. Biol. Macromol.* **2015**, *72*, 269–281.

(18) Xue, R.; Qian, Y.; Li, L.; Yao, G.; Yang, L.; Sun, Y. Polycaprolactone Nanofiber Scaffold Enhances the Osteogenic Differentiation Potency of Various Human Tissue-Derived Mesenchymal Stem Cells. *Stem Cell Res. Ther.* **2017**, *8*, 148.

(19) Xu, T.; Miszuk, J. M.; Zhao, Y.; Sun, H.; Fong, H. Electrospun Polycaprolactone 3D Nanofibrous Scaffold with Interconnected and Hierarchically Structured Pores for Bone Tissue Engineering. *Adv. Healthcare Mater.* **2015**, *4* (15), 2238–2246.

(20) Guduric, V.; Metz, C.; Siadous, R.; Bareille, R.; Levato, R.; Engel, E.; Fricain, J.-C.; Devillard, R.; Luzanin, O.; Catros, S. Layer-by-Layer Bioassembly of Cellularized Polylactic Acid Porous Membranes for Bone Tissue Engineering. *J. Mater. Sci.: Mater. Med.* **2017**, *28* (5), 78.

(21) Chen, Y.; Xu, J.; Huang, Z.; Yu, M.; Zhang, Y.; Chen, H.; Ma, Z.; Liao, H.; Hu, J. An Innovative Approach for Enhancing Bone Defect Healing Using PLGA Scaffolds Seeded with Extracorporeal-Shock-Wave-Treated Bone Marrow Mesenchymal Stem Cells (BMSCs). *Sci. Rep.* **2017**, *7*, 44130.

(22) Albrektsson, T.; Johansson, C. Osteoinduction, Osteoconduction and Osseointegration. *Eur. Spine J.* **2001**, *10*, S96–S101.

(23) Lao, L.; Wang, Y.; Zhu, Y.; Zhang, Y.; Gao, C. Poly(Lactide-Co-Glycolide)/Hydroxyapatite Nanofibrous Scaffolds Fabricated by Electrospinning for Bone Tissue Engineering. *J. Mater. Sci.: Mater. Med.* **2011**, *22* (8), 1873–1884.

(24) Wongsupa, N.; Nuntanaranont, T.; Kamolmattayakul, S.; Thuaksuban, N. Assessment of Bone Regeneration of a Tissue-Engineered Bone Complex Using Human Dental Pulp Stem Cells/Poly(ε-Caprolactone)-Biphasic Calcium Phosphate Scaffold Constructs in Rabbit Calvarial Defects. *J. Mater. Sci.: Mater. Med.* **2017**, *28* (5), 77.

(25) Huang, J.; Lin, Y. W.; Fu, X. W.; Best, S. M.; Brooks, R. A.; Rushton, N.; Bonfield, W. Development of Nano-Sized Hydroxyapatite Reinforced Composites for Tissue Engineering Scaffolds. *J. Mater. Sci.: Mater. Med.* **2007**, *18* (11), 2151–2157.

(26) Xu, C.; Su, P.; Chen, X.; Meng, Y.; Yu, W.; Xiang, A. P.; Wang, Y. Biocompatibility and Osteogenesis of Biomimetic Bioglass-Collagen-Phosphatidylserine Composite Scaffolds for Bone Tissue Engineering. *Biomaterials* **2011**, *32* (4), 1051–1058.

(27) Shimizu, H.; Jinno, Y.; Ayukawa, Y.; Atsuta, I.; Arahira, T.; Todo, M.; Koyano, K. Tissue Reaction to a Novel Bone Substitute Material Fabricated With Biodegradable Polymer-Calcium Phosphate Nanoparticle Composite. *Implant Dent* **2016**, *25* (5), 567–574.

(28) Shor, L.; Güçeri, S.; Chang, R.; Gordon, J.; Kang, Q.; Hartsock, L.; An, Y.; Sun, W. Precision Extruding Deposition (PED) Fabrication of Polycaprolactone (PCL) Scaffolds for Bone Tissue Engineering. *Biofabrication* **2009**, *1* (1), 015003.

(29) Bendtsen, S. T.; Quinnell, S. P.; Wei, M. Development of a Novel Alginate-Polyvinyl Alcohol-Hydroxyapatite Hydrogel for 3D

DOI: 10.1021/acsbiomaterials.8b00521
ACS Biomater. Sci. Eng. 2018, 4, 3317–3326

Bioprinting Bone Tissue Engineered Scaffolds. *J. Biomed. Mater. Res., Part A* **2017**, *105* (5), 1457−1468.
(30) Sankar, S.; Sharma, C. S.; Rath, S. N.; Ramakrishna, S. Electrospun Nanofibres to Mimic Natural Hierarchical Structure of Tissues: Application in Musculoskeletal Regeneration. *J. Tissue Eng. Regener. Med.* **2018**, *12*, e604−e619.
(31) Kishan, A. P.; Cosgriff-Hernandez, E. M. Recent Advancements in Electrospinning Design for Tissue Engineering Applications: A Review. *J. Biomed. Mater. Res., Part A* **2017**, *105* (10), 2892−2905.
(32) Wu, Y.; Dong, Z.; Wilson, S.; Clark, R. Template-Assisted Assembly of Electrospun Fibers. *Polymer* **2010**, *51*, 3244.
(33) Ripamonti, U. Biomimetism, Biomimetic Matrices and the Induction of Bone Formation. *J. Cell. Mol. Med.* **2009**, *13* (9B), 2953−2972.
(34) Graziano, A.; d'Aquino, R.; Cusella-De Angelis, M. G.; De Francesco, F.; Giordano, A.; Laino, G.; Piattelli, A.; Traini, T.; De Rosa, A.; Papaccio, G. Scaffold's Surface Geometry Significantly Affects Human Stem Cell Bone Tissue Engineering. *J. Cell. Physiol.* **2008**, *214* (1), 166−172.
(35) Takabatake, K.; Yamachika, E.; Tsujigiwa, H.; Takeda, Y.; Kimura, M.; Takagi, S.; Nagatsuka, H.; Iida, S. Effect of Geometry and Microstructure of Honeycomb TCP Scaffolds on Bone Regeneration. *J. Biomed. Mater. Res., Part A* **2014**, *102* (9), 2952−2960.
(36) Wittmer, C. R.; Hébraud, A.; Nedjari, S.; Schlatter, G. Well-Organized 3D Nanofibrous Composite Constructs Using Cooperative Effects between Electrospinning and Electrospraying. *Polymer* **2014**, *55* (22), 5781−5787.
(37) Nedjari, S.; Hébraud, A.; Eap, S.; Siegwald, S.; Mélart, C.; Benkirane-Jessel, N.; Schlatter, G. Electrostatic Template-Assisted Deposition of Microparticles on Electrospun Nanofibers: Towards Microstructured Functional Biochips for Screening Applications. *RSC Adv.* **2015**, *5* (102), 83600−83607.
(38) Clarke, B. Normal Bone Anatomy and Physiology. *Clin. J. Am. Soc. Nephrol.* **2008**, *3*, S131−S139.
(39) Smolewski, P.; Bedner, E.; Gorczyca, W.; Darzynkiewicz, Z. Liquidless" Cell Staining by Dye Diffusion from Gels and Analysis by Laser Scanning Cytometry: Potential Application at Microgravity Conditions in Space. *Cytometry* **2001**, *44* (4), 355−360.
(40) Livak, K. J.; Schmittgen, T. D. Analysis of Relative Gene Expression Data Using Real-Time Quantitative PCR and the 2(-Delta Delta C(T)) Method. *Methods* **2001**, *25* (4), 402−408.
(41) Duval, J.-L.; Dinis, T.; Vidal, G.; Vigneron, P.; Kaplan, D. L.; Egles, C. Organotypic Culture to Assess Cell Adhesion, Growth and Alignment of Different Organs on Silk Fibroin. *J. Tissue Eng. Regener. Med.* **2017**, *11* (2), 354−361.
(42) Komori, T. Regulation of Osteoblast Differentiation by Runx2. *Adv. Exp. Med. Biol.* **2009**, *658*, 43−49.
(43) Lee, N. K.; Sowa, H.; Hinoi, E.; Ferron, M.; Ahn, J. D.; Confavreux, C.; Dacquin, R.; Mee, P. J.; McKee, M. D.; Jung, D. Y.; et al. Endocrine Regulation of Energy Metabolism by the Skeleton. *Cell* **2007**, *130* (3), 456−469.
(44) Schweitzer, R.; Chyung, J. H.; Murtaugh, L. C.; Brent, A. E.; Rosen, V.; Olson, E. N.; Lassar, A.; Tabin, C. J. Analysis of the Tendon Cell Fate Using Scleraxis, a Specific Marker for Tendons and Ligaments. *Development* **2001**, *128* (19), 3855−3866.
(45) Shukunami, C.; Takimoto, A.; Oro, M.; Hiraki, Y. Scleraxis Positively Regulates the Expression of Tenomodulin, a Differentiation Marker of Tenocytes. *Dev. Biol.* **2006**, *298* (1), 234−247.
(46) Baudequin, T.; Bedoui, F.; Dufresne, M.; Paullier, P.; Legallais, C. Towards the Development and Characterization of an Easy Handling Sheet-like Biohybrid Bone Substitute. *Tissue Eng., Part A* **2015**, *21* (11−12), 1895−1905.
(47) Parfitt, A. M. Osteonal and Hemi-Osteonal Remodeling: The Spatial and Temporal Framework for Signal Traffic in Adult Human Bone. *J. Cell. Biochem.* **1994**, *55* (3), 273−286.
(48) Wu, H.; Fan, J.; Chu, C.-C.; Wu, J. Electrospinning of Small Diameter 3-D Nanofibrous Tubular Scaffolds with Controllable Nanofiber Orientations for Vascular Grafts. *J. Mater. Sci.: Mater. Med.* **2010**, *21* (12), 3207−3215.
(49) Borden, M.; El-Amin, S. F.; Attawia, M.; Laurencin, C. T. Structural and Human Cellular Assessment of a Novel Microsphere-Based Tissue Engineered Scaffold for Bone Repair. *Biomaterials* **2003**, *24*, 597−609.
(50) Götz, H. E.; Müller, M.; Emmel, A.; Holzwarth, U.; Erben, R. G.; Stangl, R. Effect of Surface Finish on the Osseointegration of Laser-Treated Titanium Alloy Implants. *Biomaterials* **2004**, *25* (18), 4057−4064.
(51) Jin, Q. M.; Takita, H.; Kohgo, T.; Atsumi, K.; Itoh, H.; Kuboki, Y. Effects of Geometry of Hydroxyapatite as a Cell Substratum in BMP-Induced Ectopic Bone Formation. *J. Biomed. Mater. Res.* **2000**, *51* (3), 491−499.
(52) Mankani, M. H.; Kuznetsov, S. A.; Fowler, B.; Kingman, A.; Gehron Robey, P. G. In Vivo Bone Formation by Human Bone Marrow Stromal Cells: Effect of Carrier Particle Size and Shape. *Biotechnol. Bioeng.* **2001**, *72*, 96−107.
(53) Jones, A. C.; Arns, C. H.; Hutmacher, D. W.; Milthorpe, B. K.; Sheppard, A. P.; Knackstedt, M. A. The Correlation of Pore Morphology, Interconnectivity and Physical Properties of 3D Ceramic Scaffolds with Bone Ingrowth. *Biomaterials* **2009**, *30* (7), 1440−1451.
(54) Bigerelle, M.; Giljean, S.; Anselme, K. Existence of a Typical Threshold in the Response of Human Mesenchymal Stem Cells to a Peak and Valley Topography. *Acta Biomater.* **2011**, *7* (9), 3302−3311.
(55) Date, T.; Doiguchi, Y.; Nobuta, M.; Shindo, H. Bone Morphogenetic Protein-2 Induces Differentiation of Multipotent C3H10T1/2 Cells into Osteoblasts, Chondrocytes, and Adipocytes in Vivo and in Vitro. *J. Orthop. Sci.* **2004**, *9* (5), 503−508.
(56) Baudequin, T.; Gaut, L.; Mueller, M.; Huepkes, A.; Glasmacher, B.; Duprez, D.; Bedoui, F.; Legallais, C. The Osteogenic and Tenogenic Differentiation Potential of C3H10T1/2 (Mesenchymal Stem Cell Model) Cultured on PCL/PLA Electrospun Scaffolds in the Absence of Specific Differentiation Medium. *Materials* **2017**, *10*, 1387.
(57) Shea, C. M.; Edgar, C. M.; Einhorn, T. A.; Gerstenfeld, L. C. BMP Treatment of C3H10T1/2 Mesenchymal Stem Cells Induces Both Chondrogenesis and Osteogenesis. *J. Cell. Biochem.* **2003**, *90* (6), 1112−1127.
(58) Takata, T.; Morimoto, C. Raspberry Ketone Promotes the Differentiation of C3H10T1/2 Stem Cells into Osteoblasts. *J. Med. Food* **2014**, *17* (3), 332−338.
(59) Gómez-Lizárraga, K. K.; Flores-Morales, C.; Del Prado-Audelo, M. L.; Álvarez-Pérez, M. A.; Piña-Barba, M. C.; Escobedo, C. Polycaprolactone- and Polycaprolactone/Ceramic-Based 3D-Bioplotted Porous Scaffolds for Bone Regeneration: A Comparative Study. *Mater. Sci. Eng., C* **2017**, *79*, 326−335.
(60) Subramony, S. D.; Dargis, B. R.; Castillo, M.; Azeloglu, E. U.; Tracey, M. S.; Su, A.; Lu, H. H. The Guidance of Stem Cell Differentiation by Substrate Alignment and Mechanical Stimulation. *Biomaterials* **2013**, *34* (8), 1942−1953.

DOI: 10.1021/acsbiomaterials.8b00521
ACS Biomater. Sci. Eng. 2018, 4, 3317−3326

Chapter IV – Towards the Development of a Tendon Tissue-Engineered Construct

Chapter IV: Towards the Development of a Tendon Tissue-Engineered Construct

In this chapter, we plan to evaluate the potential of electrospun PCL scaffolds to guide C3H10T1/2 differentiation towards tendon lineage. PCL was chosen because it will ensure continuity in the future process (for the bone-tendon reconstruction), and also based on the previous data generated by our group. We orientated the cell choice to this progenitor cell line (kind gift of Dr. Delphine Duprez, IPBS) because they have also the capacity to derive to tendon lineage.[72] To remember, this cell line successfully differentiated towards bone lineage using honeycomb PCL-HA scaffolds (see chapter 3). We thus hypothesized that the same progenitor cells can follow different fates according to their environment. As the final goal of our project is the establishment of a reconstructed bone-tendon continuum in the same culture, the use of differentiation factors to guide cells to either bone or tendon lineage is not acceptable. Following the preliminary data for our group (Baudequin et al., 2017) and results found in the literature, we plan to investigate several hypothesis and conditions that could promote cell differentiation towards tenocyte's phenotype:

(I) size of the fibers: T. Baudequin suggested a link between fiber diameter and C3H10T1/2 differentiation

(II) alignment of the fibers: according to the literature, cells differentiation into tenocytes can be guided by fiber alignment [134–137]

(III) mechanical stimulation: static stretching or uniaxial cyclic strain appeared to promote expression of some tendon-related markers [137–139]

Of note, some of these results are still controversy. Therefore, it seemed important to us to set up our own experiments and analysis, first with C3H10T1/2 cells.

In this part, we benefitted from the collaborations of Dr D. Duprez's group (RT-PCR analysis) and Prof. B. Glasmacher's group (IMP, Leibniz University Hanover) for electrospinning the aligned scaffold. This last collaboration was supported by a yESAO exchange grant and the presence of a Master student from Hanover University for a five month training period at UTC (Moritz von Wrangel).

1. Effect of Fiber Size

1.1. Synthesis and Characterization of the Electrospun Scaffolds

In order to analyze the impact of different fiber sizes on cell behavior, three different polymer concentrations were prepared. For this purpose, 10, 12.5 and 15 wt % of PCL granules were added to a DCM/DMF solution. Previous studies carried in our laboratory showed that a co-solvent of dichloromethane (DCM) and dimethylformamide (DMF) led to a suitable solution for electrospinning. The DCM/DMF 4:1 ratio gave the best results in terms of electrospinning process stability and controlled fibers diameter and was thus employed here.

PCL scaffolds were produced by fiber deposition over a rotating collector. Scanning electron microscope (SEM) revealed that each scaffold consisted in an interpenetrating network of randomly distributed fibers **(Figure 8)**.

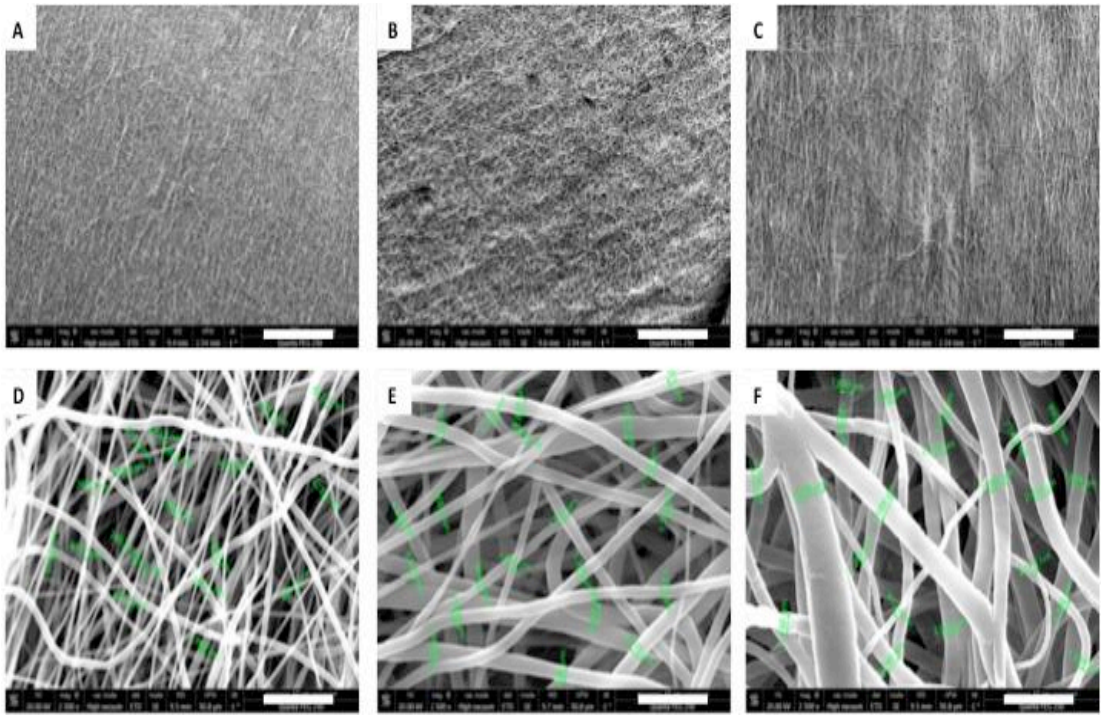

Figure 8: SEM images of three scaffolds obtained by electrospinning different concentrations of PCL A, D. PCL 10%. B, E. PCL 12.5%. C, F. PCL 15%. Top images: scale bar of 500µm. Bottom images: scale bar of 10µm

In the electrospinning process, beads might form. These pearls have to be avoided in order to ensure the mechanical properties and the homogenous porosity of the scaffolds. While the quasi-totality of the scaffold surface was homogenous for all the PCL concentrations, 10 wt % remained the most homogenous one without imperfections and fiber aggregates. In

addition, SEM observation allowed us to analyze the average diameter of each scaffold fibers, summarized in **Figure 9:** the higher the polymer concentration, the larger the fibers' diameter. Within this range, we created PCL scaffolds with variable diameters of 0.52 ± 0.25 µm for 10-wt%, 1.44 ± 0.52 µm for 12.5-wt% and 2.21 ± 0.8 µm for 15-wt%.

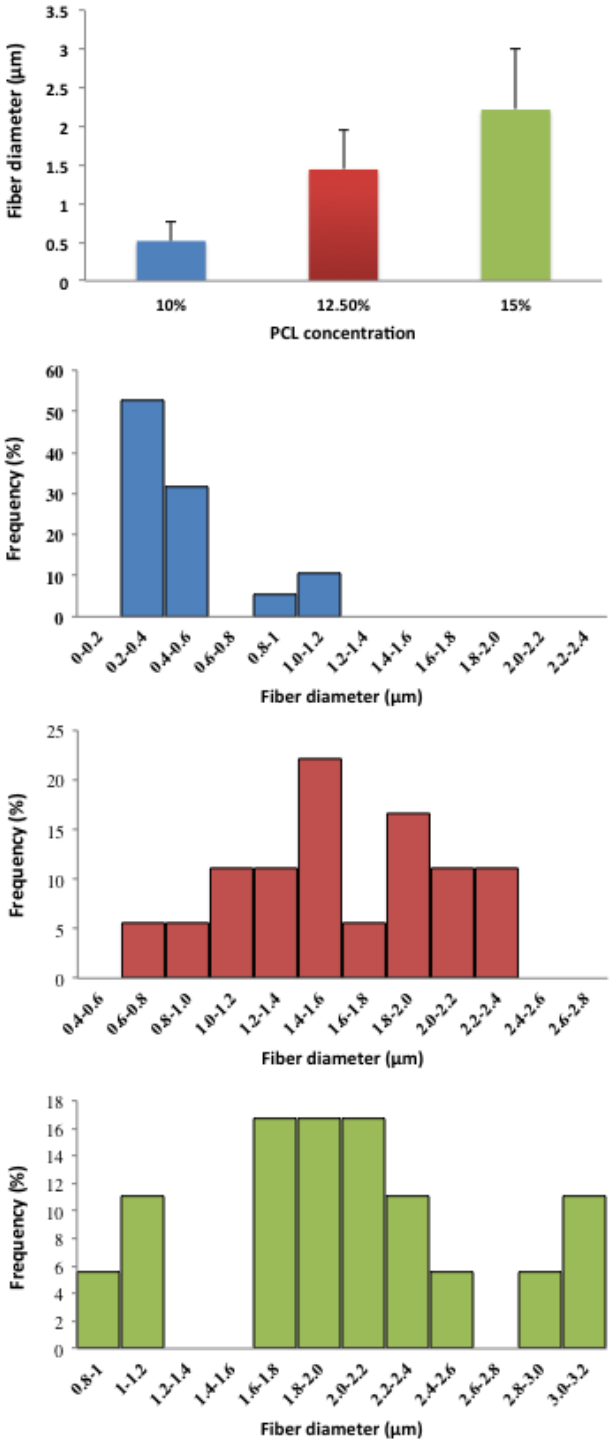

Figure 9: Average fiber diameter relative to the PCL concentration. Fibers' size distribution for the different electrospun scaffolds (10 % in blue, 12.5 % in red and 15 % in green).

The elastic modulus was calculated using uniaxial tensile tests, as described in Materials and Methods section. For this purpose, dry or wet scaffolds (immersion for 45 minutes in ethanol then immersed in PBS for 1 day) were analyzed. Wetting the material corresponded to conditions for cell culture. The thickness of each sample was measured with a caliper (0.1mm accuracy without taking into account the porosity (**Figure 10)**.

The results showed a significant difference ($p<0.001$) between 15-wt % scaffolds, for both dry and wet conditions, and the other groups (10 and 12.5-wt %). 15-wt % scaffold was the most rigid one, with an elastic modulus twice higher than those of 10 and 12.5-wt % scaffolds. No difference was observed for each group between the dry or wet conditions.

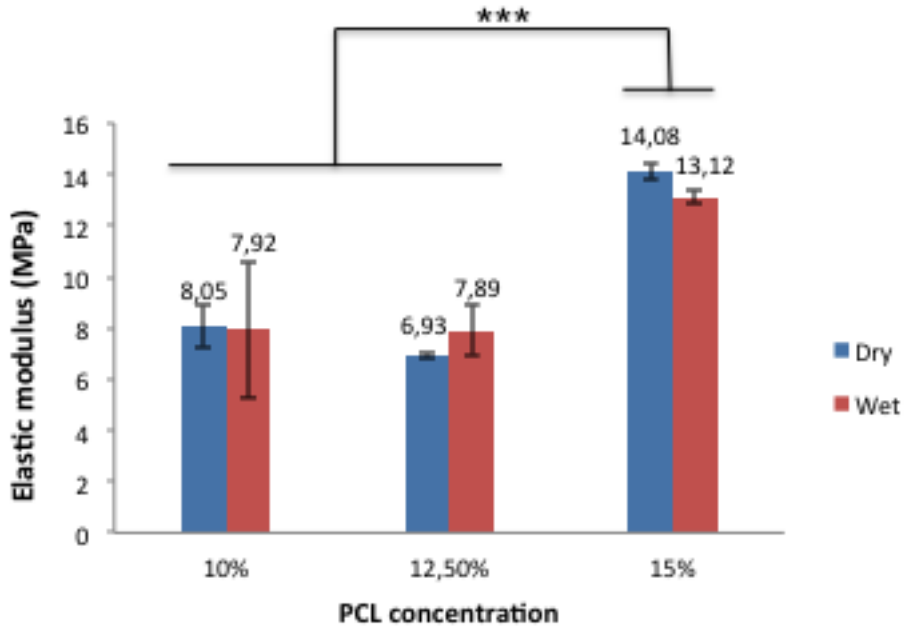

Figure 10. Average elastic modulus relative to PCL concentration analyzed in dry (bleu) or wet conditions (red). The p values are indicated for the tests showing a significant difference. (*** For p value <0.001).

1.2. Early Cells Response

The next step consisted in the evaluation of the impact of fiber diameter on C3H10T1/2 cell culture and potential differentiation. The scaffolds (surface area = 17 x 17 mm) were seeded with cells at a density of 10^5 cells/cm^2. MTT assay was performed after 1, 2 or 3 days of culture in order to evaluate the early influence of fiber diameter on cell proliferation. Results are shown in **Figure 11**. After 1 day of culture, each scaffold plated with cells presented a similar number of cells colonizing the surface with $2.4x10^5$, $2x10^5$ and $2.2x10^5$ cells/scaffold for 10, 12.5, 15-wt % of PCL respectively. At day 2, the cell population present in each

scaffold appeared almost doubled relative to day 1, with the largest fibers (15-wt % PCL) showing the highest number of cells. This difference is significant ($p<0.001$). After 3 days of culture, the number of cells was similar for each scaffold (near $4.0x10^5$ cells/scaffold). Indeed, C3H10 are known to rapidly expand. As the cells' seeding density was high, this stable state was rapidly achieved.

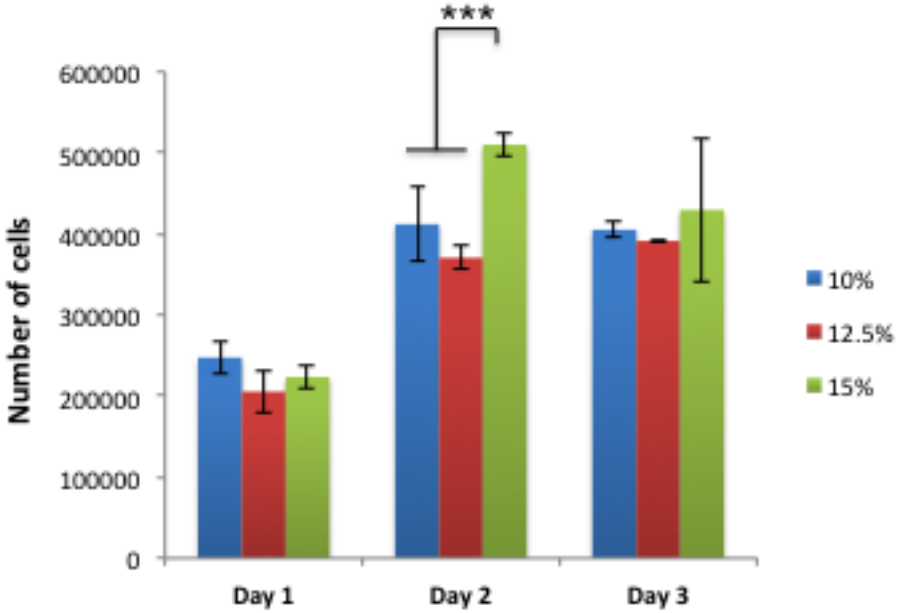

Figure 11. MTT analysis for comparing proliferation of C3H10T1/2 on different PCL scaffolds: 10-wt % (bleu), 12.5-wt % (red) and 15-wt % (green) at day 1, 2 and 3. The p values are indicated between each day tests, showing a significant difference (*** for p-value <0.001).

To better understand the impact of fibers diameter on cell behavior, the preferential differentiation outcomes of C3H10T1/2 cells cultured in each scaffold is evaluated through the expression of genes of interest by means of RT-qPCR at the end of 5 days of culture. Bone differentiation was analyzed with *Dlx5* (transcription factor involved in the activation of bone specific markers[140,141]), *RunX2* (early bone specific transcription factor[142,143]) and *Bglap* (late marker involved in bone mineralization[144,145]) while Scx (bHLH transcription factor involved in early events of tendon differentiation[146,147]), *Tnmd* (a late tendon-specific marker[148,149]) and *Aqp1* (Involved in tendon development[150]) were used for tendon differentiation. Col1, a non-specific marker can be expressed in both tendon and bone. The relative expression levels are shown in **Figure 12**.

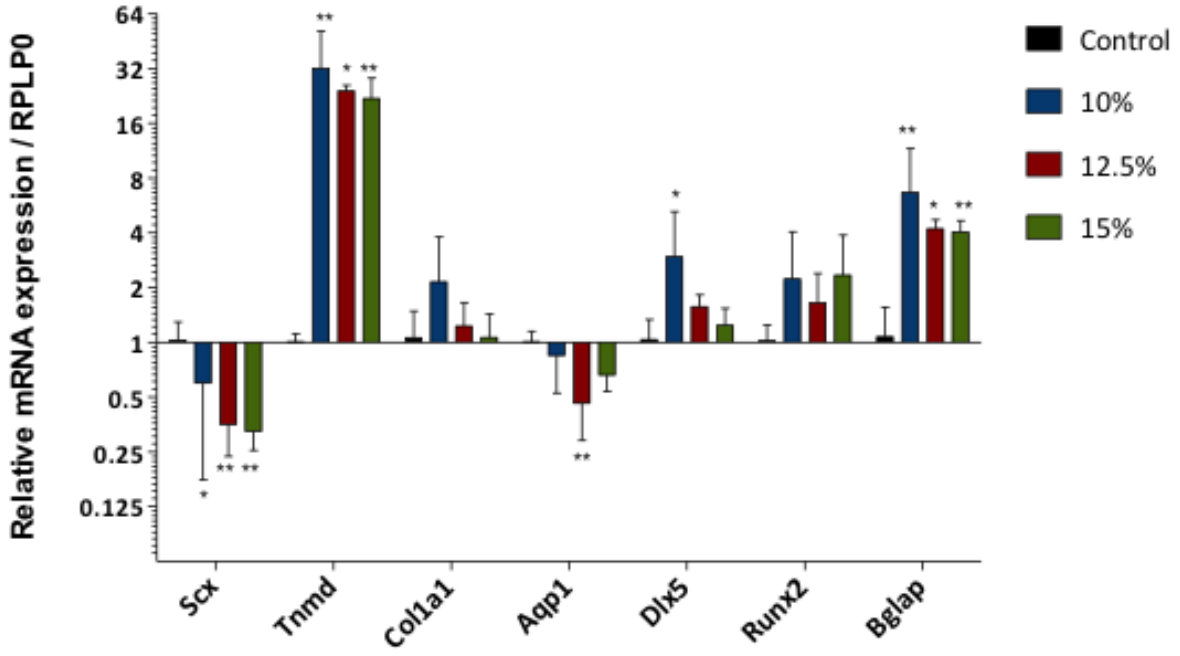

Figure 12. Gene expression of tendon- and bone-related markers in C3H10T1/2 cells cultured on the different scaffolds. The data obtained for gene expression of the cells cultured over the scaffolds were compared to those of the control cells (tissue culture plate) with the Mann-Whitney nonparametric statistical test. (* for p value <0.05, ** for p value <0.01).

After 5 days of culture over the different scaffolds, C3H10T1/2 cells presented similar response whatever the scaffold employed. Related to the control (tissue culture plate), we could observe on the one hand a high increase of *Tnmd*, a tendon-related marker, for each group with values 32, 24 and 21-fold high. In parallel, the expression of *Scx*, an early marker of tendon differentiation decreased for each condition. On the other hand, *Dlx5, RunX2* and *Bglap*, bone-related markers also increased in each condition. Particularly *Bglap, which* is a bone mineralization marker, suggested the presence of C3H10T1/2 cells shifting towards bone lineage **(Figure 12)**.

1.3. Discussion

Based on previous results and bibliography, our first hypothesis was that electrospun fibers' diameter could modulate the cell response, particularly leading to a shift towards tendon differentiation of C3H10T1/2 cultured on fibers with large diameter (>2 µm) or towards bone differentiation for smaller fibers (<1 µm). Increasing polymer concentration led indeed to an

increase of fiber diameter in a range from 500 nm to 2.2 µm. From a mechanical point of view, all scaffolds could be easily handled, the 15-wt % scaffold appearing as the most "rigid" (14.08 ± 0.30 MPa) although these values are far from the native tendon. From a biological point of view, the cells cultivated over the different scaffolds presented similar adhesion (day 1) and proliferation (day 3). The analysis of gene expression by RT-qPCR was then performed to better elucidate the effect of fiber diameters on C3H10T1/2, especially in terms of cells differentiation. The results are not easy to interpret. The down regulation of *Scx* together with the up regulation of *Tnmd* could be explained as an engaged tendon differentiation. Indeed, it has been shown that *Scx*, involved in the activation of *Tnmd*, is naturally attenuated after the activation of the *Tnmd*-related genes.[146,151] Bone-related markers, appeared also being up regulated, for any fiber diameter. At this stage, and in the absence of any differentiation factor, it is thus impossible to validate our initial hypothesis. The increase of both tendon and bone markers suggests the presence of two different engaged populations in the same scaffold. This might be due to the heterogeneity in the fibers' diameters.

As this parameter cannot be exploited to guide cellular behavior, we decided to keep PCL 10-wt % scaffolds whose fibers diameter is 0.52 ± 0.25 µm, being the scaffold most homogeneous and to play on others to favor C3H10T1/2 differentiation towards tendon lineage.

2. Towards a Biomimetic Model

In this section, the objective is to investigate two different strategies allowing the guidance of C3H10T1/2 to achieve a tendinous differentiation based on biomimetic strategies: 1) the development and characterization of aligned scaffolds mimicking the anisotropic structure of collagen fibers in native tendon and 2) the development of an in vitro protocol to reproduce the mechanical sollitations that tendons overcome in vivo.

2.1. Electrospun Fibers Alignment

Tendon is an anisotropic and viscoelastic tissue capable of withstanding high tensile forces. To mimic this inherent alignment of tendon, particularly the alignment of collagen fibers,

several groups developed an aligned network of electrospun fibers. Such aligned scaffolds, in comparison with random ones, showed greater efficacy as a support for the tendon reconstruction recapitulating better mechanical properties, cellular alignment similar to that found for tenocytes in vivo, a greater production of a tendinous extracellular matrix and an up-regulated tendon related genetic expression as found on hTSPC,[2,] hMSCs [6,] and on human rotator cuff fibroblasts[20] in the absence of any growth factor.

To get aligned fibers, one of the most widespread strategies rely on the increase of the rotating collector speed[153]. As this technique was not available at UTC at that time, we collaborated with the group of Prof. B. Glasmacher (IMP, Leibniz University Hanover, Germany).

2.1.1. Synthesis and Mechanical Characterization of Aligned Scaffolds

Aligned fibers were successfully produced by electrospinning over a rotating drum collector turning at high speed (2000rpm), using the same PCL 10% solution (**Figure 13)**.

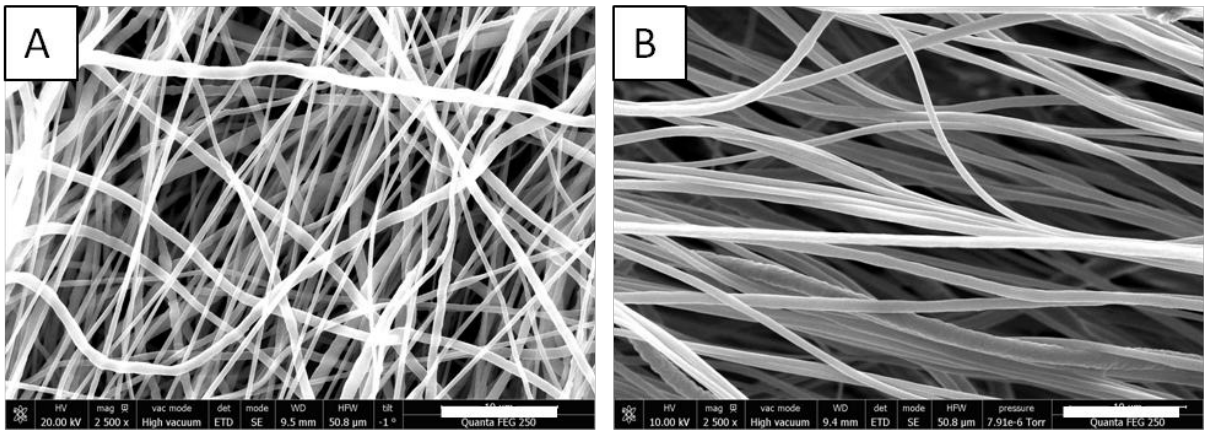

Figure 13. SEM images of two scaffold obtained by electrospinning PCL 10-wt % under different rotatation speeds. . A. Random PCL 10-wt % at medium speed (1000rpm). B. Aligned PCL 10-wt % at high speed (2000 rpm). Scale bars of 10µm.

The diameter distribution of the aligned fibers seemed to be more homogeneous than random ones, with fewer size variations along the fiber axis. In addition, the fibers were larger when generated on the high speed collector (0.81 ± 0.1 µm) compared to random ones (0.52 ± 0.25 µm). It is well known that changing the electrospinning process, although

keeping the same polymer, may lead to different response. In the present case, the different collector size might also affect the fiber diameter.

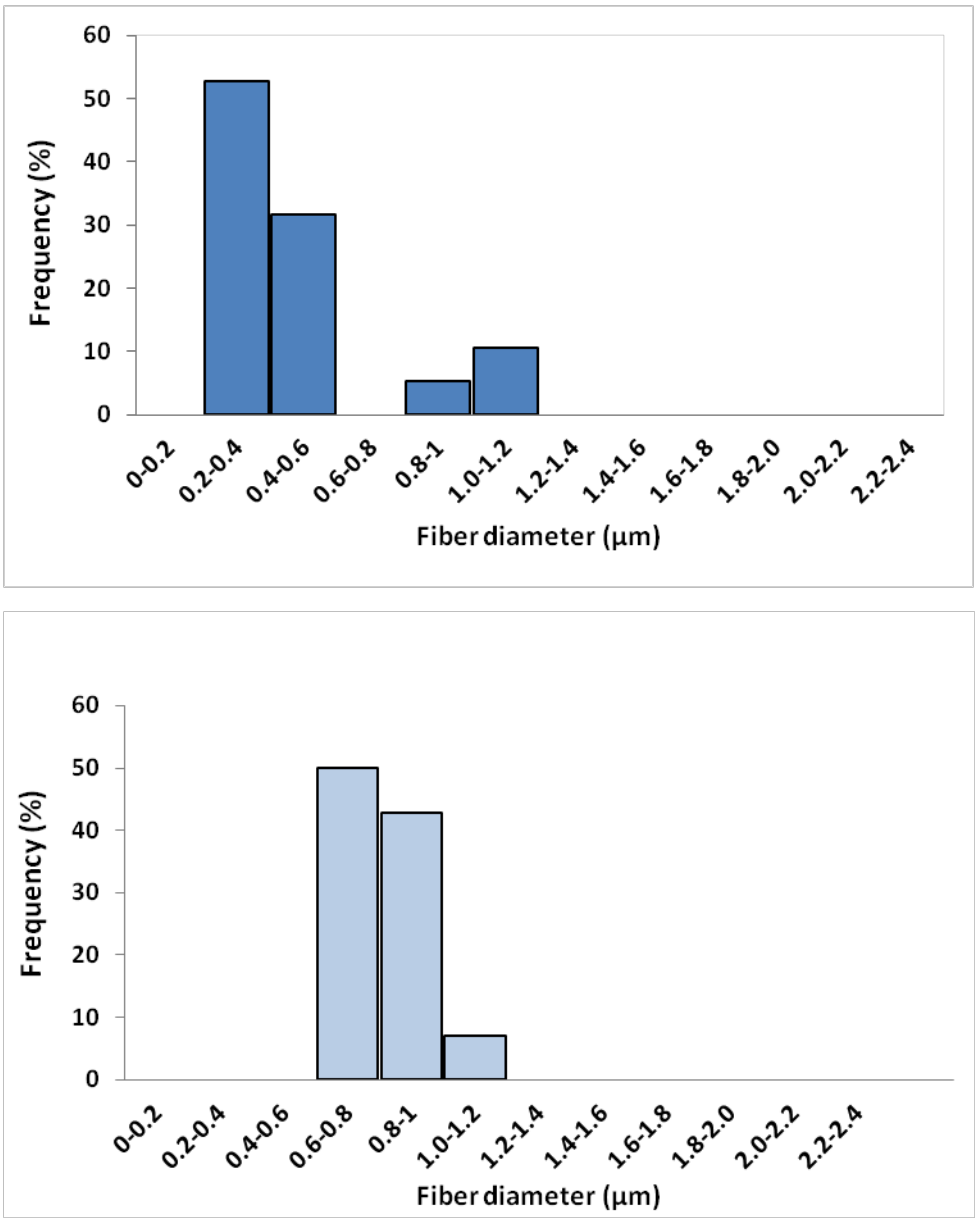

Figure 14. Fiber size distribution for random 10-wt % (up) and aligned 10-wt % (down) scaffolds.

The aligned fibers scaffold presented higher stiffness, with an elastic modulus of 15.757 ± 1.28 MPa vs 8.05 ± 0.82 MPa for scaffolds based on random fibers **(Figure 15B)**. The shape of the stress-strain curve **(Figure 15A)** revealed a purely elastic behaviour for aligned scaffolds (almost linear response), compared to a more viscoelastic behaviour for random ones (J form).

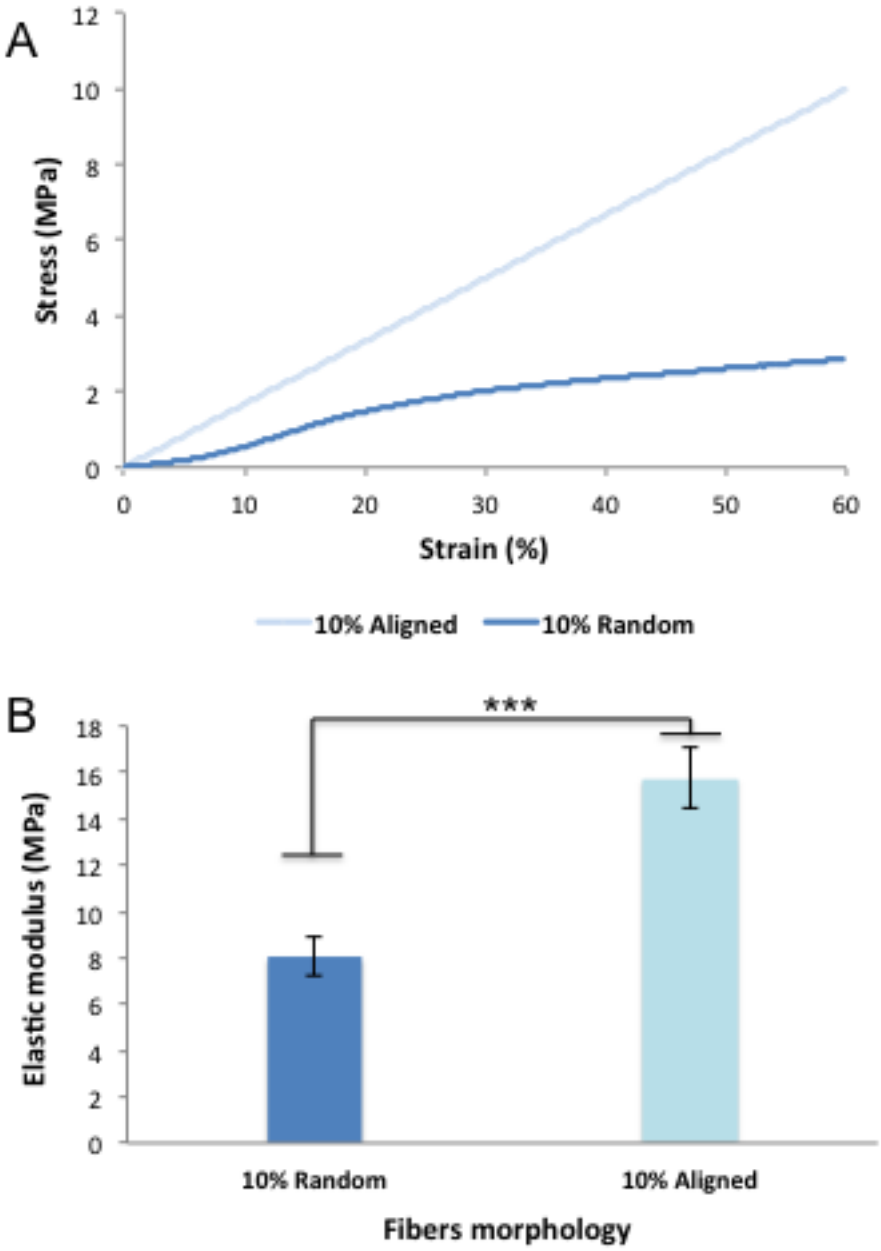

Figure 15. Average elastic modulus relative to fiber alignment. **A**. Representative stress vs strain curves for each morphology. **B.** Average elastic modulus. The p values are indicated for the tests showing a significant difference. (*** For p value <0.001).

2.1.2. Impact of Fiber Alignment on Cell Response

C3H10T1/2 cells were cultured under the same conditions (10^5 cells/cm^2) on each type of scaffolds. After 2 days of culture, confocal microscopy showed a random morphology when cells were cultured over random PCL scaffolds **(Fig 16A)** while cells cultured over aligned scaffolds spread along the fibers with an elongated shape **(Fig 16C)**. After 5 days, both

conditions presented a complete cell colonization of the scaffold surface. Regarding the cell morphology, the same tendency was observed, with cells spreading over the fiber alignment **(Fig 16D)** and without a particular orientation when cultured over random PCL scaffolds **(Fig 16B)**.

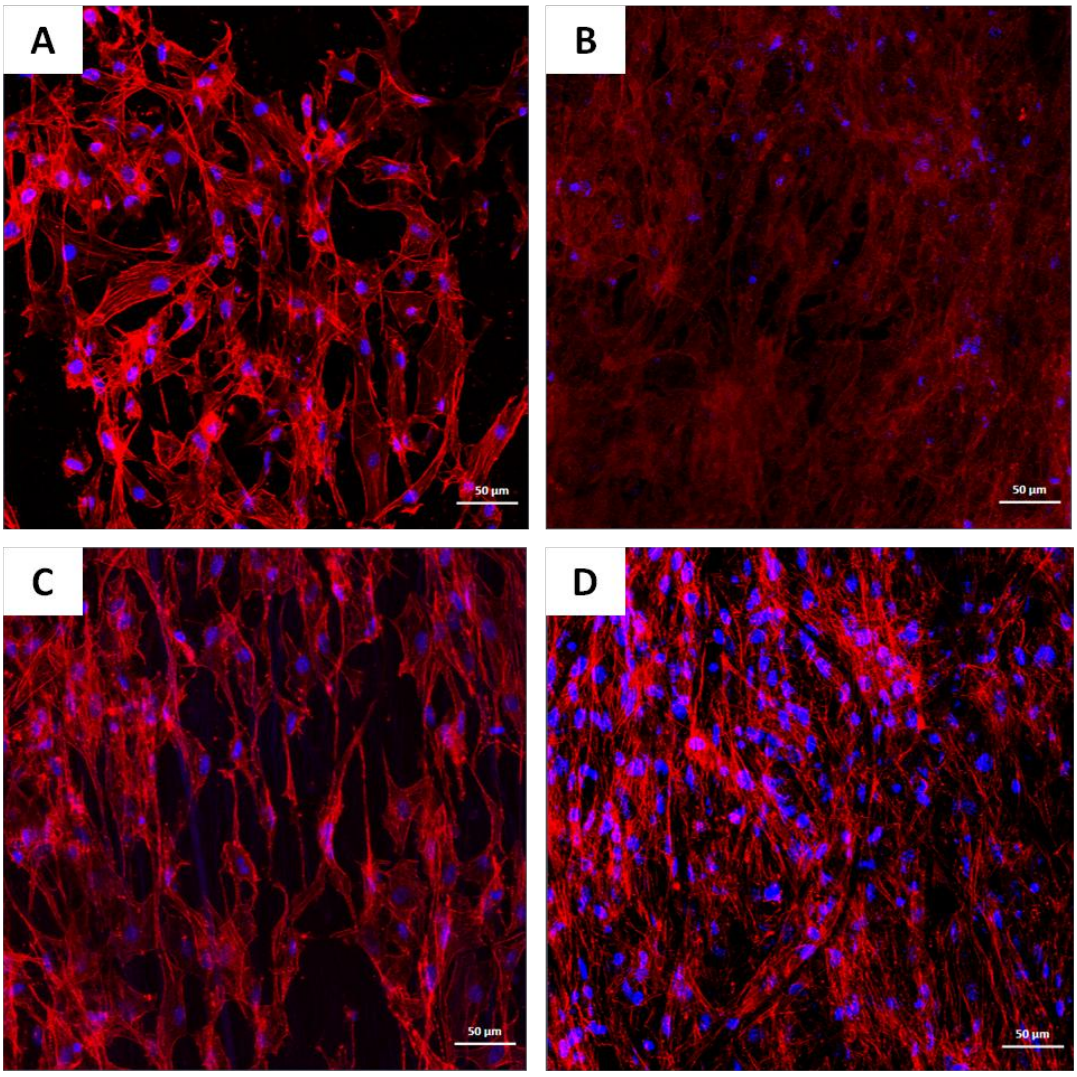

Figure 16. Effect of fibers alignment on cell morphology. Fluorescence staining of actin cytoskeleton (red) and nuclei (blue) of C3H10T1/2. The cells were cultured for 2 days (A,C) or 5 days (B,D) free of grow factors over random (A,B) or aligned PCL 10-wt % scaffolds (C,D). Scale bars 50 µm.

Then, we analyzed the gene expression of prior detailed tendon markers (*Scx*, *Tnmd*, *Aqp1*), bone related markers (*Dlx5*, *Runx2* and *Bglap*) and common markers (*Col1a1*) (**Figure 17)**. We prolonged the culture time for three weeks to also investigate long-term effects.

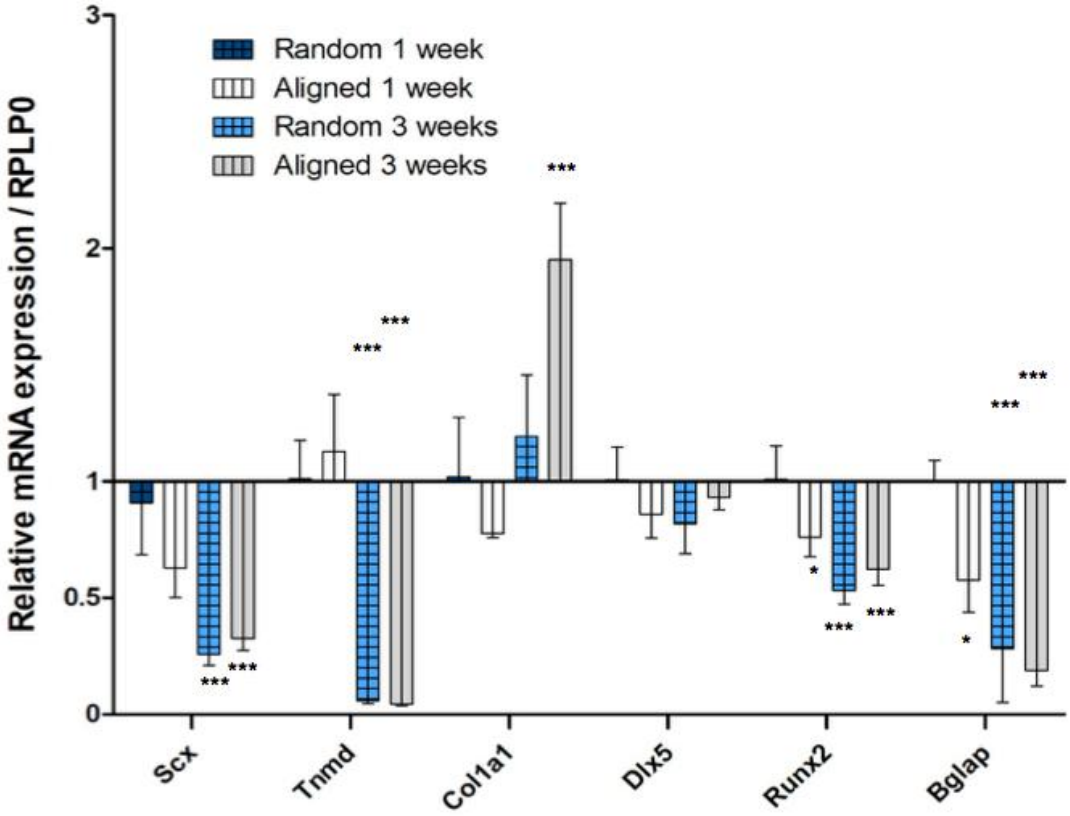

Figure 17. Gene expression of tendon- and bone-related markers in C3H10T1/2 cells cultured on aligned or random scaffolds for 1 or 3 weeks (n=6). 10-wt % random scaffold (Random 1 week) was chosen as a control. The data obtained for gene expression were compared with the Mann-Whitney nonparametric statistical test. (* for p value <0.05, *** for p value <0.001).

After a week of culture, only Runx2 and Blap appeared statistically decayed ($p<0.05$) when cells were cultured over aligned scaffolds compared to random ones. Thus, after a brief period of culture, the bone differentiation potential of C3H10T1/2 might decrease when cultured on aligned scaffolds. After 3 weeks of culture, interestingly both tendon (*Scx* and *Tnmd*) and bone (*Runx2* and *Bglap*) related markers decreased ($p<0.001$). This decrease was found both in the early markers (*Scx* and *Runx2*) and in the late markers (*Tnmd* and *Bglap*). Regarding a common marker, Col1a1, only the C3H10T1/2 cultured over aligned fibers showed a significant increase ($p<0.001$), indicating that aligned fibers favor the expression of collagen over time.

2.1.3. Discussion

Based on previously reported studies analyzing the positive impact of aligned scaffolds for tendon tissue engineering[134,154,155], we produced aligned PCL fibers in cooperation with the IMP Hanover. Unfortunately, once electrospun, the same PCL contration (10%) led to scaffolds presenting higher fiber diameters when aligned compared to random fibers. This effect have been previously reported on another study that compared PLGA scaffolds with differents fibers morphologies. Under the same polymer concentration, aumgenting the rotation speed resulted in aligned fibers with higher diameters than random ones.[152]

Related to the mechanical properties, aligned scaffolds presented a higher elastic modulus compared to random ones. This result is in concordance with previous studies in with aligned mats resulted in improved mechanical properties. This is explained as an improvement of the anisotropic mechanical behaviour of electrospun scaffold by the alignment of the fibers. [134,152,156]

If the fibers are aligned, C3H10T1/2 took a spindle shape morphology aligned with the fibers, similar to tendon cells aligned with collagen fibers. With random fibers, cells were found sparsely directed in all the axes without any predilection. This was previously reported and described as a contact guidance of aligned substrate that induce a change in the morphology of cells, addapting their morphology in the same axe as fibers[95]. However, fiber and cell alignment did not drive their differentiation towards tendon lineage, as far as genomic markers were concerned. Moreover, we observed that prolonging culture time resulted in a decrease of all related markers compared to shorter times. This may be to a self renewal of C3H10T1/2 multipotency over time.

2.2. Dynamic Culture as a Key Factor Guiding Tendon Differentiation

As reported in bibliography study, mechanical stimulaton is another environmental factor that can promote cell differentiation, activity and ECM deposition similar to those found on tendon tissue. The technical difficulty to perform such dynamic culture is mainly to generate controlled stretching while respecting the constraints of an in vitro culture in an incubator: maintain temperature, sterility, gaz exchange and a suitable culture medium for cell development. Besides the technical hurdles, one should note the lack of standardized

protocols or even recommendations to guide cells towards the right performance, in this case tendon-like differentiation.

The procedure to define a protocol for mechanical solicitation will therefore be presented here. The main objectives are : i) to analyze the impact of mechanical solicitation on cell behaviour (morphology and differentiation), and ii) to evaluate the impact of this stimulation on the mechanical properties of the biohybrid material over time.

2.2.1. Development of a Mechanical Stimulation Protocol

Taking into account the previously described requirements, the bioreactor Bose Biodynamic 5100 allowed us to perform mechanical stimulations in a controlled atmosphere, as it is possible to place the device into an incubator allowing the temperature and $C0_2$ to be controlled at 37ºC and 5% respectively. The bioreactor consists in one culture chamber with up to 200 ml volume capacity with two rods connected to one motor and the other to a force transducer of 22N. The scaffold can be fixed between the rods and the cell culture media can continuously circulate thanks to a system of peristaltic pumps connected to the cell chamber. In addition all the pieces can be autoclaved, allowing maintaining the sterility as long as the culture time take place. The entire device is shown in **Figure 18**.

The existence of the force transducer allows either to apply the force (stress), leading to the deformation (strain) as an output or to use the deformation as an input and to obtain a force as the output. The software provided by the manufacturer records all the stress strain data. Although the device offers a complete monitoring, a first part of the workwas dedicated to the implementation of the experiments.

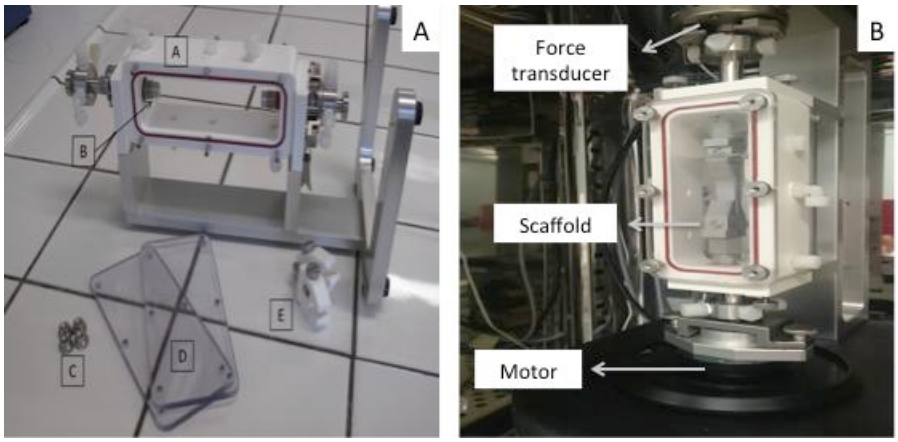

Figure 18. (A) Bose Biodynamic cell culture room. A. Bioreactor chamber. B. Rods. C. Clamping scews of glazed walls. D. Glazed walls. E. Clamps. **(B)** Mounted bioreactor inside an incubator.

Before starting, two fundamental questions had to be adrressed : 1) time of culture, i.e. short test vs. long culture assay and 2) choice of a dynamic stretching protocol to perform. Regarding the time, in order to compare the cell activity under a mechanical environment with our previous results, we decided to perform a 5-day mechanical loading regime. Moreover, as cells needs some time to attach, 11h of static culture were performed out of the culture chamber. The cell seeded scaffoldwas then integrated into the bioreactor under sterile conditions and rest for other additional 11h prior starting the mechanical stimulation cycles. The objective was to let the cells time to attach and to spread all over the surface of the scaffold prior starting stretching. As the culture chamber's volume was 170 mL, we chose to keep it for the 5 days and avoid the use of the peristaltic pump to renew the medium. To guarantee air exchange, we plug a 0.2µm air filter to avoid any contamination.

As first phase of investigation, we applied cycles of 1 h stretching + 11h of rest twice a day, imposing the strain as input and recording the resulting stress with the force transducer as output. We decided to work with 1% amplitude of strain at 1 Hz frequency, following literature with electrospun scaffolds[138,157] (physiological range). During the rest periods (11h) a static strain of ϵ_0 = 0.5% was applied. This "preload" was intended to ensure a permanent tension during both the stretching and resting phases, avoiding any compression. An illustration of the variables can be seen in **Figure 19**.

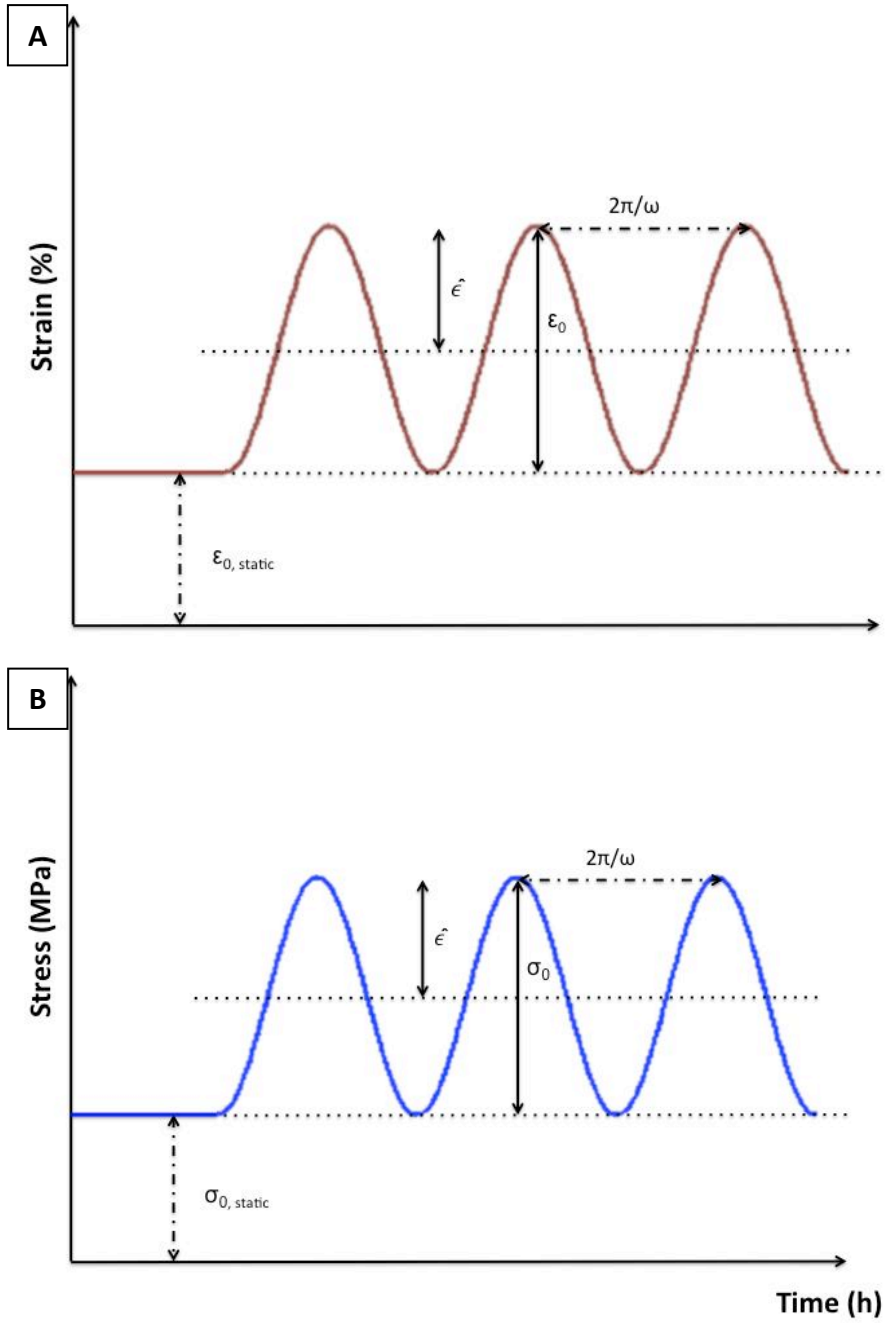

Figure 19. Dynamic cultivation protocol. **(A). Representation of the applied strain.** Amplitude $\hat{\epsilon}$ and $\epsilon_{0,static}$ are set to 0.5% strain. The offset ϵ_0 is 1% and the period T 1s. **(B). Representation of the resulting stress.**

2.2.2. Impact of Mechanical Load on Cell Response

After 5 days of static culture, as previously reported, C3H10T1/2 spread over all directions **(Fig 20A)**. Under dynamic conditions, they presented an aligned morphology following the axis of the mechanical stimulus **(Fig 20B)**. The difference between both conditions show that cells successfully perceived the mechanical stimulation despite its low range (1%). In

addition, cells were presented all over the surface of the scaffold, indicating a successful culture inside the bioreactor.

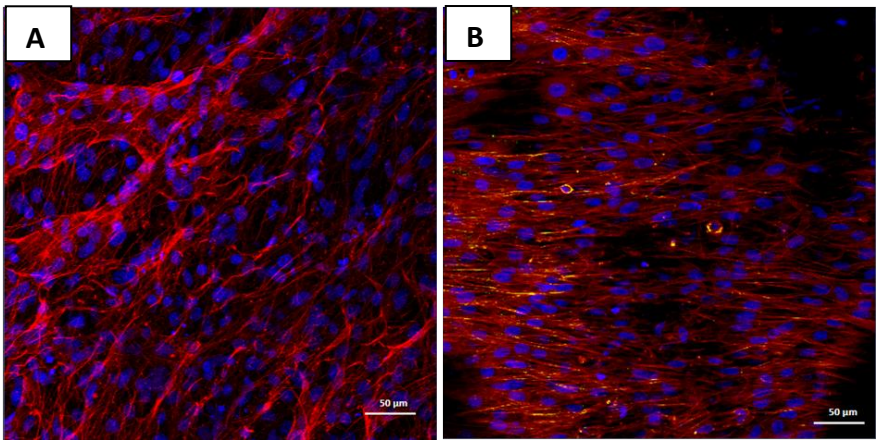

Figure 20. Fluorescence staining of actin cytoskeleton (red) and nuclei (blue) of C3H10T1/2 after 5 days of static (A-B) or dynamic culture (C-D). Scale bars of 50µm.

Gene expression analysis for cells under static vs dynamic culture did not show significant difference **(Figure 21)**, but for *Bglap*, which slightly increased in dynamic culture, compared to static one, with no statistical difference.

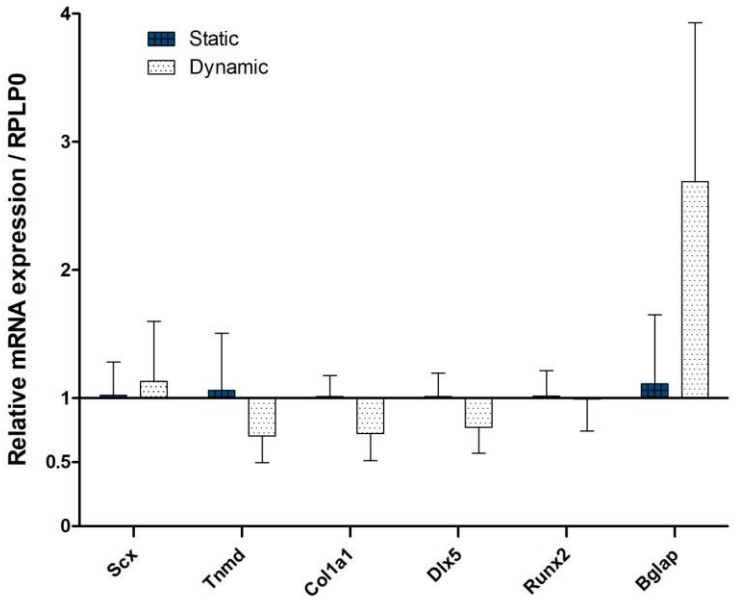

Figure 21. Gene expression of tendon- and bone-related markers in C3H10T1/2 cells cultured on random scaffolds under static or dynamic culture conditions for 5 days inside the Bose Biodynamic 5100 bioreactor (n=6). Static culture was chosen as a control.

2.2.3. Impact of Mechanical Load on Scaffold Mechanical Response

Besides the cellular behaviour, it is interesting to follow the mechanical evolution of the biohybrid construct (i.e scaffold + cells) during the whole duration of the stimulation test. Compared to a control without cells, wa aimed at determining the potential mechanical impact of the presence of cells on the scaffold.

As explained earlier, for each sinus of an imposed strain (1%), a resulting force was collected thanks to a force transducer. Every second, the software imposed to record at least 20 points. A first analysis consisted in representing all the points saved for both the stimulation cycles (1 hour) and the rest periods (11h) during the 5 days, for the control without cells and the cell-construct **(Figure 22 and 23)**.

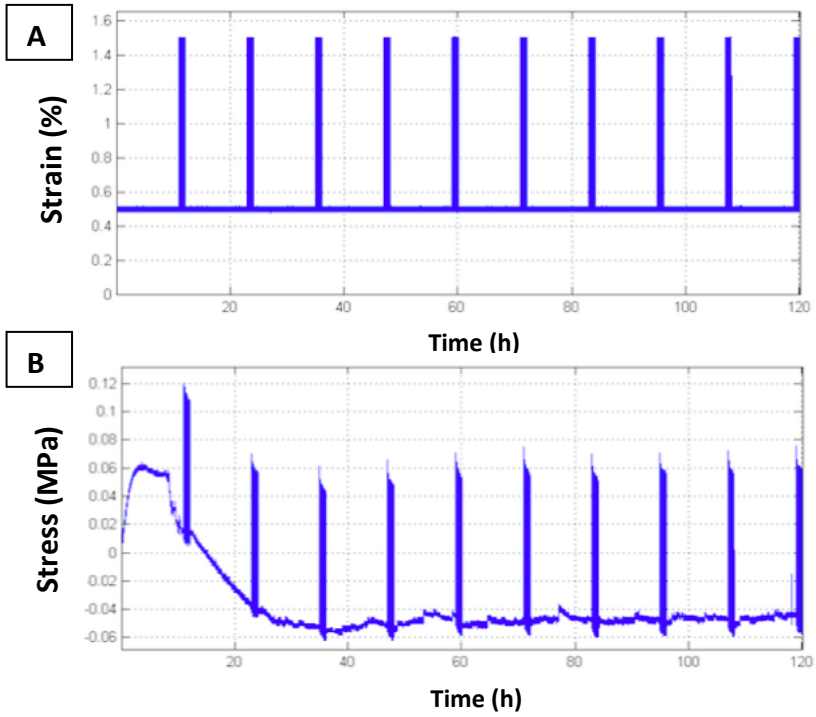

Figure 22. Strain vs time (**A**) and stress vs time (**B**) for a 5 days mechanically stimulated control scaffold without cells.

Once the “native” sample was secured between the grips and maintained at 0.5% strain prior to the first stretching, the force exerted on the sensor increased without any additional load. Then the recorded force started to decrease until it reached equilibrium **(Fig 22)**. We hypothesized that these changes were the results of water up-take and creep of the

material, respectively. After about 24h, these permutations seemed to stabilize and the resulting force remained stable until the end. In addition, by looking closely at each stimulation cycle, the force seemed to decay throughout each cycle.

When the scaffold was equipped with cells, the changes in the first 24 h response were less pronounced. The stress remained stable during the 5 days. The force needed to deform the scaffold was in the same range of magnitude than control, but always slightly higher **(Figure 23)**.

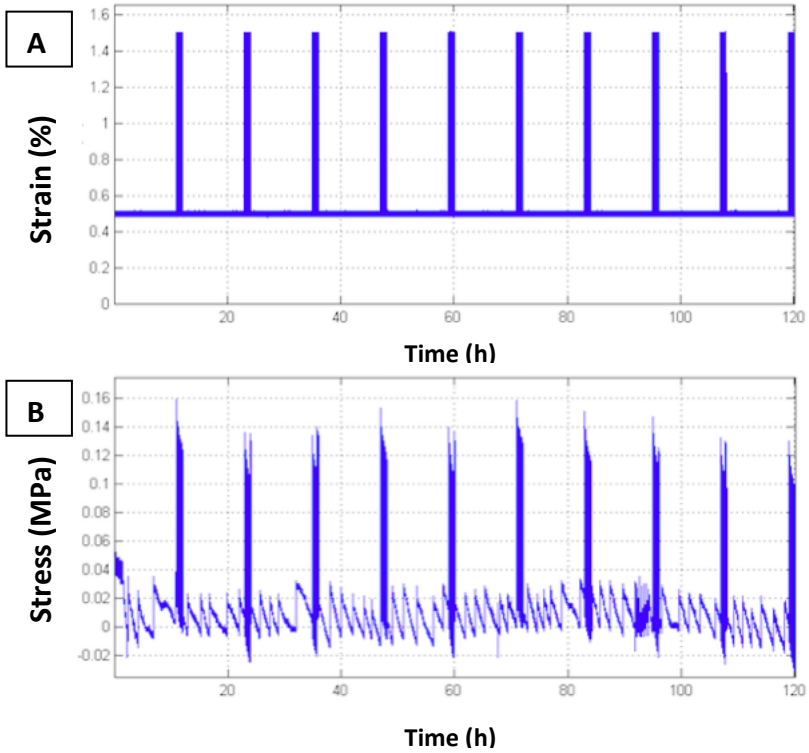

Figure 23. Strain vs time (**A**) and stress vs time (**B**) for a 5 days mechanically stimulated cell-construct.

For more detailed analyses, we focused on each sinus of each dynamic stretching. We chose to represent here the first sinus of the first cycle and the last sinus of the last cycle for the control (**Figure 24)** and the cell-seeded scaffold (**Figure 25)**.

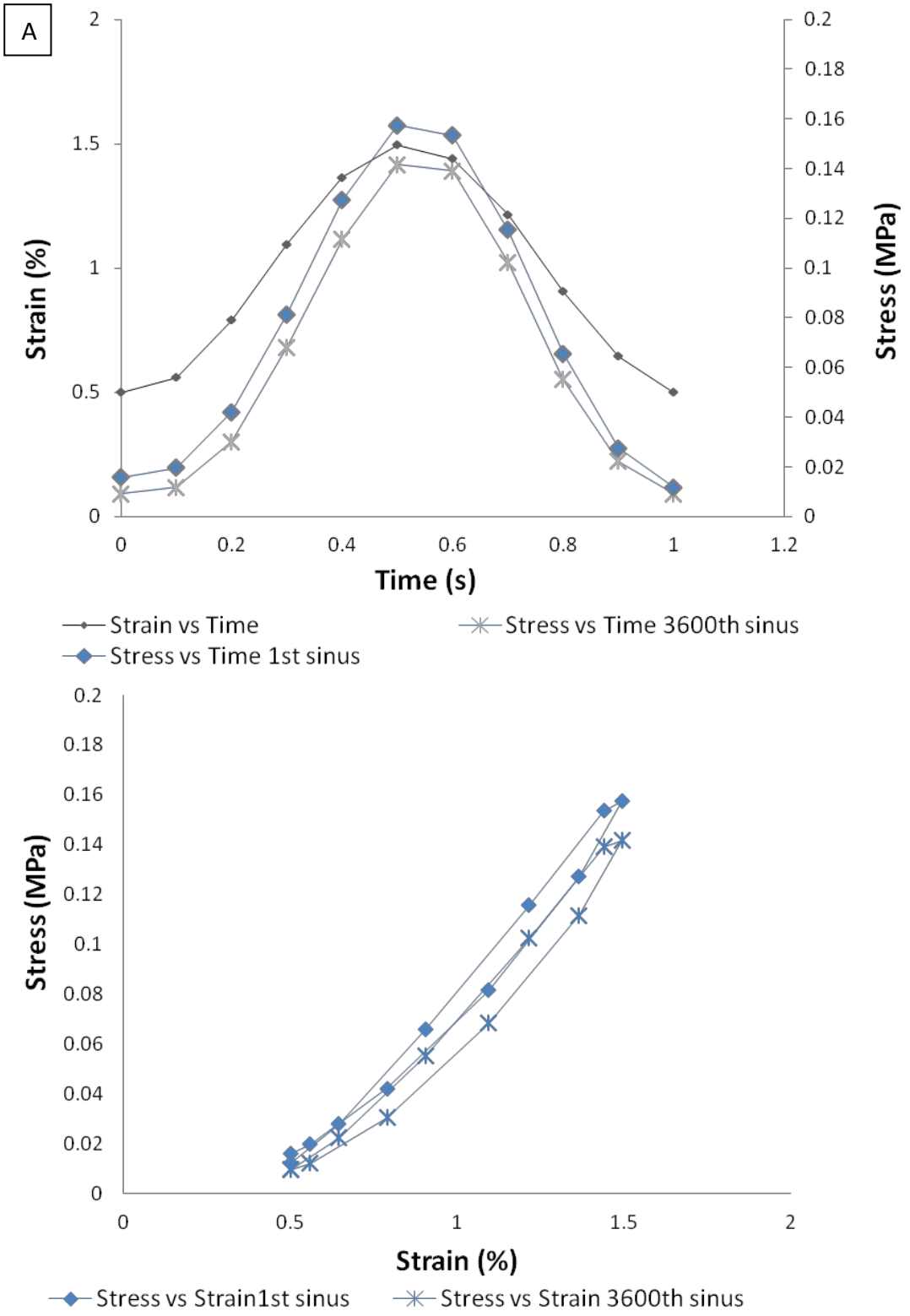

Figure 24. Representation of the strain and stress vs. time **(A)** and stress vs. strain **(B)** curves of the first sinus from the first cycle at day 1 and the last sinus from the last cycle at day 5. Scaffold 10-wt % control without cells

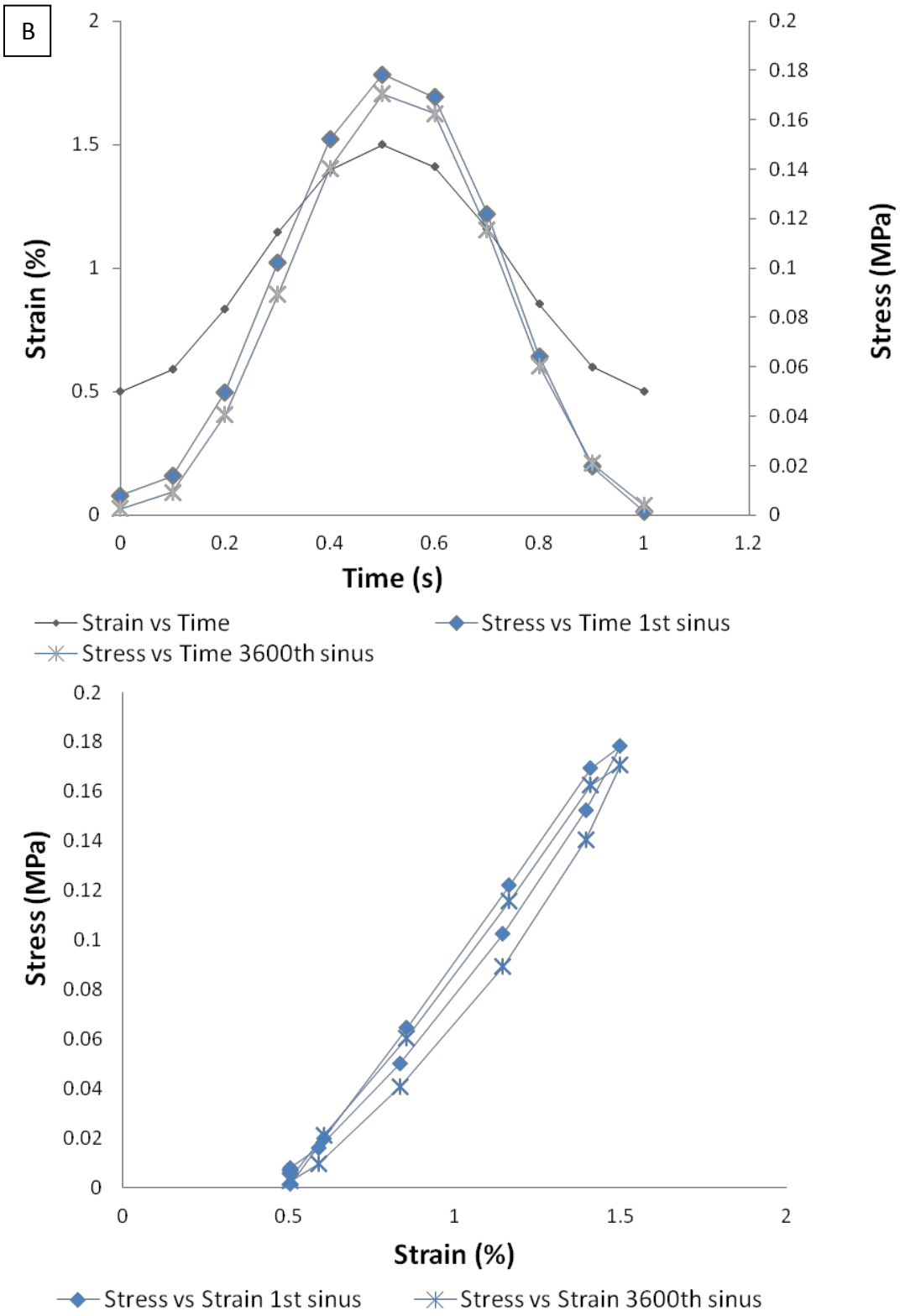

Figure 25. A. Representation of the strain and stress vs. time **(A)** and stress vs. strain **(B)** curves of the first sinus from the first cycle at day 1 and the last sinus from the last cycle at day 5. Scaffold 10-wt % with cells.

For both conditions (with or without cells), the displayed graphs were quite similar. It is worth to mention that for both conditions, the stress vs. time curves always appeared slightly lower for the last sinus when compared to the first sinus. This indicated that less force was needed to deform the scaffold when repeated stimulations are applied for a time. Of note, the range (22N) of the force transducer available for these experiments was not really adapted for these small deformations, although the results were quite repeatable.

Plotting on the same graph the stress and strain curves vs time allows the estimation of the phase lag (δ) between the curves. This could provide us in the future some information on the viscoelastic nature of the scaffolds. On **Fig 26A**, a lag between force and displacement was indeed noticeable. Changes of phase lag over the five days of dynamic stimulation is shown in **Fig 26B**. The results indicate that cultured specimens and controls (without cells) presented the same δ around 6º. Of note, only one specimen is shown for each condition. The results are therefore not suitable to proof statistical evidence. Nevertheless, at this low range of strain tested, the presence of these cells did not seem to have any impact on the phase lag. Moreover, remaining constant over time (5 days) for each condition, it indicated the mechanical stability of the scaffolds for this time period.

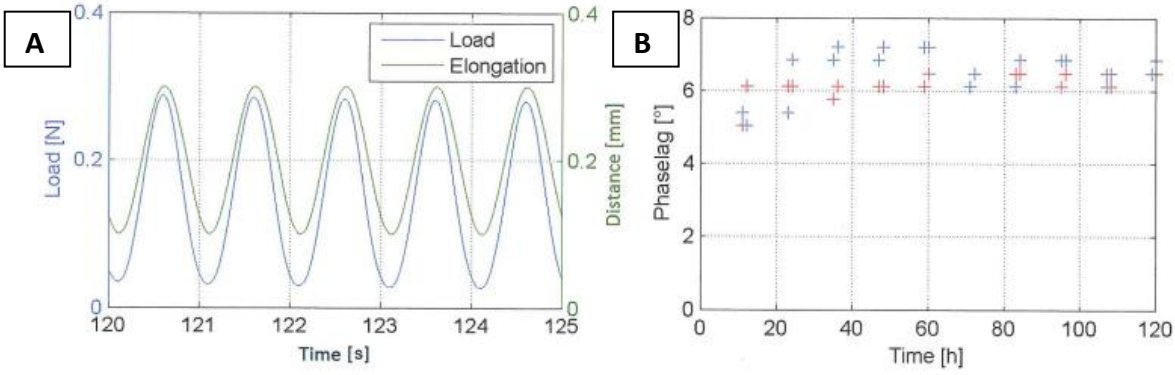

Figure 26. Effect of 5 days of dynamic culture (with or without cells) on the viscosity of the material. **(A).** Stress vs. time and displacement vs. time curves. **(B).**Phase lag between the applied displacement and the obtained force. Blue represents the control experience without cells. Red represents the cell-construct experience.

2.2.4. Discussion

As explained above, mechanical stimulation has been used during the last years as a relevant environmental factor to guide cells towards a tendon activity in tissue engineering strategies. In this chapter, we decided to apply a low range of deformation (1%) to asses the impact on C3H10T1/2 differentiation.

After 5 days of mechanical stimulation, cells appeared to be aligned in the stretching axis, indicating that they have positively responded to the stimuli, orientating their morphology as previously described in other works.[138,139,158,159] These changes are attributed to mechanotransduction. However, this guidance in morphology did not result in any positive cell differentiation.

From a mechanical point of view, we confirmed that the set up was efficient for several days and allowed us to record strain and stress parameters, although the sensor's sensitivity was not fully adapted to the electrospun materials. We did not observe significant differences between bare scaffolds and cell seeded ones.

Five days of culture might not be long enough for complete cell colonization and production of an important extracellular matrix, which could result in relative change in mechanical properties. Despite these results, our system revealed promising results. Both in the presence or absence of cells, after 5 days of mechano-culture the scaffold did not present signs of mechanical degradation, supporting the mechanical stress without this being irreversible, which is necessary for a long-time culture.

3. Conclusion

In this chapter, we investigated several ways to drive cells differentiation towards tendon lineage, using electrospun PCL as scaffold. The challenge was high, since we intentionally chose not to use any differentiation factor, to assess the only impact of physical parameters: size, orientation or stretching of the fibers. Unfortunately, we did not succeed in these investigations with C3H10T1/2 cells. The choice of this cell line was guided by the previous expertise of our lab, as well as the potential to use their progenitor status to guide them either to bone or tendon. Based on the results presented here, we should now reconsider this choice: indeed, their capacity for high proliferation might lead to a "permanent"

pluripotency, with cells concomitantly found at different stages. In addition, collagen synthesis appeared very low, which was not favorable to study the impact of cells on the mechanical properties of the biohybrid scaffold. The conclusion of this study regarding the choice of cells now guides us towards using mesenchymal stem cells.

We learnt also a lot on the mechanical stimulation process. Taking into account the overall obtained results, the next stage will consist in increasing the mechanical culture time inside the bioreactor, as well as modifying the strain range. This deformation should be larger to expect a significant cell response.

Chapter V: (Submitted Article) Monitoring Mechanical Stimulation for Optimal Tendon Tissue Engineering: a Mechanical and Biological Multiscale Study.

Monitoring mechanical stimulation for optimal tendon tissue engineering: a mechanical and biological multiscale study

Garcia Garcia A.[1], Perot JB.[1], Beldjilali-Labro M.[1], Dermigny Q.[1], Naudot M.[2], Le Ricousse S.[2], Legallais C.[1], Bedoui F.[3,*]

[1] CNRS, UMR 7338 Laboratory of Biomechanics and Bioengineering, Sorbonne Universités, Université de Technologie de Compiègne, 60200 Compiegne, France; alejandro.garcia-garcia@utc.fr (A.G.G); megane.beldjilali-labro@utc.fr (M.B.L); quentin.dermigny@utc.fr (QD); cecile.legallais@utc.fr (C.L)

[2] EA4666-LNPC-Immunologie Therapie Cellulaire Hématologie Cancers, CURS, Hopital Sud Avenue René Laennec, 80054 Salouel, France; marie.naudot@u-picardie.fr (M.N); sophie.le.ricousse@u-picardie.fr (S.L.R)

[3] FRE CNRS 2012 Roberval Laboratory for Mechanics, Sorbonne Universités, Université de Technologie de Compiègne, 60200 Compiègne, France; fahmi.bedoui@utc.fr (F.B)

* Correspondence: fahmi.bedoui@utc.fr; Tel.: +33- 3 44 23 45 28

Abstract

The aim of this work is to evaluate in tendon tissue engineering the effects of cyclic stretching on both the differentiation of mesenchymal stem cells and the mechanical properties of the resulting viscoelastic biohybrid scaffold. In our approach, electrospun poly(ε-caprolactone) (PCL) nanofibers inspired by the random healing structure of tendon were produced to both provide an appropriate environment for cells, and ensure mechanical stability during the application of mechanical stimulation. Rat bone marrow stromal cells (BMSCs) were cultured in the absence of any tenogenic growth factors, on the assumption that both cell-material interactions and mechanical stretching in a bioreactor (5% strain at 1Hz for 2H/day for 12 days) would guide their differentiation. After 12 days of mechanical stimulation, the cells effectively presented an elongated morphology and produced an aligned collagen and tenomodulin extracellular matrix (ECM). When stimulated, tendon constructs showed upgraded viscous and elastic properties, related to the ECM deposition, compared to non-stimulated ones or to native materials (devoid of cells). Changes in these

mechanical properties could be monitored throughout the culture process. Our study highlights the importance of correlation between cellular and mechanical changes when submitted to a mechanical stimulation protocol. This model can be adapted to any material or mechanical load, making it possible to determine both the range of stimulation and the cell response in the scaffold.

1. Introduction

Native tendon is made of an anisotropic and viscoelastic material capable of resisting high tensile forces. Tendon cells, mainly tenocytes, are rather scarce, and are responsible for synthesising extracellular matrix, which is mainly composed of type I collagen with a highly organised structure.

The main objective of tendon tissue engineering is to design and produce a cell-construct that will help to regenerate damaged tissue or mimic it for comprehensive in vitro studies. To achieve this goal, researchers have searched in recent years for the most efficient cells, the right materials, and the appropriate chemical or mechanical environment [1,2]. Although the holy grail is still a long way off, most studies have clearly demonstrated the advantages of reproducing the mechanical environment in order to guide the cell-scaffold constructs towards tendon repair [2].

Bone marrow stromal cells (BMSC) are the most widely-used stem cells for tendon tissue engineering [3,4], among other stem or progenitor cells, as they have the potential for self-renewal, clonogenicity, and multi-lineage differentiation, including tenogenicity. In many studies, biochemical factors – mainly from the transforming growth factor family (TGF-β) – are added to the culture medium to foster this differentiation [5,6].

Regarding the scaffold issue, electrospinning has been used for several years to tailor an environment for cell development and differentiation similar to that of extracellular matrix, but with different fibre sizes, porosity, elasticity and mechanical properties for tendon tissue engineering [7]. Some researchers have shown the influence of alignment as the first guiding point for aligning cells as in tendons [3]. Fibre size is also a parameter that may influence cell activity. Recently, Lee et al. showed that small, nano-scale random fibres provided a cell environment similar to that found in the inflammatory phase of the tendon healing process, promoting the synthesis of the extracellular matrix (ECM) and cell

proliferation, while larger aligned fibres mimicked the normal structure of collagen in tendon, maintaining the tendon cell phenotype [8].

Mechanical stimulation is another key environmental factor for reproducing in vivo conditions. Physiotherapists recommend periodic stretching in training to heal defects or to improve capacity [9–12]. In vitro, some studies have stated that proper stimuli applied to biohybrid scaffolds could act on cell proliferation, differentiation or function, following mechanotransduction pathways [13–15]. While different stimuli have been tested with a wide range of amplitudes, frequencies and time, it should be noted that little is known about how mechanical stress may affect both cell and material responses throughout the tissue engineering process [16].

In order to better understand the inter-dependency between mechanical stimulations and biohybrid scaffold responses (both biological and mechanical), we performed static and dynamic cultures of rat BMSCs on dedicated electrospun PCL scaffolds using bioreactors (T6 CellScale and Bose Biodynamic 5200). The mechanical behaviour and cellular activity of the cell-constructs during the stimulation period were recorded and analysed for 12 days, then compared with those obtained under static conditions. At the biological level, we focused on cell proliferation, differentiation towards tendon lineage (in the absence of specific differentiation factors) and organisation of the neo-synthetized ECM. At the mechanical level, we followed up the changes in both the viscous and elastic properties of the pure and cell-seeded scaffolds.

2. Materials and Methods

2.1 Scaffold preparation and characterisation

Poly(ε-caprolactone) (PCL, MW=80kg.mol^{-1} Sigma Aldrich, United States) was dissolved in dichloromethane (DCM, Sigma-Aldrich)/*N,N*-dimethylformamide (DMF, ReagentPlus® Sigma-Aldrich, USA) (80/20 v/v) for 24h to make an electrospinning solution at 10 wt %. Once dissolved, the solution was poured into a 10 ml glass syringe. Scaffold fabrication was performed over a rotating collector for 3H (distance 15 cm, flow rate 0.017ml/min, needle diameter 18G, voltage 15kV). In order to evaluate the morphology and mechanical

properties of the PCL scaffolds, scanning electron microscopy and tensile testing were carried out retrospectively.

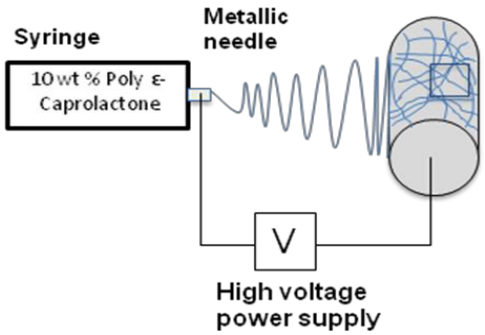

Figure 1. Electrospinning device.

- **Morphological characterisation**

The morphology of the electrospun scaffolds was observed using scanning electron microscopy (Philips XL30 ESEM-FEG). Electrospun mats were cleaned with ethanol and gold-coated prior to observation. To analyse the diameter of the electrospun 10 wt % PCL fibres, ImageJ software was used. After setting up the scale, a line was drawn manually across the diameter of randomly-selected fibres (n=50) from 3 different SEM micrographs. The degree of isotropy in two samples from three scaffolds (n=6) was analysed using Mountain™ software. The main directions of the fibres were analysed using the Fourier Transform method.

- **Elastic properties**

The scaffold modulus for dry and wet scaffolds was quantified using uniaxial tensile testing. Three samples for each scaffold (n=3) were shaped into a strip measuring 1.0 cm x 3.0 cm. For wet samples, the scaffolds were immersed in ethanol 70% (Sigma-Aldrich, USA) for 45 min then washed three times with PBS 7.4 (phosphate buffered saline, Gibco Invitrogen, USA). The thickness was evaluated using a precision dial thickness gauge (Mitutoyo Corporation, Japan). The samples were secured within the metallic grips of the tensile tester (Bose Electroforce 3200, TA, USA) and elongation at 0.1 mm s^{-1} was performed with a

working load of 22N. The applied force was measured each second and the modulus obtained from the slope of the linear region.

2.2 Pre-culture preparation

- **Cell harvesting and culture**

Bone marrow stromal cells (BMSCs) were isolated from rat bone marrow thanks to their short-time adherence to plastic, in accordance with previously described protocols [17,18]. Briefly, 6-week-old male Sprague Dawley rats (n=4) were sacrificed, and both right and left femurs were aseptically removed and washed 3 times with 1x PBS 7.4 (phosphate buffered saline, Gibco Invitrogen, USA). Next, bone marrow was flushed out using α-MEM culture medium (PAN BIOTECH, Germany) supplemented with 10% foetal bovine serum (FBS, Gibco Invitrogen, USA), 1% penicillin-streptomycin (Gibco Invitrogen, USA) and 1% amphotericin B (PAN BIOTECH, Germany). The released cells were then collected into 6-well dishes (BD Falcon™, USA). After 24h, non-adherent cells were carefully discarded and adherent cells were cultured with fresh α-MEM for 6-7 days, the time needed for BMSC colonies to reach confluence. The cell culture media were replaced every 3 days. When the culture dishes started to approach confluence, the cells were detached and serially subcultured. The cells at the third passage (P3) were used for the cell seeding experiments.

- **Cell seeding on scaffolds**

Electrospun mats were cut into strips measuring 40 x 12.5 mm or 35 x 9 mm as shown in **Table 1**, disinfected with ethanol 70% (Sigma-Aldrich, USA) for 45 min, and then washed three times with PBS for 10 min. Disinfected scaffolds were soaked in fresh α-MEM for 48h before seeding the cells. After that, the media was discarded and each scaffold was plated with a density of $6x10^4$ cells cm^{-2}.

- **Mechanical stimulation**

After two days of static culture, each construct was placed in a bioreactor for mechanical stimulation or in well dishes for static culture. Mechanically-stimulated cell constructs were stretched twice a day at 5% strain for 1h at 1Hz with 11h of rest between each cycle for 5 or 12 days (considered as 1 or 2 weeks of culture time respectively). For this purpose, two different bioreactors were used: (1) the MechanoCulture T6 Mechanical Stimulation System

(CellScale Biomaterials Testing, Waterloo, ON, Canada), consisting of an actuator and screw-driven clamp grips mounted inside a cell culture chamber capable of applying uniaxial stretching to 6 parallel samples, was chosen for the biological assays. Cell culture media were replaced every 5 days, and (2) the Bose Biodynamic 5100 (TA Electroforce®, USA), consisting of a cell culture chamber connected to a flow pump in which one sample was attached thanks to a system of rods and clamps. One rod was attached to a step motor making it possible to apply uniaxial displacement. The other rod was connected to a force transducer of 22N making it possible to constantly monitor the force applied to each displacement. Cell culture media circulated continuously through the flow pump connected to a reservoir of 500 mL, making it possible to maintain the culture for up to two weeks. This system was chosen for biomechanical evaluation. For static culture, each construct was cultured for 5 or 12 days without tension and the cell culture media were replaced every 3 days.

2.3 Post-culture evaluation

To investigate the effects of dynamic culture on cell activity, seeded PCL 10-wt % scaffolds were secured in the grips of the T6 CellScale bioreactor after two days of static culture and cultured for 5 or 12 days under dynamic culture conditions (5% strain for 1h at 1Hz with 11h of rest). After this time, the cell-constructs were removed for biological analyses.

- **DNA and hydroxyproline content**

Total DNA and collagen from each sample were extracted at 5 or 12 days of static or dynamic culture with the reagent, Trizol (TRI Reagent®, Sigma-Aldrich, USA) according to the manufacturer´s protocol. Briefly, once lysed by the action of 1ml of Trizol, chloroform (Sigma-Aldrich, USA) was added to obtain a colourless upper aqueous phase with RNA, an interphase with DNA, and a lower red phenol-chloroform phase with proteins. DNA was then isolated and quantified using NanoDrop ND-1000 (Thermo Scientific, USA). Proteins were isolated and hydrolysed in 6N HCl (Sigma-Aldrich, USA), and total hydroxyproline content was determined using hydroxyproline assay (Hydroxyproline Assay Kit, Sigma-Aldrich, USA) [19]. Hydroxyproline content was related to the collagen content [20].

- **Morphology and ECM components**

After 5 or 12 days of static or dynamic culture, cells-constructs were fixed in a solution of 4% (w/v) paraformaldehyde solution (PAF, Agar Scientific, United Kingdom) in PBS for 15 min then rinsed three times with PBS 7.4. After 10 min of permeabilisation in a solution of PBS-Triton X-100 0.5% (v/v) (VWR, United Kingdom), cell-constructs were blocked at 4ºC overnight with a solution of 1% (w/v) BSA (Sigma-Aldrich, USA). The morphology of the rBMSCs under static or dynamic culture was assessed using rhodamine phalloidin (Invitrogen, USA) to selectively stain the F-actin. For immunofluorescence staining, cell-constructs were treated with primary antibodies to collagen type I (COL1, 1:100, Abcam, United Kingdom) or to tenomodulin (TNMD, 1:200, Abcam, United Kingdom) overnight at 4ºC. After incubating overnight at 4ºC with secondary fluorescent antibodies, Hoechst 33342 (Sigma-Aldrich, USA) was added as counterstaining for cell nuclei.

- **Biomechanical evaluation of cell construct**

Bose Biodynamic 5100 consists of one culture chamber with two rods, one connected to a motor and the other to a force transducer of 22N. The entire system is placed in an incubator making it possible to control the temperature and CO_2 at 37ºC and 5% respectively. Cell culture media circulated continuously thanks to a system of peristaltic pumps connected to the cell chamber. Either stress (σ) or strain (ε) could be set up as the driving parameter. We decided to set deformation, 5% cyclic sinusoidal strain as the control parameter. We recorded the resulting force at 20 points per second, corresponding to 20 points per sinus, during the 12 days of dynamic culture.

$$\text{Strain } \varepsilon = \varepsilon_0 \sin \omega t \quad (1)$$

$$\text{Stress } \sigma = \sigma_0 \sin(\omega t - \delta) \quad (2)$$

Where ε_0 and σ_0 are the initial strain and stress respectively, and ω and δ are the frequency and dephasage angle between stress and strain respectively. Plotting together stress vs strain, we were able to calculate the relative dissipation energy by calculating the surface between the curves in each sinus. Because sinusoidal stress was applied, we also determined the storage modulus (E'), loss modulus (E''), complex modulus (E*) and tan δ. All equations are indicated below:

$E' = E^* \cos\delta$ (Pa) (3)

$E'' = E^* \sin\delta$ (Pa) (4)

$E^* = \sqrt{E'^2 + E''^2}$ (Pa) (5)

tan δ = (E''/E') (6)

Each 1h cycle, consisting of 3600 sinuses, was divided into six intervals of 600 sinus and the results are given as an arithmetic average. After the first analysis, we decided to represent the results from 1200 to 3600 sinus of each cycle, where a closed loop region was found. For statically-cultured cell-constructs and controls, each sample was placed on the bioreactor and, once secured between the rods, one cycle of 3600 sinus was set at a given time (7 and 14 days) to compare in the same way as the dynamic conditions. For the control without cells, scaffolds were submitted at the same parameters as the cell-constructs, including disinfestations and incubation with cell culture media.

3. Results

3.1. PCL scaffold synthesis and characterisation

Electrospinning PCL into a DCM/DMF 4:1 co-solvent led to the production of a homogenous scaffold without pearls. SEM images showed a final material composed of a dense network of continuous smooth fibres **(Fig 2A),** as found in [21]. These fibres presented an average diameter of 0.52 ± 0.25 µm. Distribution analyses of the fibres revealed a random conformation, a with 53.3 % of anisotropy **(Fig 2B)**.

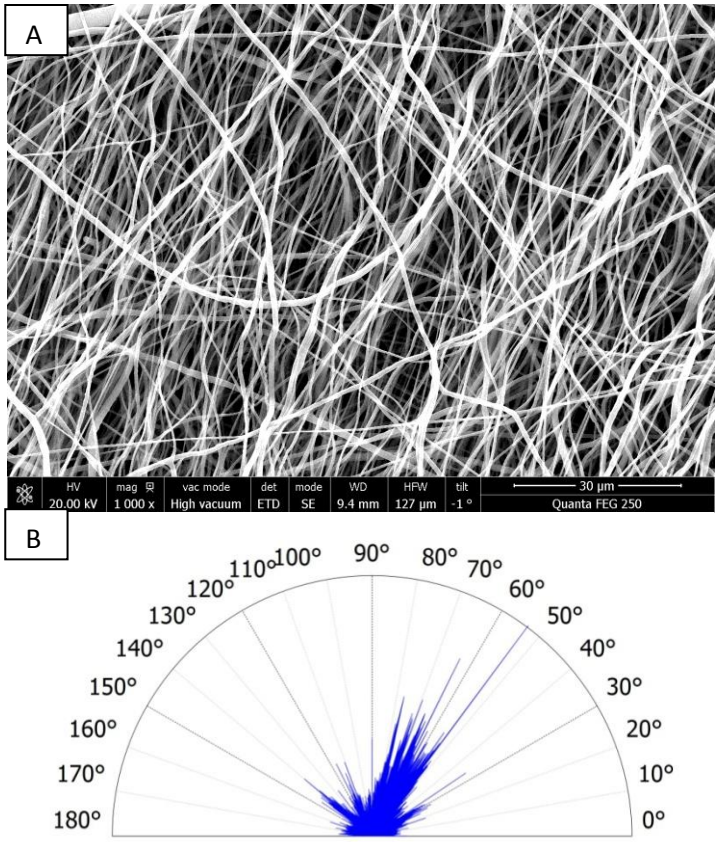

Figure 2. SEM pictograph of a 10-wt % PCL scaffold **(A)**. Fibre orientation distribution in PCL scaffolds **(B)**.

The scaffolds were then characterised following the uniaxial traction test described in the Materials and Methods section. In order to evaluate potential alteration of the mats in an aqueous solution, the scaffolds were analysed in both dry and wet conditions. Stress/strain profiles were similar, showing a "J" zone, characteristic of the nonlinear mechanical response of a viscoelastic material, in which we were able to identify three different regions; the toe region (<2% strain), heel region (<8% strain) and linear region (<18% strain) **(Fig 3A)**. Both elastic moduli were similar, with 8.05 ± 0.82 MPa for the dry scaffolds and 7.93 ± 2.66 MPa for the wet ones **(Fig 3B).**

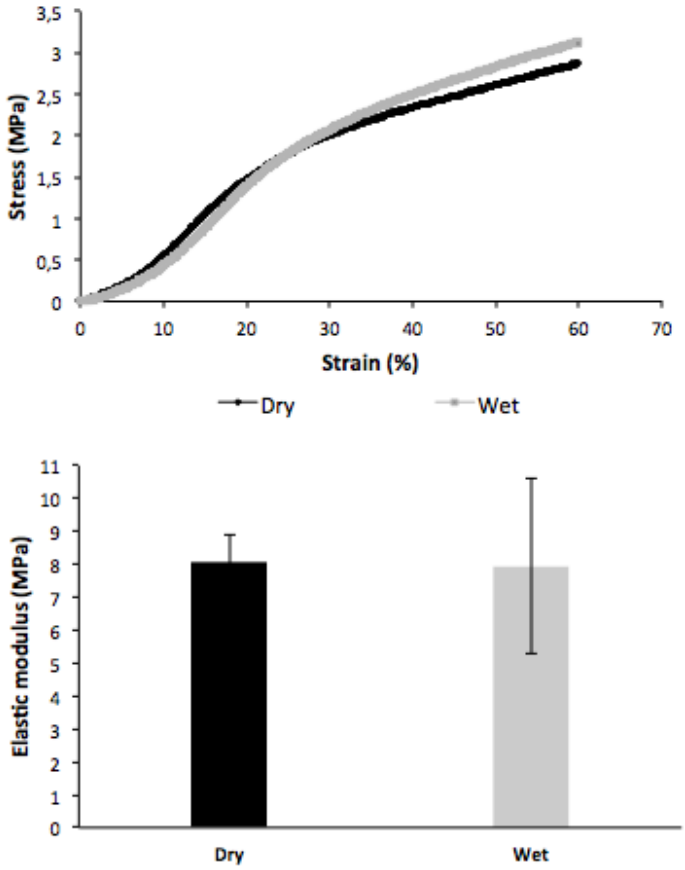

Figure 3. Stress (MPa) vs strain (%) curve for 10-wt % PCL scaffolds in a dry (dark grey) or wet (light grey) state, obtained using the Electroforce 3200 system.

3.2. Biological outcomes and tendon extracellular matrix deposition

The number of cells presented on the constructs was assessed by means of DNA quantification. Cell proliferation was observed in either static or dynamic conditions, with an almost 4-fold increase after 2 weeks **(Fig 4A)**. Dynamic stimulated cell-constructs appeared to have greater proliferation compared to static cultures with $4.1 \pm 1.3 \times 10^6$ vs $2.91 \pm 0.8 \times 10^6$ respectively, after 2 weeks of culture, although the difference was not statistically significant.

In order to determine the effect of the mechanical stretching on ECM neo-synthesis, hydroxyproline was measured **(Fig 4B)**. Hydroxyproline concentration is related to fibrillar collagen and comprises around 13.5% of the collagen [22]. It could be detected in all the culture conditions. After a week of culture, no difference in collagen production was observed between the static or dynamic conditions. After two weeks, a significant increase

in collagen synthesis under dynamic stretching was noted, with 18.8 ± 2.6 µg vs 12.1 ± 1.4 µg of hydroxyproline for the static culture. Mechanical stimulation thus induced elevated collagen content in the scaffold, compared to the static culture, most probably in relation to cell numbers.

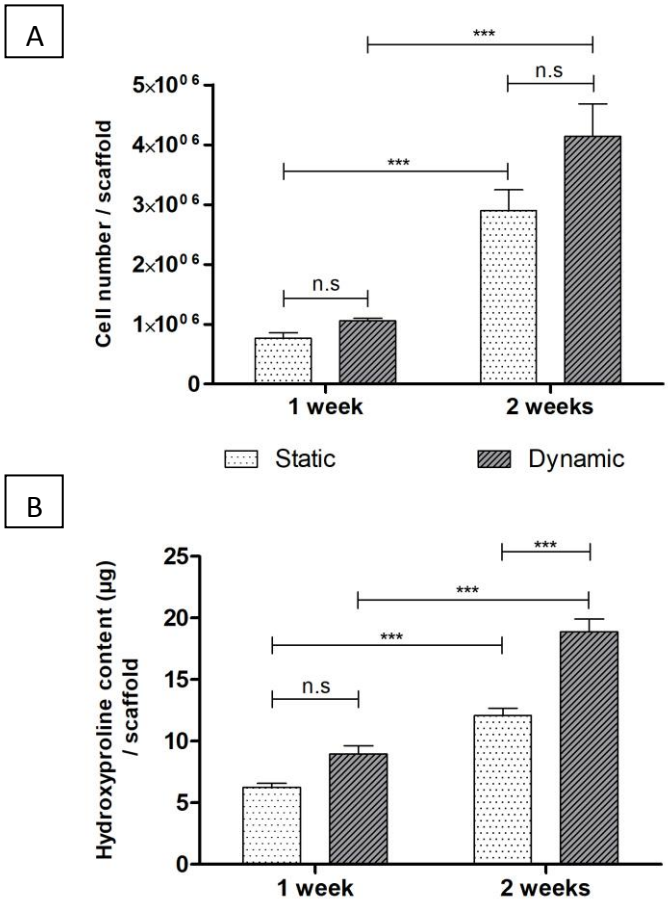

Figure 4. Cell proliferation **(A)** and hydroxyproline synthesis **(B)** over time, at 1 and 2 weeks of static and dynamic culture performed with the T6 CellScale. Hydroxyproline concentration was related to collagen content. (n = 6) (*** are indicated for p <0.001)

To better understand cell organisation, fluorostaining of the actin cytoskeleton was performed **(Fig 5)**. Cells cultured in the absence of mechanical stimulation presented a random morphology on the scaffold. This behaviour did not evolve with culture time, with the same observations at 1 or 2 weeks **(Fig 5A-D).** On the contrary, when submitted to mechanical stimulation, cells presented an elongated shape and appeared aligned with the

stretching direction. This effect seemed more pronounced after two weeks of stimulation, with thinner elongated cells at the surface of the material **(Fig 5D).**

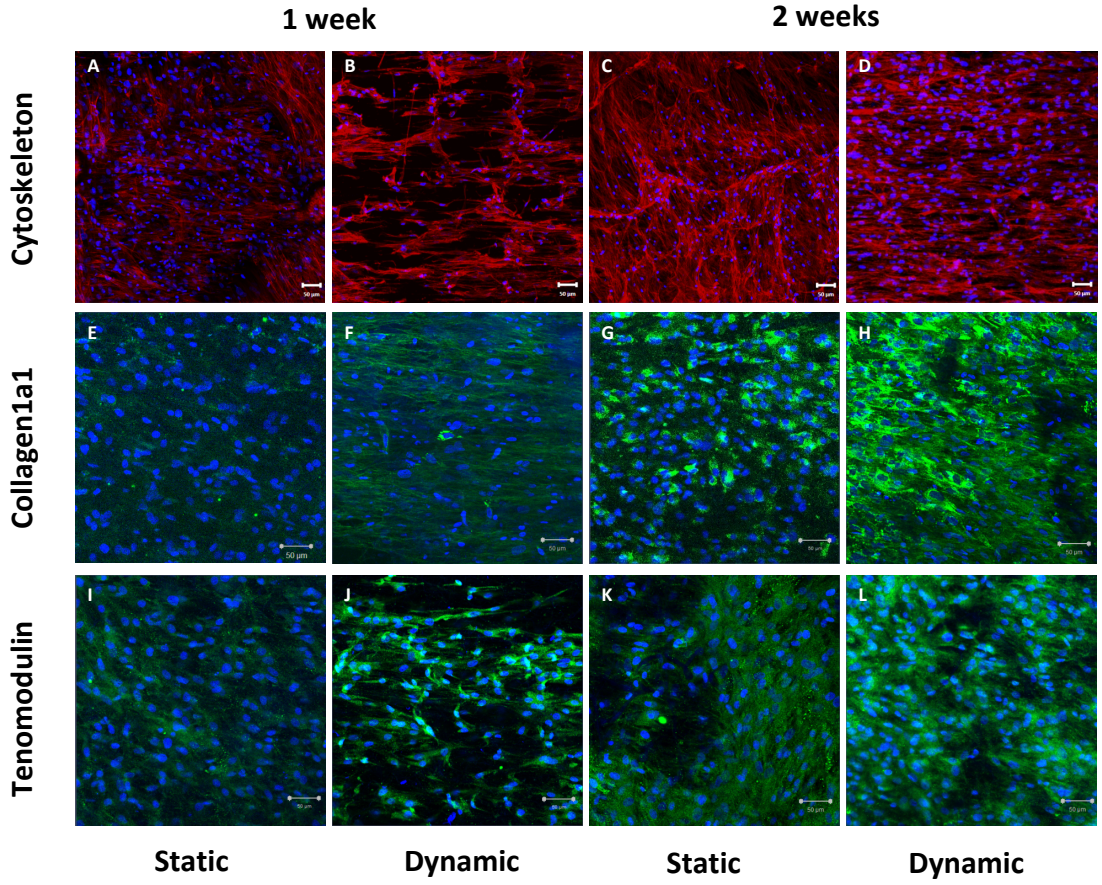

Figure 5. Fluorescence staining of the actin cytoskeleton (red) **(A-D)**, type-1 collagen (green) **(E-H)** and tenomodulin (green) **(I-L)**, of rat BMSCs cultured in static and dynamic conditions for 1 or 2 weeks with MechanoCulture T6. Cell nuclei were stained blue as a counter-stain. Scale bar of 50µm.

To determine the possible differentiation of BMSCs towards tendon lineage under both static and dynamic culture conditions, immunofluorescence staining of type 1 collagen, the main constituent of tendon ECM, and tenomodulin, a tendon specific marker, was performed at different time points**.** Type-1 collagen was found in both conditions at 1 or 2 weeks of culture **(Fig 5E-H)**. After 1 week of culture, type-1 collagen structures were aligned with the stretching under dynamic conditions **(Fig 5F)**, while in static culture they were present in a random manner **(Fig 5E).** After 2 weeks of culture, the same trend was confirmed. Collagen fibres seemed to be more abundant compared with the first week of culture **(Fig 5G, H)**. While there were some clusters of aligned collagen on the static culture

(Fig 5G), under the effect of mechanical stimulation, the collagen was highly organised, with collagen fibres aligned towards the stretching axis.

Immunoflorescence staining revealed the presence of tenomodulin on both culture conditions. In the same manner as collagen fibres, an alignment was observed when the cell-constructs where mechanically stretched **(Fig 5 I-L)**. After one week of culture, tenomodulin appeared to be clearly aligned under dynamic conditions **(Fig 5J)** compared to the static culture **(Fig 5I)**. This effect was more difficult to visualise after two weeks due to the total distribution of tenomodulin and the high cell density **(Fig 5K, L)**.

3.3. Mechanical stimulation and biomechanical evaluation of cell constructs

The Biodynamic device Bose Biodynamic 5100 makes it possible to apply defined cyclic (sinusoidal) strain to the cell-seeded or empty scaffolds, and to concomitantly record the resulting stress. After 2 days of static culture, the cell-construct or the control scaffolds were fixed inside the bioreactor chamber and the mechanical test was launched. Both signal force and displacement were recorded over time and found to be smooth, without any background noise, making it possible to plot the stress/strain curves **(Fig 6B)**. We could thus calculate the elastic modulus by plotting the slope of the stress vs strain curve, and the relative dissipation energy by calculating the surface area between the curves, along with the damping factor **(Fig 6B).** All the relevant parameters were extracted following the equations described previously and presented in **Fig 7**.

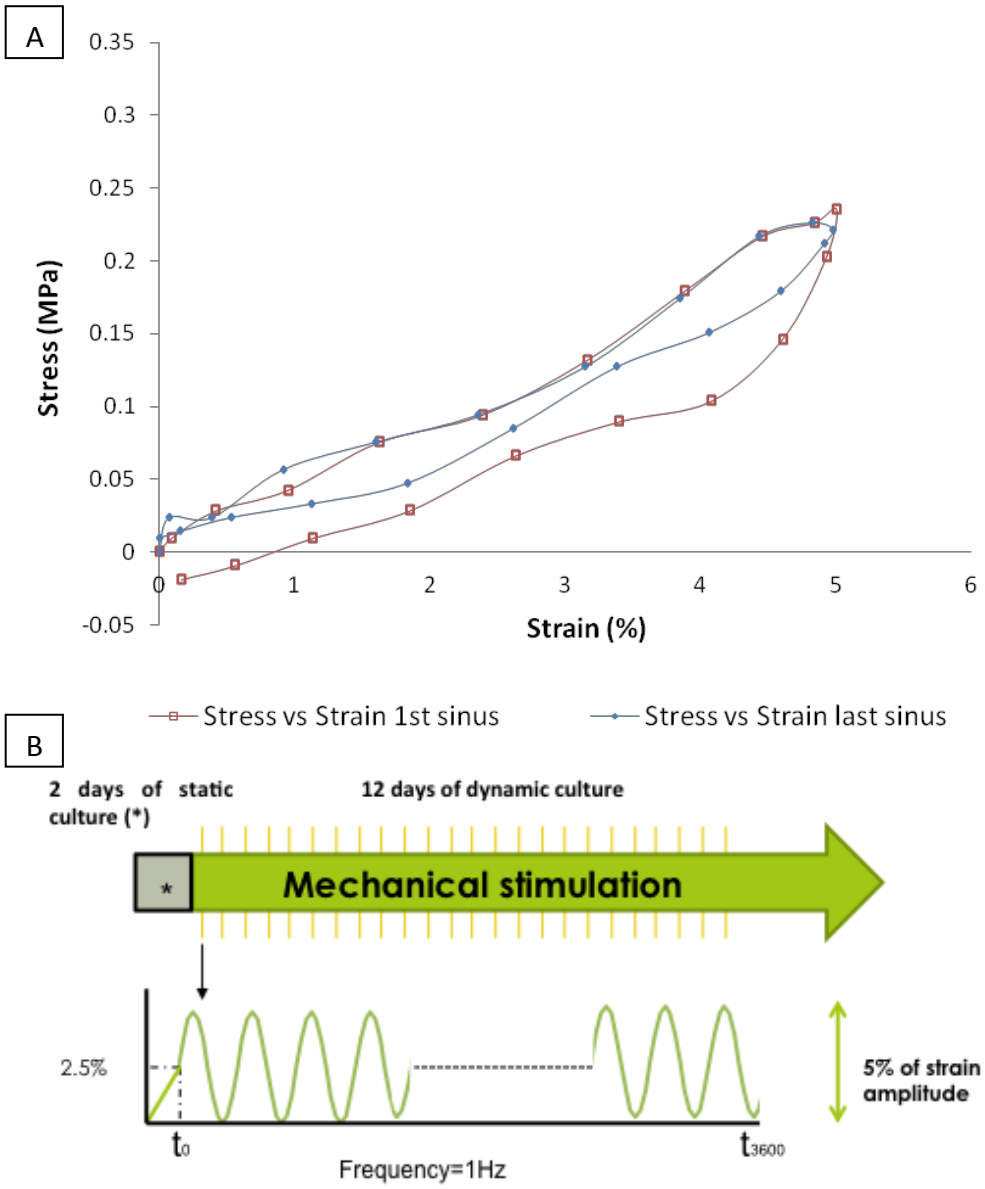

Figure 6. Design of the dynamic culture process during 12 days of stimulation **(A)**. Representative stress vs strain curve **(B)** of the first sinus from the first cycle and the last sinus from the last cycle for cell-constructs subjected to dynamic culture conditions.

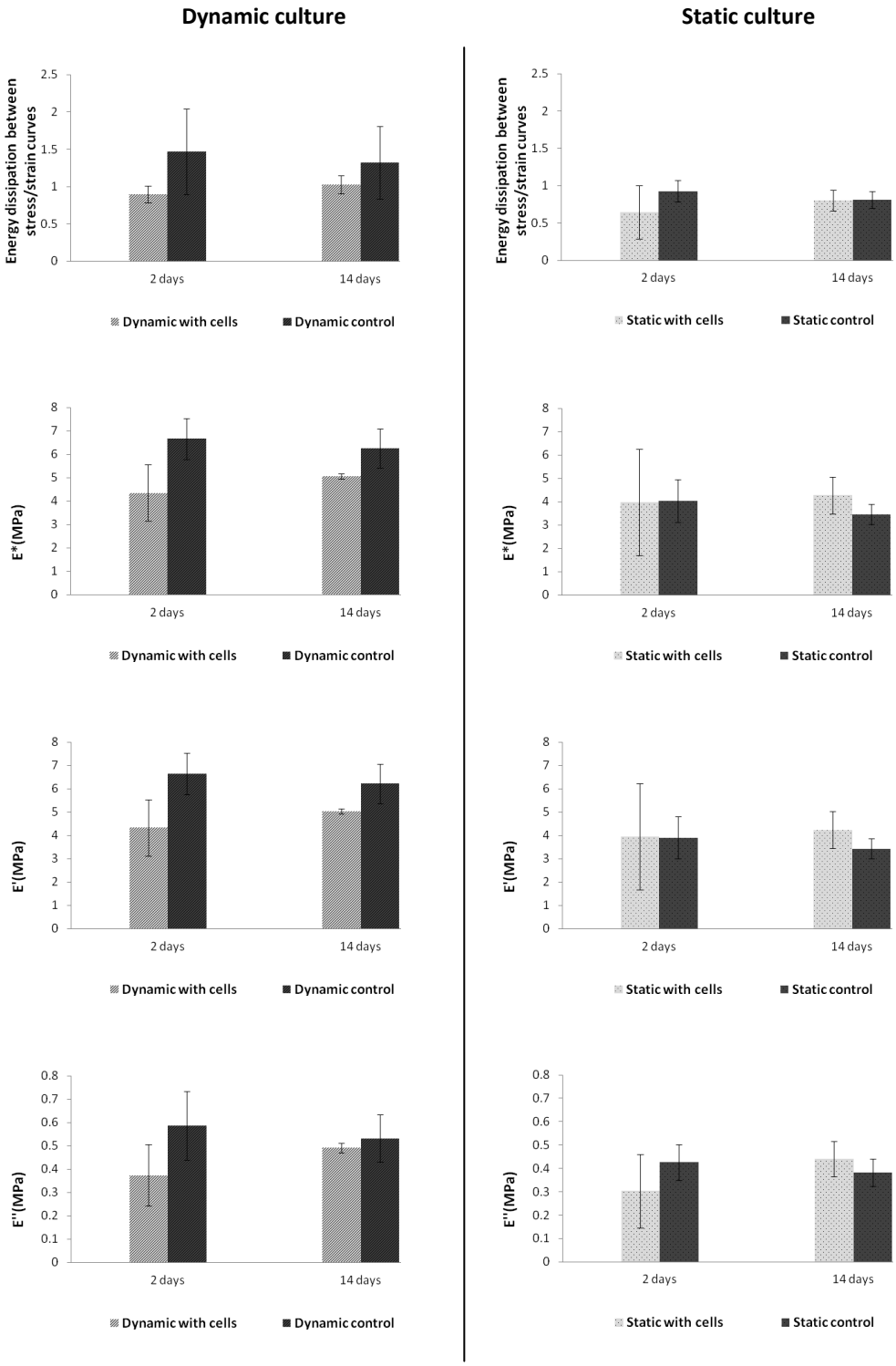

Figure 7. Energy dissipation values, E*, E' and E'' for both dynamic **(left column)** and static **(right column)** conditions cultured with or without cells for both days 2 and 14. Tests were performed in the Bose BioDynamic 5100. Bar plots represent the arithmetic average for each value from 1200 to 3600 sinuses (n=3). There was no statistical difference between the conditions.

Initially (i.e. on day 2), in terms of viscous (tan □, dissipated energy and E´´) and elastic (E´) properties, along with the complex modulus (E*), no significant differences were found between the different parameters for the different culture conditions with or without cells. For tan □, similar values were found for each condition. For the dissipated energy (hysteresis), cell-constructs seemed to present lower values than controls, with 0.64 ± 0.35 vs 0.92 ± 0.14 in static conditions and 0.90 ± 0.11 vs 1.47 ± 0.57 in dynamic ones **(Fig 7)**. For E'', another parameter related to viscosity, the same trend was found, with lower values for cell-constructs (0.30 ± 0.16MPa & 0.37 ± 0.13MPa) in both static and dynamic conditions, compared to controls (0.42 ± 0.07MPa & 0.59 ± 0.14MPa). In terms of elastic properties, the storage modulus (E') appeared higher for the dynamic control with 6.63 ± 0.89 MPa. E* followed the same trends as E', with the highest value found for dynamic control (6.68 ± 0.87 MPa).

After 14 days of culture, the results showed a slight increase in tan □, dissipated energy and E" for cell-constructs, both static and dynamically cultured **(Fig 7**), compared to both static and dynamic controls. For E' and E*, the same trend was found after 14 days of culture, with values for statically cultured cell-constructs of 4.24 ± 0.78 MPa and 0.44 ± 0.08MPa respectively and 5.04 ±0.11 MPa and 0.49 ± 0.02MPa for cell-constructs under dynamic stimulation.

To better determine the effects of mechanical stimulation and cell culture on different groups, we decided to analyse the variation (V%) in the mechanical parameters (P) between the first cycle of day 2 (i.e. the first day of mechanical stimulation) and the last cycle of day 14 (i.e. the last day of culture) **(Fig 8)**. $V\% = 100*(P_{d14} - P_{d2})/ P_{d2}$.

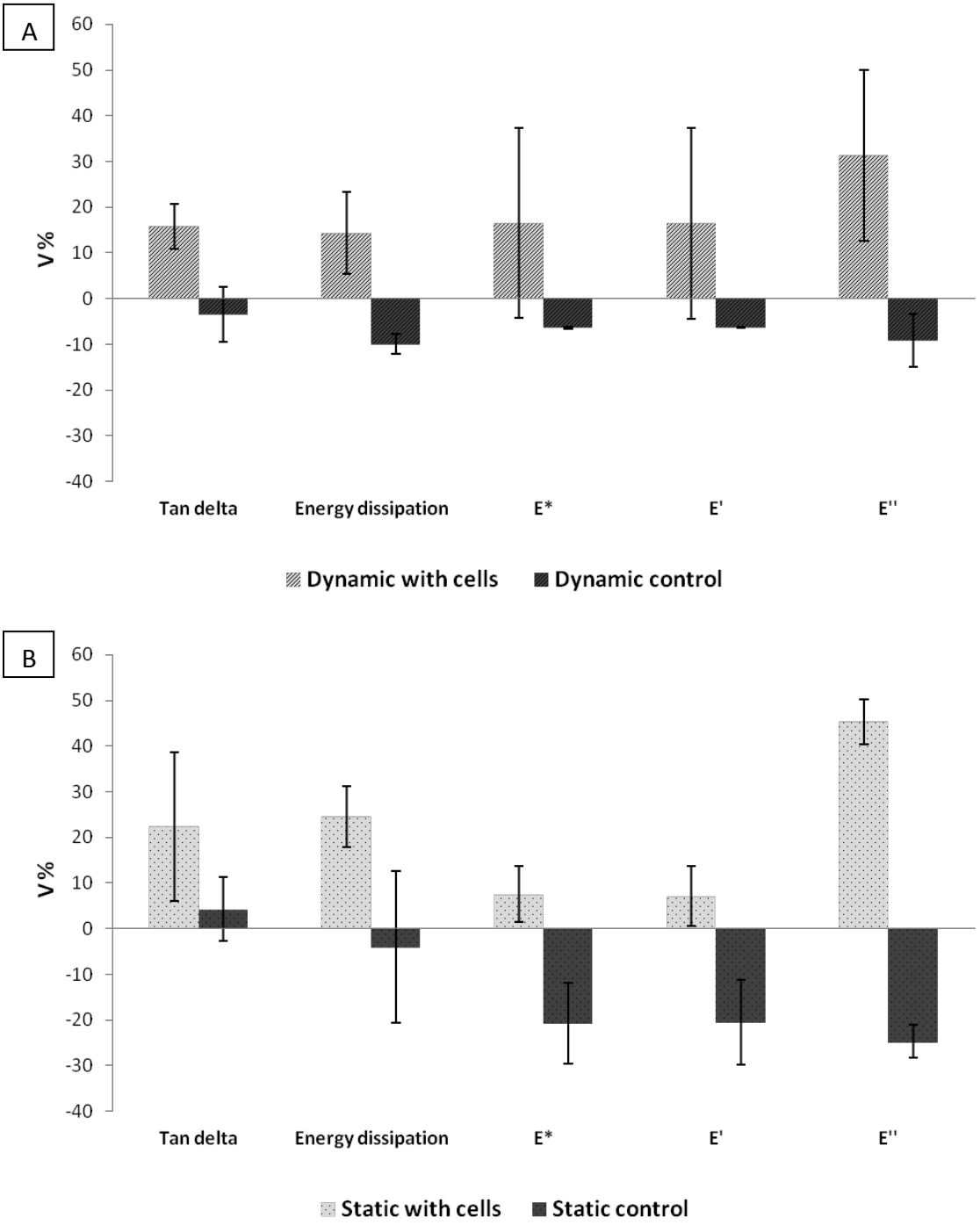

Figure 8. Evolution in the mechanical properties of the scaffolds under both dynamic **(A)** and static **(B)** conditions. These percentages were expressed in terms of variation (V%). V% resulted from the following equation: ((Last cycle - First cycle) / (First cycle))*100.

In the absence of cells, all mechanical parameters presented lower percentages than those obtained in cell-constructs. Tan δ remained almost constant for the static controls (4 ± 7%) and decreased for dynamic ones (-3 ± 6%). For dissipated energy, controls presented a

decrease of -4 ± 17% and -10 ± 2% for static and dynamic conditions respectively. E'' presented the same trend as dissipated energy, with the highest decrease obtained for static conditions (-25 ± 4) compared to dynamic ones (-9 ± 6%). The elastic parameter (E') appeared to decrease particularly for the static control (-20 ± 9%), compared to a slight reduction for the dynamic control (-6 ± 0.1%). E* followed the same trends as E', with the highest decrease found with the static control with -20 ± 9% vs -6 ± 0.2% for the dynamic control.

In the presence of cells, Tan δ seemed to increase particularly in both static and dynamic cultures, with an enhancement of 22 ± 16% and 16 ± 5% respectively. Dissipated energy presented a similar trend with enhancement of 25 ± 7% and 14 ± 9% for static and dynamic culture of cell-constructs, respectively. In terms of E'', cell-constructs presented an increase of 45 ± 5% for static and 31 ± 19% for dynamically-cultured cell-constructs. For E', dynamically-cultured cell-constructs presented the highest increase, with 16 ± 20%, while for static cultures a slight increase of 7 ± 6% was found. Regarding E*, the same trends appeared as for E', with the highest increase for dynamic conditions (16 ± 20%).

Static control appeared to have the lowest values for E', E" and E*, followed by dynamic control. On the other hand, both cell-constructs (dynamic or static cultured) presented the highest enhancement of mechanical properties over time, with higher viscosity for static conditions and higher elasticity for dynamic ones.

4. Discussion

The aims of this study were: i) to investigate the role of mechanical stimulation on BMSC differentiation towards tendon lineage when cultured on adapted scaffolds; ii) to understand whether or not there is any correlation between the changes on the mechanical properties of the biohybrid scaffold and the activity of the seeded BMSCs, in association with the production and arrangement of the newly-formed ECM produced by cells. To the best of our knowledge, the second point, which effectively depends on the first one, has not yet been investigated.

Our first goal was thus to develop a biomaterial suitable for this approach. Electrospinning has been widely used in the development of materials mimicking the fibrous nature of the tendon extracellular matrix [23]. While our PCL scaffold presented an elastic modulus of 8.05

± 0.82MPa **(Fig 3)**, which is still a long way from native tendon [24], the stress-strain curve revealed three regions similar to those found in tendons [4]. Taking into account this stress-strain response, and comparing them with the mechanical behaviour of tendon, we decided to apply a cyclic sinusoidal strain of 5% (0-5%) corresponding to the heel region of both tendon and our electrospun scaffold. Within this region, tendon collagen fibres began to organise and stretch, and the stiffness began to increase [25]. This was intended to calculate the viscoelastic behaviour of our cell-constructs when submitted to cyclic stretching with repeated stretching cycles and strain rates within a low range. This type of strain range represents a more physiological testing method, simulating physiological activities for tendons [26]. For this study, then, repeated sinus strain with a strain rate of 0-5% at 1Hz was used not only as mechanical stimulation but also as mechanical evaluation of the cell-constructs.

After one week of culture, there was no difference in terms of proliferation between static and dynamic conditions **(Fig 4A)**. After two weeks, the number of cells was found to have tripled for the static culture and even quadrupled for cells submitted to dynamic stretching. We can thus conclude that the mechanical stimulation enhanced the proliferative ability of BMSCs, inducing an increase in cell proliferation in response to mechanical load. This result is consistent with other experiments conducted with BMSCs, where more cells were found after 2 weeks of culture compared to shorter culture times under 5% of stretching [27]. Other studies have shown similar results with fibroblasts [28] and TDSCs [29]. While an increase in cell proliferation is found as a response to mechanical stimulation, the mechanisms involved in this mechano-response still need to be clarified [30].

When stimulated, BMSCs presented an elongated morphology aligned with the stretching direction **(Fig 5B,D)**, while cells cultured under static conditions were randomly organised on the scaffold **(Fig 5A,C)**. Similar behaviour was found in another study that analysed the impact of mechanical stimulation on cell alignment when cultured on randomly-oriented scaffolds in the same range of nanofiber size [31].

Regarding collagen synthesis, the cell-constructs showed continuous production over time, with more collagen found after 2 weeks of culture for each condition **(Fig 4B)**. After two

weeks of culture, more collagen was found on cell-constructs subjected to mechanical stretching, in agreement with several other studies [32–34]. This effect has been shown consistently in in vivo studies carried out on tendons where an increase in collagen synthesis was observed as a part of the tendon adaptation response to continuous mechanical loading [35].

Analysis of the ECM produced by cells in both static and dynamic cultures was also performed by immunofluorescence staining of type I collagen and tenomodulin **(Fig 5)**. Collagen I is the most abundant collagen in tendons, and tenomodulin is a late tendon differentiation marker, and a key glycoprotein for the mature state of tendons [36,37]. Both were more abundant under mechanical stimulation when compared to static culture samples. Furthermore, they appeared to be arranged in the stretching direction. Taken together, these data with cell alignment achieved in dynamic conditions, revealed a tendon-like phenotype of BMSCs under dynamic culture conditions, similar to native tendon arrangement [38].

Native tendon is a viscoelastic material, combining viscous liquid-like, and solid-like behaviour. While the notion of viscoelasticity includes time dependency, meaning that the mechanical response depends on the deformation rate (ε), tendon tissue engineered constructs tend to be characterised by quasi-static mechanical tests at ranges of strain that do not reproduce physiological conditions [26,39]. In this study, we decided to follow the cell-constructs' mechanical properties with a set of relevant parameters (tan δ, relative dissipation energy, E*, E' and E'') throughout the entire dynamic stimulation. Our experiment, generating 5% of strain at 1Hz, was intended as a continuous dynamic tension-compression test, and it was monitored continuously throughout the culture period. As we found that during the first 1200 stretching cycles the mechanical behaviour was not stable (Annexed figure), we decided to analyse and represent the V% resulting from 1200 to 3600 sinus where a neat loop was observed, similar to the mechanical behaviour observed in tendons [40]. Unexpectedly, our results showed different initial values between the conditions **(Fig 7)**, whereas the stimulation had not yet started. The presence of such wide variability led us to consider an initial disparity in terms of mechanical properties between the scaffolds tested in each group. When mechanical tests were carried out in the linearity

domain, this variability remained attenuated **(Fig 3)**, but in the present study, under a regime of low deformation within the non-linearity range, the differences were accentuated. For the controls, our results showed that E' declined over time. This decrease was more pronounced for static (-20%) than for dynamic controls (-6%) **(Fig 8)**. This could be explained as water-induced softening of the polymer. Water absorption effectively leads to a loss of the polymer's mechanical properties, resulting in a slight decrease in its elastic properties. This effect has already been shown on PCL electrospun materials [41]. Dynamic stretching seems to attenuate these effects, probably by reducing the water uptake due to the continuous stretching cycles.

For cell-constructs, our results showed that the presence of cells on the surface of our material made possible the increase in E´ after 14 days of culture **(Fig 8)**. In addition, mechanical stimulation presented the highest increase in E' (16%) compared to static culture (7%). These results may be explained as the result of newly-deposited type I collagen fibres. Type I collagen is effectively an important stress-bearing component of connective tissues. It is secreted by cells and hierarchically assembled into fibrils from a packaging of collagen molecules, embedded in a soft matter formed of water and proteoglycans. This organisation gives the collagen structure enough rigidity to be considered an elastic beam [42]. In addition, the aligned orientation adopted by collagen fibres through the stretching direction could explain the higher E' percentage for dynamically-cultured cell-constructs, as aligned collagen fibres are better suited up to supporting tensile stress [43].

The value of tan δ is an indicator of how efficiently the material absorbs and dissipates energy due to molecular rearrangements and internal friction. When we compared its evolution over time **(Fig 8)**, the controls presented the lowest values. While the static control presented a slight increase of 4%, the dynamic control presented a decrease in tan δ of 3%. This can be explained as a consequence of water uptake. While water absorption decreased for dynamically-stimulated controls as a consequence of continuous dynamic loadings, thus resulting in a reduction in dissipated energy, the static controls remained waterlogged, resulting in an increase in water movement through the scaffold. As a result, a higher tan δ percentage was found.

Cell-constructs, in both static and dynamic cultures, presented an enhanced tan δ of 22% and 16% respectively, compared to cell-free control scaffolds **(Fig 8)**. Because tan δ represents the ratio of viscosity to elasticity, the highest values of tan δ were related to a higher damping factor. In a rabbit Achilles tendon regeneration model, Nagasawa et al. found higher values of tan δ for regenerated tendons after surgery compared to controls [37]. This increase was explained as the result of the neosynthesis of collagen fibres. As this "new" fibre presented a lower amount of mature cross-linking, collagen mobility was increased within the tissue, resulting in more energy dissipation. This may explain the increase in tan □ in our cell-constructs, where cells produced collagen, compared to controls without cells. In addition, the random organisation of collagen fibres for static conditions may explain the greater tan δ percentages.

Hysteresis, here represented as relative dissipation energy, is another viscoelastic parameter on which we focused. It represents the difference between the loading and the unloading curves, or mean energy dissipation [44], and is a cross-validation of tan δ. Greater hysteresis means a more viscous material that dissipated more energy. Hysteresis on tendons depends primarily on water movements through the tissue and the reordering of the collagen fibres that make up the tendon [45]. After two weeks, while both static and dynamic controls presented a decrease of 4% and 10% respectively, the scaffolds where cells were cultured presented an increase in dissipated energy, with 25% and 15% for static and dynamic cultures respectively **(Fig 8)**. The reduced values for controls may be explained as a result of the hydrophobic nature of PCL, which hinders the movement of water molecules through the scaffold, resulting in a loss of energy dissipation. The increase in cell-constructs presented over time **(Fig 8)** may be explained as the gain in water retention caused by the production of an ECM by cells. Interestingly, in a rabbit Achilles tendon model, most of the water molecules were found bundled within the collagen fibres [26]. The same phenomenon can explain the increased values for cell-constructs compared to controls. In addition, the highest values of hysteresis for static cultures may be the result of higher mobility of water through the newly randomly deposited collagen fibres compared to the aligned fibres produced under dynamic loads.

As with tan δ and hysteresis, the loss modulus (E'') also took into account the energy dissipation and confirmed our previous results. As seen before, when initial and last values were compared **(Fig 8)**, the controls without cells presented a reduction in E'' with -25% for static and -9% for dynamic controls. The cell-constructs presented an increased loss modulus over time, with 45% for static and 31% for dynamic cultures. Taken together, these results consistently demonstrated that cell-constructs, either in static or dynamic culture conditions, presented increased viscosity over time, compared to nude biomaterials. Finally, dynamic cultures exhibited a greater increase in the elastic properties of the cell-constructs, with a lesser gain in viscous properties, while the static cultures had a greater influence on the viscous properties, with a lower increase in elasticity. This effect may be explained by the effect of the alignment of the extracellular matrix, particularly the collagen fibres, which align through the tensile axis, resulting in an increase in the elastic properties of the cell-constructs submitted to dynamic culture conditions **(Fig 9)**.

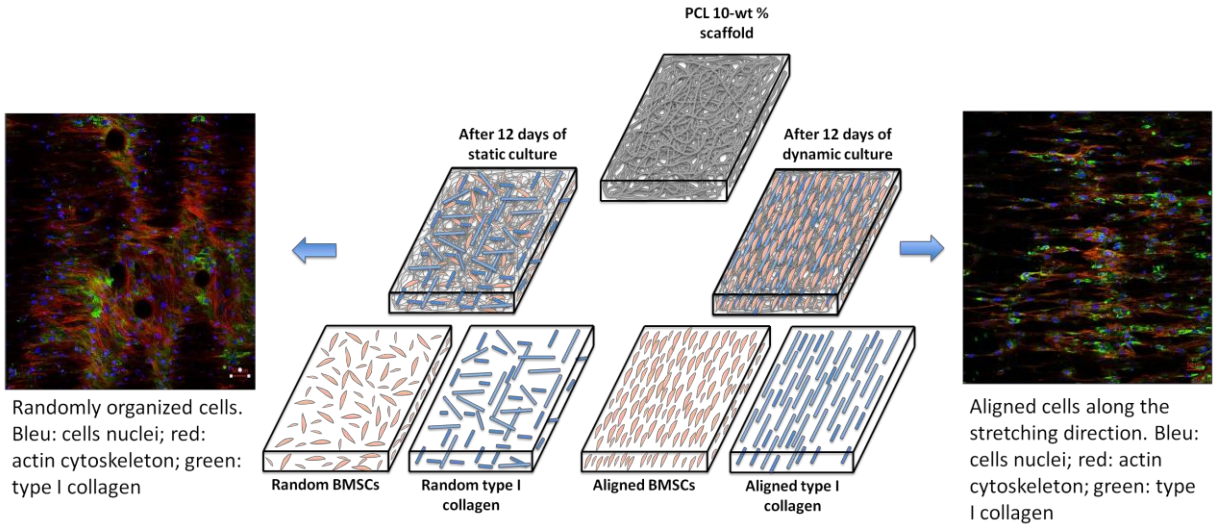

	Tan delta	E*	E'	E''
Static with cells	↑↑	↑	↑	↑↑
Dynamic with cells	↑	↑↑	↑↑	↑

Figure 9. Schematic representation of evolution in the mechanical properties for cellular constructions in the absence or presence of mechanical stimulation.

Conclusion

Correlating both the biological and mechanical results, it seems that mechanical stimulation has a positive effect on cell proliferation and collagen synthesis, which was greater than static culture conditions. Cell and collagen alignment, together with an increase in tenomodulin under dynamic culture conditions, provides a better environment for BMSCs to differentiate towards a tendon-like phenotype. Furthermore, the mechanical properties of the cell-constructs were enhanced over time compared to the control scaffolds without cells. This could be explained as a result of the cellular activity, translated into the production of an ECM. By synthesising collagen, which in tendons and ligaments is responsible for its mechanical properties, the viscous properties (tan delta, dissipated energy and E'') were increased in both the static and dynamic cultures. The random nature of this ECM conferred higher viscous properties for cells cultured under static conditions, explained as an increase in the mobility of collagen and the associated water molecules within these random fibres, while dynamically-stimulated cell-constructs presented aligned collagen fibres towards the direction of the stretching. These aligned fibres could better retain water molecules, resulting in less mobility compared to random ones. In addition, due to the elastic nature of the collagen fibres when they are stretched, the alignment may explain a greater increase in elasticity (E') under mechanical cultivation.

Citations

[1] J.T. Shearn, K.R. Kinneberg, N.A. Dyment, M.T. Galloway, K. Kenter, C. Wylie, D.L. Butler, Tendon tissue engineering: progress, challenges, and translation to the clinic, J. Musculoskelet. Neuronal Interact. 11 (2011) 163–173.

[2] D.L. Butler, N. Juncosa-Melvin, G.P. Boivin, M.T. Galloway, J.T. Shearn, C. Gooch, H. Awad, Functional tissue engineering for tendon repair: A multidisciplinary strategy using mesenchymal stem cells, bioscaffolds, and mechanical stimulation, J. Orthop. Res. Off. Publ. Orthop. Res. Soc. 26 (2008) 1–9. doi:10.1002/jor.20456.

[3] Z. Yin, X. Chen, J.L. Chen, W.L. Shen, T.M. Hieu Nguyen, L. Gao, H.W. Ouyang, The regulation of tendon stem cell differentiation by the alignment of nanofibers, Biomaterials. 31 (2010) 2163–2175. doi:10.1016/j.biomaterials.2009.11.083.

[4] M. Beldjilali-Labro, A. Garcia Garcia, F. Farhat, F. Bedoui, J.-F. Grosset, M. Dufresne, C. Legallais, Biomaterials in Tendon and Skeletal Muscle Tissue Engineering: Current Trends and Challenges, Mater. Basel Switz. 11 (2018). doi:10.3390/ma11071116.

[5] S. Testa, M. Costantini, E. Fornetti, S. Bernardini, M. Trombetta, D. Seliktar, S. Cannata, A. Rainer, C. Gargioli, Combination of biochemical and mechanical cues for tendon tissue engineering, J. Cell. Mol. Med. 21 (2017) 2711–2719. doi:10.1111/jcmm.13186.
[6] G. Yang, B.B. Rothrauff, H. Lin, S. Yu, R.S. Tuan, Tendon-Derived Extracellular Matrix Enhances Transforming Growth Factor-β3-Induced Tenogenic Differentiation of Human Adipose-Derived Stem Cells, Tissue Eng. Part A. 23 (2017) 166–176. doi:10.1089/ten.tea.2015.0498.
[7] A.P. Kishan, E.M. Cosgriff-Hernandez, Recent advancements in electrospinning design for tissue engineering applications: A review, J. Biomed. Mater. Res. A. 105 (2017) 2892–2905. doi:10.1002/jbm.a.36124.
[8] N.M. Lee, C. Erisken, T. Iskratsch, M. Sheetz, W.N. Levine, H.H. Lu, Polymer fiber-based models of connective tissue repair and healing, Biomaterials. 112 (2017) 303–312. doi:10.1016/j.biomaterials.2016.10.013.
[9] N. Maffulli, U.G. Longo, M. Loppini, F. Spiezia, V. Denaro, New options in the management of tendinopathy, Open Access J. Sports Med. 1 (2010) 29. https://www.ncbi.nlm.nih.gov/pmc/articles/PMC3781852/ (accessed March 5, 2019).
[10] S.P. Magnusson, H. Langberg, M. Kjaer, The pathogenesis of tendinopathy: balancing the response to loading, Nat. Rev. Rheumatol. 6 (2010) 262–268. doi:10.1038/nrrheum.2010.43.
[11] T. Andersson, P. Eliasson, M. Hammerman, O. Sandberg, P. Aspenberg, Low-level mechanical stimulation is sufficient to improve tendon healing in rats, J. Appl. Physiol. 113 (2012) 1398–1402. doi:10.1152/japplphysiol.00491.2012.
[12] P. Eliasson, T. Andersson, P. Aspenberg, Influence of a single loading episode on gene expression in healing rat Achilles tendons, J. Appl. Physiol. Bethesda Md 1985. 112 (2012) 279–288. doi:10.1152/japplphysiol.00858.2011.
[13] J.D. Humphrey, E.R. Dufresne, M.A. Schwartz, Mechanotransduction and extracellular matrix homeostasis, Nat. Rev. Mol. Cell Biol. 15 (2014) 802–812. doi:10.1038/nrm3896.
[14] J. Lee, V. Guarino, A. Gloria, L. Ambrosio, G. Tae, Y.H. Kim, Y. Jung, S.-H. Kim, S.H. Kim, Regeneration of Achilles' tendon: the role of dynamic stimulation for enhanced cell proliferation and mechanical properties, J. Biomater. Sci. Polym. Ed. 21 (2010) 1173–1190. doi:10.1163/092050609X12471222313524.
[15] B. Engebretson, Z.R. Mussett, V.I. Sikavitsas, Tenocytic extract and mechanical stimulation in a tissue-engineered tendon construct increases cellular proliferation and ECM deposition, Biotechnol. J. 12 (2017). doi:10.1002/biot.201600595.
[16] B. Engebretson, Z.R. Mussett, V.I. Sikavitsas, The effects of varying frequency and duration of mechanical stimulation on a tissue-engineered tendon construct, Connect. Tissue Res. 59 (2018) 167–177. doi:10.1080/03008207.2017.1324431.
[17] X. Li, Y. Zhang, G. Qi, Evaluation of isolation methods and culture conditions for rat bone marrow mesenchymal stem cells, Cytotechnology. 65 (2013) 323–334. doi:10.1007/s10616-012-9497-3.
[18] S.K. Maiti, Mesenchymal Stem Cells Derived from Rat Bone Marrow (rBM MSC): Techniques for Isolation, Expansion and Differentiation, J. Stem Cell Res. Ther. 3 (2017). doi:10.15406/jsrt.2017.03.00101.
[19] M.R. Neidert, E.S. Lee, T.R. Oegema, R.T. Tranquillo, Enhanced fibrin remodeling in vitro with TGF-beta1, insulin and plasmin for improved tissue-equivalents, Biomaterials. 23 (2002) 3717–3731.

[20] J.E. Marturano, J.D. Arena, Z.A. Schiller, I. Georgakoudi, C.K. Kuo, Characterization of mechanical and biochemical properties of developing embryonic tendon, Proc. Natl. Acad. Sci. 110 (2013) 6370–6375. doi:10.1073/pnas.1300135110.
[21] A. Gholipour Kanani, S.H. Bahrami, Effect of Changing Solvents on Poly(□-Caprolactone) Nanofibrous Webs Morphology, J. Nanomater. (2011). doi:10.1155/2011/724153.
[22] I. Stoilov, B.C. Starcher, R.P. Mecham, T.J. Broekelmann, Chapter 7 - Measurement of elastin, collagen, and total protein levels in tissues, in: R.P. Mecham (Ed.), Methods Cell Biol., Academic Press, 2018: pp. 133–146. doi:10.1016/bs.mcb.2017.08.008.
[23] N. Bölgen, 10 - Electrospun materials for bone and tendon/ligament tissue engineering, in: T. Uyar, E. Kny (Eds.), Electrospun Mater. Tissue Eng. Biomed. Appl., Woodhead Publishing, 2017: pp. 233–260. doi:10.1016/B978-0-08-101022-8.00004-1.
[24] R.B. Martin, D.B. Burr, N.A. Sharkey, D.P. Fyhrie, Mechanical Properties of Ligament and Tendon, in: R.B. Martin, D.B. Burr, N.A. Sharkey, D.P. Fyhrie (Eds.), Skelet. Tissue Mech., Springer New York, New York, NY, 2015: pp. 175–225. doi:10.1007/978-1-4939-3002-9_4.
[25] C.T. Thorpe, H.L. Birch, P.D. Clegg, H.R.C. Screen, Chapter 1 - Tendon Physiology and Mechanical Behavior: Structure–Function Relationships, in: M.E. Gomes, R.L. Reis, M.T. Rodrigues (Eds.), Tendon Regen., Academic Press, Boston, 2015: pp. 3–39. doi:10.1016/B978-0-12-801590-2.00001-6.
[26] K. Ikoma, M. Kido, M. Nagae, T. Ikeda, T. Shirai, K. Ueshima, Y. Arai, R. Oda, H. Fujiwara, T. Kubo, Effects of stress-shielding on the dynamic viscoelasticity and ordering of the collagen fibers in rabbit Achilles tendon, J. Orthop. Res. Off. Publ. Orthop. Res. Soc. 31 (2013) 1708–1712. doi:10.1002/jor.22424.
[27] K.-M. Choi, Y.-K. Seo, H.-H. Yoon, K.-Y. Song, S.-Y. Kwon, H.-S. Lee, J.-K. Park, Effects of mechanical stimulation on the proliferation of bone marrow-derived human mesenchymal stem cells, Biotechnol. Bioprocess Eng. 12 (2007) 601–609. doi:10.1007/BF02931075.
[28] R. Kuang, Z. Wang, Q. Xu, S. Liu, W. Zhang, Influence of mechanical stimulation on human dermal fibroblasts derived from different body sites, Int. J. Clin. Exp. Med. 8 (2015) 7641–7647. https://www.ncbi.nlm.nih.gov/pmc/articles/PMC4509256/ (accessed March 7, 2019).
[29] Y. Xu, S. Dong, Q. Zhou, X. Mo, L. Song, T. Hou, J. Wu, S. Li, Y. Li, P. Li, Y. Gan, J. Xu, The effect of mechanical stimulation on the maturation of TDSCs-poly(L-lactide-co-e-caprolactone)/collagen scaffold constructs for tendon tissue engineering, Biomaterials. 35 (2014) 2760–2772. doi:10.1016/j.biomaterials.2013.12.042.
[30] Y.-K. Wang, C.S. Chen, Cell adhesion and mechanical stimulation in the regulation of mesenchymal stem cell differentiation, J. Cell. Mol. Med. 17 (2013) 823–832. doi:10.1111/jcmm.12061.
[31] S.D. Subramony, B.R. Dargis, M. Castillo, E.U. Azeloglu, M.S. Tracey, A. Su, H.H. Lu, The guidance of stem cell differentiation by substrate alignment and mechanical stimulation, Biomaterials. 34 (2013) 1942–1953. doi:10.1016/j.biomaterials.2012.11.012.
[32] H.R.C. Screen, J.C. Shelton, D.L. Bader, D.A. Lee, Cyclic tensile strain upregulates collagen synthesis in isolated tendon fascicles, Biochem. Biophys. Res. Commun. 336 (2005) 424–429. doi:10.1016/j.bbrc.2005.08.102.

[33] E. Huisman, A. Lu, R.G. McCormack, A. Scott, Enhanced collagen type I synthesis by human tenocytes subjected to periodic in vitro mechanical stimulation, BMC Musculoskelet. Disord. 15 (2014) 386. doi:10.1186/1471-2474-15-386.
[34] S. Wu, Y. Wang, P.N. Streubel, B. Duan, Living nanofiber yarn-based woven biotextiles for tendon tissue engineering using cell tri-culture and mechanical stimulation, Acta Biomater. 62 (2017) 102–115. doi:10.1016/j.actbio.2017.08.043.
[35] K.M. Heinemeier, M. Kjaer, In vivo investigation of tendon responses to mechanical loading, J. Musculoskelet. Neuronal Interact. 11 (2011) 115–123.
[36] S. Dex, P. Alberton, L. Willkomm, T. Söllradl, S. Bago, S. Milz, M. Shakibaei, A. Ignatius, W. Bloch, H. Clausen-Schaumann, C. Shukunami, M. Schieker, D. Docheva, Tenomodulin is Required for Tendon Endurance Running and Collagen I Fibril Adaptation to Mechanical Load, EBioMedicine. 20 (2017) 240–254. doi:10.1016/j.ebiom.2017.05.003.
[37] K. Nagasawa, M. Noguchi, K. Ikoma, T. Kubo, Static and dynamic biomechanical properties of the regenerating rabbit Achilles tendon, Clin. Biomech. Bristol Avon. 23 (2008) 832–838. doi:10.1016/j.clinbiomech.2008.02.002.
[38] D.M. Doroski, K.S. Brink, J.S. Temenoff, Techniques for biological characterization of tissue-engineered tendon and ligament, Biomaterials. 28 (2007) 187–202. doi:10.1016/j.biomaterials.2006.08.040.
[39] Tendon Physiology and Mechanical Behavior: Structure–Function Relationships - ScienceDirect, (n.d.). https://www.sciencedirect.com/science/article/pii/B9780128015902000016 (accessed February 7, 2019).
[40] K. Kubo, H. Kanehisa, T. Fukunaga, Effect of stretching training on the viscoelastic properties of human tendon structures in vivo, J. Appl. Physiol. 92 (2002) 595–601. doi:10.1152/japplphysiol.00658.2001.
[41] R.A. Sabu Thomas, In Vitro Degradation of Electrospun Polycaprolactone Membranes in Simulated Body Fluid, ResearchGate. (n.d.). https://www.researchgate.net/publication/286926828_In_Vitro_Degradation_of_Electrospun_Polycaprolactone_Membranes_in_Simulated_Body_Fluid (accessed March 14, 2019).
[42] A.J. Licup, S. Münster, A. Sharma, M. Sheinman, L.M. Jawerth, B. Fabry, D.A. Weitz, F.C. MacKintosh, Stress controls the mechanics of collagen networks, Proc. Natl. Acad. Sci. U. S. A. 112 (2015) 9573–9578. doi:10.1073/pnas.1504258112.
[43] R.B. Martin, J. Ishida, The relative effects of collagen fiber orientation, porosity, density, and mineralization on bone strength, J. Biomech. 22 (1989) 419–426. doi:10.1016/0021-9290(89)90202-9.
[44] T. Finni, J. Peltonen, L. Stenroth, N.J. Cronin, Viewpoint: On the hysteresis in the human Achilles tendon, J. Appl. Physiol. Bethesda Md 1985. 114 (2013) 515–517. doi:10.1152/japplphysiol.01005.2012.
[45] C.T. Thorpe, H.L. Birch, P.D. Clegg, H.R.C. Screen, The role of the non-collagenous matrix in tendon function, Int. J. Exp. Pathol. 94 (2013) 248–259. doi:10.1111/iep.12027.

Annexes

Mechanically stimulated	Yes				No			
Cells	Yes		No		Yes		No	
Length (mm)	40	35*	40	35*	40	35*	40	35*
Width (mm)	12.5	9*	12.5	9*	12.5	9*	12.5	9*
Thickness (mm)	0.12 ± 0.02		0.11 ± 0.03		0.13 ± 0.03		0.1 ± 0.01	

Table 1. Initial scaffold length, width and thickness of the cell-constructs for Bose Biodynamic 5100 and T6 CellScale. * Represents values for scaffolds destined for the T6 CellScale bioreactor.

100*(Last cycle-First cycle)/First cycle	Tan delta	Hysteresis	E*	E'	E''
	%	%	%	%	%
Static with cells	22.38±16.34	24.55±6.64	7.56±6.19	7.14±6.55	45.03±4.83
Static control	4.29±6.95	-3.99±16.59	-20.70±8.87	-20.55±9.38	-24.77±3.63
Dynamic with cells	15.77±4.85	14.37±8.89	16.57±20.84	16.52±20.88	31.28±18.63
Dynamic control	-3.49±6.03	-9.98±2.22	-6.36±0.20	-6.35±0.14	-9.22±5.79

Table 2. Percentage of evolution between the first cycle and the last one, corresponding to day 2 and day 14 of culture. All data were obtained by doing the arithmetic media of all data between each group and an SEM of the percentage between each group.

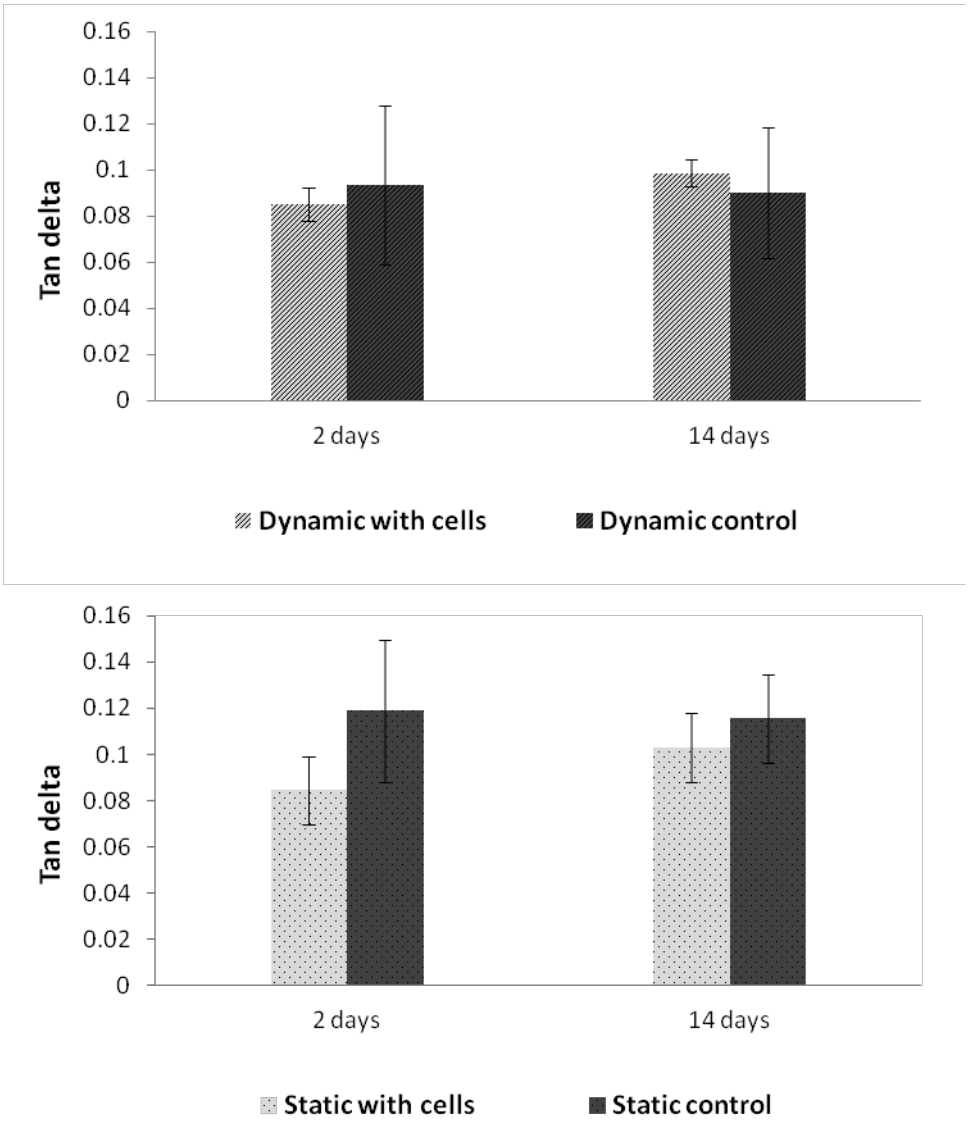

Figure 1. Tan delta values for both dynamic **(A)** and static **(B)** conditions cultured or not with cells for days 2 and 14. Tests were performed in the Bose BioDynamic 5100. Bar plots represent the arithmetic media of both cycles from 1200 to 3600 sinuses.

Chapter VI – Conclusion and Perspectives

Chapter VI: Conclusion and Perspectives

1. Conclusion

The initial goal of this PhD thesis was the design of a biohybrid system recapitulating part of the musculo-skeletal system, i.e. tendon and bone with specific attention on the junction - the enthesis. Our approach focused on the development by tissue engineering of such a biohybrid system taking into account the biological and mechanical properties of each subsystem. To this end, the versatility of electrospinning had been chosen for the achievement of a continuum between each subsystem, as well as future basis for the enlargements towards the total bone-tendon-muscle system, as defined in the challenge supported by the Labex MSST (Maitrise de Systèmes de Systèmes Technologiques) at UTC.

One of the strength of the whole project was to elaborate such biohybrid constructs from the knowledge acquired at BMBI on "native" tissues, thanks to the interaction with researchers from C2MUST team, from bibliographical survey, as well as from discussions with clinicians to understand their expectations. Instead of directly focusing on the interface between reconstructed tissues, we wanted in the present work to ensure that the built-up of the continuum was achievable using electrospinning methods that should be adapted and evaluated for each type of tissue. For clinical perspectives, we also postulated that cell differentiation towards different lineages (here bone and tendon) should be obtained without any differentiation factor (that are specific for each tissue), playing only on cell-materials interactions and mechano-transduction.

First, the development of a material for bone tissue regeneration was achieved using a combination of electrospinning PCL and electrospraying hydroxyapatite, resulting from the collaboration with Dr. G. Schlatter and Dr. A. Hébraud at ICPEES (Strasbourg). Besides its fibrillar and mineral components close to the extracellular bone matrix, the final substitute was shaped into a macroscopic "honeycomb" organization similar to the osteons that form part of the bone. This configuration was designed on purpose to create a cell niche that supports biological activity, based on the structure-function premise, to accentuate the effect on cell differentiation. This end point has been achieved in vitro with C3H10T1/2 cell line and organotypic culture, in collaboration with Dr. Delphine Duprez (IBPS, Paris). In vivo trials were then performed by our collaborators at Institut Faire Faces, Amiens, in the EA 4666 from UPJV (Dr. M Naudot, Dr. S. Le Ricousse). Seeding the honeycomb PCL-HA with

BMSCs 24h pre-implantation allowed to speed up bone reconstruction in a critical size calvarial defect. With promising results, the process can nevertheless be improved, involving the automation of electrospinning and electrospraying steps to reduce the errors of the manipulator, or changes in environmental conditions. While in vitro and in vivo assays have been carried out with animal primary cells, future work must be carried out with humanmesenchymal stem cells whose origins are still questionable.

Then and in parallel, we addressed the question of engineering a tendon structure, based on electrospinning process, considering both biological and mechanical properties of such biohybrid system, with an original perspective: we studied not only the cell response to mechanical solicitations, but also the changes in mechanical properties of the biohybrid constructs due to cell arrangement and extracellular matrix neosynthesis. As there were no literature consensus on the guidelines to drive progenitor cells or stem cells towards tendon lineage in the absence of any differentiation factor, we investigated, for the PCL-based scaffold: (1) the effect of electrospun fibers size and alignment, with some materials prepared by IMP Hannover, (2) the effect of cyclic stretching in dedicated bioreactors (Bose BioDynamic 5100 and MechanoCulture T6). So far, the results obtained are rather promising with BMSCs, and were less successful with our initial progenitor cell line (C3H10T1/2), may be due to its high proliferation and renewal potential. We demonstrated that BMSCs were able to align on random scaffold under cyclic stretching strain, and to produce an extracellular matrix that reinforced the biomaterials structure. To our knowledge, it is the first time that such a biomechanical study was conducted. We therefore develop robust protocols using the above mentioned bioreactor that could be transferred to other materials. We consider thus this study as a success of interdisciplinary approaches involving two laboratories at UTC (BMBI/Roberval) and many collaborators.

This thesis work has therefore made it possible to go through different stages for the development of a continuum between the bone and the tendon, obtaining each subsystem in an isolated manner, with the final objective of a future junction between each of them.

2. Perspectives

Unfortunately, in the time framework, we were not able to achieve the design of the interface between bone and tendon biohybrid structure. This part of the work, based on the proofs, is currently carried out by a post-doc student C.Y. Leon-Valdiviesoat Roberval laboratory. A collector with a special topography should allow us to develop a honeycomb shaped material that evolves into a random material for the tendon. In a short period of time, biological tests will be carried out to evaluate the cell behavior of BMSCs cultured on this material and the incidence of each sub-unit on cell differentiation. Later on, in the framework of the PhD of M. Beldjilali Labro, the muscle part could be added.

These biohybrid systems of systems will not be applied directly to human. They will be nevertheless very helpful to understand what is occurring at the tissue or cell level during embryogenesis, or during healing process, since it will let scientists access to data that are impossible to collect in vivo. These kinds of organoids could be employed to reduce animal trials, being more relevant in case human cells have to be used.

In parallel, future opportunities may arise in the field of tissue engineering for the improvement of the mechanical properties of our biohybrid substitutes, such as 3D (bio) impression or melt-spinning, as well as a cooperation with physiologists to evaluate the training effect on our biohybrid system as a parallel model for the development of an optimal in vivo training method, in which different frequencies or deformations in the physiological range can be used to increase the cellular and mechanical behavior of the biohybrid substitute.

Intern Citations

(1) Baudequin, T. Caractérisation biologique et mécanique d'un subsitut osseux biohybride et développement de scaffolds par électrospinning: vers un pansement vivant pour la reconstruction maxillo-faciale. 297.

(2) Grabowski, P. Physiology of Bone. *Endocr. Dev.* **2009**, *16*, 32–48. https://doi.org/10.1159/000223687.

(3) Young, M. F. Bone Matrix Proteins: Their Function, Regulation, and Relationship to Osteoporosis. *Osteoporos. Int. J. Establ. Result Coop. Eur. Found. Osteoporos. Natl. Osteoporos. Found. USA* **2003**, *14 Suppl 3*, S35-42. https://doi.org/10.1007/s00198-002-1342-7.

(4) Gentili, C.; Cancedda, R. Cartilage and Bone Extracellular Matrix. *Curr. Pharm. Des.* **2009**, *15* (12), 1334–1348.

(5) Buck, D. W.; Dumanian, G. A. Bone Biology and Physiology: Part I. The Fundamentals. *Plast. Reconstr. Surg.* **2012**, *129* (6), 1314–1320. https://doi.org/10.1097/PRS.0b013e31824eca94.

(6) Clarke, B. Normal Bone Anatomy and Physiology. *Clin. J. Am. Soc. Nephrol. CJASN* **2008**, *3 Suppl 3*, S131-139. https://doi.org/10.2215/CJN.04151206.

(7) Hadjidakis, D. J.; Androulakis, I. I. Bone Remodeling. *Ann. N. Y. Acad. Sci.* **2006**, *1092*, 385–396. https://doi.org/10.1196/annals.1365.035.

(8) Oftadeh, R.; Perez-Viloria, M.; Villa-Camacho, J. C.; Vaziri, A.; Nazarian, A. Biomechanics and Mechanobiology of Trabecular Bone: A Review. *J. Biomech. Eng.* **2015**, *137* (1), 0108021–01080215. https://doi.org/10.1115/1.4029176.

(9) Chen, C.; Jin, D.; Liu, Y.; Wehrli, F. W.; Chang, G.; Snyder, P. J.; Regatte, R. R.; Saha, P. K. Trabecular Bone Characterization on the Continuum of Plates and Rods Using in Vivo MR Imaging and Volumetric Topological Analysis. *Phys. Med. Biol.* **2016**, *61* (18), N478–N496. https://doi.org/10.1088/0031-9155/61/18/N478.

(10) Cowin, E., SC; Telega, R., JJ. Bone Mechanics Handbook, 2nd Edition. -. *Appl. Mech. Rev.* **2003**, *56* (4), B61–B63. https://doi.org/10.1115/1.1579463.

(11) Downey, P. A.; Siegel, M. I. Bone Biology and the Clinical Implications for Osteoporosis. *Phys. Ther.* **2006**, *86* (1), 77–91.

(12) Raggatt, L. J.; Partridge, N. C. Cellular and Molecular Mechanisms of Bone Remodeling. *J. Biol. Chem.* **2010**, *285* (33), 25103–25108. https://doi.org/10.1074/jbc.R109.041087.

(13) Garcia Garcia, A.; Hébraud, A.; Duval, J.-L.; Wittmer, C. R.; Gaut, L.; Duprez, D.; Egles, C.; Bedoui, F.; Schlatter, G.; Legallais, C. Poly(ε-Caprolactone)/Hydroxyapatite 3D Honeycomb Scaffolds for a Cellular Microenvironment Adapted to Maxillofacial Bone Reconstruction. *ACS Biomater. Sci. Eng.* **2018**, *4* (9), 3317–3326. https://doi.org/10.1021/acsbiomaterials.8b00521.

(14) Dimitriou, R.; Jones, E.; McGonagle, D.; Giannoudis, P. V. Bone Regeneration: Current Concepts and Future Directions. *BMC Med.* **2011**, *9*, 66. https://doi.org/10.1186/1741-7015-9-66.

(15) Black, C. R. M.; Goriainov, V.; Gibbs, D.; Kanczler, J.; Tare, R. S.; Oreffo, R. O. C. Bone Tissue Engineering. *Curr. Mol. Biol. Rep.* **2015**, *1* (3), 132–140. https://doi.org/10.1007/s40610-015-0022-2.

(16) Shi, R.; Huang, Y.; Ma, C.; Wu, C.; Tian, W. Current Advances for Bone Regeneration Based on Tissue Engineering Strategies. *Front. Med.* **2018**. https://doi.org/10.1007/s11684-018-0629-9.
(17) Shibuya, N.; Jupiter, D. C. Bone Graft Substitute: Allograft and Xenograft. *Clin. Podiatr. Med. Surg.* **2015**, *32* (1), 21–34. https://doi.org/10.1016/j.cpm.2014.09.011.
(18) Fillingham, Y.; Jacobs, J. Bone Grafts and Their Substitutes. *Bone Jt. J.* **2016**, *98-B* (1 Suppl A), 6–9. https://doi.org/10.1302/0301-620X.98B.36350.
(19) Bauer, T. W.; Muschler, G. F. Bone Graft Materials. An Overview of the Basic Science. *Clin. Orthop.* **2000**, No. 371, 10–27.
(20) Pape, H. C.; Evans, A.; Kobbe, P. Autologous Bone Graft: Properties and Techniques. *J. Orthop. Trauma* **2010**, *24 Suppl 1*, S36-40. https://doi.org/10.1097/BOT.0b013e3181cec4a1.
(21) Rogers, G. F.; Greene, A. K. Autogenous Bone Graft: Basic Science and Clinical Implications. *J. Craniofac. Surg.* **2012**, *23* (1), 323–327. https://doi.org/10.1097/SCS.0b013e318241dcba.
(22) Roberts, T. T.; Rosenbaum, A. J. Bone Grafts, Bone Substitutes and Orthobiologics: The Bridge between Basic Science and Clinical Advancements in Fracture Healing. *Organogenesis* **2012**, *8* (4), 114–124. https://doi.org/10.4161/org.23306.
(23) Beaman, F. D.; Bancroft, L. W.; Peterson, J. J.; Kransdorf, M. J. Bone Graft Materials and Synthetic Substitutes. *Radiol. Clin. North Am.* **2006**, *44* (3), 451–461. https://doi.org/10.1016/j.rcl.2006.01.001.
(24) Benefits and Associated Risks of Using Allograft, Autograft and Synthetic Bone Fusion Material for Patients and Service Providers - A Systematic Review. *JBI Database Syst. Rev. Implement. Rep.* **2010**, *8* (8), 1. https://doi.org/10.11124/jbisrir-2010-851.
(25) Laurencin, C.; Khan, Y.; El-Amin, S. F. Bone Graft Substitutes. *Expert Rev. Med. Devices* **2006**, *3* (1), 49–57. https://doi.org/10.1586/17434440.3.1.49.
(26) Liu, Y.; Lim, J.; Teoh, S.-H. Review: Development of Clinically Relevant Scaffolds for Vascularised Bone Tissue Engineering. *Biotechnol. Adv.* **2013**, *31* (5), 688–705. https://doi.org/10.1016/j.biotechadv.2012.10.003.
(27) Mendelson, B. C.; Jacobson, S. R.; Lavoipierre, A. M.; Huggins, R. J. The Fate of Porous Hydroxyapatite Granules Used in Facial Skeletal Augmentation. *Aesthetic Plast. Surg.* **2010**, *34* (4), 455–461. https://doi.org/10.1007/s00266-010-9473-2.
(28) LeGeros, R. Z. Properties of Osteoconductive Biomaterials: Calcium Phosphates. *Clin. Orthop.* **2002**, No. 395, 81–98.
(29) Välimäki, V. V.; Aro, H. T. Molecular Basis for Action of Bioactive Glasses as Bone Graft Substitute. *Scand. J. Surg. SJS Off. Organ Finn. Surg. Soc. Scand. Surg. Soc.* **2006**, *95* (2), 95–102. https://doi.org/10.1177/145749690609500204.
(30) van Gestel, N. A. P.; Geurts, J.; Hulsen, D. J. W.; van Rietbergen, B.; Hofmann, S.; Arts, J. J. Clinical Applications of S53P4 Bioactive Glass in Bone Healing and Osteomyelitic Treatment: A Literature Review. *BioMed Res. Int.* **2015**, *2015*. https://doi.org/10.1155/2015/684826.
(31) Wang, W.; Yeung, K. W. K. Bone Grafts and Biomaterials Substitutes for Bone Defect Repair: A Review. *Bioact. Mater.* **2017**, *2* (4), 224–247. https://doi.org/10.1016/j.bioactmat.2017.05.007.
(32) Amini, A. R.; Laurencin, C. T.; Nukavarapu, S. P. Bone Tissue Engineering: Recent Advances and Challenges. *Crit. Rev. Biomed. Eng.* **2012**, *40* (5), 363–408.

(33) Samavedi, S.; Whittington, A. R.; Goldstein, A. S. Calcium Phosphate Ceramics in Bone Tissue Engineering: A Review of Properties and Their Influence on Cell Behavior. *Acta Biomater.* **2013**, *9* (9), 8037–8045. https://doi.org/10.1016/j.actbio.2013.06.014.
(34) Yoshikawa, H.; Myoui, A. Bone Tissue Engineering with Porous Hydroxyapatite Ceramics. *J. Artif. Organs Off. J. Jpn. Soc. Artif. Organs* **2005**, *8* (3), 131–136. https://doi.org/10.1007/s10047-005-0292-1.
(35) Sulaiman, S. B.; Keong, T. K.; Cheng, C. H.; Saim, A. B.; Idrus, R. B. H. Tricalcium Phosphate/Hydroxyapatite (TCP-HA) Bone Scaffold as Potential Candidate for the Formation of Tissue Engineered Bone. *Indian J. Med. Res.* **2013**, *137* (6), 1093–1101.
(36) Trombetta, R.; Inzana, J. A.; Schwarz, E. M.; Kates, S. L.; Awad, H. A. 3D Printing of Calcium Phosphate Ceramics for Bone Tissue Engineering and Drug Delivery. *Ann. Biomed. Eng.* **2017**, *45* (1), 23–44. https://doi.org/10.1007/s10439-016-1678-3.
(37) Deville, S.; Saiz, E.; Tomsia, A. P. Freeze Casting of Hydroxyapatite Scaffolds for Bone Tissue Engineering. *Biomaterials* **2006**, *27* (32), 5480–5489. https://doi.org/10.1016/j.biomaterials.2006.06.028.
(38) Vitale-Brovarone, C.; Di Nunzio, S.; Bretcanu, O.; Verné, E. Macroporous Glass-Ceramic Materials with Bioactive Properties. *J. Mater. Sci. Mater. Med.* **2004**, *15* (3), 209–217.
(39) Jones, J. R.; Ehrenfried, L. M.; Hench, L. L. Optimising Bioactive Glass Scaffolds for Bone Tissue Engineering. *Biomaterials* **2006**, *27* (7), 964–973. https://doi.org/10.1016/j.biomaterials.2005.07.017.
(40) Liu, X.; Rahaman, M. N.; Fu, Q. Oriented Bioactive Glass (13-93) Scaffolds with Controllable Pore Size by Unidirectional Freezing of Camphene-Based Suspensions: Microstructure and Mechanical Response. *Acta Biomater.* **2011**, *7* (1), 406–416. https://doi.org/10.1016/j.actbio.2010.08.025.
(41) Fu, Q.; Rahaman, M. N.; Bal, B. S.; Kuroki, K.; Brown, R. F. In Vivo Evaluation of 13-93 Bioactive Glass Scaffolds with Trabecular and Oriented Microstructures in a Subcutaneous Rat Implantation Model. *J. Biomed. Mater. Res. A* **2010**, *95* (1), 235–244. https://doi.org/10.1002/jbm.a.32827.
(42) Shor, L.; Güçeri, S.; Chang, R.; Gordon, J.; Kang, Q.; Hartsock, L.; An, Y.; Sun, W. Precision Extruding Deposition (PED) Fabrication of Polycaprolactone (PCL) Scaffolds for Bone Tissue Engineering. *Biofabrication* **2009**, *1* (1), 015003. https://doi.org/10.1088/1758-5082/1/1/015003.
(43) Ahn, S. H.; Lee, H. J.; Kim, G. H. Polycaprolactone Scaffolds Fabricated with an Advanced Electrohydrodynamic Direct-Printing Method for Bone Tissue Regeneration. *Biomacromolecules* **2011**, *12* (12), 4256–4263. https://doi.org/10.1021/bm201126j.
(44) Gregor, A.; Filová, E.; Novák, M.; Kronek, J.; Chlup, H.; Buzgo, M.; Blahnová, V.; Lukášová, V.; Bartoš, M.; Nečas, A.; et al. Designing of PLA Scaffolds for Bone Tissue Replacement Fabricated by Ordinary Commercial 3D Printer. *J. Biol. Eng.* **2017**, *11*. https://doi.org/10.1186/s13036-017-0074-3.
(45) Grémare, A.; Guduric, V.; Bareille, R.; Heroguez, V.; Latour, S.; L'heureux, N.; Fricain, J.-C.; Catros, S.; Le Nihouannen, D. Characterization of Printed PLA Scaffolds for Bone Tissue Engineering. *J. Biomed. Mater. Res. A* **2018**, *106* (4), 887–894. https://doi.org/10.1002/jbm.a.36289.

(46) Ortega-Oller, I.; Padial-Molina, M.; Galindo-Moreno, P.; O'Valle, F.; Jódar-Reyes, A. B.; Peula-García, J. M. Bone Regeneration from PLGA Micro-Nanoparticles. *BioMed Res. Int.* **2015**, *2015*, 415289. https://doi.org/10.1155/2015/415289.

(47) Sun, X.; Xu, C.; Wu, G.; Ye, Q.; Wang, C. Poly(Lactic-Co-Glycolic Acid): Applications and Future Prospects for Periodontal Tissue Regeneration. *Polymers* **2017**, *9* (6), 189. https://doi.org/10.3390/polym9060189.

(48) Lavrador, C.; Mascarenhas, R.; Coelho, P.; Brites, C.; Pereira, A.; Gogolewski, S. Elastomeric Enriched Biodegradable Polyurethane Sponges for Critical Bone Defects: A Successful Case Study Reducing Donor Site Morbidity. *J. Mater. Sci. Mater. Med.* **2016**, *27* (3), 61. https://doi.org/10.1007/s10856-016-5667-8.

(49) Yu, J.; Xia, H.; Teramoto, A.; Ni, Q.-Q. Fabrication and Characterization of Shape Memory Polyurethane Porous Scaffold for Bone Tissue Engineering. *J. Biomed. Mater. Res. A* **2017**, *105* (4), 1132–1137. https://doi.org/10.1002/jbm.a.36009.

(50) Marzec, M.; Kucińska-Lipka, J.; Kalaszczyńska, I.; Janik, H. Development of Polyurethanes for Bone Repair. *Mater. Sci. Eng. C Mater. Biol. Appl.* **2017**, *80*, 736–747. https://doi.org/10.1016/j.msec.2017.07.047.

(51) Groppo, M. F.; Caria, P. H.; Freire, A. R.; Figueroba, S. R.; Ribeiro-Neto, W. A.; Bretas, R. E. S.; Prado, F. B.; Haiter-Neto, F.; Aguiar, F. H.; Rossi, A. C. The Effect of a Hydroxyapatite Impregnated PCL Membrane in Rat Subcritical Calvarial Bone Defects. *Arch. Oral Biol.* **2017**, *82*, 209–215. https://doi.org/10.1016/j.archoralbio.2017.06.018.

(52) Totaro, A.; Salerno, A.; Imparato, G.; Domingo, C.; Urciuolo, F.; Netti, P. A. PCL-HA Microscaffolds for in Vitro Modular Bone Tissue Engineering. *J. Tissue Eng. Regen. Med.* **2017**, *11* (6), 1865–1875. https://doi.org/10.1002/term.2084.

(53) Eftekhari, H.; Jahandideh, A.; Asghari, A.; Akbarzadeh, A.; Hesaraki, S. Assessment of Polycaprolacton (PCL) Nanocomposite Scaffold Compared with Hydroxyapatite (HA) on Healing of Segmental Femur Bone Defect in Rabbits. *Artif. Cells Nanomedicine Biotechnol.* **2017**, *45* (5), 961–968. https://doi.org/10.1080/21691401.2016.1198360.

(54) Santos, D.; Silva, D. M.; Gomes, P. S.; Fernandes, M. H.; Santos, J. D.; Sencadas, V. Multifunctional PLLA-Ceramic Fiber Membranes for Bone Regeneration Applications. *J. Colloid Interface Sci.* **2017**, *504*, 101–110. https://doi.org/10.1016/j.jcis.2017.05.032.

(55) Qi, H.; Ye, Z.; Ren, H.; Chen, N.; Zeng, Q.; Wu, X.; Lu, T. Bioactivity Assessment of PLLA/PCL/HAP Electrospun Nanofibrous Scaffolds for Bone Tissue Engineering. *Life Sci.* **2016**, *148*, 139–144. https://doi.org/10.1016/j.lfs.2016.02.040.

(56) Bhuiyan, D. B.; Middleton, J. C.; Tannenbaum, R.; Wick, T. M. Bone Regeneration from Human Mesenchymal Stem Cells on Porous Hydroxyapatite-PLGA-Collagen Bioactive Polymer Scaffolds. *Biomed. Mater. Eng.* **2017**, *28* (6), 671–685. https://doi.org/10.3233/BME-171703.

(57) van Houdt, C. I. A.; Ulrich, D. J. O.; Jansen, J. A.; van den Beucken, J. J. J. P. The Performance of CPC/PLGA and Bio-Oss® for Bone Regeneration in Healthy and Osteoporotic Rats. *J. Biomed. Mater. Res. B Appl. Biomater.* **2018**, *106* (1), 131–142. https://doi.org/10.1002/jbm.b.33801.

(58) Liao, H.; Félix Lanao, R. P.; van den Beucken, J. J. J. P.; Zhou, N.; Both, S. K.; Wolke, J. G. C.; Jansen, J. A. Size Matters: Effects of PLGA-Microsphere Size in Injectable CPC/PLGA on Bone Formation. *J. Tissue Eng. Regen. Med.* **2016**, *10* (8), 669–678. https://doi.org/10.1002/term.1840.

(59) Dhandayuthapani, B.; Yoshida, Y.; Maekawa, T.; Kumar, D. S. Polymeric Scaffolds in Tissue Engineering Application: A Review https://www.hindawi.com/journals/ijps/2011/290602/ (accessed Jan 8, 2019). https://doi.org/10.1155/2011/290602.
(60) Polo-Corrales, L.; Latorre-Esteves, M.; Ramirez-Vick, J. E. Scaffold Design for Bone Regeneration. *J. Nanosci. Nanotechnol.* **2014**, *14* (1), 15–56.
(61) Bone Engineering: A Matter of Cells, Growth Factors and Biomaterials | IntechOpen https://www.intechopen.com/books/regenerative-medicine-and-tissue-engineering/bone-engineering-a-matter-of-cells-growth-factors-and-biomaterials (accessed Feb 22, 2019).
(62) Mondal, D.; Lin, S.; Rizkalla, A. S.; Mequanint, K. Porous and Biodegradable Polycaprolactone-Borophosphosilicate Hybrid Scaffolds for Osteoblast Infiltration and Stem Cell Differentiation. *J. Mech. Behav. Biomed. Mater.* **2019**, *92*, 162–171. https://doi.org/10.1016/j.jmbbm.2019.01.011.
(63) Wu, Q.; Yang, B.; Hu, K.; Cao, C.; Man, Y.; Wang, P. Deriving Osteogenic Cells from Induced Pluripotent Stem Cells for Bone Tissue Engineering. *Tissue Eng. Part B Rev.* **2017**, *23* (1), 1–8. https://doi.org/10.1089/ten.TEB.2015.0559.
(64) Medvedev, S. P.; Shevchenko, A. I.; Zakian, S. M. Induced Pluripotent Stem Cells: Problems and Advantages When Applying Them in Regenerative Medicine. *Acta Naturae* **2010**, *2* (2), 18–28.
(65) Asatrian, G.; Pham, D.; Hardy, W. R.; James, A. W.; Peault, B. Stem Cell Technology for Bone Regeneration: Current Status and Potential Applications. *Stem Cells Cloning Adv. Appl.* **2015**, *8*, 39–48. https://doi.org/10.2147/SCCAA.S48423.
(66) Romagnoli, C.; Brandi, M. L. Adipose Mesenchymal Stem Cells in the Field of Bone Tissue Engineering. *World J. Stem Cells* **2014**, *6* (2), 144–152. https://doi.org/10.4252/wjsc.v6.i2.144.
(67) Park, S. Y.; Ki, C. S.; Park, Y. H.; Jung, H. M.; Woo, K. M.; Kim, H. J. Electrospun Silk Fibroin Scaffolds with Macropores for Bone Regeneration: An in Vitro and in Vivo Study. *Tissue Eng. Part A* **2010**, *16* (4), 1271–1279. https://doi.org/10.1089/ten.TEA.2009.0328.
(68) Fang, R.; Zhang, E.; Xu, L.; Wei, S. Electrospun PCL/PLA/HA Based Nanofibers as Scaffold for Osteoblast-like Cells. *J. Nanosci. Nanotechnol.* **2010**, *10* (11), 7747–7751.
(69) Terranova, L.; Mallet, R.; Perrot, R.; Chappard, D. Polystyrene Scaffolds Based on Microfibers as a Bone Substitute; Development and in Vitro Study. *Acta Biomater.* **2016**, *29*, 380–388. https://doi.org/10.1016/j.actbio.2015.10.042.
(70) Guo, Z.; Xu, J.; Ding, S.; Li, H.; Zhou, C.; Li, L. In Vitro Evaluation of Random and Aligned Polycaprolactone/Gelatin Fibers via Electrospinning for Bone Tissue Engineering. *J. Biomater. Sci. Polym. Ed.* **2015**, *26* (15), 989–1001. https://doi.org/10.1080/09205063.2015.1065598.
(71) Yu, Y.; Hua, S.; Yang, M.; Fu, Z.; Teng, S.; Niu, K.; Zhao, Q.; Yi, C. Fabrication and Characterization of Electrospinning/3D Printing Bone Tissue Engineering Scaffold. *RSC Adv.* **2016**, *6* (112), 110557–110565. https://doi.org/10.1039/C6RA17718B.
(72) Baudequin, T.; Gaut, L.; Mueller, M.; Huepkes, A.; Glasmacher, B.; Duprez, D.; Bedoui, F.; Legallais, C. The Osteogenic and Tenogenic Differentiation Potential of C3H10T1/2 (Mesenchymal Stem Cell Model) Cultured on PCL/PLA Electrospun Scaffolds in the Absence of Specific Differentiation Medium. *Materials* **2017**, *10* (12). https://doi.org/10.3390/ma10121387.

(73) Yang, S. Y.; Hwang, T. H.; Che, L.; Oh, J. S.; Ha, Y.; Ryu, W. Membrane-Reinforced Three-Dimensional Electrospun Silk Fibroin Scaffolds for Bone Tissue Engineering. *Biomed. Mater.* **2015**, *10* (3), 035011. https://doi.org/10.1088/1748-6041/10/3/035011.
(74) Prabhakaran, M. P.; Venugopal, J.; Ramakrishna, S. Electrospun Nanostructured Scaffolds for Bone Tissue Engineering. *Acta Biomater.* **2009**, *5* (8), 2884–2893. https://doi.org/10.1016/j.actbio.2009.05.007.
(75) Zhang, Y.; Venugopal, J. R.; El-Turki, A.; Ramakrishna, S.; Su, B.; Lim, C. T. Electrospun Biomimetic Nanocomposite Nanofibers of Hydroxyapatite/Chitosan for Bone Tissue Engineering. *Biomaterials* **2008**, *29* (32), 4314–4322. https://doi.org/10.1016/j.biomaterials.2008.07.038.
(76) Kartsogiannis, V.; Ng, K. W. Cell Lines and Primary Cell Cultures in the Study of Bone Cell Biology. *Mol. Cell. Endocrinol.* **2004**, *228* (1), 79–102. https://doi.org/10.1016/j.mce.2003.06.002.
(77) Kaur, G.; Dufour, J. M. Cell Lines. *Spermatogenesis* **2012**, *2* (1), 1–5. https://doi.org/10.4161/spmg.19885.
(78) De Witte, T.-M.; Fratila-Apachitei, L. E.; Zadpoor, A. A.; Peppas, N. A. Bone Tissue Engineering via Growth Factor Delivery: From Scaffolds to Complex Matrices. *Regen. Biomater.* **2018**, *5* (4), 197–211. https://doi.org/10.1093/rb/rby013.
(79) Bonewald, L. F.; Mundy, G. R. Role of Transforming Growth Factor-Beta in Bone Remodeling. *Clin. Orthop.* **1990**, No. 250, 261–276.
(80) Chen, D.; Zhao, M.; Mundy, G. R. Bone Morphogenetic Proteins. *Growth Factors Chur Switz.* **2004**, *22* (4), 233–241. https://doi.org/10.1080/08977190412331279890.
(81) Su, N.; Jin, M.; Chen, L. Role of FGF/FGFR Signaling in Skeletal Development and Homeostasis: Learning from Mouse Models. *Bone Res.* **2014**, *2*, 14003. https://doi.org/10.1038/boneres.2014.3.
(82) Hu, K.; Olsen, B. R. The Roles of Vascular Endothelial Growth Factor in Bone Repair and Regeneration. *Bone* **2016**, *91*, 30–38. https://doi.org/10.1016/j.bone.2016.06.013.
(83) McCarthy, T. L.; Centrella, M.; Canalis, E. Insulin-like Growth Factor (IGF) and Bone. *Connect. Tissue Res.* **1989**, *20* (1–4), 277–282.
(84) Wu, M.; Chen, G.; Li, Y.-P. TGF-β and BMP Signaling in Osteoblast, Skeletal Development, and Bone Formation, Homeostasis and Disease. *Bone Res.* **2016**, *4*, 16009. https://doi.org/10.1038/boneres.2016.9.
(85) Itonaga, I.; Sabokbar, A.; Sun, S. G.; Kudo, O.; Danks, L.; Ferguson, D.; Fujikawa, Y.; Athanasou, N. A. Transforming Growth Factor-Beta Induces Osteoclast Formation in the Absence of RANKL. *Bone* **2004**, *34* (1), 57–64.
(86) Blackwood, K. A.; Bock, N.; Dargaville, T. R.; Ann Woodruff, M. Scaffolds for Growth Factor Delivery as Applied to Bone Tissue Engineering https://www.hindawi.com/journals/ijps/2012/174942/ (accessed Feb 26, 2019). https://doi.org/10.1155/2012/174942.
(87) Sahni, A.; Khorana, A. A.; Baggs, R. B.; Peng, H.; Francis, C. W. FGF-2 Binding to Fibrin(Ogen) Is Required for Augmented Angiogenesis. *Blood* **2006**, *107* (1), 126–131. https://doi.org/10.1182/blood-2005-06-2460.
(88) Behr, B.; Leucht, P.; Longaker, M. T.; Quarto, N. Fgf-9 Is Required for Angiogenesis and Osteogenesis in Long Bone Repair. *Proc. Natl. Acad. Sci.* **2010**, *107* (26), 11853–11858. https://doi.org/10.1073/pnas.1003317107.

(89) Moreaux, J.; Hose, D.; Kassambara, A.; Rème, T.; Moine, P.; Requirand, G.; Goldschmidt, H.; Klein, B. Osteoclast-Gene Expression Profiling Reveals Osteoclast-Derived CCR2 Chemokines Promoting Myeloma Cell Migration. *Blood* **2011**, *117* (4), 1280–1290. https://doi.org/10.1182/blood-2010-04-279760.
(90) Klein-Nulend, J.; Bacabac, R. G.; Bakker, A. D. Mechanical Loading and How It Affects Bone Cells: The Role of the Osteocyte Cytoskeleton in Maintaining Our Skeleton. *Eur. Cell. Mater.* **2012**, *24*, 278–291.
(91) Saunders, M. M.; Lee, J. S. The Influence of Mechanical Environment on Bone Healing and Distraction Osteogenesis. *Atlas Oral Maxillofac. Surg. Clin. North Am.* **2008**, *16* (2), 147–158. https://doi.org/10.1016/j.cxom.2008.04.006.
(92) Duncan, R. L.; Turner, C. H. Mechanotransduction and the Functional Response of Bone to Mechanical Strain. *Calcif. Tissue Int.* **1995**, *57* (5), 344–358.
(93) Baudequin, T.; Legallais, C.; Bedoui, F. In Vitro Bone Cell Response to Tensile Mechanical Solicitations: Is There an Optimal Protocol? *Biotechnol. J.* **2019**, *14* (1), 1800358. https://doi.org/10.1002/biot.201800358.
(94) Ma, Z.; Kotaki, M.; Inai, R.; Ramakrishna, S. Potential of Nanofiber Matrix as Tissue-Engineering Scaffolds. *Tissue Eng.* **2005**, *11* (1–2), 101–109. https://doi.org/10.1089/ten.2005.11.101.
(95) Wang, X.; Ding, B.; Li, B. Biomimetic Electrospun Nanofibrous Structures for Tissue Engineering. *Mater. Today* **2013**, *16* (6), 229–241. https://doi.org/10.1016/j.mattod.2013.06.005.
(96) Norouzi, M.; Boroujeni, S. M.; Omidvarkordshouli, N.; Soleimani, M. Advances in Skin Regeneration: Application of Electrospun Scaffolds. *Adv. Healthc. Mater.* **2015**, *4* (8), 1114–1133. https://doi.org/10.1002/adhm.201500001.
(97) Horner, C. B.; Low, K.; Nam, J. 10 - Electrospun Scaffolds for Cartilage Regeneration. In *Nanocomposites for Musculoskeletal Tissue Regeneration*; Liu, H., Ed.; Woodhead Publishing: Oxford, 2016; pp 213–240. https://doi.org/10.1016/B978-1-78242-452-9.00010-8.
(98) Brennan, D. A.; Conte, A. A.; Kanski, G.; Turkula, S.; Hu, X.; Kleiner, M. T.; Beachley, V. Mechanical Considerations for Electrospun Nanofibers in Tendon and Ligament Repair. *Adv. Healthc. Mater.* **2018**, *7* (12), e1701277. https://doi.org/10.1002/adhm.201701277.
(99) Mu, Y.; Wu, F.; Lu, Y.; Wei, L.; Yuan, W. Progress of Electrospun Fibers as Nerve Conduits for Neural Tissue Repair. *Nanomed.* **2014**, *9* (12), 1869–1883. https://doi.org/10.2217/nnm.14.70.
(100) Ramachandran, K.; Gouma, P.-I. Electrospinning for Bone Tissue Engineering. *Recent Pat. Nanotechnol.* **2008**, *2* (1), 1–7.
(101) Bhardwaj, N.; Kundu, S. C. Electrospinning: A Fascinating Fiber Fabrication Technique. *Biotechnol. Adv.* **2010**, *28* (3), 325–347. https://doi.org/10.1016/j.biotechadv.2010.01.004.
(102) Haider, A.; Haider, S.; Kang, I.-K. A Comprehensive Review Summarizing the Effect of Electrospinning Parameters and Potential Applications of Nanofibers in Biomedical and Biotechnology. *Arab. J. Chem.* **2018**, *11* (8), 1165–1188. https://doi.org/10.1016/j.arabjc.2015.11.015.
(103) Shih, Y.-R. V.; Chen, C.-N.; Tsai, S.-W.; Wang, Y. J.; Lee, O. K. Growth of Mesenchymal Stem Cells on Electrospun Type I Collagen Nanofibers. *Stem Cells Dayt. Ohio* **2006**, *24* (11), 2391–2397. https://doi.org/10.1634/stemcells.2006-0253.

(104) Ekaputra, A. K.; Zhou, Y.; Cool, S. M.; Hutmacher, D. W. Composite Electrospun Scaffolds for Engineering Tubular Bone Grafts. *Tissue Eng. Part A* **2009**, *15* (12), 3779–3788. https://doi.org/10.1089/ten.TEA.2009.0186.
(105) Haslauer, C. M.; Moghe, A. K.; Osborne, J. A.; Gupta, B. S.; Loboa, E. G. Collagen-PCL Sheath-Core Bicomponent Electrospun Scaffolds Increase Osteogenic Differentiation and Calcium Accretion of Human Adipose-Derived Stem Cells. *J. Biomater. Sci. Polym. Ed.* **2011**, *22* (13), 1695–1712. https://doi.org/10.1163/092050610X521595.
(106) Zhang, Y.; Ouyang, H.; Lim, C. T.; Ramakrishna, S.; Huang, Z.-M. Electrospinning of Gelatin Fibers and Gelatin/PCL Composite Fibrous Scaffolds. *J. Biomed. Mater. Res. B Appl. Biomater.* **2005**, *72* (1), 156–165. https://doi.org/10.1002/jbm.b.30128.
(107) Wang, M.; Jin, H.-J.; Kaplan, D. L.; Rutledge, G. C. Mechanical Properties of Electrospun Silk Fibers. *Macromolecules* **2004**, *37* (18), 6856–6864. https://doi.org/10.1021/ma048988v.
(108) Li, C.; Vepari, C.; Jin, H.-J.; Kim, H. J.; Kaplan, D. L. Electrospun Silk-BMP-2 Scaffolds for Bone Tissue Engineering. *Biomaterials* **2006**, *27* (16), 3115–3124. https://doi.org/10.1016/j.biomaterials.2006.01.022.
(109) Shalumon, K. T.; Lai, G.-J.; Chen, C.-H.; Chen, J.-P. Modulation of Bone-Specific Tissue Regeneration by Incorporating Bone Morphogenetic Protein and Controlling the Shell Thickness of Silk Fibroin/Chitosan/Nanohydroxyapatite Core-Shell Nanofibrous Membranes. *ACS Appl. Mater. Interfaces* **2015**, *7* (38), 21170–21181. https://doi.org/10.1021/acsami.5b04962.
(110) Yoshimoto, H.; Shin, Y. M.; Terai, H.; Vacanti, J. P. A Biodegradable Nanofiber Scaffold by Electrospinning and Its Potential for Bone Tissue Engineering. *Biomaterials* **2003**, *24* (12), 2077–2082. https://doi.org/10.1016/S0142-9612(02)00635-X.
(111) Rodrigues, M. T.; Martins, A.; Dias, I. R.; Viegas, C. A.; Neves, N. M.; Gomes, M. E.; Reis, R. L. Synergistic Effect of Scaffold Composition and Dynamic Culturing Environment in Multilayered Systems for Bone Tissue Engineering. *J. Tissue Eng. Regen. Med.* **2012**, *6* (10), e24-30. https://doi.org/10.1002/term.499.
(112) Canha-Gouveia, A.; Rita Costa-Pinto, A.; Martins, A. M.; Silva, N. A.; Faria, S.; Sousa, R. A.; Salgado, A. J.; Sousa, N.; Reis, R. L.; Neves, N. M. Hierarchical Scaffolds Enhance Osteogenic Differentiation of Human Wharton's Jelly Derived Stem Cells. *Biofabrication* **2015**, *7* (3), 035009. https://doi.org/10.1088/1758-5090/7/3/035009.
(113) Ko, E. K.; Jeong, S. I.; Rim, N. G.; Lee, Y. M.; Shin, H.; Lee, B.-K. In Vitro Osteogenic Differentiation of Human Mesenchymal Stem Cells and in Vivo Bone Formation in Composite Nanofiber Meshes. *Tissue Eng. Part A* **2008**, *14* (12), 2105–2119. https://doi.org/10.1089/ten.tea.2008.0057.
(114) Kim, S. J.; Jang, D. H.; Park, W. H.; Min, B.-M. Fabrication and Characterization of 3-Dimensional PLGA Nanofiber/Microfiber Composite Scaffolds. *Polymer* **2010**, *51* (6), 1320–1327. https://doi.org/10.1016/j.polymer.2010.01.025.
(115) Three Dimensional Honeycomb Patterned Fibrinogen Based Nanofibers Induce Substantial Osteogenic Response of Mesenchymal Stem Cells | Scientific Reports https://www.nature.com/articles/s41598-017-15956-8 (accessed Feb 11, 2019).
(116) Chen, Z.; Song, Y.; Zhang, J.; Liu, W.; Cui, J.; Li, H.; Chen, F. Laminated Electrospun NHA/PHB-Composite Scaffolds Mimicking Bone Extracellular Matrix for Bone Tissue Engineering. *Mater. Sci. Eng. C* **2017**, *72*, 341–351. https://doi.org/10.1016/j.msec.2016.11.070.

(117) Nedjari, S.; Awaja, F.; Altankov, G. Three Dimensional Honeycomb Patterned Fibrinogen Based Nanofibers Induce Substantial Osteogenic Response of Mesenchymal Stem Cells. *Sci. Rep.* **2017**, *7* (1), 15947. https://doi.org/10.1038/s41598-017-15956-8.
(118) Cai, Y.-Z.; Zhang, G.-R.; Wang, L.-L.; Jiang, Y.-Z.; Ouyang, H.-W.; Zou, X.-H. Novel Biodegradable Three-Dimensional Macroporous Scaffold Using Aligned Electrospun Nanofibrous Yarns for Bone Tissue Engineering. *J. Biomed. Mater. Res. A* **2012**, *100* (5), 1187–1194. https://doi.org/10.1002/jbm.a.34063.
(119) Vaquette, C.; Cooper-White, J. J. Increasing Electrospun Scaffold Pore Size with Tailored Collectors for Improved Cell Penetration. *Acta Biomater.* **2011**, *7* (6), 2544–2557. https://doi.org/10.1016/j.actbio.2011.02.036.
(120) Apostolakos, J.; Durant, T. J.; Dwyer, C. R.; Russell, R. P.; Weinreb, J. H.; Alaee, F.; Beitzel, K.; McCarthy, M. B.; Cote, M. P.; Mazzocca, A. D. The Enthesis: A Review of the Tendon-to-Bone Insertion. *Muscles Ligaments Tendons J.* **2014**, *4* (3), 333–342.
(121) Boys, A. J.; McCorry, M. C.; Rodeo, S.; Bonassar, L. J.; Estroff, L. A. Next Generation Tissue Engineering of Orthopedic Soft Tissue-to-Bone Interfaces. *MRS Commun.* **2017**, *7* (3), 289–308. https://doi.org/10.1557/mrc.2017.91.
(122) Benjamin, M.; Kumai, T.; Milz, S.; Boszczyk, B. M.; Boszczyk, A. A.; Ralphs, J. R. The Skeletal Attachment of Tendons—Tendon 'Entheses.' *Comp. Biochem. Physiol. A. Mol. Integr. Physiol.* **2002**, *133* (4), 931–945. https://doi.org/10.1016/S1095-6433(02)00138-1.
(123) Schlecht, S. H. Understanding Entheses: Bridging the Gap between Clinical and Anthropological Perspectives. *Anat. Rec. Hoboken NJ 2007* **2012**, *295* (8), 1239–1251. https://doi.org/10.1002/ar.22516.
(124) Zhang, X.; Levine, W. N.; Lu, H. H. Chapter 15 - Scaffold Design for Integrative Tendon–Bone Repair. In *Tendon Regeneration*; Gomes, M. E., Reis, R. L., Rodrigues, M. T., Eds.; Academic Press: Boston, 2015; pp 413–437. https://doi.org/10.1016/B978-0-12-801590-2.00015-6.
(125) Paxton, J. Z.; Baar, K.; M.Grover, L. Current Progress in Enthesis Repair: Strategies for Interfacial Tissue Engineering. *Orthop. Muscular Syst. Curr. Res.* **2012**, *3* (1). https://doi.org/10.4172/2161-0533.S1-003.
(126) Sharma, P.; Maffulli, N. Tendon Injury and Tendinopathy: Healing and Repair. *J. Bone Joint Surg. Am.* **2005**, *87* (1), 187–202. https://doi.org/10.2106/JBJS.D.01850.
(127) Font Tellado, S.; Balmayor, E. R.; Van Griensven, M. Strategies to Engineer Tendon/Ligament-to-Bone Interface: Biomaterials, Cells and Growth Factors. *Adv. Drug Deliv. Rev.* **2015**, *94*, 126–140. https://doi.org/10.1016/j.addr.2015.03.004.
(128) Kim, B. S.; Kim, E. J.; Choi, J. S.; Jeong, J. H.; Jo, C. H.; Cho, Y. W. Human Collagen-Based Multilayer Scaffolds for Tendon-to-Bone Interface Tissue Engineering. *J. Biomed. Mater. Res. A* **2014**, *102* (11), 4044–4054. https://doi.org/10.1002/jbm.a.35057.
(129) Erisken, C.; Kalyon, D. M.; Wang, H. Functionally Graded Electrospun Polycaprolactone and Beta-Tricalcium Phosphate Nanocomposites for Tissue Engineering Applications. *Biomaterials* **2008**, *29* (30), 4065–4073. https://doi.org/10.1016/j.biomaterials.2008.06.022.
(130) Liu, W.; Lipner, J.; Xie, J.; Manning, C. N.; Thomopoulos, S.; Xia, Y. Nanofiber Scaffolds with Gradients in Mineral Content for Spatial Control of Osteogenesis. *ACS Appl. Mater. Interfaces* **2014**, *6* (4), 2842–2849. https://doi.org/10.1021/am405418g.

(131) Spalazzi, J. P.; Dagher, E.; Doty, S. B.; Guo, X. E.; Rodeo, S. A.; Lu, H. H. In Vivo Evaluation of a Multiphased Scaffold Designed for Orthopaedic Interface Tissue Engineering and Soft Tissue-to-Bone Integration. *J. Biomed. Mater. Res. A* **2008**, *86* (1), 1–12. https://doi.org/10.1002/jbm.a.32073.
(132) Patel, S.; Caldwell, J.-M.; Doty, S. B.; Levine, W. N.; Rodeo, S.; Soslowsky, L. J.; Thomopoulos, S.; Lu, H. H. Integrating Soft and Hard Tissues via Interface Tissue Engineering. *J. Orthop. Res. Off. Publ. Orthop. Res. Soc.* **2018**, *36* (4), 1069–1077. https://doi.org/10.1002/jor.23810.
(133) Calejo, I.; Costa-Almeida, R.; Gomes, M. E. Cellular Complexity at the Interface: Challenges in Enthesis Tissue Engineering. **2019**, 1–20. https://doi.org/10.1007/5584_2018_307.
(134) Yin, Z.; Chen, X.; Chen, J. L.; Shen, W. L.; Hieu Nguyen, T. M.; Gao, L.; Ouyang, H. W. The Regulation of Tendon Stem Cell Differentiation by the Alignment of Nanofibers. *Biomaterials* **2010**, *31* (8), 2163–2175. https://doi.org/10.1016/j.biomaterials.2009.11.083.
(135) Kishore, V.; Bullock, W.; Sun, X.; Van Dyke, W. S.; Akkus, O. TENOGENIC DIFFERENTIATION OF HUMAN MSCs INDUCED BY THE TOPOGRAPHY OF ELECTROCHEMICALLY ALIGNED COLLAGEN THREADS. *Biomaterials* **2012**, *33* (7), 2137–2144. https://doi.org/10.1016/j.biomaterials.2011.11.066.
(136) Younesi, M.; Islam, A.; Kishore, V.; Anderson, J. M.; Akkus, O. Tenogenic Induction of Human MSCs by Anisotropically Aligned Collagen Biotextiles. *Adv. Funct. Mater.* **2014**, *24* (36), 5762–5770. https://doi.org/10.1002/adfm.201400828.
(137) Qin, T.-W.; Sun, Y.-L.; Thoreson, A. R.; Steinmann, S. P.; Amadio, P. C.; An, K.-N.; Zhao, C. Effect of Mechanical Stimulation on Bone Marrow Stromal Cell-Seeded Tendon Slice Constructs: A Potential Engineered Tendon Patch for Rotator Cuff Repair. *Biomaterials* **2015**, *51*, 43–50. https://doi.org/10.1016/j.biomaterials.2015.01.070.
(138) Subramony, S. D.; Dargis, B. R.; Castillo, M.; Azeloglu, E. U.; Tracey, M. S.; Su, A.; Lu, H. H. The Guidance of Stem Cell Differentiation by Substrate Alignment and Mechanical Stimulation. *Biomaterials* **2013**, *34* (8), 1942–1953. https://doi.org/10.1016/j.biomaterials.2012.11.012.
(139) Cardwell, R. D.; Kluge, J. A.; Thayer, P. S.; Guelcher, S. A.; Dahlgren, L. A.; Kaplan, D. L.; Goldstein, A. S. Static and Cyclic Mechanical Loading of Mesenchymal Stem Cells on Elastomeric, Electrospun Polyurethane Meshes. *J. Biomech. Eng.* **2015**, *137* (7). https://doi.org/10.1115/1.4030404.
(140) Robledo, R. F.; Rajan, L.; Li, X.; Lufkin, T. The Dlx5 and Dlx6 Homeobox Genes Are Essential for Craniofacial, Axial, and Appendicular Skeletal Development. *Genes Dev.* **2002**, *16* (9), 1089–1101. https://doi.org/10.1101/gad.988402.
(141) Samee, N.; Geoffroy, V.; Marty, C.; Schiltz, C.; Vieux-Rochas, M.; Levi, G.; de Vernejoul, M.-C. Dlx5, a Positive Regulator of Osteoblastogenesis, Is Essential for Osteoblast-Osteoclast Coupling. *Am. J. Pathol.* **2008**, *173* (3), 773–780. https://doi.org/10.2353/ajpath.2008.080243.
(142) Komori, T. Regulation of Osteoblast Differentiation by Runx2. *Adv. Exp. Med. Biol.* **2010**, *658*, 43–49. https://doi.org/10.1007/978-1-4419-1050-9_5.
(143) McGee-Lawrence, M. E.; Carpio, L. R.; Bradley, E. W.; Dudakovic, A.; Lian, J. B.; van Wijnen, A. J.; Kakar, S.; Hsu, W.; Westendorf, J. J. Runx2 Is Required for Early Stages of Endochondral Bone Formation but Delays Final Stages of Bone Repair in Axin2-

Deficient Mice. *Bone* **2014**, *66*, 277–286. https://doi.org/10.1016/j.bone.2014.06.022.
(144) Neve, A.; Corrado, A.; Cantatore, F. P. Osteocalcin: Skeletal and Extra-Skeletal Effects. *J. Cell. Physiol.* **2013**, *228* (6), 1149–1153. https://doi.org/10.1002/jcp.24278.
(145) Zoch, M. L.; Clemens, T. L.; Riddle, R. C. New Insights into the Biology of Osteocalcin. *Bone* **2016**, *82*, 42–49. https://doi.org/10.1016/j.bone.2015.05.046.
(146) Schweitzer, R.; Chyung, J. H.; Murtaugh, L. C.; Brent, A. E.; Rosen, V.; Olson, E. N.; Lassar, A.; Tabin, C. J. Analysis of the Tendon Cell Fate Using Scleraxis, a Specific Marker for Tendons and Ligaments. *Dev. Camb. Engl.* **2001**, *128* (19), 3855–3866.
(147) Shukunami, C.; Takimoto, A.; Oro, M.; Hiraki, Y. Scleraxis Positively Regulates the Expression of Tenomodulin, a Differentiation Marker of Tenocytes. *Dev. Biol.* **2006**, *298* (1), 234–247. https://doi.org/10.1016/j.ydbio.2006.06.036.
(148) Docheva, D.; Hunziker, E. B.; Fässler, R.; Brandau, O. Tenomodulin Is Necessary for Tenocyte Proliferation and Tendon Maturation. *Mol. Cell. Biol.* **2005**, *25* (2), 699–705. https://doi.org/10.1128/MCB.25.2.699-705.2005.
(149) Dex, S.; Alberton, P.; Willkomm, L.; Söllradl, T.; Bago, S.; Milz, S.; Shakibaei, M.; Ignatius, A.; Bloch, W.; Clausen-Schaumann, H.; et al. Tenomodulin Is Required for Tendon Endurance Running and Collagen I Fibril Adaptation to Mechanical Load. *EBioMedicine* **2017**, *20*, 240–254. https://doi.org/10.1016/j.ebiom.2017.05.003.
(150) Havis, E.; Bonnin, M.-A.; Olivera-Martinez, I.; Nazaret, N.; Ruggiu, M.; Weibel, J.; Durand, C.; Guerquin, M.-J.; Bonod-Bidaud, C.; Ruggiero, F.; et al. Transcriptomic Analysis of Mouse Limb Tendon Cells during Development. *Dev. Camb. Engl.* **2014**, *141* (19), 3683–3696. https://doi.org/10.1242/dev.108654.
(151) Bashur, C. A.; Shaffer, R. D.; Dahlgren, L. A.; Guelcher, S. A.; Goldstein, A. S. Effect of Fiber Diameter and Alignment of Electrospun Polyurethane Meshes on Mesenchymal Progenitor Cells. *Tissue Eng. Part A* **2009**, *15* (9), 2435–2445. https://doi.org/10.1089/ten.tea.2008.0295.
(152) Moffat, K. L.; Kwei, A. S.-P.; Spalazzi, J. P.; Doty, S. B.; Levine, W. N.; Lu, H. H. Novel Nanofiber-Based Scaffold for Rotator Cuff Repair and Augmentation. *Tissue Eng. Part A* **2009**, *15* (1), 115–126. https://doi.org/10.1089/ten.tea.2008.0014.
(153) Beldjilali-Labro, M.; Garcia Garcia, A.; Farhat, F.; Bedoui, F.; Grosset, J.-F.; Dufresne, M.; Legallais, C. Biomaterials in Tendon and Skeletal Muscle Tissue Engineering: Current Trends and Challenges. *Mater. Basel Switz.* **2018**, *11* (7). https://doi.org/10.3390/ma11071116.
(154) Orr, S. B.; Chainani, A.; Hippensteel, K. J.; Kishan, A.; Gilchrist, C.; Garrigues, N. W.; Ruch, D. S.; Guilak, F.; Little, D. Aligned Multilayered Electrospun Scaffolds for Rotator Cuff Tendon Tissue Engineering. *Acta Biomater.* **2015**, *24*, 117–126. https://doi.org/10.1016/j.actbio.2015.06.010.
(155) Schoenenberger, A. D.; Foolen, J.; Moor, P.; Silvan, U.; Snedeker, J. G. Substrate Fiber Alignment Mediates Tendon Cell Response to Inflammatory Signaling. *Acta Biomater.* **2018**, *71*, 306–317. https://doi.org/10.1016/j.actbio.2018.03.004.
(156) Bosworth, L. A.; Alam, N.; Wong, J. K.; Downes, S. Investigation of 2D and 3D Electrospun Scaffolds Intended for Tendon Repair. *J. Mater. Sci. Mater. Med.* **2013**, *24* (6), 1605–1614. https://doi.org/10.1007/s10856-013-4911-8.
(157) Subramony, S. D.; Su, A.; Yeager, K.; Lu, H. H. Combined Effects of Chemical Priming and Mechanical Stimulation on Mesenchymal Stem Cell Differentiation on Nanofiber

Scaffolds. *J. Biomech.* **2014**, *47* (9), 2189–2196. https://doi.org/10.1016/j.jbiomech.2013.10.016.
(158) Xu, Y.; Dong, S.; Zhou, Q.; Mo, X.; Song, L.; Hou, T.; Wu, J.; Li, S.; Li, Y.; Li, P.; et al. The Effect of Mechanical Stimulation on the Maturation of TDSCs-Poly(L-Lactide-Co-e-Caprolactone)/Collagen Scaffold Constructs for Tendon Tissue Engineering. *Biomaterials* **2014**, *35* (9), 2760–2772. https://doi.org/10.1016/j.biomaterials.2013.12.042.
(159) Engebretson, B.; Mussett, Z. R.; Sikavitsas, V. I. The Effects of Varying Frequency and Duration of Mechanical Stimulation on a Tissue-Engineered Tendon Construct. *Connect. Tissue Res.* **2018**, *59* (2), 167–177. https://doi.org/10.1080/03008207.2017.1324431.